APPLICATION OF BIOINFORMATICS IN STUDIES OF SPHINGOLIPID BIOSYNTHESIS

A Dessertation
Presented to
The Academic Faculty

by

Amin Altaf Momin

In Partial Fulfillment
of the Requirements for the Degree
Doctor of Philosophy in the
School of Biology, College of sciences

Georgia Institute of Technology
August 2010

APPLICATION OF BIOINFORMATICS IN STUDIES OF SPHINGOLIPID BIOSYNTHESIS

Approved by:

Dr. Alfred H Merrill Jr, Advisor
School of Biology
Georgia Institute of Technology

Dr. Stephen C Harvey
School of Biology
Georgia Institute of Technology

Dr Cameron Sullards
School of Chemistry and Biochemistry
Georgia Institute of Technology

Dr. Marion B. Sewer
School of Pharmacy and
Pharmaceutical Sciences
University of California, San Diego

Dr I King Jordan
School of Biology
Georgia Institute of Technology

Date Approved: 05/14/2010

This thesis is dedicated to my parents

ACKNOWLEDGEMENTS

I wish to thanks my Advisor Dr Alfred Merrill for all his kind advice and support during my graduate study. His encouragement and insight has been instrumental in shaping studies and overcoming challenging during my project. I would also like to think my committee members Dr Marion Sewer, Dr King Jordan, Dr Cameron Sullards, Dr Steve Harvey and a previous member Dr John Cairney for their valuable advice and constructive feedback during my dissertation.

All this work wouldn't be possible without the support of all my co-workers in the Merrill lab including Samuel Kelly, Chris Haynes, Hyejung Park, Kacee Sim, Kristin Jones, Jeremy Allegood, Jia Wei, Rebecca Shaner, Ying Liu, Martina Liepelt and Brent Portz. I am especially thankful to Elaine Wang for her advice and support during all these years in graduate school.

I would like to think my collaborators Dr John McDonald, Dr Nathan Bowen and Dr Lijuan Wang for their support and advice in the ovarian cancer project.

Living in Atlanta wouldn't be exciting and fun without the group of friends at Georgia Tech. I greatly appreciate all their support and encouragement.

Most of all, I am thankful to my parents. Their love, encouragement and support made all my work possible.

TABLE OF CONTENTS

LIST OF TABLES

LIST OF FIGURES

LIST OF SYMBOLS AND ABBREVIATIONS

1-deoxy-Sa	1-deoxysphinganine and 1-desoxymethylsphinganine
1-desoxymethyl-Sa	1-desoxymethylsphinganine
3KSR	3-Ketosphinganine reductase
BSA	Bovine serum albumin
CHO	Chinese hamster ovary
Cer	Ceramide
DMSO	Dimethyl sulfoxide
FBS	Fetal bovine serum
FB_1	Fumonisin B_1
FVT1	Folicular lymphoma variant type 1
GluCer	Glucosylceramide
GalCer	Galactosylceramide
GEO	Gene expression omnibus
GAPDH	Glyceraldehyde 3-phosphate dehydrogenase
HA	Human influenza hemagglutin
HexCer	Hexosylceramide
HPLC	High performance liquid chromatography
HSN1	Hereditary sensory neuropathy type 1
LCB	Long chain base
LC ESI-MS/MS	Liquid chromatography electrospray ionization mass spectrometry
LY-B	Chinese hamster ovary cells strain with defective SPT

LY-B/cLCB1	LY-B cells stably transfection with LCB1 cDNA
PBS	Phosphate buffer saline
PDB	Protein data bank
Sa	Sphinganine
SaP	Sphinganine 1-phosphate
SM	Sphingomyelin
So	Sphingosine
SoP	Sphingosine 1-phosphate
TLC	Thin layer chromatography
TBST	Tris buffered saline Tween-20

SUMMARY

Sphingolipids are diverse family of molecules found in all eukaryotes and some prokaryotes. They modulate critical functions related to cell survival, apoptosis, migration and membrane structures. As sphingolipids and their biosynthetic pathways are highly complex, studies in sphingolipid metabolism have been challenging. This dissertation addresses this challenge by the novel application of bioinformatics analysis to investigate sphingolipid and glycosphingolipid alterations at the system, as well as molecular levels.

As part of this thesis, updated pathway maps were prepared based on recent reports to visualize differences in gene expression and metabolites in the different branches of sphingolipid biosynthesis. Supporting Perl scripts were written to extract and format gene expression datasets for pathway visualization.

Cancer gene expression datasets were examined for sphingolipid gene expression differences using the pathway maps and compared to metabolites that were either reported or analyzed by mass spectrometry analysis conducted during this study. Comparison of 9 gene expression datasets and corresponding sphingolipid alterations identified a 72.8% correlation between transcript and metabolite pattern at a significance $p < 0.0001$using the Fisher's exact test. This study also discovered hydroxyl sphingolipids (phyto-sphingolipids) and short chain ceramides in MCF-7 and MDA-MB-231 cells respectively that were initially predicted by a gene expression pathway diagram.

The next study focuses on the discovery of the transcript that encodes the human 3-Ketosohinganine reductase (3KSR) which was not identified during the preparation of the pathway map. By blast comparison to the yeast enzyme sequence, Follicular

lymphoma type 1 (FVT1) was identified as the human homolog of 3KSR. After over expressing FVT1 in Hela cells and E.coli, its 3KSR activity was verified by an invitro enzyme activity assay. In Hela cells we have further discovered that the absence of FOXC1, a putative transcription regulator of FVT1 results in lower 3KSR activity and the accumulation of intermediate sphingolipids.

One of the critical factors influencing de novo sphingolipid biosynthesis is the expression of serine palmitoyltransferase (SPTLC1 and SPTLC2 subunits) and its role has been widely studied using a Chinese hamster ovary cells (LY-B) that lack the enzyme. Because the molecular abnormality of LY-B cells in the cells was unknown, we cloned the SPTLC1 transcript and discovered a point mutation. Homology modeling of the mutant protein suggested that the substitution would cause the protein to misfold and degrade. The use of chemical chaperones, DMSO and glycerol resulted in the partial stabilization of the SPT peptide but no significant SPT activity was determined.

These studies demonstrate the application of bioinformatics to investigate different molecular aspects of the sphingolipid biosynthesis.

CHAPTER 1

INTRODUCTION

1.1 Sphingolipids and their structural diversity

Sphingolipids are diverse family of lipids found in most eukaryotes and some prokaryotes [1]. They play important roles in cellular processes such as proliferation [2], migration, apoptosis [3, 4] and membrane structure. Abnormalities in their biosynthesis have been linked to neurodegenerative diseases [5, 6], lipid storage disorders [7] and carcinogenesis [8, 9]. Structurally, they are comprised of a sphingoid base (Fig 1), that may be N-acylated with a fatty acid of chain lengths C14-C30 (Fig 1.1). The 1-hydroxy (1-OH) position of sphingolipids can be modified by a phosphocholine, phosphate or complex carbohydrate headgroup (Fig 1). Besides sphinganine and sphingosine (sphingoid bases without and with a 4,5 unsaturation, respectively), other detected variations in sphingoid bases include 4-hydroxylation, iso and ante-iso methylation [10]. Recent reports have shown that shorter sphingoid bases can be produced by the condensation of palmitoyl-CoA with alanine and glycine [11] or the condensation of myristyl-CoA with serine to produce d16:1 sphingoid base [12, 13].

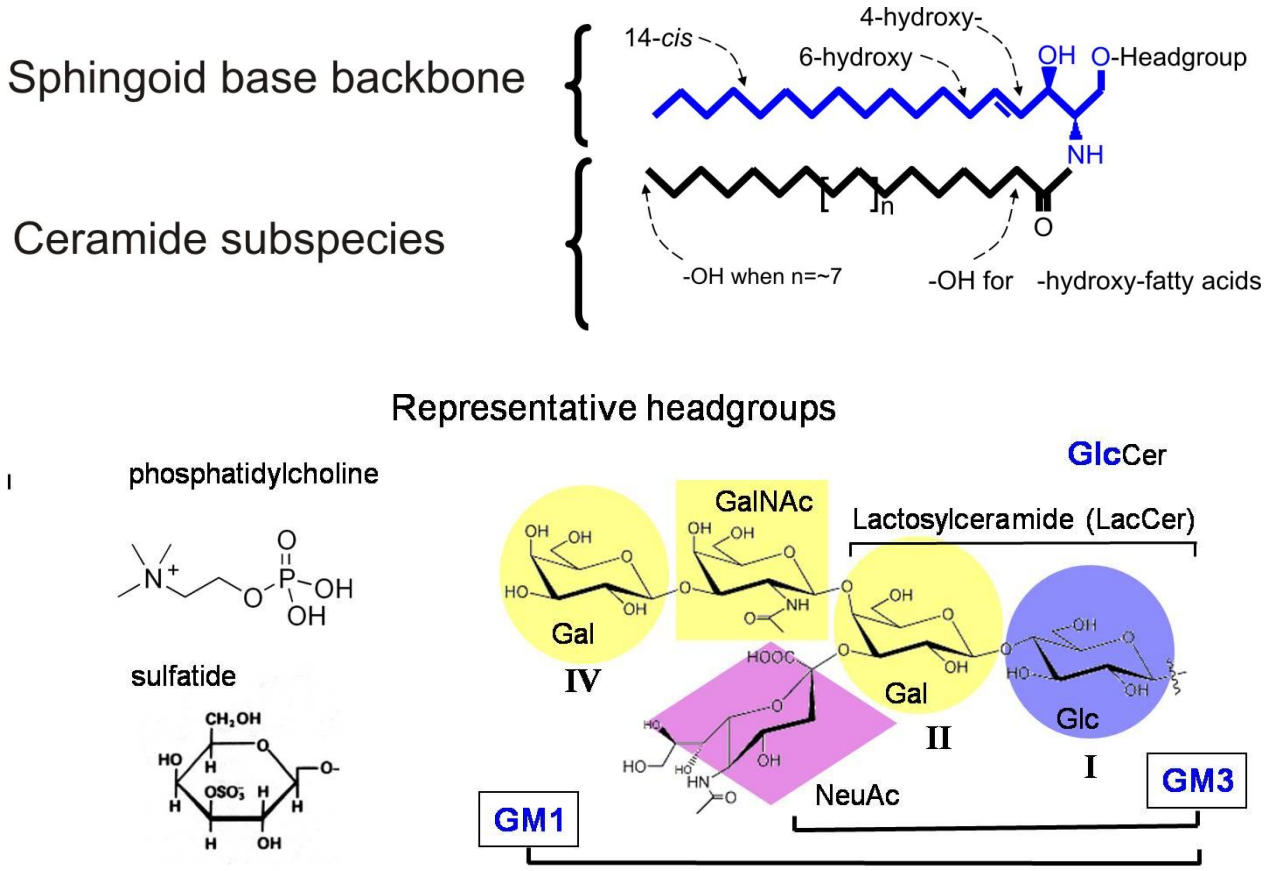

Fig 1.1. Illustration of backbone sphingolipid structure and putative headgroup modifications. The figure displays variations in sphingoid base and some of the possible headgroup modifications. Variations of the sphingoid base include Sphingosine, d18:1 (also called sphingenine) (shown), Sphinganine, d18:0 (dihydrosphingosine), 4-Hydroxysphinganine, t18:0 (phytosphingosine), Sphingadiene, d18:2 (e.g., 4-*trans*,14-*cis*) and others. Modifications in fatty acids include Amide-linked fatty acids (C14 to 30)/ mostly saturated (or mono-unsaturated)/sometimes with an α- or ω-hydroxyl group (abbreviation for compound shown: d18:1/16:0). The 1-position of the sphingoid base can be modified by moieties including phosphocholine sulfatides or glycans. Representative combinations of sugar residues in ganglioside are also displayed. This figure is adapted from a previous article [1]

1.2 De novo biosynthesis of ceramide and less complex glycosphingolipids

De novo biosynthesis of backbone sphingolipids [1] begins with the condensation of L-serine and palmitoyl-CoA by serine palmitoyltransferase (SPT) (Fig 1.1 A) to produce 3-ketosphinganine (3-KSa) that is reduced to sphinganine (Sa) by 3-ketosphinganine reductase (3KSR). Sphinganine can be N-acylated by fatty acid specific (dihydro) ceramide synthases (CerS1-6) (Fig 1.1 A) [14-18] to produce dihydroceramides with variable chain length fatty acids. A 4,5-double bond can then be introduced by dihydroceramide desaturase (DES1 and DES2) to generate different ceramide subspecies. In addition to 4,5 desaturation, DES2 also catalyzes a 4-hydroxylation reaction which is responsible for the synthesis of phytoceramide [19]. Glucosylceramide (GlcCer) and galactosylceramide (GalCer) are produced by the addition of glucose and galactose residues respectively, at the 1-hydroxy position of ceramide (Fig 1.1 A), whereas sphingomyelin and ceramide 1-phosphate are formed by the attachment of phosphatidylcholine and phosphate headgroups respectively.

An alternate approach to generate ceramides is by the turnover of complex sphingolipids [20], such as sphingomyelin (SM), GlcCer and GalCer by degradative enzymes. Ceramides can also be catabolized to sphingosine and then to sphingosine 1-phosphate (So 1-P) by acid ceramidase (ASAH 1) and sphingosine kinase (SPHK1, SPHK2), respectively, and So 1-P is degraded as ethanolamine phosphate and hexadecenal by sphingosine phosphate lyase (SoP lyase1).

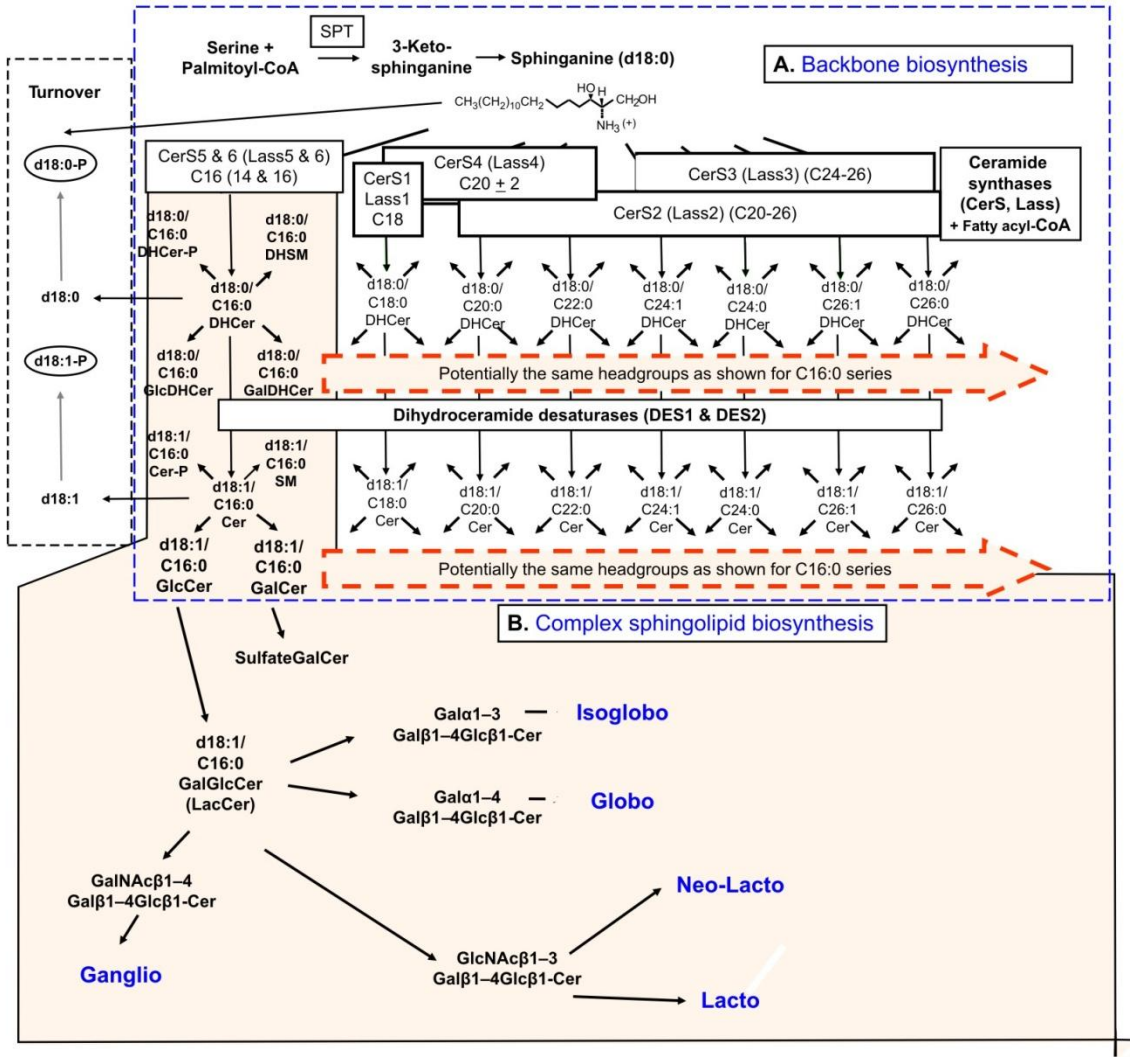

Figure 1.2. Biosynthesis of backbone sphingolipids and initial steps of complex sphingolipid metabolism. The illustration depicts early step of sphingolipid backbone formation and conversion to different branches of complex sphingolipid A) Backbone synthesis begins with the condensation of serine and palmitoyl-CoA by Serine palmitoyltransferase (SPT) to produce 3-Ketosphinganine, sphinganine, dihydroceramide, ceramide , ceramide 1-phosphate, glucosylceramide, galactosylceramide and sphingomyelin. Fatty acid specific ceramide synthases attaches N-acyl chain of different chain length to the sphingoid base backbone. Ceramides are degraded by conversion to sphingosine and then to sphingosine 1-phosphate. B) Metabolism of glucosylceramide to different branches of glycosphingolipids; ganglioside, isogloboseries, globoseries, neo-lacto-series and lacto-series begins with the attachment of different sugar groups. This figure is adapted from a previous article [1]

1.3 Biosynthesis of more complex glycosphingolipids

Synthesis of glycosphingolipid (GSL) species is initiated by the attachment of charged and uncharged sugar residues to GlcCer and GalCer (Fig 1.2 B) in a combinatorial fashion to produce acidic (charged) and neutral GSLs. While neutral GSL contain uncharged sugar residues such as glucose (Glc), galactose (Gal), N-acetylglucoseamine (GlucNAc) , N-acetylgalactoseamine and Fucose (Fuc) sugars, acidic GSL contain charged sugar residues such as sialic acid and glucuronic acid or headgroups such as phosphate and sulphate in addition to neutral sugar residues.

Acidic and neutral GSL are further classified based on the combination of a few initial sugar residues and the presence and absence of charged sugar residues, (Fig 1.2 B) such as ganglioside (Galβ1–3GalNacβ1–4Galβ1–4Glcβ1–1 Cer), Lactoseries (Galβ1–3GlcNacβ1–3Galβ1–4Glcβ1–1 Cer), Neolacto-series (Galβ1–4GlcNacβ1–3Galβ1–4Glcβ1–1 Cer), Globo-series (GalNacβ1–3Galα1–4Galβ1–4Glcβ1–1 Cer) and Isoglobo-series (GalNacβ1–3Galα1–3Galβ1–4Glcβ1–1 Cer). While most of the ganglioside and globoseries headgroups are specific to GSL, glycans belonging to other classes such as lacto-series and neo-lacto series are shared between glycolipids and glycoproteins. The biosynthesis of two abundant branches of GSL is described below.

1.3.1 Ganglioside biosynthesis

Stepwise addition of sialic acids to the carbohydrate headgroup of lactosylceramide(LacCer) results in the formation of simple gangliosides, i.e. monosialyl ganglioside (GM3) , disialyl ganglioside (GD3) and trisialyl ganglioside (GT3) (Fig 1.3

A). These species are further metabolized to more complex gangliosides by the attachment of charged and uncharged sugar residues for example GM3 is the precursor to GM2, GM1a, GD1a and GT1a, GD3 is converted to GD2, GD1b, GT1b and GQ1b, and GT3 is metabolized to GT2, GT1c, GQ1c and GP1c. In contrast, direct linkage of non-sialic acid residues to LacCer results in the formation of asialo-gangliosides species, GA2 and GA1. GSL formed using GM3, GD3 and GT3 as precursors are referred as A-, B- and C-series ganglioside respectively, and are usually indicated by the suffix 'a', 'b' and 'c' attached with their name (Fig 1.3 A).

1.3.2 Globoseries biosynthesis

Neutral GSL are formed by the metabolism of LacCer (Fig. 1.3 B) to ceramidetrihexoside (Gb3) that is converted to globoside (Gb4), which serves as the precursor to the formation of Forssman and para-forssman antigen), stage specific embryonic antigen-3 (Gb5, which is the precursor for Globo-H and Type IV A and B antigens) and stage specific embryonic antigen-4 (monosialyl-Gb5, which can be sialated to Disialyl-Gb5).

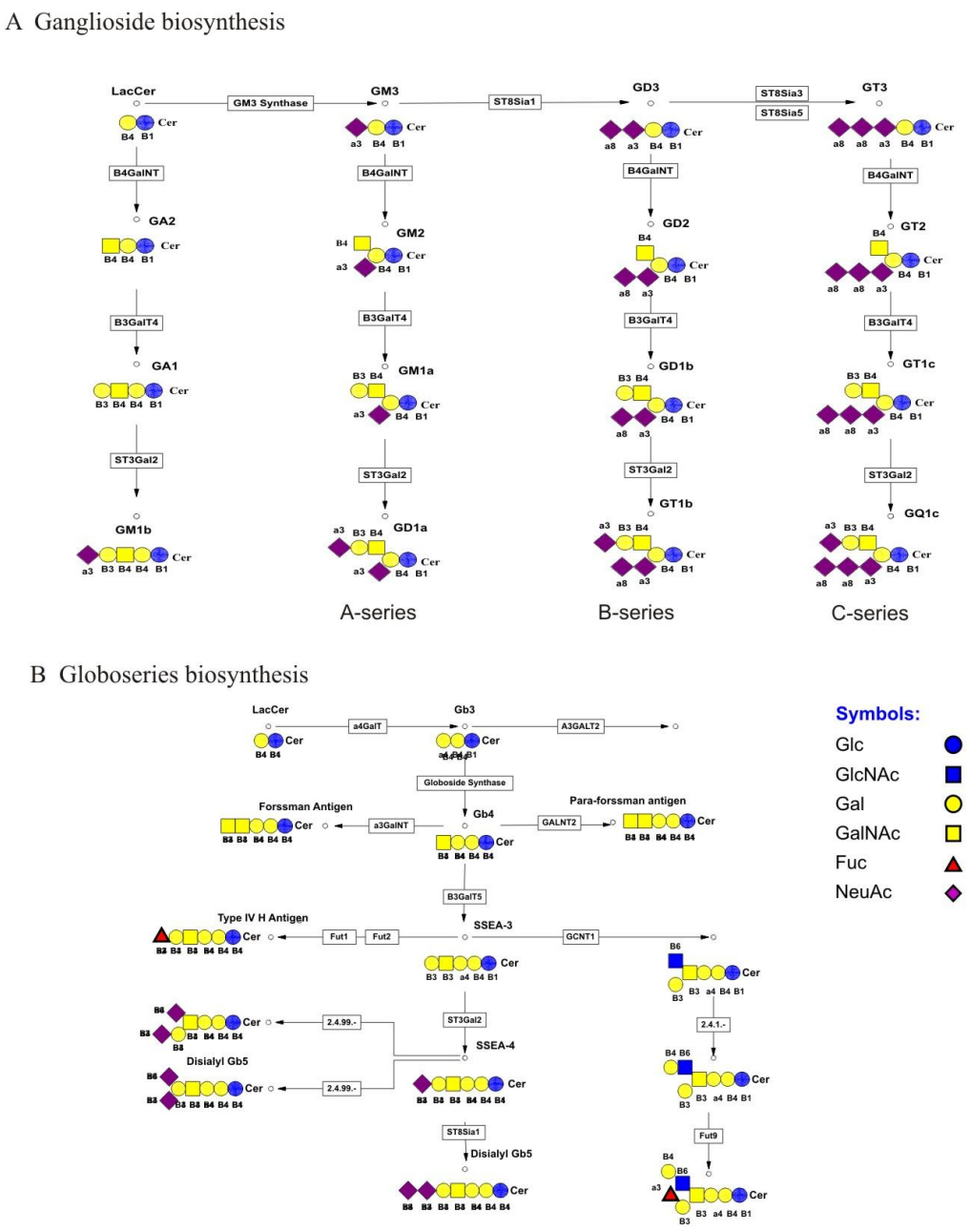

Figure 1.3 Biosynthesis of gangliosides and globoseries glycosphingolipids
Ganglioside
biosynthesis illustrated in (A) results in the formation of asialo-ganglioside (GA2 and Ga1), monosialyl-ganglioside(GM3, GM2, GM1a and GD1a), disialyl-ganglioside (GD3, GD2, GD1b and Gt1b) and trisialyl-ganglioside (GT3, GT2, GT1c and GQ1c). Structural isomers belonging to A, B or C series are indicated with a suffix 'a', 'b' and 'c'. B) shows the metabolism of LacCer to globoseries glycolipids; ceramidetrihexoside

(Gb3), globoside (Gb4), Forssman and para-forssman antigen, stage specific embryonic antigen-3 (SSEA-3), Globo-H antigen, stage specific embryonic antigen-4 (SSEA-4) and disialyl-Gb5. The layout of the modified pathway maps is based on KEGG (Kyoto Encyclopedia of Genes and Genomes, map00603 and map00604) pathway diagram, which were prepared using a GenMapp v2.1. The objects with different shapes and colors represent different sugar residues as indicated in the figure legend. Glucose (Glc), N-acyl glucose amine (GlcNAc), Galactose (Gal), N-acyl galactose amine (GalNAc), Fucose (Fuc) and Neuraminic acid (NeuAc).

1.4 Biological functions of sphingolipids

1.4.1 Membrane structure

Sphingolipids are components of lipids rafts [21] (detergent insoluble glycolipids enriched complexes) and glycosynapses in the plasma membrane [22]. Lipid rafts tend to cluster other important cell signaling proteins and G-protein coupled receptors including CD95/FAS [23, 24], EGFR [25] and nitric oxide synthase [26, 27]. Therefore changes in membrane lipid composition of sphingolipids and glycolipids have been noted to cause alterations of Serotonin (5-hydroxytryptamine) receptor activity [28] and bacterial adhesion to cell membrane (Helicobacter pylori) [29]. Another form of membrane micro-domain shown to contain sphingolipid molecules are "glycosynapses", wherein GSL accumulate with their binding proteins such as tetraspanins, integrins [30], growth factor receptors [31] and signaling molecules [32]. Through these interactions [33] GSL mediate adhesion, signal transduction and other functions pertinent to cancer.

1.4.2 Adhesion

GSL are largely localized to the outer leaflet of the plasma membrane and the lumens of the Golgi and endosomes, where they interact with receptors, glycoconjugates and extracellular proteins of neighboring cells through direct carbohydrate-carbohydrate interaction and carbohydrate-protein interactions [34].Their interactions with selectins [35], siglecs [36] and galectins [37], facilitate cell recognition and adhesion. One example is the adhesion and invasion of macrophages into inflamed renal tissue is

dependent upon the interaction between sulfatides and L-selectins [35]. In contrast, interaction of GM3 with CD9 tetraspanin inhibits haptotactic motility [38]. GSL have the capability to bind molecules on the same cell surface, for example GM3 binds and modulates epidermal growth factor receptor signaling (EGFR) through carbohydrate-carbohydrate interaction [39, 40].Glycan headgroups of GSLs are also recognized by viruses, bacteria and pathogens, and aid in binding and invasion of the host cells [41, 42].

1.4.3 Cell signaling

Backbone sphingolipids such as sphingosine, ceramide, sphingosine 1-phosphate and ceramide 1-phosphate serve as important second messenger molecules [43]. Sphingosine (So) and its N-methyl derivatives have been shown to inhibit protein kinase C (PKC) [19, 44, 45] and induce cell death. Ceramide, like sphingosine also interact with various members of the PKC family to initiate cell signaling through Bad/Bax, ERK and prostate apoptosis response-4 (PAR4) [46, 47] [48]. It induces apoptosis by promoting the phosphorylation and Golgi translocation of PKCα, PKCδ and PKCε [49-51], while it interacts with PKCβ2 and inhibits its juxtanuclear translocation [52]. Direct binding of ceramide to PKCξ was shown to cause the formation of a pro-apoptotic complex, PAR4 and induce cell death [48]. Ceramide also binds and activates protein phosphatase 2A (PP2A) and protein phosphatase 1 (PP1), which induces apoptosis by activating pro-apoptotic factors BAD and BAX [46, 47] and inactivating anti-apoptotic factors, bcl-2 and bcl-$_{XL}$ [53, 54]. The interaction of ceramide with cathepsin D causes caspase independent apoptosis [55].

In contrast, sphingoid base 1-phosphates (Sa1P and So1P) stimulate cell motility and proliferation through the activation of *platelet-derived growth factor* (PDGF) receptor [56] and the sphingosine 1-phosphate receptor family (S1P receptor, previously known as EDG receptors) [57]. S1P was shown to block apoptosis induced by ceramide, through the inhibition of caspase and SAPK/JNK activation, or by stimulating ERK pathway [58]. It has been proposed that the opposing effects of ceramide and So1P resulting in apoptosis and cell proliferation respectively, may function as a "switch" that can "dial" between growth, senescence and death depending on which combination is produced [59].

GSLs are involved in cell signaling via interaction with various tyrosine kinase receptors and cell adhesion molecules. GM3 caused complete inhibition of fibroblast growth factor receptor (FGFR) signaling and epidermal growth factor receptor (EGFR) signaling by blocking tyrosine phosphorylation in cells BHK [31, 60]. In contrast *platelet derived growth factor receptor (*PDGFR) signaling was inhibited by GD1a, GD1b, GT1b and GM1 [61, 62].

Another signaling mechanism involving GM3 is through the activation of c-Src, Rho and focal adhesion kinase (FAK) [63] in glycosphingolipid enriched microdomains (GEM). The binding of B16 cells expressing GM3 to Gg3 coated dishes enhanced tyrosine phosphorylation of FAK and c–Src [32], resulting in higher loading of GTP in Rho and Ras, resulting in their activation. Interaction of GM3 was also noted with the CD_4 –LCK protein complex [64].

As sphingolipids play critical roles in wide range of cell processes, their biosynthesis is highly regulated [65, 66]. However, an altered composition of these compounds has been found in a number of disorders, including neurodegenerative diseases [5, 6], lipid storage disorders [7] and carcinogenesis [8, 9]. The abnormal changes in sphingolipids have been linked to either their incomplete breakdown (degradation) caused by defective enzymes [7] or due to changes in gene expression and enzyme activity [8, 9].

1.5 Abnormal sphingolipid metabolism in cancer

Malignant transformation of cells is accompanied by aberrant changes in sphingolipid metabolites [34]. These were initially characterized as tumor antigens using immunological approaches, but later studies showed that they were glycosphingolipids (GSL). It is suggested that the abnormal composition of GSL's was caused by either the suppression of a downstream enzyme, also termed as 'blocked synthesis', or due to the induction of precursor enzyme, known as 'neosynthesis' [34]. Some of the alterations in tumors are summarized in Table 1.1.

Table 1.1 Comparison of sphingolipid alteration in tumors and cell lines.

Cancer type	Subtype comparison	Elevated	Depleted
Glioma	**Astrocytoma Vs Normal brain**	GM3 and GD3 [67, 68]	GD1a, GD1b, GT1b and GQ1b [67, 68]
	Gliosarcoma Vs Normal brain	GM3, GD2, GT3, 3'-isoLM1 and GD3 [69]	GM1a, GM1b, GD1a, GD1b, GM2, GT1b and GQ1b [69]
Melanoma	**Metastatic Normal/primary**	GD3 [70, 71], 9-O-acetylGD3, de-N-acetylGD3, O-acetyl GM2, O-actylGD2 and sialyl-Le^a [72-74]	
Ovarian	**Serous Vs normal ovary**	Gb1, Gb2, Gb3, and sulfatide[75, 76]	
	Mucinous Vs normal ovary	Gb1, Gb2, Gb3, Lewis A , Lewis B and sulfatide [75, 76]	
Prostate	**Metastatic Vs Normal**		Gb1, Gb2, Gb3 and GD2 [77]
	PC3 Vs PREC	GT1b, GD1b, GD1a and GM2.	
Breast	**Invasive ductal carcinoma (tissue) Vs normal**	GM3, GD3, N- and O-acetyl GD3, and GT3 [78], SSEA-3 and Globo-H [79, 80]	
	Invasive ductal carcinoma (serum) Vs normal	GD1b, GT1b and GQ1b [81]	
	MCF7 Vs MDA-MB-231	Gb4, SSEA3, Globo H [82]	GM3, GM2 and GD1a [82]

Table 1.1 Comparison of sphingolipid alteration in tumors and cell lines. The table depicts the differences in sphingolipid metabolites from published literature of glioma, melanoma, ovarian, prostate and breast tumors or cell lines. These studies quantified differences in sphingolipid species were quantified using analytical techniques such as thin layer chromatography (TLC), TLC immunostaining, high performance liquid chromatography or mass spectrometry. Calculated results were used to determine increase (elevated) or decrease (depleted) in metabolites amounts, while quantitative differences in TLC images were determined by densitometry analysis using the Flurchem 5500 (Alpha Innotech).

The Mechanisms used by sphingolipids to influence cancer processes are discussed in the section below.

1.5.1 Backbone sphingolipids

Sphingolipid backbone species participate in a number of cancer cell processes such as cell signaling, proliferation, motility and the induction of apoptosis. Sphingosine inhibits classical PKC and induces cell death [83]. Sphingosine and dimethyl sphingosine have been implicated in promoting sphingosine dependent kinase 1 (SDK1) dependent phosphorylation of 14-3-3 that prevents its dimerization and inactivation of proapoptotic factors, BAD and BAX [84].

Ceramide, like sphingosine, interacts with various members of the PKC family to initiate cell signaling through Bad/Bax, ERK and prostate apoptosis response-4 (PAR4) [46, 47] [48]. It binds and activates protein phosphatase 2A (PP2A) and protein phosphatase 1 (PP1), which induces apoptosis by activating pro-apoptotic factors BAD and BAX [46, 47] and inactivating anti-apoptotic factors BCL-2 and BCL-XL [53, 54], while the interaction of ceramide with cathepsin D results in caspase independent apoptosis [55]. In addition, chemotherapeutic agents [85-87] induce apoptosis by stimulating the production of ceramides through the turnover of sphingomyelin or induction of de novo biosysnthesis. Recently, induction of ceramides by tamoxifen was shown to induce autophagy [88], a critical pathway for the degradation and turnover of cellular organelles and proteins, and an important mechanism for non-apoptotic programmed cell death [89]. In addition a study performed in our lab has revealed that

generation of dihydroceramide by the inhibition of DES by fenretnide caused dihydroceramide mediated autophagy [90].

S1P plays a critical role in the process of angiogenesis [91] and the formation of blood vessels [92], through activation of $S1P_1$ receptor. This function is critical for tumor angiogenesis and vascularization [93], and was suppressed by the siRNA mediated silencing of $S1P_1$ receptor [94] . In addition, a recent study has demonstrated that a monoclonal antibody specific against S1P, arrested tumor angiogenesis and vascularization by inhibiting proangiogenic factors, IL-8, VEGF and bFGF [95]. S1P not only promote cell proliferation, but also blocks ceramide induced apoptosis by the inhibition of caspase and SAPK/JNK pathways and the activation of ERK pathway [58]. The activation of $S1P_1$ receptor by S1P was also essential for PGDF induced cell motility [56].

1.5.2 Gangliosides

Gangliosides play critical roles in both cell adhesion and signaling. GM3 binds and inhibits epidermal growth factor receptor (EGFR) signaling by inhibiting its phosphorylation, which results in stimulated phosphorilation of EGF receptor and growth inhibition by cell cycle arrest [60]. In contrast, reduction in GM3 levels leads to higher motility and invasiveness of YST-1 cells, which is reversible by the addition of exogenous GM3 [96]. In addition GM3 has been shown to inhibit FGFR signaling [167]. It also binds a number of extracellular proteins in the glycosynapse such as cSrc, RhoA and Csk. GM3 dependent activation of cSrc resulted in the induced differentiation of neurobalstoma cells, Neuro-2a [97], through the activation of MAPK signaling pathway

and the inhibition of Csk, an inhibitor of cSrc. The prophylactic treatment with anti-GM3 vaccine caused substantial reduction in tumor metastasis in B16 mouse model by eliciting the production of anti-GM3 IgG [98]. It was later shown that it elicited its effect through the through $CD8^+$ T cells [99].

GD3 is another important tumor associated ganglioside that has been detected in many tumors including melanoma [100-103], neuroblastoma [104-107] and lymphoma [108, 109]. In melanoma, high quantities of GD3 promotes enhanced cell proliferation and invasion through the phosphorylation of paxillin and P130CAS [110], while the suppression of paxillin and P130CAS inhibited GD3 mediated invasion and proliferation. Increase in ceramide amounts also augments GD3 level that triggers apoptosis through mitochondrial permeability transition [111-114], cytochrome-c release [115, 116] and caspase activation [108, 117, 118]. The treatment of cancer cells with fenretnide results in GD3 dependent formation of reactive oxygen species that triggers caspase-3 dependent apoptosis [118-120].

1.5.3 Sulfatides

Sulfatides are essential sulfated glycolipids that are mainly found on the cell surface where they interact with extracellular membrane proteins such as laminin [121, 122], L-selectins [35], P-selectins [123, 124] and thrombospondin [125, 126]. These interactions facilitate cell adhesion in metastasis [127] and immune responses [35]. Sulfatide was shown to bind P-selectin during adhesion and invasion of MC-38 cancerous cells injected in mice [124], which was significantly diminished when the sulfate group

was cleaved. During infiltration of monocytes into inflamed kidney during unilateral uretral obstruction, sulfatide act as a binding ligand to L-selectin to permit monocyte adhesion. This interaction was disrupted in CST $^{-/-}$ mouse where the monocytes were unable to infiltrate the kidney during inflammation due to the inability of L-selectins on monocytes to interact with their ligand [35]. The potential role of sulfatide in cancer metastatic may not be restricted to its interaction with different extra cellular matrix proteins but could also be due to their ability to interact with hepatocyte growth factors [128], cytokines and their receptors [129] as well as regulation of cytokine signaling (CXCR4) [130] and NF-KB signaling [131]. The importance of sulfatide binding a number of ligands, makes them a potential target for investigative therapeutics. In a study conducted in endometrial carcinoma patients, medroxyprogesterone acetate (progesterone) was able to reduce expression of sulfatide ligand on the surface of cancerous tissue, which may reduce their adhesion laminin and reduce the chances of invasion and metastasis [132]. The sulfatide binding to some of these ligands makes them a potential target for investigative therapeutics. In a study conducted in endometrial carcinoma patients, medroxyprogesterone acetate (progesterone) was able to reduce surface expression of sulfatide ligand and on cancerous tissue, which may reduce their adhesion laminin and reduce the chances of invasion and metastasis [132].

1.6 Systems biology analysis of sphingolipid biosynthesis

Given the structural diversity of sphingolipids and the complexity of their biosynthesis pathway, application of systems biology and data integration approaches

may provide insight into their alterations. Comparison of differences in individual gene expression (or enzyme activity) with corresponding metabolites from previous studies have revealed interesting correlations. For example, elevated expression of mRNA for GD3 synthase has been correlated with the amounts of GD3 in melanoma cell lines [133]. Conversely, reduction of C18 ceramide (Cer) in head and neck cancer correlates with lower CerS1 and abnormal growth control [134].

The wide availability of high throughput gene expression platforms have made it feasible to measure mRNA abundance of multiple genes and more than 10000 microarray datasets are accessible through public repositories such as NCBI GEO [135] , Array express [136] and Oncomine [137]. The analysis of gene expression from published datasets could help identify alterations in sphingolipid composition which can be evaluated by mass spectrometry or though published literature. However, the large number of genes, and the existence of multiple branch points in sphingolipid biosynthesis pose challenges that can best be addressed with the aid of computational tools that can automatically define relationships between different omics datasets.

Pathway maps prepared by *Kyoto Encyclopedia of Genes and Genomes (KEGG)* have played a critical role in studies of metabolic pathway as they provide information about the relationship between enzymes and compounds. However these maps for sphingolipid biosysnthesis are have not been updated and remain incomplete and not specific to mammals. Despite these short comings they have been used in number of bioinformatics and genomics application for gene expression analysis such as GenMapp and PathwayExpress.

1.7 Conclusions

Despite the increasing knowledge about the regulation of sphingolipid biosynthesis, significant challenges remain in the study of these compounds due to their structural diversity and complex metabolic pathways. One of the problems facing researchers is the absence of accurate pathway maps to visualize differences in the expression of transcripts encoding different steps of the pathway and methods to predict alterations sphingolipid biosynthesis. Another challenge is the lack of knowledge about the transcripts encoding some of the biosynthetic enzymes. Questions also remain about the molecular abnormalities associated with models used to experimentally study sphingolipid biosynthesis.

This thesis demonstrates the first broad application of bioinformatics and data mining to study sphingolipid biosynthesis. In chapter 2 we describe the preparation of mammalian sphingolipid biosynthesis pathway maps for simultaneous visualization of gene expression and metabolite differences. These pathway diagrams were applied to cancer gene expression datasets in chapter 3, to compare correlation between transcript and sphingolipid alterations as well as predict novel metabolic changes in cancer cells. Chapter 4 describes ongoing studies and published reports that have used the gene expression pathway maps prepared during this dissertation. In chapter 5 we demonstrate the discovery of gene encoding 3-Ketosphinganine reductase and analyze the effect of the absence of FOXC1, a putative transcription regulator of the enzyme. In chapter 6, we employed sequence analysis and homology modeling to identify the reason for the

abnormal biosynthesis of sphingolipids in the LY-B cell lines, a model for defective *de novo* sphingolipid biosynthesis.

CHAPTER 2

PREPARATION OF SPINGOLIPID PATHWAY MAPS TO VISUALIZE DIFFERENCES IN GENE EXPRESSION AND METABOLITES

2.1 Abstract

Sphingolipids are a structurally diverse family of molecules (www.lipidmaps.org) that modulate cell functions that are abnormal in cancer, such as growth, adhesion, migration and survival. Because these compounds and their metabolic pathways are highly complex, it is difficult to analyze all of the subspecies associated with cancer. A useful approach might be to utilize gene expression datasets to predict metabolic changes and direct attention to particular sphingolipids for analysis. To this effect an updated list of genes that facilitate the biosynthesis of both early as well as higher order glycosphingolipids was prepared. Using their input and an open access pathway browser, Pathvisio v1.1, updated and expanded maps to visualize data from analyses of gene expression and sphingolipid metabolites were prepared. In addition, perl scripts were developed for extraction and formatting data for pathway visualization are available through this study.

2.2 Introduction

Sphingolipids are bioactive lipids that have been shown to be differentially regulated in diseases such as cancer [8, 9]. However, due to the wide diversity and the complexity of their metabolic pathway it is not feasible to characterize differences in all

subspecies. With greater access to public gene expression data [135, 136], it would feasible to use this wealth of information to predict and study sphingolipid alteration. This approach has been applied to specific steps of sphingolipid metabolism: for example, elevated expression of mRNA for GD3 synthase has been correlated with the amounts of GD3 in melanoma cell lines [133]. Conversely, the finding of differences in the amounts of particular sphingolipid subspecies has directed attention to altered gene expression. For example, reduction of C18 ceramide (Cer) in head and neck cancer correlates with lower CerS1 [134] and elevation of GalCer, LacCer, Gb3Cer in drug resistant ovarian cancer cells [138] were accompanied by changes in expression of GalCer synthase and LacCer synthase.

Nonetheless, there is currently no accurate pathway map for the visualization of datasets for large categories of genes and metabolites involved in sphingolipid biosynthesis. Therefore, the goal of these studies was to develop a tool for this purpose. Using an open access pathway browser, Pathvisio v1.1 [139], updated and expanded maps to visualize data from analyses of human gene expression and sphingolipid metabolites were prepared. In addition, we prepared a list of preselected gene probes associated with sphingolipid biosynthesis and complementary perl scripts for efficient retrieval and formatting of gene values. The results of pathway visualization could be used for targeted lipidomic analysis using techniques such as mass spectrometry.

2.3 Methods

2.3.1 Modification of Pathvisio v1.1 and construction of sphingolipid pathway maps

An open source java software, Pathvisio v1.1 [139] was selected for the construction of pathway maps for different branches of sphingolipid biosynthesis and the visualization of differentially expressed genes. To differentiate metabolites from genes, the program source code was modified to display metabolites as circular objects, while genes retained the rectangular shape.

New pathway maps were constructed to complement the features of Pathvisio v1.1 by altering KEGG pathway diagrams to include metabolite identifiers at the nodes, while the genes were updated to reflect new discoveries and changes in nomenclature. Some of the prominent changes in the sphingolipid pathway maps are listed as follows; the addition of ceramide synthase gene isoforms (CerS1-6) [14-18], dihydroceramide desaturase (DEGS1, DEGS2) [19] and alpha(1,2)fucosyltransferases (FUT1 and FUT2) [79]. The layout of the backbone biosynthesis map was modified to differentiate changes in sphingolipids with dihydroceramide backbones, and another branch for the synthesis of phyto-sphingolipids was included. Updated pathway maps for sphingolipid backbone, gangliosides, globoseries, Lacto-series and Neo-lacto-series biosynthesis can also be obtained from the wikipathways database [140].

2.3.2 Selection of gene probes

To identify the best probes for sphingolipid genes , the sequences of all probes directed to individual transcripts were retrieved from the Affymetrix Netaffx tool [141] and compared to the mRNA using the Blat search [142] in the UCSC genome browser [143]. The probe that recognized the catalytic transcript and hybridized nearest to its 3' UTR was selected to represent the gene for pathway model visualization, while others

were excluded. The procedure was repeated for all sphingolipid genes for Affymetrix chips HG-U95 A-E and HG-U133 plus 2 (Appendix A).

2.3.3 Perl algorithm for extraction of expression values

A Perl script was written to search and extract gene expression values for sphingolipid related transcripts. This program transforms the list of probe IDs or Gene IDs into an array, and then searches for similar objects in a normalized gene expression data file, where the rows represent probe IDs and columns individual experiments. The loop function efficiently extracts values and writes the matching sphingolipid gene expression values into a text file, which is used to calculate gene fold changes. A copy of the Perl script and instructions for use are provided in Appendix A**.**

2.4 Results

2.4.1 Summary of the sphingolipid biosynthetic pathway as the basis for construction of gene expression pathway maps

The following summary described the initial steps of sphingolipid biosynthesis as illustrated in Figure 2.1 (Detailed description of the pathway can be obtained from a previous article [1]), and the genes references for individual steps are listed in Table 2.1. The pathway is initiated by the condensation of serine and palmitoyl-CoA by serine palmitoyltransferase (SPT, gene annotation: SPTLC 1, 2 and 3) (shown in the upper left corner of Fig. 2.1) to produce 3-ketosphinganine (3KSa), which is reduced to sphinganine (Sa) by 3KSa reductase (3KSR, gene annotation: FVT1). Sa is either acylated by one of the ceramide synthases (CerS) to dihydroceramide (DHCer) or phosphorylated by sphingosine kinase (SphK, gene annotated: SPHK1 or 2) to Sa 1-phosphate (Sa1P)

(which can be terminally degraded to hexadenanal, C16:0-al, and ethanolamine phosphate, EP, by a lyase, SGPL1) (Fig 2.1). DHCer is at another branchpoint of the pathway and is either desaturated to Cer (by DHCer desaturase 1 or 2, gene annotation: DES1 and DES2), hydroxylated to 4-hydroxyDHCer (also called phytoCer, by DES2) [19], converted to a more complex dihydrosphingolipids, as will be discussed later, or hydrolyzed to Sa by ceramidases (ASAH 1-3, 3L and PCHA). For most cells, the major route is thought to be desaturation to Cer because Cer is the major lipid backbone of most complex sphingolipids [1, 10]. Cer is used for the biosynthesis of SM by SM synthases (gene annotation: SMS1 or 2) [144], glucosylCer (GlcCer) by GlcCer synthase (gene annotation: UGCG), galactosylCer (GalCer) by GalCer synthase (gene annotation: UGT8), or Cer 1-phosphate (Cer1P) by Cer kinase (gene annotation: CERK). Cer is also hydrolyzed by ceramidases (gene annotation: ASAH1-3,3L and PCHA) to sphingosine (So) which can be phosphorylated to S1P and terminally degraded to hexadenenal, C16:1-al, and EP, as shown in Fig. 2.1. Also shown on the pathway in Fig. 2.1 is a protein, CERT (gene annotation: COL4A3BP), that participates in Cer transport for the biosynthesis of SM, CerP and GlcCer. The headgroup additions are circumscribed by a dashed line in Fig. 1 because these enzymes can sometimes accommodate the other types of ceramide backbones (e.g., DHCer and PhytoCer), therefore, for simplicity, these steps have not been shown explicitly for those branches of the pathway in Fig. 1. Also shown in Fig. 1 are the sphingomyelinases (SMase; gene annotation: SMPD1-3) which are responsible for degradation of SM to Cer. GlcCer is further glycosylated to lactosylCer (LacCer) by LacCer synthase (gene annotation: B4GALT6), which is the branch point for the five families of complex glysosphingolipids in the five so-called root structure series

(globo-series, isoglobo-series, ganglio-series, lacto-series and neo-lacto-series), which will be discussed later. GalCers can be sulfated by sulfatide transferase (gene annotation: GAL3ST1) to produce sulfatides (ST).

In addition to this pathway overview, there are additional variations in the lipid backbones that are difficult to depict in a simple diagram (a discussion of an alternative graphical display format can be found in [1, 10]), such as chain length of sphingoid base and the fatty acid distribution of ceramide backbones. Different isoforms of the first enzyme of the pathway (SPT) have been linked to these alterations.

In sphingoid base, where the SPTLC2 was shown to synthesize C18 bases, the newly identified SPTLC3 subunit has been shown to produce sphingoid base of C16 chain length (Fig 2.1, upper left corner). Similarly, ceramide synthase isoforms (CerS1-6, Fig 1 lower panel) facilitate the selective N-acylation of sphingoid bases to produce dihydroceramides (DHCer) with different N-acyl chain lengths [14-18]. These CerS isoforms either possess narrow substrate specificity (Eg CerS 5 and 1) or broad chain length specificity such as CerS 6, 2, 4 and 3 (Fig 2.1, lower panel). The alterations of Cer subspecies has gained prominence due to recent findings that elevation in C18-Cer caused by overexpression of CerS1 induced growth arrest in head and neck small cell carcinoma cells [134].

Another factor that can influence fatty acid composition of ceramides is the abundance of the different fatty acyl-CoAs (produced by fatty acid elongases, gene annotation: ELOVL 1-7) [145] and their desaturated subspecies (catalyzed by stearoyl-CoA desaturase, gene annotation: SCD) [146] since they are essential precursors of sphingoid bases and their N-acyl products.

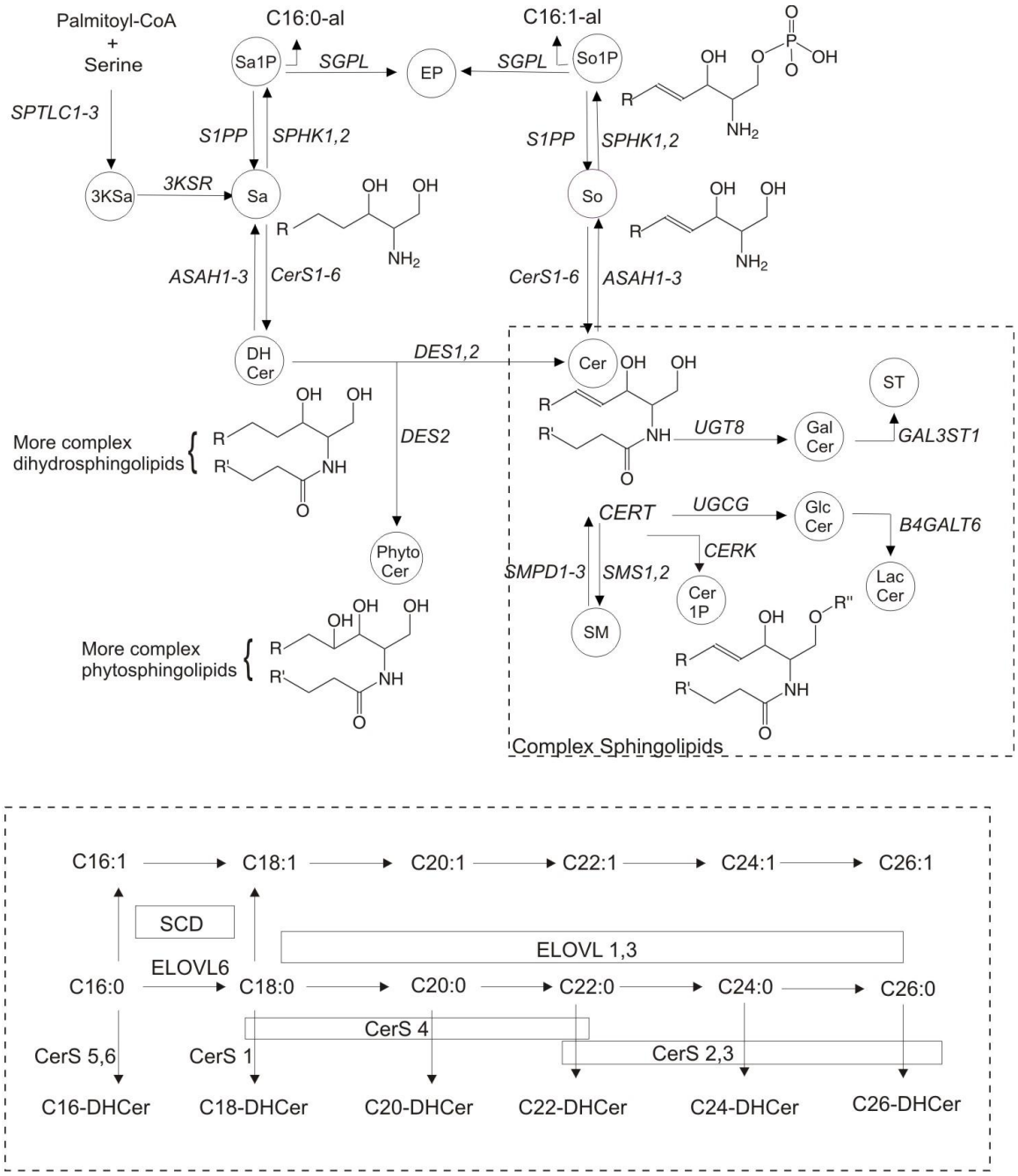

Fig 2.1. Early steps of sphingolipids biosynthesis The pathway begins with the condensation of serine and palmitoyl-CoA by serine palmitoyltransferase (SPTLC) to produce 3-ketosphinganine (3KSa), which is reduced (by 3KSa reductase, 3KSR) to sphinganine (Sa). Dihydroceramide (DHCer) synthases (CerS 1-6) N-acylate Sa with

different fatty acyl-CoA (R') to produce DHCers, which are converted to ceramides (Cer) or Phyto-Cer by DHCer desaturases (DES1,2). Substitution of the 1-OH with different head groups (R") produces Cer 1-phosphate (Cer1P by Cer kinase, CERK), sphingomyelin (SM by SM synthase, SMS1,2), galactosylceramide (GalCer by GalCer synthase, UGT8) and glucosylceramide (GluCer by GluCer synthase, UGCG), which can be further metabolized to sulfatide (ST by ST transferase, GAL3ST1) and lactosylceramide (LacCer by LacCer synthase, B4GALT6), respectively. CERT is a transporter of Cer from the ER to Golgi and is thought to play a role in the synthesis of SM, Cer1P and GluCer. These headgroup modifications are shown for Cer in the area circumscribed by a dashed line (complex sphingolipids) and also pertain to DHCer, Phyto-Cer and other backbones. Also shown is the catabolism of Cer to sphingosine (So) (and analogous DHCer to Sa) by ceramidase (ASAH1-3), phosphorylation by So (Sa) kinases (SPHK1,2) to So 1-phosphate (S1P) (and Sa to Sa1P), and cleavage by S1P lyase (SGPL1) to ethanolamine phosphate (EP) and hexadecanal (C16:0al for Sa1P) and hexadecenal (C16:1al for S1P). The lower panel illustrates the synthesis of the precursor fatty acyl-CoA by a combination of fatty acid elongases (ELOVL 1-7) and stearoyl CoA desaturase (SCD), and their utilization for the N-acylation of sphingoid bases by different CerS isoforms (CerS1-7).

Table 2.1 List of genes involved in *de novo* sphingolipid biosynthesis.

Gene ID	Gene Name	Reference
SPTLC1, SPTLC2, SPTLC 3	Serine palmitoyltransferase subunits (1, 2 & 3)	[147]
KDSR, 3KSR, FVT1	3-Ketosphinganine reductase	[148]
CerS1, CerS2, CerS3, CerS4 Cers5, CerS6	Ceramide synthase (1 to 6)	[14-18]
SPHK1, SPHK2	Sphingosine kinase (1,2)	[149]
SGPL1	Sphingosine 1-phosohate lyase	[150]
DES1, DES2 , DEGS1, 2	Dihydroceramide desaturase (1 & 2)	[19]
ASAH1, ASAH2, ASAH3, ASAH3L, PCHA	Ceramidases (Acid, neutral, phytoceramidase)	[151-155]
SMS1,SMS2, SMSr,	Sphingomyelin synthase (1, 2 and atypical)	[144, 156]
UGCG, Gba	Glucosylceramide synthase	[157]
UGT8, CGT	Galactosylceramide synthase	[158]
CERK	Ceramide kinase	[159, 160]
CERT	Ceramide transporter	[161, 162]
SMPD1, SMPD2 ,SMPD3, SMPD4	Sphingomyelinases (Acidic, neutral)	[163, 164]
B4GALT6	Lactosylceramide synthase	[165]
GAL3ST1	galactose-3-O-sulfotransferase 1	[35]
ELOVL 1-7	Fatty acid CoA elongases (1 to 7)	[145]
SCD	Stearoyl CoA desaturase	[146]
ssSPTa, ssSPTb	Small subunits of SPT	[166]

The table lists alternative gene abbreviations and complete names for genes encoding enzymes for different steps of *de novo* sphingolipid biosynthesis as displayed in Fig 2.1.

2.4.2 Construction of gene expression pathway maps for human and mouse sphingolipid biosynthesis

Based on the current understanding of sphingolipid biosynthesis discussed above, updated pathway maps were prepared to visualize gene expression and metabolites differences in *de novo* sphingolipid biosynthesis using Pathvisio v1.1 [139] (Fig. 2.2). In addition, pathway maps to visualize mRNA abundance relevant to biosynthesis of higher order glysosphingolipids have been prepared for ganglio-series (Fig. 2.3) and globo-series, (Fig. 2.4). The associated gene references for higher order glycosphingolipid biosynthesis are provided in Table 2.2.

2.4.3 Preparation of data for visualization in sphingolipid gene expression pathway diagrams

To visualize differences in mRNA abundance pertinent to the sphingolipid biosynthesis pathway, published gene expression datasets for cancer cells and normal and tumors [167-169] were obtained from public microarray repositories [135, 136] . Platform specific tools were used to normalize raw expression values for samples within studies (as discussed in methods section). A perl script was written (Appendix A) to sort out expression values for transcripts involved in sphingolipid biosynthesis, and fold differences were computed by either taking the ratio between two conditions (such as two cell lines or cancer stages), or by normalizing the individual gene expression by the average among all samples (in the case of multiple cell lines). The fold differences between conditions were visualized by updated sphingolipid biosynthesis pathway maps using the Pathvisio v1.1**.**

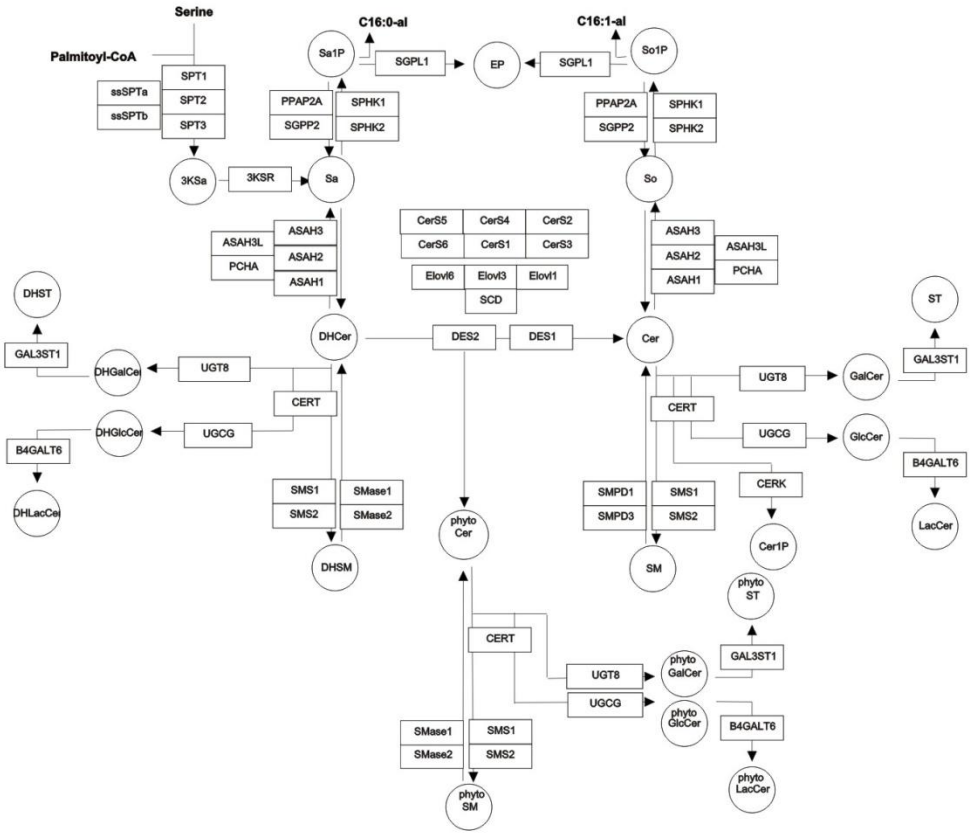

Fig 2.2 Illustration of early step of sphingolipid biosynthesis in Pathvisio v1.1. The *de novo* sphingolipid biosynthesis pathway map was prepared using Pathvisio v1.1 [139]. The rectangular boxes represent the genes while the circles depict the metabolites.

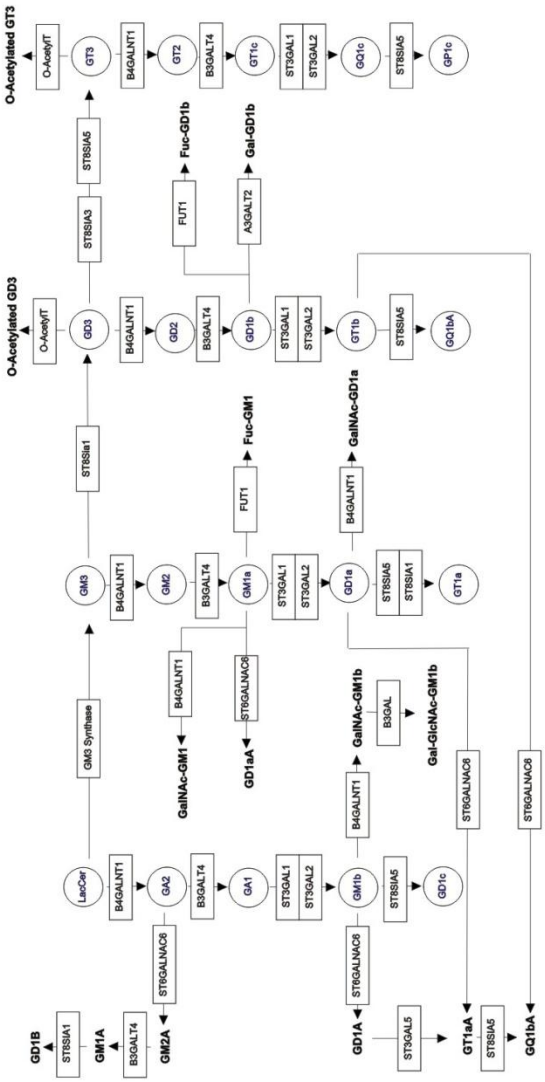

Fig 2.3 Illustration of ganglio-series gene expression pathway map in Pathvisio v1.1. The ganglio-series biosynthesis pathway map was prepared using Pathvisio v1.1 [139]. The rectangular boxes represent the genes while the circles depict the metabolites.

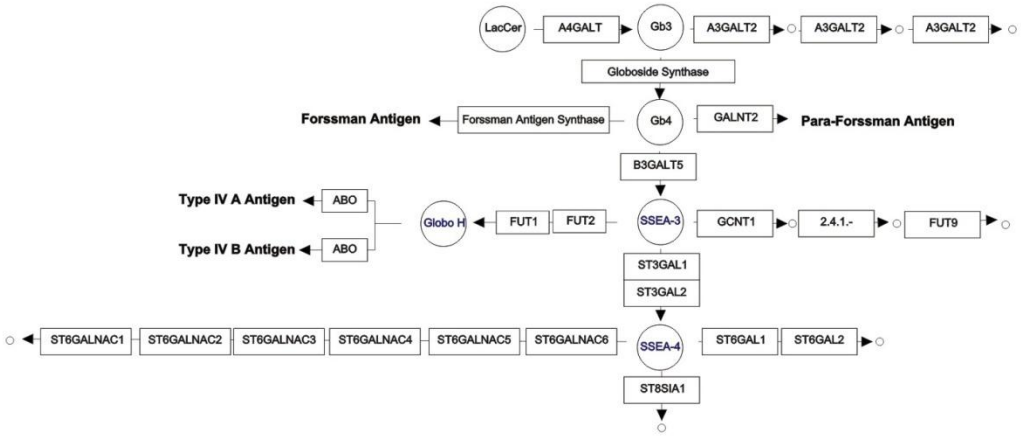

Fig 2.4 Illustration of globo-series gene expression pathway map in Pathvisio v1.1. The globo-series biosynthesis pathway map was prepared using Pathvisio v1.1 [139]. The rectangular boxes represent the genes while the circles depict the metabolites.

Table 2.2 List of genes involved in higher order glycosphingolipids biosynthesis.

Homo sapiens Gene	Gene Name	Abbreviation	References
UGCG	Ceramide glucosyltransferase	GlcCer Synthase, UGCG, GlcT-I, GCS	[157]
UGT8, CGT	GalCer synthase	CGT	[158]
β4GALTI, B4GALT1	β-*N*-acetylglucosaminyl-glycopeptide β-1,4-galactosyltransferase I	β4GalT-I, B4GALT1	[170]
B4GALT2, β4Gal-T2	β-*N*-acetylglucosaminyl-glycopeptide β-1,4-galactosyltransferase II	β4GalT-II, B4GALT2	[171]
B4GALT3	β-*N*-acetylglucosaminyl-glycopeptide β-1,4-galactosyltransferase IIII	β4GalT-III,	[171]
B4GALT4	β-N-acetylglucosaminyl-glycopeptide β-1,4-galactosyltransferase IV	β4GalT-IV	
B4GALT5	β-N-acetylglucosaminyl-glycopeptide β-1,4-galactosyltransferase V	β4GalT-V	[172]
B4GALT6	β-N-acetylglucosaminyl-glycopeptide β-1,4-galactosyltransferase VI	β4GalT-VI	[173]
B3GALT1	β3-galactosyltrasferase I	β3GalT-I	
B3GALT2	β3-galactosyltrasferase II	β3GalT-II	[174]
B3GALT4, GalT4, β3GalT4	β3-galactosyltrasferase IV	β3GalT-IV, GM1/GD1b/GA1 synthase, β3GalT, Gal-T2	[174]
B3GalT5	β3-galactosyltrasferase V	β3GalT-V	[175]
A3GALT2	*N*-acetyllactosaminide 3-α-galactosyltransferase	α3GalT, iGb_3 synthase	[176]
β3GlcNAcT1 (iGnT1)	β3-N-Acetylglucosaminyltrasferase (iGnT)	β3GalNAcT, iGnT	[177]
β3GlcNAcT2			
β3GlcNAcT3			
β3GlcNAcT4			
β3GlcNAcT5			
IGnT	β6-N-Acetylglucosaminyltrasferase (IGnT)	β6GalNAcT, IGnT	
Core2GlcNAcT-I	Core 2 β6-N-Acetylglucosaminyltransferase I	β6GlcNAcT, Core2GlcNAcT-I, GNT	[178]
B4GALNT1	β4-N-Acetylgalactosaminyltrasferase	β4GalNAcT, GM2/GD2 synthase	[179]
	Histoblood group A transferase		[180]
	Histoblood group B transferase		
Forssman synthase	Forssman Glycolipid Synthase	α3GalNAcT	[181, 182]
	para-Forssman Glycolipid Synthase		Y. Yoda et al. / J. Biochem (Tokyo) 88 (1980) 1887-1890
Fut1, Fut2	α1/2-Fucosyltransferase	FUT1, H, HH, HSC	[183]

Table 2.2 continued

Homo sapiens	Gene Name	Abbreviation	References
FUT2		FUT2, SE, Se2, sej	[184]
FUT3, Fuc-TIII	α3/4-Fucosyltransferase	FUT3, Lewis enzyme, LE, Les, CD174, MGC131739	[185]
FUT4, ELFT, FCT3A, FUC-TIV	α3-Fucosyltransferase-IV	FUT4, CD15, ELFT, FCT3A, FUC-TIV	[186]
FUT5, FUC-TV	α3-Fucosyltransferase-V	FUT5, FUC-TV	[187]
FUT6	α3-Fucosyltransferase-VI	FUT6, FT1A, FLJ40754	[188]
FUT7, Fuc-TVII	α3-Fucosyltransferase-VII	FUT7	[189]
FUT9, Fuc-TIX	α3-Fucosyltransferase-IX	FUT9, FUC-TIX	[190, 191]
	Sialyltransferase 3	SAT-III	
SIAT4B	ST3Gal-II	SAT-IV	[192, 193]
SIAT9	ST3Gal-V	GM3 synthase, SAT-I	[194]
ST6GALNAC3	ST6GalNAc-III	STY	[195]
ST6GALNAC5	ST6GalNAc-V	GD1α synthase	[196]
ST6GALNAC6	ST6GalNAc-VI		[197]
ST8SIA1, SIAT8A, GD3 synthase	ST8Sia-I	GD3 synthase, SAT-II	[198]
ST8SIA3	ST8Sia-III	GT3 synthase	[199]
ST8SIA5	ST8Sia-V	SAT-V/SAT-III, GQ1b/GT1a/GD1c synthase	[200]
GlcAT-P, B3GAT1	HNK-1 Glucuronlytransferase		[201]
	HNK-1 Sulfotransferase	HNK-1 SulfoT	[202]
GAL3ST1, CST	βGal 3-Osulfotransferase-1	Gal3ST-1	[35]
A4galt, Gb3 synthase	LacCer 4-α-galactosyltransferase	Gb3/CD77 synthase, α1,4-GalT	[203]
beta3GalNAc-T1	Gb3 3-β-N-acetylgalactosaminyltransferase	Globoside synthase	[204]
SLC33A1, ACATN	O-Acetyltransferase		[205]

The table list the genes involved in the biosynthesis of glycosphingolipids of the ganglio-series, globo-series, lacto-series and neo-lacto-series with suitable references.

The presence of multiple probes for individual transcripts and large category of transcripts posed a challenge during the analysis. To address the former, probes specific to the 3' UTR of the mRNA were chosen by a Blat search [142] of the UCSC genome browser [143]. A list of the optimum probes for sphingolipid biosynthesis in human HG-U133 Plus2 and HG-U95 affymetrix gene chips is provided in Appendix A. In case of the latter, a search algorithm was written in perl (Appendix A) to sort out the expression values for the optimum probes using the list of preselected probes.

2.5 Conclusion

This tool facilitates the visualization of differential gene expression in sphingolipid biosynthesis pathway using public or in-house transcriptomic data. Predictions using these mammalian specific pathway diagrams can help direct attention to sphingolipid alterations in specific branches of the metabolic pathway. In addition, these maps also serve as a resource for comparative analysis of genomic and metabolomic data.

CHAPTER 3

PREDICTION OF SPHINGOLIPID ALTERATIONS IN CANCER CELLS LINES, TUMORS AND NORMAL TISSUE USING GENE EXPRESSION PATHWAY MAPS

3.1 Abstract

Sphingolipids play critical roles in cancer processes and their composition differs in tumors. However, it is difficult to characterize differences in all sphingolipid subspecies due to the complexity of their metabolic pathway and their wide structural diversity. Pathway visualization of gene expression data could help predict altered branches of sphingolipid biosynthesis. Therefore, the updated pathway diagrams were applied to data for cancer cell lines, tumors and normal tissues from published literature and analyses described here, which revealed significant relationships. For example, differences in gene expression for two breast cancer cell lines, the highly metastatic MDA-MB-231 versus MCF7 cells (representing estrogen receptor, ER, negative and positive cells, respectively), predicted that sphingolipid biosynthesis would be lower for MDA-MB-231 cells, which was confirmed by labeling studies. MDA-MB-231 cells also had lower expression of DES2, the hydroxylase that produces phytoceramides, and mass spectrometric analysis found lower phyto-sphingomyelins. In addition, gene expression differences between invasive ductal carcinoma and normal ductal breast tissue predicted elevated SSEA3 and Globo-H antigen in breast tumors, and this is consistent with published results. Comparison of available data for a wide range of cancer types revealed

a 72.8 % probability of match between the gene expression data and the sphingolipid composition ($P < 0.001$ by the Fishers exact test). The tool was also used to explore the metabolic implications of differences in gene expression for ER-negative versus ER-positive breast cancer cells identified by traditional hierarchical clustering. In conjunction with these studies, pathway maps for the panel of 59 human cancer cell lines (the NCI-60) have been provided in the supplement for further study. These findings demonstrate that a pathway visualization map can facilitate the integration of two types of "omic" technologies ("transcriptomics" and "sphingolipidomics") to predict and identify correlations relevant to cancer, which might lead to a better understanding of tumor biology and discovery of new biomarkers.

3.2 Introduction

Sphingolipids and glycosphingolipids (GSL) are structurally diverse family of compounds that are characterized by a sphingoid base backbone that can be modified by the addition of an amide linked fatty acid and wide range of head groups [1]. Sphingolipids play important roles in cancer processes, such as growth, survival, adhesion, and migration [34], and tumors often display alterations in sphingolipid composition [8, 9] and been proposed as cancer markers [76, 79, 81]. Because these compounds and their metabolic pathways are highly complex, integration of gene expression data with sphingolipid analysis might aid the understanding of the molecular changes associated with cancer, and identify novel biomakers.

Comparison of gene expression and metabolite differences for specific steps of sphingolipid metabolism has identified relationships between mRNA and sphingolipid alterations in tumors [133, 134, 138]. However as wide range of gene expression datasets have become accessible through public repositories (NCBI GEO [135] , Array express [136] and Oncomine [137]), it is now possible to evaluate gene expression differences in different branches of sphingolipid biosynthesis using the updated pathway maps using an open access pathway browser, Pathvisio v1.1 [139].

In this study visualization of public gene expression datasets for cancer cell line, tumors and normal tissue using sphingolipid biosynthesis pathway maps identified substantial agreement between gene expression and metabolite profiles in different branches of the pathway. Among the significant findings, prediction of gene expresson diffrerences between MCF7 and MDA-MB-231 cells resulted in the identification of novel sphingolipid subspecies with phyto-ceramides and d16:1 sphingoid bases.

3.3 Methods

3.3.1 Materials

MCF7 cells were purchased from ATCC **(Manassas, VA), while** MDA-MB-231 cells were provided by Dr. Nathan Bowen (School of biology, Georgia Institute of Technology, Atlanta, GA). Cell culture medium was procured from Gibco (Carlsbad, CA) and fetal bovine serum was obtained from Hyclone (Logan, UT). U-^{13}C labeled palmitic acid was obtained from Cambridge Isotopes (Andover, MA). The mass spectrometry internal standards were procured from Avanti Polar Lipids (Alabaster, AL), while GSL standards were obtained from Sigma (St louis, MO) and Matreya (Pleasant Gap, PA). All other reagents and solvents were HPLC grade.

3.3.2 Selection of DNA microarray datasets and statistical analysis

In the present study, keyword search was conducted on NCBI GEO [135] , Array express [136] and Oncomine [137] for ‘cancer type’ or ‘cancer cell line’ , and the outcomes were examined to identify expression datasets having multiple replicates of control and cancer tissues, or all cell lines to be compared. The Affymetrix expression files (.CEL file) for the selected datasets were downloaded and processed by Affymetrix expression console v1.1 (Affymetrix, Santa Clara, CA) using the MAS5 algorithm. For non-Affymetrix studies the normalized and background corrected expression datasets (GDS file, NCBI GEO format) were accessed using the GEOquery package [206] of Bioconductor v1.8 [207], and exported as tab delineated text files. Sphingolipid specific gene expression values were filtered using a Perl search algorithm and a list of preselected Affymetrix probe ids or Gene ID (see below). The gene expression fold change was determined using Excel (Microsoft Inc, Seattle, WA), after which the data set was formatted as a Pathvisio input file (comma separated values) with ‘gene ids’, ‘system code’ and ‘fold change’.

3.3.3 Pathway visualization

In the modified Pathvisio v1.1 browser, the appropriate gene and metabolite database was selected and the expression dataset was created after importing the saved input file using the ‘import expression dataset’ tab. The color criteria for the expression dataset were specified by the ‘visualization option’ function. Gene and metabolite expression changes were visualized on the pathway maps by opening the pathway

diagram and then selecting the saved expression dataset and visualization criteria. A detailed tutorial is available at www.Pathvisio.org. The pictures were prepared by exporting the images as PDF files; while changes to font colors were performed with Corel draw X4 (Mountain view, CA).

3.3.4 Selection and analysis of GSL profiles from literature

To select sphingolipid metabolite changes in cancer cells and tissues, published literature was reviewed through a keyword search of Pubmed and Google Scholar with the terms 'cancer type/cell name and glycosphingolipids'. The abstracts of the selected manuscripts were manually screened to identify articles that characterize sphingolipids in cancer specimens using analytical methods such as thin layer chromatography (TLC) or mass spectrometry (MS). In addition, the experimental design and the cancer subtypes were verified to match the microarray study. Quantitative data for metabolites were directly used to compute fold changes, while changes observed in TLC experiments were compared by densitometry analysis of JPEG images using Fluorchem 5500 (Alpha Innotech , San Leandro, CA).

3.3.5 Tissue culture and sphingolipid analysis by LC-MS/MS analysis

The MCF7 and MDA-MB-231 cells were grown in 100 mm tissue culture dishes using RPMI 1640 medium containing 5% fetal bovine serum using conditions described previously [167]. When the cells reached 80-90% confluency they were washed once with PBS solution, before being scraped into screw capped glass test tubes for sphingolipid extraction as previously described [208]. An aliquot of the cells was retained

from each dish to measure the protein concentration by the BCA assay (Pierce Biotechnology, Rockford, IL). During stable isotope labeling studies, the media was supplemented with 0.1 mM [U-^{13}C]-palmitic acid complexed with equimolar fatty acid free BSA (Calbiochem, Gibbstown, NJ). After 12 or 24 h, depending on the experiment, the incorporation of stable isotope into sphingolipids was measured by liquid-chromatography, electrospray ionization-tandem mass spectrometry (LC ESI-MS/MS) as previously described [208].

Complex sphingolipids and long chain bases were analyzed using ABI 3000 and ABI 4000 LC-tandem mass spectrometers (Applied Biosystems, Foster City, CA) as described previously [208].

3.3.6 Cluster analysis of breast cancer cell lines

The gene expression dataset for ER-positive and ER-negative breast cancer cell lines were obtained from NCBI GEO (GSE12777) [169] and the '.CEL' file were processed as previously described. Expression values for sphingolipid specific genes were extracted and the average fold change ER-positive and ER-negative was computed by Excel. Genes with significant expression difference (p-value < 0.05) between the two groups were compared by unsupervised hierarchical clustering using the average linkage method and visualized by a heatmap diagram using the Genesis software [209].

3.4 Results and Discussion

3.4.1 Comparison of gene expression and sphingolipid differences between MCF7 and MDA-MB-231 breast cancer cells

Gene expression differences between the ER-positive MCF7 and highly metastatic ER-negative MDA-MB-231 cell lines were compared using published microarray data [167], and the ratios of mRNA abundance between the latter and former cells (the numerator and denominator, respectively) were visualized by the sphingolipid biosynthetic pathway diagrams (Fig 3.1). Analysis of the initial steps of sphingolipid biosynthesis (Fig 3.1) predicts that MDA-MB-231 cells have lower expression of SPTLC1 and SPTLC2 (Fig 3.1, dashed box A), the genes responsible for the first step of *de novo* sphingolipid biosynthesis. In contrast, MDA-MB-231 cells have higher expression of SPTLC3 compared to MCF7, indicating an elevation of sphingolipids with C16 sphingoid base. The map also predicts that MDA-MB-231 cells have lower mRNA for the desaturases, SCD (multiple transcript) (Fig 3.1, dashed box B), that converts C18:0-CoA to C18:1-CoA, which is subsequently elongated to other FA-CoA (C24:1 and C26:1)[210]. This visualization also reveals that MDA-MB-231 cells have lower DES2 (Fig 3.1, dashed box C), which is responsible for the addition of 4-OH to dihydro-Cer to make phyto-Cer. In addition, MDA-MB-231 cells displayed lower mRNA for UGT8 and higher UGCG and B4GALT6 (Fig 3.1, dashed box D), which biosynthesize GalCer, GlcCer and LacCer, respectively.

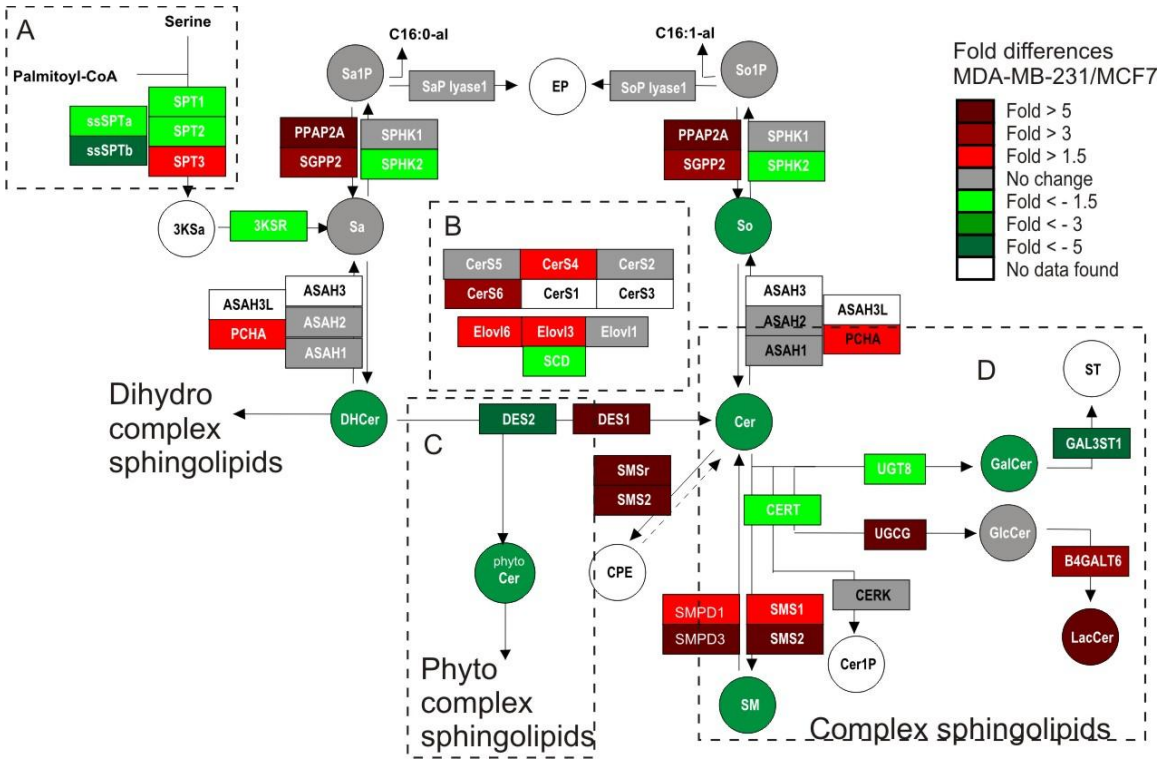

Fig 3.1. Visualization of transcription and metabolite differences in early steps of sphingolipids biosynthesis between MCF7 and MDA-MB-231 cells using and expanded pathway map and Pathvisio v1.1. The figure depicts sphingolipid genes (indicated as rectangles) and metabolites (circles) that participate in early steps of sphingolipid biosynthesis (ref Fig1) prepared in the Pathvisio v1.1 [139]. The updated and expanded pathway map was overlaid by gene expression fold change difference between MDA-MB-231 and MCF7 cells that were obtained from a previous study [167]. Variations in sphingolipid composition (shaded circles) between the two cell lines were determined by LC-ESI-MS/MS as previously described [211] and compared to gene expression as highlighted by circumscribed dash boxes (A,B, C and D) and are discussed in Fig 3-6. The shade of the box and circles represents the degree of up and down regulation as indicated by the color chart.

To test the prediction that MDA-MB-231 cells have lower SPTLC1 and SPTLC2, which are the primary SPT genes responsible for d18 sphingoid base biosynthesis (Fig 3.1, dashed box A) and hence lower *de novo* sphingolipid biosynthesis, cells were incubated with [U-^{13}C]-palmitic acid and the labeled sphingolipids were extracted and quantified by LC-ESI-MS/MS. After 6 hr, MDA-MB-231 cells made 79.9 $\pm$ 6.6 pmol [U-^{13}C] SL/10^6 cells (Fig 3.2A, black bars, p-value = 0.003), as compared to 226 $\pm$ 14 pmol [U-^{13}C] SL/10^6 MCF7 cells (Fig 3.2A, white bars) (changes at other time points are depicted in the figure) . The term [U-^{13}C] SL refers to the sum of SL and DHSL which have [U-^{13}C] palmitate incorporated in both the sphingoid base as well as the N-acyl chain as determined by multiple reaction monitoring (MRM).

Another intensity difference between MDA-MB-231 and MCF7 cells was a higher expression of SPTLC3, which has been proposed to metabolize a shorter chain (d16:1) [12, 13]. Preliminary analysis of the Cer subspecies of these cells using a recently developed method [211] indicated that MDA-MB-231 cells had a higher proportion of d16:1-Cer (1.85 $\pm$ 0.4 pmol /10^6 cells) than (1.09 $\pm$ 0.16 pmol /10^6 cells) MCF7 cells (p-value < 0.05, n = 3), which agrees with the higher SPTLC3 expression.

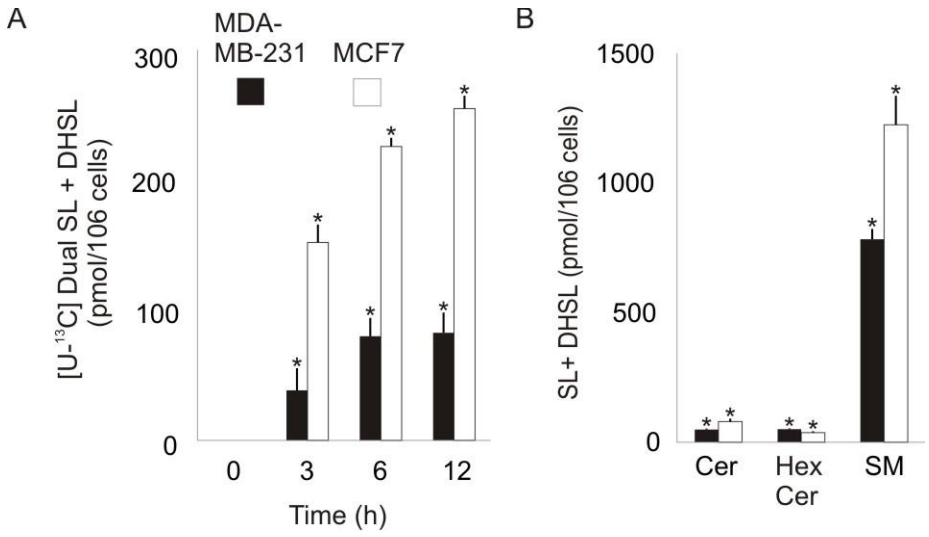

Fig 3.2. Comparison of *de novo* sphingolipid biosynthesis between MDA-MB-231 and MCF7 cells with gene expression of serine palmitoyltransferase. The two cells were grown as previously described [167] and incubated with and without 0.1 mM [13C]-palmitic acid for 0, 3 and 6hr and the sphingolipids labeled in sphingoid base and fatty acid (Dual) were measured by LC-ESI-MS/MS [211]. In parallel experiments, unlabelled sphingolipids were also measured in both cell types. A) sum of Dual [13C]-palmitate labeled complex sphingolipids with SL (Cer) and DHSL (DHCer) backbone, B) sum of unlabeled complex SL and DHSL in ceramide, Cer, monohexosylceramide, HexCer and sphingomyelin, SM. The significance as indicated by an asterisk was determined by a t-test at $p < 0.05$ for $n = 3$ (labeling study) and $n = 6$ (for unlabeled cells).

To test the predictions of lower mono unsaturated fatty acyl-CoA (FA-CoA) in MDA-MB-231 compared to MCF7 cells due to lower expression of the mRNA for SCD (Fig 3.1, dashed box B), the FA-CoA were analyzed within the two cells . MDA-MB-231 cells have significantly lower amounts of mono-unsaturated fatty acyl-CoA (Fig 3.3A, black bars, 6.3 $\pm$ 0.22 pmol C18:1 /10^6 cells; 1.4 $\pm$ 0.2 pmol C24:1 /10^6 cells; 4.6 $\pm$ 2.1 pmol C26:1 /10^6 cells), as compared to MCF7 cell (Fig 3.3A, white bars, 14.3 + 0.6 pmol C18:1 /10^6 cells, p-value < 0.001; 5.3 $\pm$ 1 pmol C24:1/10^6 , p-value < 0.001; 10.8 + 0.9 pmol C26:1 /10^6 cells, p-value < 0.001). In contrast, no significant difference was observed in saturated FA-CoAs (Fig 4A, C18:0, C24:0 and C26:0). Furthermore, because FA-CoAs are precursors for N-acylation of sphingoid bases, the Cer subspecies were also evaluated. MDA-MB-231 cells have significantly lower amounts of Cer with mono-unsaturated fatty acids (Fig 3.3B, black bars, 0.28 $\pm$ 0.07 pmol C18:1-Cer /10^6 cells, 24.8 $\pm$ 4.5 pmol C24:1-Cer / 10^6 cells and 3.88 $\pm$ 0.64 pmol C26:1-Cer / 10^6 cells), as compared to MCF7 cell (Fig 3.3B, white bars, 0.21 $\pm$ 0.04 pmol C18:1-Cer / 10^6 cells, p-value = 0.02; 7.07 $\pm$ 0.95 pmol C24:1-Cer / 10^6 cells, p-value < 0.001; and 0.5 $\pm$ 0.07 pmol C26:1-Cer / 10^6 cells, p-value < 0.001). Also consistent with the absence of differences in saturated fatty acids, no change was observed in their corresponding Cer subspecies (Fig 3.3B; C18:0-Cer, C24:0-Cer and C26:0-Cer). These findings suggest that alterations of FA-CoA precursor pool may be reflected by changes in cogent sphingolipid molecular species.

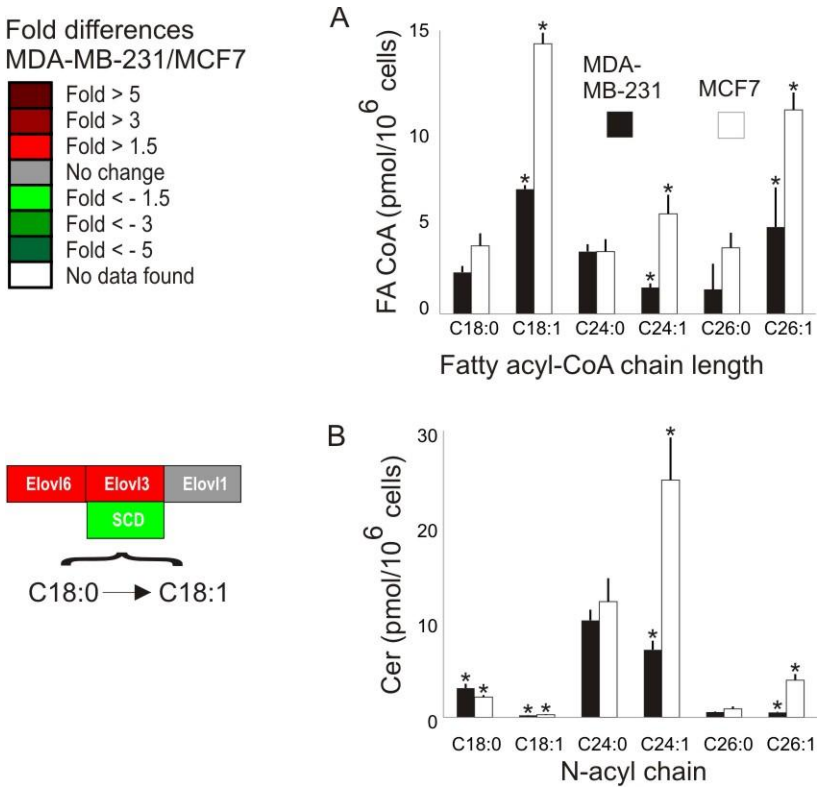

Fig 3.3. Comparison of gene expression differences of stearoyl CoA desaturase with the composition of fatty acyl CoA and ceramide chain lengths. MDA-MB-231 and MCF7 cells were grown as previously described [167] and the fatty acyl-CoA (FA-CoA) and ceramides (Cer) were measured by LC-ESI-MS/MS [208, 212]. A) composition of saturated and monounsaturated FA-CoA chain lengths, B) N-acyl chain distribution of Cer corresponding to the FA-CoA measured in A. The changes in the metabolites were compared to differences in the expression of steroyl CoA desaturase (SCD), fatty acid elongases (ELOVL) and ceramide synthase (CerS) (Fig 2, Box B). The significance as indicated by an asterisk was determined by a t-test at $p < 0.05$ for $n = 6$. The shade of the box represents the degree of up and down regulation as indicated by the color chart.

To test if the lower production of the mRNA for DES2 would cause lower amounts of phyto-sphingolipids in MDA-MB-231 compared to MCF7 cells (Fig 3.1, dashed box C), these subspecies were analyzed by LC-ESI-MS/MS. MDA-MB-231 cells had 1.4 $\pm$ 0.25 pmol phyto-Cer / 10^6 cells, 0.06 + 0.02 pmol phyto-HexCer / 10^6 cells and 0.6 $\pm$ 0.05 pmol phyto-SM / 10^6 cells (Fig 3.4, black bars, different scale) and all of which were higher in MCF7 cells 6 $\pm$ 1.4 pmol phyto-Cer / 10^6 cells (p-value < 0.001), 0.21 + 0.036 pmol phyto-HexCer / 10^6 cells (p-value < 0.001) and 17.6 $\pm$ 1.9 pmol phyto-SM / 10^6 cells (p-value < 0.001) (Fig 3.4, white bars, different scale).

Furthermore, the pathway diagram predicted lower biosynthesis of GalCer due to lower expression of UGT8 and higher GluCer due to higher UGCG in MDA-MB-231 compared to MCF7 cells (Fig 3.1, dashed box D). Consistent with these predictions, MDA- MB-231 cells have 0.6 $\pm$ 0.6 pmol/10^6 cells GalCer (Fig 3.5, left panel black bars), as compared to 9 $\pm$ 2 pmol GalCer /10^6 MCF7 cells (p-value < 0.001) (Fig 3.5, left panel white bars). In contrasts, no significant difference in GlcCer was measured between the two cell lnes (60.9 $\pm$ 11.4 pmol GlcCer /10^6 MDA-MB-231 cells and 66.1 $\pm$ 10.1 pmol GlcCer /10^6 MCF7 cells, p-value = 0.41). In addition, the higher expression of LacCer synthase matched elevated amounts of LacCer reported in MDA-MB-231 compared to MCF7 cells (Fig 6, right panel densitometric analysis) [82].

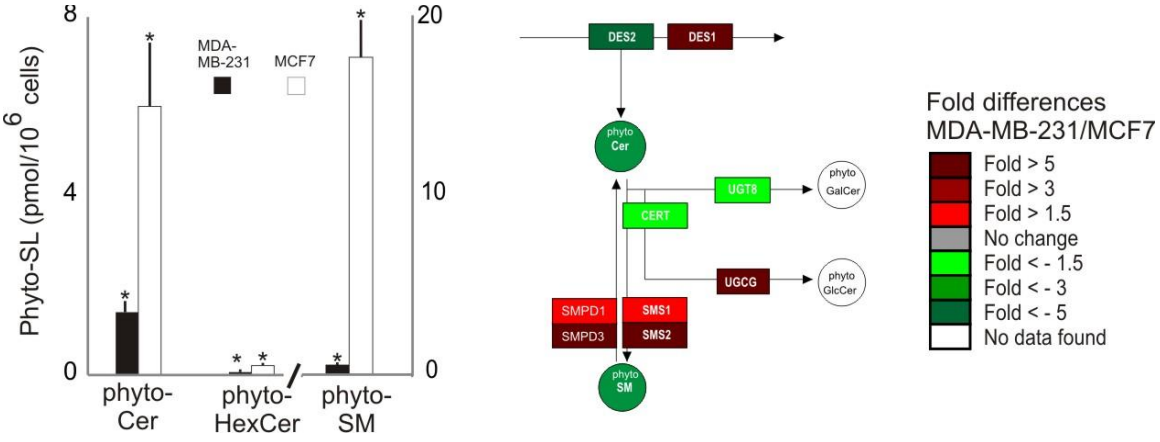

Fig 3.4. Comparison of changes in the DES2 expression with differences in Phyto-sphingolipids. Shown is the LC-ESI-MS/MS comparison of phyto-sphingolipids (phyto-SL), phyto-ceramide, phyto-Cer, phyto-monohexosylceramide, phyto-HexCer and phyto-sphingomyelin, phyto-SM (different scale) for MDA-MB-231 and MCF7 cells. The significance as indicated by an asterisk was determined by a t-test at $p < 0.05$ for $n = 6$. The metabolites were compared to gene expression differences in dihydroceramide desaturase 2 (DES2), where the shade of the box represents the degree of up and down regulation as indicated by the color chart.

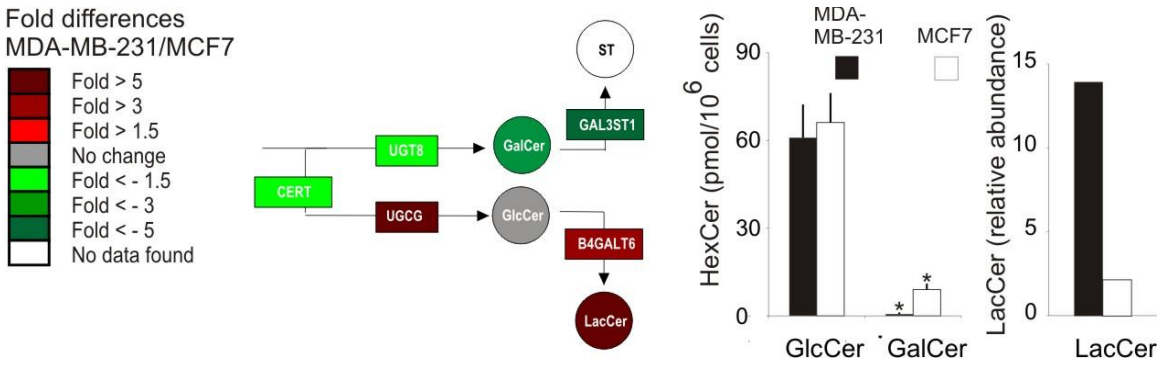

Fig 3.5. Pathway visualization of changes in gene expression and complex sphingolipids. The figure compares gene expression differences in GluCer synthase, UGCG and GalCer synthase, UG8 with LC-ESI-MS/MS analysis of GluCer and GalCer within MDA-MB-231 and MCF7 cells as previously described [211]. The significance as indicated by an asterisk was determined by a t-test at $p < 0.05$ for $n = 6$. LacCer synthase, B4GALT6 expression between the two cells was compared with densitometry analysis of LacCer quantization from a previous study [82]. The shade of the box and circles represents the degree of up and down regulation as indicated by the color chart.

3.4.2 Correlation of gene predictions and metabolite analysis in breast tumor tissues

In addition to changes in gene expression observed in breast cancer cell lines, gene expression differences between invasive ductal carcinoma (IDC, breast tumors) and normal ductal tissue were compared using a previously published microarray dataset [168]. Visualization of the ganglioside biosynthesis pathway gene differences (Fig. 3.6) predicted higher GM_3 synthase, B4GALNT1 (responsible for GM_2, GD_2 and GT_2 synthesis), ST3gal2 (responsible for GD_{1a}, GT_{1b} and GQ_{1c} synthesis) and ST8SIA5 (responsible for GT_3, GT_{1a}, GQ_{1b} and GP_{1c} synthesis). In agreement with these predictions, higher quantities of GM_3 have been previously reported in IDC tissue (Fig 3.6, shaded circles) [78]. On the other hand, GD_3, and N- and O-acetyl GD_3 and GT_3 are also higher, but the mRNAs for the proximal enzymes are not elevated. Therefore the changes in these sphingolipids may be result of higher levels of the precursor, GM3 (Fig 3.6, shaded circles) [78]. Also consistent with gene predictions, serum from IDC patients have been shown to have significant elevation in GD_{1b}, GT_{1b} and GQ_{1b} (Fig 3.6, circles with colored edges) as compared to healthy volunteers [81].

Comparison of the globoseries biosynthesis pathway map for normal ductal tissue versus IDC (Fig 3.7) showed that B3GalT5 and Fut2 (which synthesize SSEA-3 and Globo-H antigen, respectively) were higher. Consistent with predictions previous reports have established elevated quantities of SSEA-3 and Globo-H antigen in 77% and 61% of breast cancer tissues respectively (Fig 3.7, circles with colored edges) [79, 80].

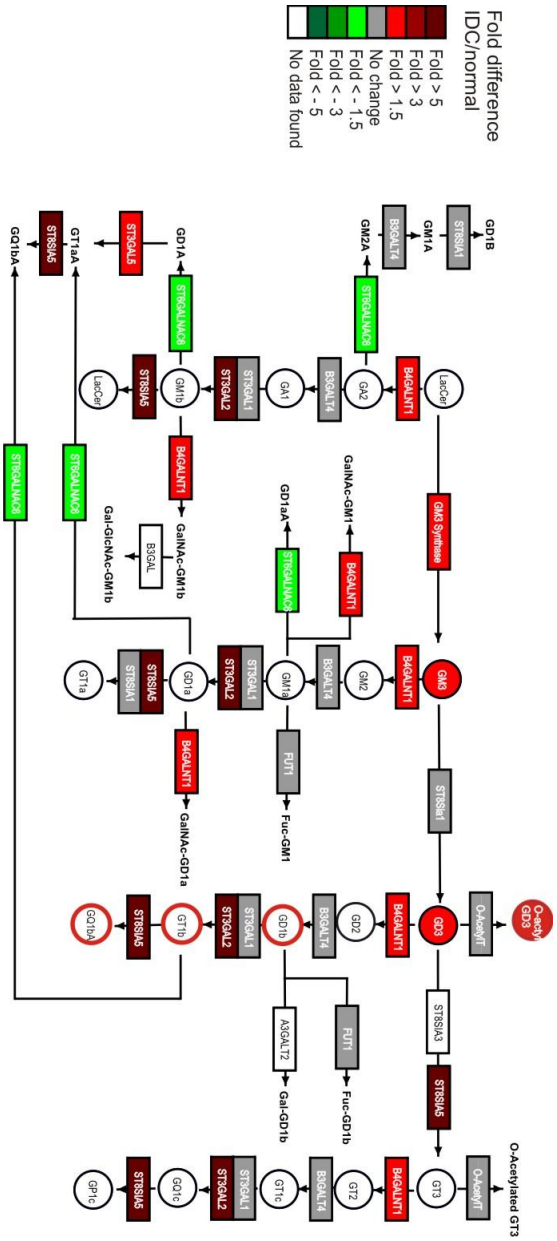

Fig 3.6. Comparison of ganglioside biosynthesis gene expression deference between invasive ductal carcinoma and normal ductal tissue to corresponding metabolites. Gene expression differences between the two breast cancer stages were visualized from a previous study [168] using updated ganglioside biosynthetic maps in Pathvisio v1.1 [139]. Ganglioside measurements reported in similar tumors (circles with solid shade) [78] and patient serum (circles with colored edges) [81] were compared to mRNA abundance . The shade of the box and circles represents the degree of up and down regulation as indicated by the color chart.

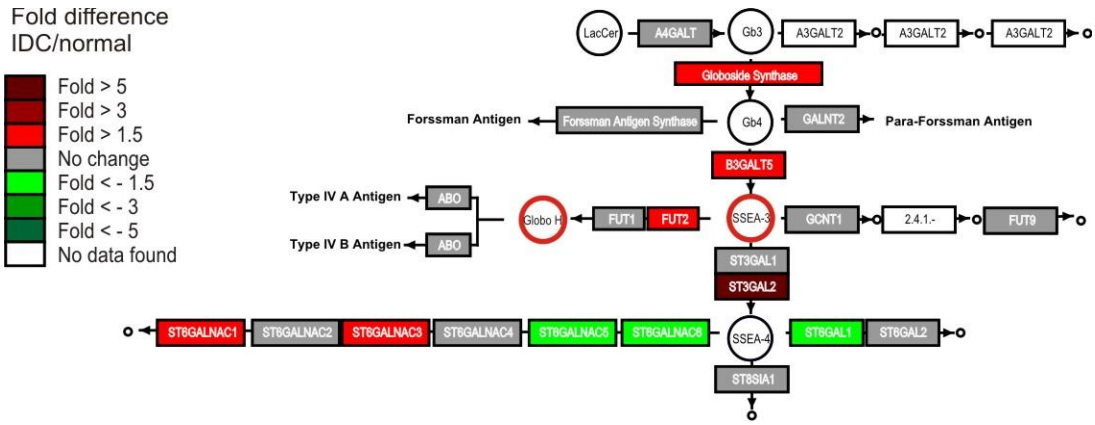

Fig 3.7. Comparison of globo-series biosynthesis gene expression deference between invasive ductal carcinoma and normal ductal tissue to corresponding metabolites. This figure compares gene expression differences between normal and invasive ductal carcinoma (IDC) from a previous study [168] using updated KEGG pathway maps for globo-series biosynthesis to metabolite changes previously reported using flow cytometry [79]. The shade of the box and circles represents the degree of up and down regulation as indicated by the color chart.

3.4.3 Comparison of the frequency of gene and sphingolipid alterations in cancers

To determine whether mRNA abundance concur with metabolite differences, 9 gene expression datasets for which corresponding metabolite data was available (for a total of 80 observations, including the present study) were analyzed. Evaluation of positive and negative correlations between gene expression differences and metabolite amounts revealed 38 instances in which both increased, whereas in 21 both decreased, for a total of 59 positive correlations (Fig 3.8, Table 3.1). In 22 cases, gene and metabolite changes showed opposing outcomes (a negative correlation). In 10 instances gene expression remained unchanged inspite of alterations in metabolites. Thus, there was 72.8% correlation between gene expression and sphingolipid differences, which was statistically significant at p-value < 0.001 by the Fisher's exact test (Fig. 3.8).

3.4.4 Sphingolipid biosynthesis gene expression differences between ER negative and ER-positive breast cancer cells

This technique was extended to identify gene expression differences that are observed between multiple breast cancer cell lines [169]. Pathway map comparison of average gene expression differences in 31 ER-negative and -positive breast cancer cell lines showed that the former had higher CERK, UGT8, GD3 synthase and Forssman antigen synthase and lower SPTLC2, CerS6 and DES2 (Fig 3.9 A and B).These findings concur with previous reports that indicated higher CERK, UGT8 and GD3 synthase and lower ASAH1, CerS6 in ER negative breast cancer [213, 214]. However, analysis of the

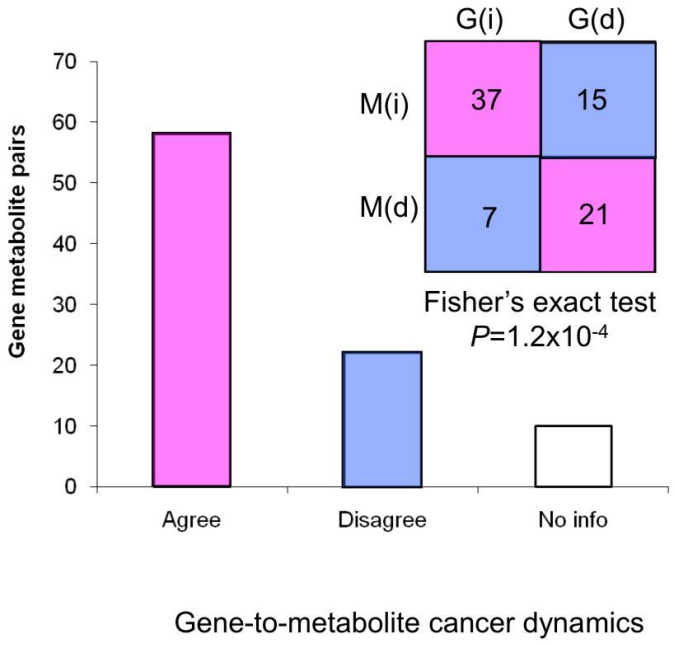

Fig 3.8. Statistical comparison of gene expression differences with metabolite amounts. The chart displays the results from survey comparing ten different gene expression datasets with corresponding sphingolipids. G(i) and G(d) indicate an increase and decrease in gene levels, while M(i) and M(d) indicate increase and decrease in metabolites. The significance of agreement and disagreement between genes and metabolites was measured by the Fisher's Exact test (p-value = 0.01).

Table 3.1. Comparison of gene expression and glycosphingolipid differences for nine cancer datasets.

Cancer type	Gene exp reference	Metabolite reference	G(i) M(i)	G(d) M(d)	G(i) M(d)	G(d) M(i)
MDA-MB231/ MCF7	[167]	Current analysis, [82]	11	1	2	3
IDC/ normal ductal	[168]	[78-81]	5			
Gliosarcoma	[215]	[69]	2	1	1	
GBM/ white matter	[215]	[68]	1	3	2	2
Serious ovarian	[216]	[75, 76]	2			1
Mucinous ovarian	[216]	[75, 76]	4			1
SSEA3/ globo-H	[167]	[217]	3	7	5	
Melanoma cells	[133]	[133]	6	9	5	
Melanoma	[218]	[72]	3			
Total			**38**	**21**	**15**	**7**

The table compares the agreement G(i)M(i) and G(d)M(d), and disagreement G(i)M(d) and G(i)M(d), between gene expression and sphingolipid differences for nine cancer datasets. G: gene expression differences, M: metabolite difference, (i): higher ratio, and (d): lower ratio. The total for each category were used to determine the statistical significance as indicated in Fig 9.

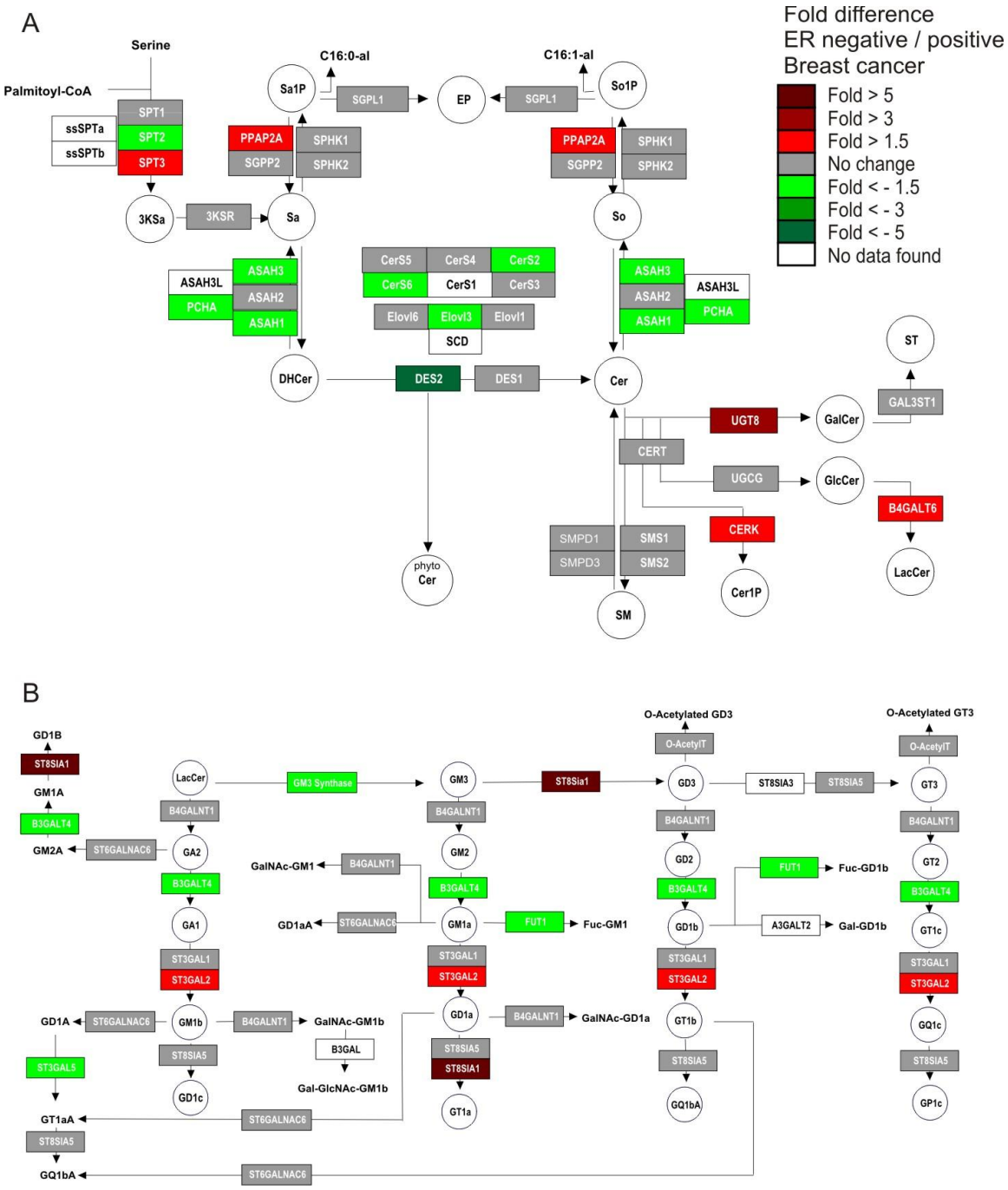

Fig 3.9. Pathway visualization of gene differences between estrogen receptor positive and negative cell lines. The sphingolipid pathway diagrams compare the average gene expression differences between estrogen receptor positive and negative breast cancer cell lines from previous study [169], and were prepared using Pathvisio v1.1 [139]. A) Illustrates the gene expression differences in the early steps of sphingolipid biosynthesis while, (B) indicates differences in mRNA of ganglioside biosynthesis genes. The shade of the box and circles represents the degree of up and down regulation as indicated by the color chart.

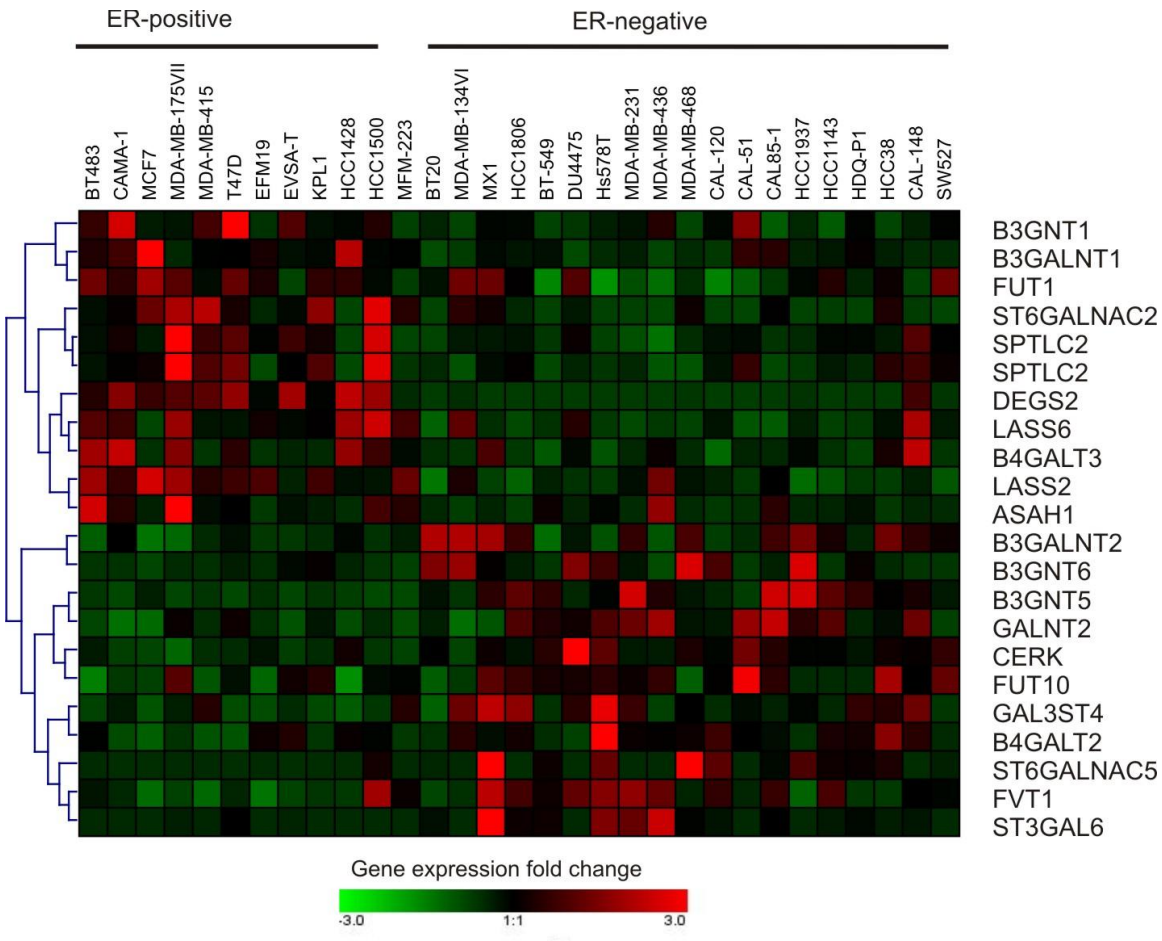

Fig 3.10. Comparison of glycosphingolipid biosynthetic gene expression between estrogen receptor positive and negative cell line. The heatmap depicts the hierarchical clustering of differentially expressed (p-value < 0.05) glycosphingolipid biosynthetic genes between the estrogen receptor positive(ER positive) and negative (ER negative) breast cancer cell lines obtained from a previous study [169]. The columns represent the cell lines and the rows correspond to individual genes. The diagram were prepared using the Genesis software [209] and are color coded as indicated by the color scale.

gene expression differences standard gene expression approaches such as hierarchical clustering and heatmap diagram (t-test, p-value < 0.05, Fig 3.10) revealed heterogeneity in between breast cancer cell lines within categories. Such variations might predict altered profile of metabolite markers within subcategories of breast cancer type.

3.4.5 Sphingolipid gene expression pathway maps for 59 cancer cell lines

The supplement for the manuscript has pathway maps based on previously published gene expression data [167] for all 59 cancer cells lines in the NCI (NCI-60, http://discover.nci.nih.gov/cellminer/) (Appendix B). From these, further studies could explain the possibility of tumor specific changes in sphingolipids as have been illustrated in the examples in the manuscript.

3.5 Conclusion

This pathway visualization map provides a tool to identify correlations between differentially expressed genes and metabolites in the sphingolipid pathway. Since there is a growing body of data on differences in gene expression in cancers and other diseases, these pathway maps can be used to predict changes in sphingolipid metabolites that can then be evaluated using an appropriate analytical technique such as, mass spectrometry.

CHAPTER 4

DESCRIPTION OF STUDIES EMPLOYING GENE EXPRESSION PATHWAY MAPS TO VISUALIZE TO STUDY SPHINGOLIPID BIOSYNTHESIS

The gene expression pathway maps prepared during this dissertation have been used in a number of studies to elucidate transcriptional changes in different branches of sphingolipid biosynthesis. The studies are listed below.

1) Visualization of gene expression data for sphingolipid and glycosphingolipid metabolism and metabolites via a pathway model and its application to cancer. This paper described the construction of the pathway maps and its application to cancer datasets. (submitted to BMC Systems Biology)

2) Comparison of gene expression differences between normal and ovarian epithelium cancer cells predicted elevated amounts of sulfatide and its precursor in cancer tissue which were confirmed by LC-ESI-MS/MS (submitted to Molecular Cancer)

3) Study of gene expression differences between mouse embryonic stem cells and embroid bodies using the pathway map showed correlation with variation in the fatty acid composition of their ceramides (J Lipid Res. 2010 Mar;51(3):480-9).

4) Sphingolipidomics: a valuable tool for understanding the roles of sphingolipids in biology and disease. (J Lipid Res. 2009 Apr;50 Suppl:S97-102).

5) Pathway visualization of gene expression differences in KDo2 treated mouse macrophage cells (RAW264.7) using high throughput qRTPCR agreed with composition of sphingolipid and sulfatides. (In collaboration with Dr Kelly Mormon and Lipidmaps)

6) Comparison of gene expression differences in ovarian cancer stem cells versus ovarian epithelial cells concurred with results of glycosphingolipids and N-acyl distribution of ceramides (study in collaboration with Dr John McDoanald)

7) Visualization of age dependant changes in gene expression in sphingolipid biosynthesis pathway in mouse T-cells. (In collaboration with Dr Meydani)

CHAPTER 5

CLONING OF HUMAN 3-KETOSPHINGANINE REDUCTASE AND ITS PUTITIVE REGULATED BY FOXC1

5.1 Abstract

3-Ketosphinganine reductase (3KSR) is the second enzyme of the *de novo* sphingolipid biosynthesis pathway that catalyzes the reduction of 3-ketosphingaine to sphinganine. During the preparation of the pathway maps its human transcript was unknown. Therefore, based on homology matches to yeast 3KSR transcript, follicular lymphoma variant type 1 (FVT1) was identified and cloned. A sensitive HPLC compatible enzyme assay was developed to measure 3KSR activity. Over-expression of FVT1 in Hela cells resulted in a 1.8-fold increase in 3KSR activity. Expression of the FVT1 transcript in E.coli cells, which lack the enzyme, produced significant 3KSR activity. Furthermore, as reports had shown that FOXC1 was a putative transcriptional regulator of FVT1 and Hela cells had a defective FOXC1, we measured sphingolipid intermediates of 3KSR in Hela and HekSPT1/2 cells. LC-ESI-MS/MS analysis of sphingolipids from the two cell lines detected significantly higher amounts of N-acetylated 3-ketosphinganine (3-keto dihydroceramide) in Hela cells as compared to Hek SPT1/2 cells. The elevated amounts of 3-keto dihydroceramide in Hela cells matched with low expression of FVT1 as confirmed by western blot analysis. These results show that FVT1 possess 3KSR activity and FOXC1 is a putative transcription regulator of FVT1 (3KSR).

5.2 Introduction

Modern molecular biology techniques have aided in the discovery of a genes encoding broad set of sphingolipid biosynthesis enzymes. However, at the outset of my thesis research the transcripts encoding some of the biosynthetic enzymes had not been found, such as 3-ketosphinganine reductase (3KSR). This enzyme catalyzes the reduction of 3-ketosphinganine in the *de novo* sphingolipid biosynthesis pathway. 3KSR activity was first found in rat tissues [219]. Because the enzyme is highly expressed, the intermediate is rapidly converted [1], but a recent report suggested the discovery of its substrate, 3-ketosphinganine [220]. At the start of this study the human gene encoding 3KSR was not identified despite the discovery of its yeast homolog [221].

Our work in this chapter focuses on identification of the human 3KSR gene by homology to the yeast transcript and its enzymatic verification in human and E.coli cells. We further describe the discovery of FOXC1 as a putative transcription regulator of 3KSR and accumulation of 3-ketodihydroceramides in cells lacking the transcription regulator (Hela cells).

5.3 Methods

5.3.1 Materials

Hela cells were obtained from ATCC, while Hek cells stably over-expressing SPT1 and SPT2 (Hek SPT1/2) were obtained from Dr David Ulinger (Johnson and Johnson pharmaceutical, Nutley, NJ). Normal human genomic DNA was obtained from invitrogen (Carlsbad, CA). The expression vector (pUC18, pCDNA3.0, pEGFP-N1 and

pET25b) were purchased from Takara Bio (Mountain view, CA). The cell culture medium DMEM and DMEM-F12 was from Gibco (Carlsbad, CA) and fetal bovine serum was obtained from Hyclone (Logan, UT). Penicillin G and streptomycin were purchased from Sigma (St Louis, MO). The sources for the antibodies were Abnova (Taipei, Taiwan) for anti-3KSR, Abcam (Cambridge, MA) for anti-FOXC1 and Ambion (Austin, TX) for the anti-GAPDH antibody. The enhanced chemifluorescence (ECF) Western blotting kit was purchased from GE healthcare (Piscataway, NJ). All other reagents and solvents were of high quality.

5.3.2 Cloning of 3KSR and FOXC1

The human expression sequence tag clone for 3KSR was obtained from Open Biosystems (image id 3636291). The clone was sequenced to confirm its match to the full-length cDNA sequences of the human FVT1 gene (Genbank accession numbers BC008797). Fragments containing the cDNA were amplified by PCR using the forward (gatg ctgctgctggctgccgcc) and reverse (gcggcagttttgtctgcattttc) primers. The purified DNA was ligated into to the pUC18 vector, and then subcloned using the introduced restrictions sites into vectors for mammalian (pCDNA3.0 & pEGFP-N1) and bacterial (pET25b) expression. The clones were sequenced to validate the orf sequence.

Because no clone was available for human FOXC1, the genes was cloned from normal human DNA, since the gene lacks any introns [222]. The FOXC1 orf was amplified by PCR using forward (cggaccgggcgcgttgccg) and reverse (aaacttgctacagtcgtagacgaaag) primers. The amplified product was ligated into pCDNA3.1 vector for mammalian expression. The sequencing of the clone detected three point

mutations (A to G substitution at nt 1329, G to A substitution at nt 975). Our attempts to correct them using the GeneTailor site directed mutagenesis kit (Invitrogen) with appropriate PCR primers were unsuccessful due to the high GC (80%) content of the gene. The three point mutations in the FOXC1 clone were corrected with the help of an outside vendor (Mutagenex, Piscataway, NJ). The sequencing of the final clones revealed no mutations.

5.3.3 Expression and enzyme activity assay of 3KSR in E.Coli

His-tagged 3KSR cloned into pUC18 was transformed into the *E. coli* strain (TunerTM (DE3)pLacI) and the protein production was induced by the addition of 1 mM isopropyl-1-thio-β-D-galactopyranoside. After growing the cells at 30 ^{o}C for 5 hr, the cells were collected by centrifugation. The expressed protein was obtained following the lysis of the cells using a solution mixture containing the BugBuster lysis buffer (Novagen), rLysozyme (Novagen), Benzonase Nuclease (Novagen) and protease inhibitor cocktail (Roche).

The 3KSR expressed in E.coli was assayed by adapting a previously developed method [221]. 3KSR enzyme assay was initiated by the addition 80 µM 3-**ketosphinganine** substrate to a 300 µl of assay mixture containing 1 mg of protein (supernatant cell lysate), 50 mM Hepes (6.9)**,** 5 mM dithiothreitol, 2.5 mM EDTA and NADPH regenerating system (Clontech). After incubating for 10 min at 37 °C, the reaction was terminated by addition of 1 ml $CHCl_3$:MeOH (1:1) and extracted for HPLC analysis.

5.3.4 Cell culture and enzyme assay of 3KSR in Hela cells

Hela cells were grown in 100 mm dishes to confluency in DMEM substituted with 10% FCS and antibiotics (penicillin and streptomycin) at 37 ^{o}C in 4% CO_2. Cells for *invitro* enzyme activity assay were scrapped in 10 mM phosphate buffer and lysed by sonication. The 200 μL reaction mixture for the enzyme assay consisted of 100 μg of protein, NADPH regenerating system, 100 μM di-thiothreotol and 5 μM 3-keto sphinganine made volume with the assay buffer. The reaction was stopped after 10 min with addition of 2:1 methanol : chloroform. 5 μM C20 sphingosine was added to each sample as an internal standard.

To determine 3KSR activity in transiently transfected Hela, cells were grown in six well plates to 50-60 % confluency and transfected with control (pEGFP) or pEGFP-3KSR using the GeneJuice transfection reagent (Epicenter). The transfection efficiency was determined by fluorescence microscopy to be 80%. After 48 hr cells were scraped into assay buffer (10 mM phosphate buffer) and the in vitro assay was performed as described above.

5.3.5 Extraction of sphingolipid long chain bases (LCB)

During the extraction of LCB from the assay mixture, 1 ml of $CHCl_3$ and 1 ml water were added along with 5 μM of C20 sphingosine as an international standard and mixed by sonication. The sample was centrifuged, and the upper aqueous layer was removed. The lower phase was washed three times with 1 ml of water, drained through a small column containing anhydrous sodium sulfate (granular), and dried by speedvac (Thermo scientific, Waltham, MA). The extracted LCBs were resuspended in 1 ml of 0.1

M KOH in methanol and $CHCl_3$ (2:1) and incubated at 37 C to cleave the acylglycerolipids. After the sample had cooled to room temperature, 1 ml each of chloroform and water were added. The LCBs were recovered in the chloroform phase, washed two times with water, and dried over sodium sulfate column, and the solvent was removed by speedvac.

5.3.6 HPLC analysis

The HPLC analysis of the 3KSR enzyme assay was performed with slight modification of a previously reported method for the analysis of free sphingosine [223]. Shortly before HPLC analysis the lipid extracts were solubalized in 100 µL of methanol by sonication, and derivatized by mixing with 50 µL of o-phthalaldehyde (OPA) solution. (The OPA solution was freshly prepared prior to derivatization by mixing 9.9ml 3% boric acid solution in water (pH adjusted to 10.5 with KOH) and 0.1 ml of ethanol containing 5 mg of OPA and 20 µL of beta-mercaptoethanol.) After 5 min of incubation at room temperature and the reaction was stopped by addition of 900 µL of mobile phase (10% v/v 5mM phosphate buffer in methanol). The LCB were resolved by a mobile phase consisting of 10% v/v potassium phosphate (pH 7.0) - methanol using a C18 packed column (Waters) and analyzed by a fluorescent detector (Shimadzu) at excitation 340 nm and emission 455 nm. The results were analyzed using the CLASS VP chromatography data system v4.3 (Shimadzu).

5.3.7 Western blot analysis

Hela cells grown as described above were collected at 80% confluency by scraping into PBS solution containing the completemini protease inhibitor cocktail. The total cell lysate was incubated with Benzonase Nuclease (Novagen, Madison, WI) for DNA cleavage for 30 min at room temperature, following which equal amounts of protein (15 μg) were separated by 12% SDS-PAGE (Pierce, Rockford, IL) minigel (10 well) in Tris-HEPES-SDS (100mM Tris, 100mM HEPES, pH 8.0, 3 mM SDS) running buffer and electrophoresed at 160 volts. The separated proteins were transferred onto a nitrocellulose membrane (Whatman, Florham park, NJ) and blocked with 5% milk-TBST (Tris buffered saline Tween-20) (20 mM Tris-HCl, pH 7.6, 137 mM NaCl, 0.1% Tween-20) solution. The membrane was incubated with primary antibodies (anti-FVT1, diluted 2 μg/ml) for 1hr at room temperature and washed with TBST solution before being probed with a secondary anti–fluorescein antibody (ECF kit) for 1 h. The protein bands were visualized by incubating the membrane with the ECF substrate for 30 min and imaged using FLA-3000 imager (Fujifilm, Stamford, CT).

5.3.8 Synthesis of 3-keto dihydroceramide internal standard

For the synthesis of C16 and C24 3-keto dihydroceramide internal standards, 2 mg of substrate (C16 and C24 dihydroceramides respectively) were dissolved in 0.2 ml of dry benzene. The oxidation reaction was by the addition of 0.2 ml (6.5 mg/ml) of CrO_3 in dry pyridine solution and the mixture was kept at room temperature for 2 hr with occasional shaking. To minimize the presence of moisture, the tube was purged with argon. The reaction was terminated by adding it to a cold solution of 5N HCl (0.6 ml), ice (0.6 ml) and chloroform (1 ml) and chilled for 10 min. After shaking, the chloroform

layer was removed and the aqueous layer was re-extracted twice with 0.5 ml chloroform and extract was added to the original chloroform layer. Combined extracts were washed with 1 ml of water and dried over anhydrous sodium sulphate. The completion of the reaction was confirmed by TLC using Silica gel 60 plates (Merck). The substrate and products were resolved using chloroform: methanol (50:1) mobile phase and visualized by staining the plates with primuline (Sigma). The standards were also validated by the infusion method using ESI-MS/MS.

5.3.9 LC-ESI-MS/MS analysis of 3-keto dihydroceramides

Cells were grown in culture as described above and extracted for mass spectrometry analysis as previously described [208]. The sphingolipid extracts were resolved by reverse phase HPLC using a discovery C18 column (supelco-Sigma Aldrich) using a gradient mobile phase containing solutions A (99:1 methanol:formic acid, 5 mM ammonium formate) and B (58:41:1 methanol:water:formic aicid, 5 mM ammonium formate). The 3-keto dihydrocermides were detected using triple quadrupole mass spectrometer (ABI3000, Applied biosystems) using MRM transitions as previously described [208].

5.4 Results

5.4.1 Identification of human of 3-ketosphinganine reductase (3KSR)

To identify the open reading frame (orf) encoding the human 3KSR a blast search was conducted against the human EST database using the yeast 3KSR homolog [221].

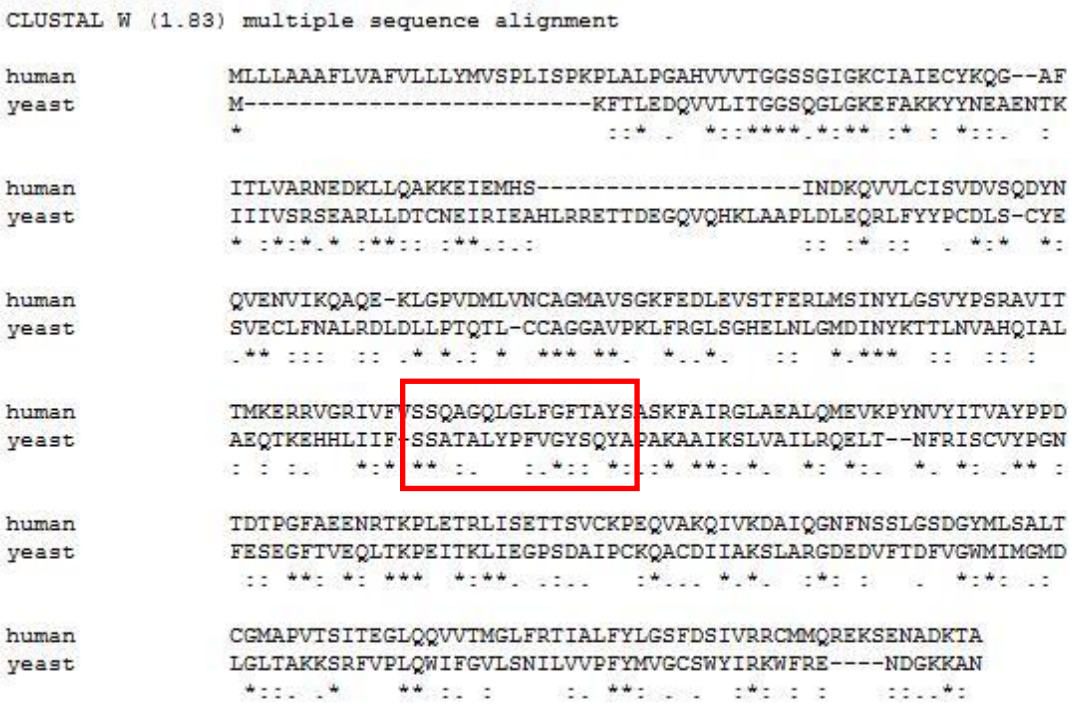

Fig 5.1 Sequence alignment comparison of human and yeast 3-Ketosphinganine peptide. The peptide sequence of yeast 3-Ketosphinganine reductase (NP_009824.1) and human follicular lymphoma variant translocation 1 (NP_002026.1) were obtained from NCBI database and aligned using the T-coffee algorithm [224]. The sequence region highlighted in red denotes the catalytic triad of short chain reductase family of enzymes.

The search identified follicular lymphoma variant translocation 1 (FVT1), sepiapterin reductase (SPR) and estradiol 17 beta-dehydrogenase 8 (17-beta-HSD 8) as the closest homologs with 24 %, 22 % and 21 % sequence identity respectively with the yeast mRNA. Since FVT1 had the sequence homology along the entire length of the yeast 3KSR peptide (Fig 5.1) and possessed the catalytic triad (Fig 5.1 residues highlighted by a red outline) required for the catalytic activity of short chain reductases [225], it was selected for experimental evaluation.

5.4.2 Development of HPLC based assay for 3-ketosphinganine reductase

In order to verify the activity of 3-ketosphinganine reductase in cells, an enzyme assay adapted for HPLC analysis was developed with modification to a previously reported protocol employing radio isotopes [219]. This protocol, as described in the methods section, is based on the principle of fluorescent derivatization of long chain bases (i.e So, Sa etc) with o-phthalaldehyde (OPA). The fluorescent conjugates are well resolved by reverse phase HPLC and detected by florescence [223]. HPLC analysis of internal standards showed that the mixture of substrate 3-ketosphinganine (C18 3-ketoSa) and C20 sphingosine (C20 So) produce a single peak (Fig 5.2 B), while a combination of product standard (C18 Sa) and C20 So produce two distinct peaks (Fig 5.2 C). The absence of a peak for 3-KetoSa was confirmed by analysis of the substrate alone (Fig 5.2 A) (except OPA fluorescence in the void volume).

To validate the separation of product and substrate from assay extracts, in vitro enzyme assays were conducted in Hela cells using equal amounts of substrates, and either

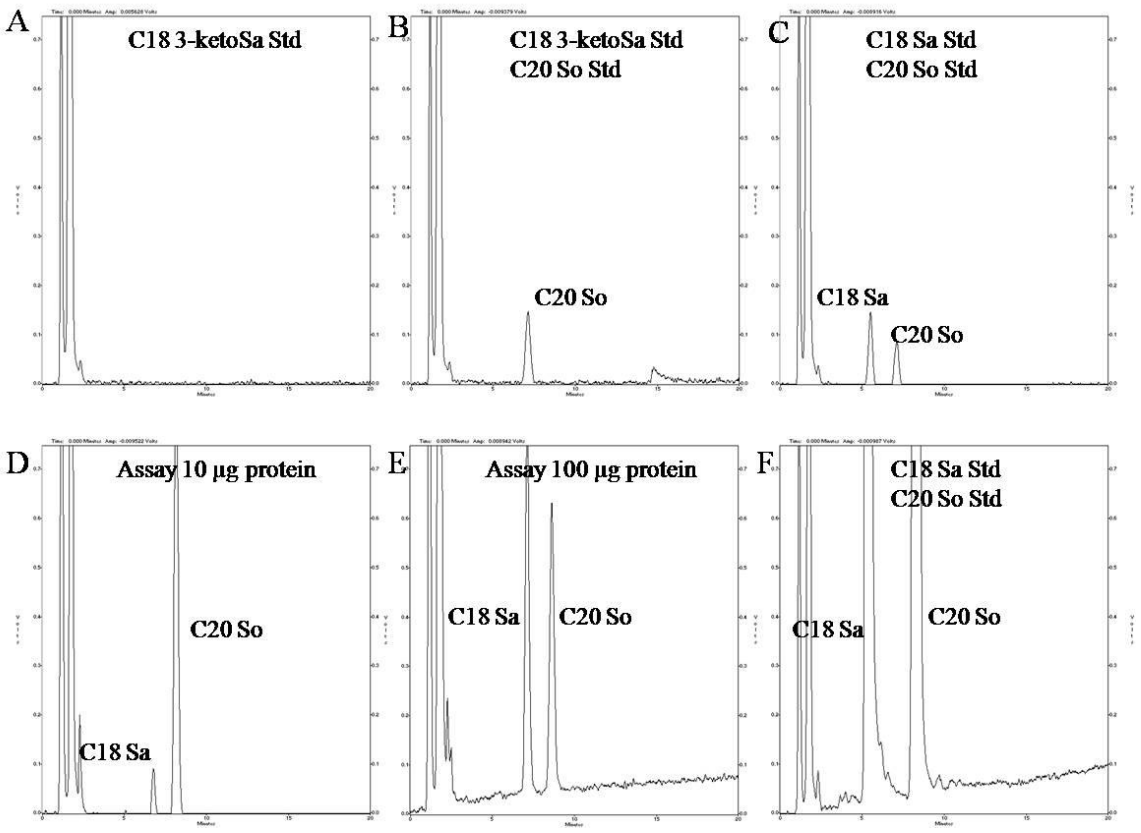

Fig 5.2 HPLC analysis of enzyme assay. HPLC analysis was performed for long chain bases internal standards and 3-ketosphinganine assay extracts following derivatization of the long chain bases with OPA and the products were resolved by reverse phase HPLC using a C18 pack column as previously described [223]. The panel depicts chromatograms for internal standards **A)** C18 3-keto sphinganine (3-ketoSa), **B)** 3-ketoSa + C20 sphingosine (C20 So) and **C)** C18 sphinganine (C18 Sa) and C20 So. The elution of internal standards were compared to extract of invitro enzyme assay that was conducted with equal quantities of substrate and either **D)** 10 µg protein or **E)** 100 µg protein as total cell lysate. Prior to extraction the assay samples with spiked with equal amounts of C20 So as internal standards. **F)** depicts the chromatogram for C18 Sa + C20 So internal standards.

10 µg, 50 µg or 100 µg protein equivalent cell lysate. Before extraction of the assay mixture all samples were spiked with 1 nmol of C20 So. Analysis of the assay extracts show that with increase in protein concentration higher proportion of C18 Sa (product) (Fig 5.2 D, E) was detected as compared to constant amounts of internal standards. The peaks for the product and show a elution profile similar to C18 Sa and C20 So standards (Fig 5.2 F)

5.4.3 Analysis of 3KSR activity in Hela cells over expressing FVT1

To assess if FVT1 possess 3KSR activity, the pEGFP control vector or FVT1 cloned into pEGFP were transiently transfected into Hela cells for 48 hr in 6-well plates. After the verification of the transfection efficiency by fluorescence microscopy, the cells were collected by scraping and *invitro* enzyme activity assays were performed. The LCBs from the assay mixture were extracted and analyzed by reverse phase HPLC. Hela cells transfected with pEGFP-FVT1 displayed 663 $\pm$ 140 pmol/mg protein/min activity for 3KSR (Fig 5.3 E), as compared to 372 $\pm$ 75 pmol/mg protein/min for empty vector transfected Hela cells ($p < 0.05$, $n = 4$) (Fig 5.3 E). The representative chromatograph for the enzyme assays (Fig 5.3 A,B) closely align with the peaks for standards. This study suggested that ectopic expression of FVT1 resulted in elevated 3KSR activity.

5.4.4 Measurement of 3KSR activity in E.coli transformed with FVT1

Because Hela cells possess background 3KSR, the activity of the peptide produced by FVT1 was verified by ectopic expression in E.coli following the induction of protein synthesis by IPTG. After 5 hr of growth the bacterial cells were lysed and the protein in

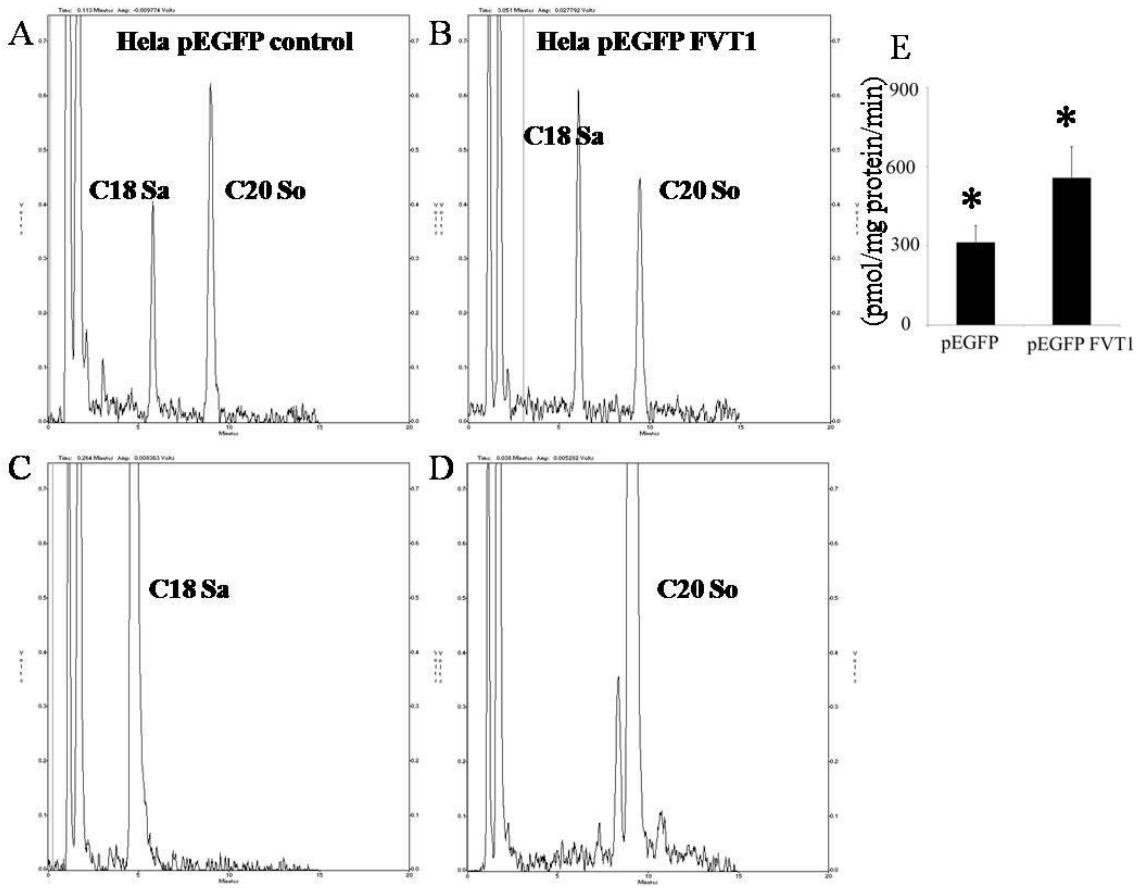

Fig 5.3 Analysis of the 3-ketosphinganine reductase activity in Hela cell transfected with FVT1. Hela cells were transfected with FVT1 cloned into the pEGFP or the vector alone in 6-well plates. The cells were harvested 48 hr after transfected and in vitro enzyme activity assay was performed as described in the methods section and analyzed by reverse phase HPLC. The representative chromatograph for **A)** control vector, **B)** FVT1transfected Hela cells were compared with chromatographic peaks for **C)** C18 Sa and **D)** C20 So standards. **E)** depicts the graphical representation of activity in **A** and **B** in pmole/mg protein/min. The significance as indicated by an asterisk was determined by a t-test at p-value < 0.05

the supernatant was used for a 3KSR *in vitro* enzyme activity assay as described in the methods section and the LCB were extracted and analyzed by reverse phase HPLC. Results showed that E.coli transformed with FVT1 produced 754 $\pm$ 117 pmol/mg protein/min C18 Sa (Fig 5.4 B, E) as compared to 11 $\pm$ 7 pmol/mg protein/min in E.coli transformed with the empty vector (Fig 5.4 A, E) ($p < 0.001$, $n = 4$). E.coli cells expressing a mutant FVT1 peptide produce 17 $\pm$ 12 pmol/mg protein/min C18 Sa (Fig 5.4 C, E), which further verifies the finding that wildtype FVT1 transcript possess 3KSR activity. These findings confirm that FVT1 possesses 3KSR activity. This conclusion has been confirmed by somewhat later study [148].

During this period a study reported that FOXC1 was a putative transcription regulator of 3KSR [226] and showed that Hela cells lack FOXC1 due to deletion of the genomic sequence [222]. Therefore, in the remaining chapter we use the Hela cell model to investigate the consequences of FOXC1 deletion on the activity of 3KSR and the composition of its metabolites.

5.4.5 Composition of 3-ketosphinganine intermediates in Hela and Hek SPT1/2 cells

Because reports showed that FOXC1 was a putative transcription regulator of FVT1 (3KSR) [226] and Hela cells had a defective FOXC1 [222] the sphingolipids of Hela and Hek SPT1/2 cells were compared. Both cell lines were grown in culture and their sphingolipids were extracted and analyzed by liquid chromatography electrospray ionization tandem mass spectrometry (LC-ESI-MS/MS). The analysis of the cells

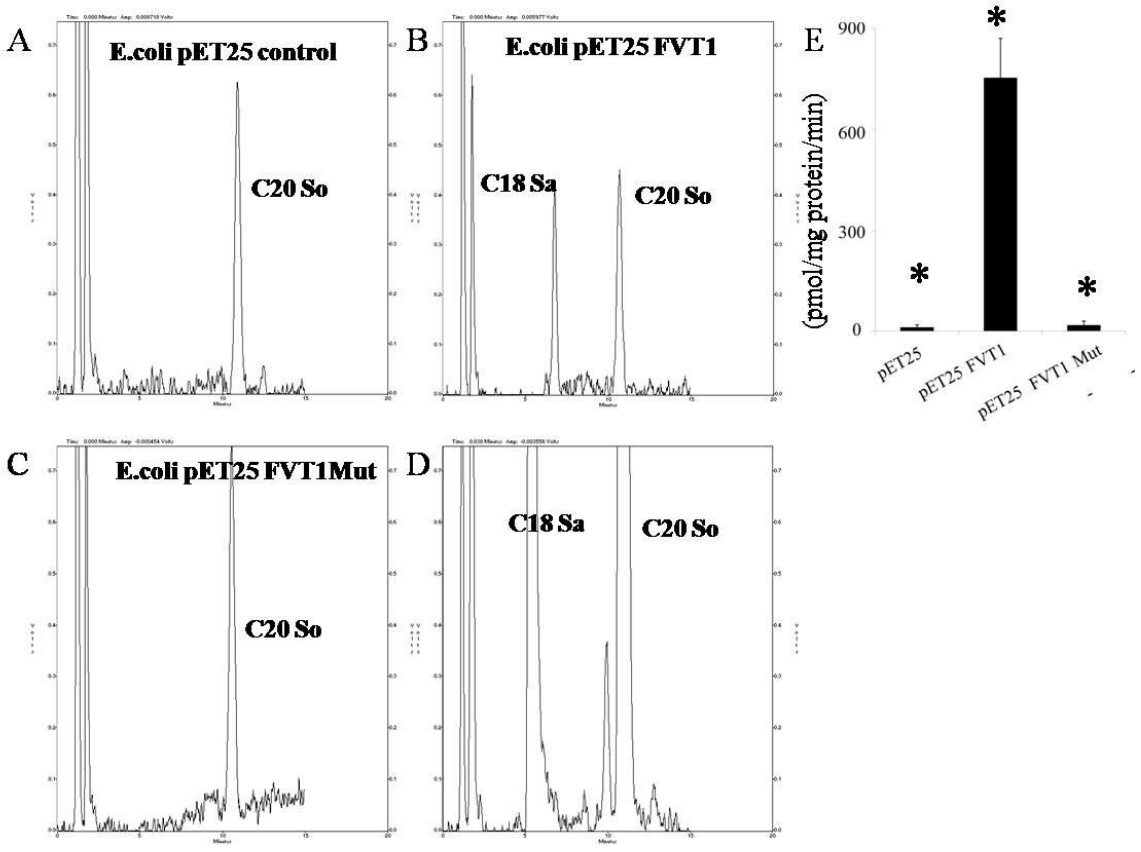

Fig 5.4 Analysis of the 3-ketosphinganine reductase activity in E.Coli transformed with FVT1. Ecoli cells were transformed with FVT1, mutant FVT or the control vector, and the peptide production was induced for 5 hr. The assay was conducted with 10 min as described in the methods section and the product was analyzed by reverse phase HPLC. The representative chromatograph for **A)** control vector, **B)** FVT1, **C)** FVT1-mut were compared to peaks for **D)** standard C18 Sa and C20 So. **E)** depicts the graphical representation of activity in **A**, **B** and **C** in pmole/mg protein/min. The significance as indicated by an asterisk was determined by a t-test at p-value < 0.001

revealed that Hela cells had 4.1 ± 0.9 pmol C16-3Keto DHCer/mg protein and 1.3 ± 0.2 pmol C18-3Keto DHCer/mg protein (Fig 5.5) versus undetectable C16-3Keto DHCer and 0.07 ± 0.04 pmol C18-3Keto DHCer/mg protein in Hek SPT1/2 cells (Fig 5.5) ($p < 0.05$, n=3). 3-keto DHCer with longer chain length fatty acids were below the limit of detection of the instrument. In comparison, no significant amounts of 3-ketosphinganine was detected in either cell lines. These findings suggest that the accumulating 3-keto sphinganine in Hela cells is rapidly N-acylated to 3-keto dihydroceramide due to a defective FOXC1 gene.

5.4.6 Verification of FOXC1 expression in Hela cells

To ascertain if the Hela cells used for sphingolipid profiling had its FOXC1 gene deleted as previously reported [222], genomics DNA from Hela and HekSPT1/2 cells were isolated. The FOXC1 orf was amplified by a PCR reaction using the primers representing the start and stop codons, as the gene doesn't contain introns [222]. The products of the PCR reaction were resolved by agarose gel, which revealed a prominent band at 1662 bp for Hek SPT1/2 cells (Fig 5.6). In contrast, no band was observed in Hela cells (Fig 5.6). These finding suggest that the accumulation of 3-keto dihydrocermides in Hela cells may possibly be regulated by the expression of FOXC1 in cells.

5.4.7 Expression of 3KSR in different cell lines

Because a report suggested that FOXC1 was a putative transcription regulator of FVT1 [226] and Hela cells displayed greater accumulation of 3-keto dihydroceramide (Fig 5.5), the expression of FVT1 peptide was measured in Hela, Hela-3KSR, Hek and

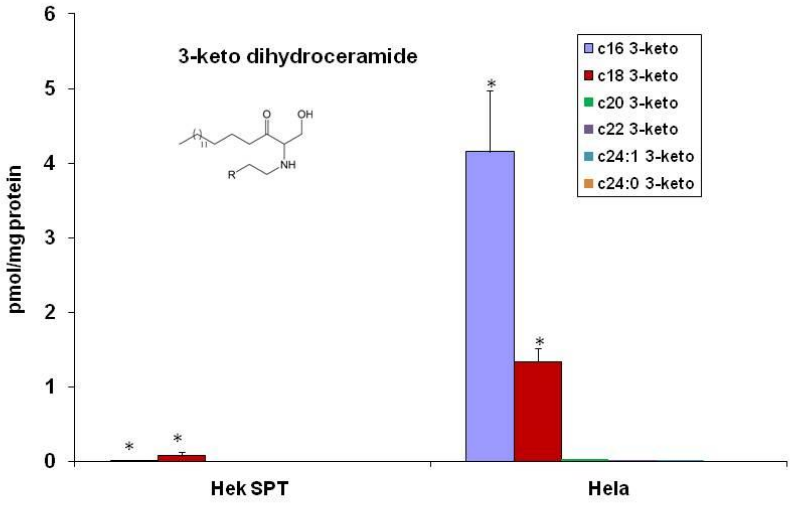

Fig 5.5 LC-ESI-MS/MS analysis of 3-ketodihydrocermide in HekSPT1/2 and Hela cells. Both the cells were grown in culture medium and the cells were collected by scraping in PBS. Sphingolipids were extracted and analyzed by LC-ESI-MS/MS using a previous protocol [208]. The chart displays the fatty acid distribution of in 3-ketodihydroceramide in pmol/ mg protein for subspecies indicated in the color chart. The significance was determined by a t-test as indicated by an asterisk at p-value < 0.05.

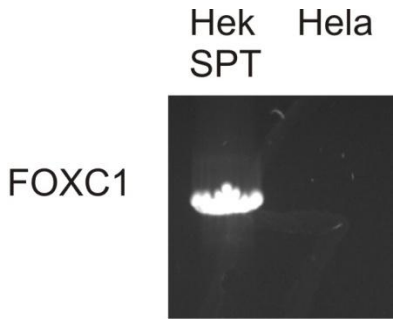

Fig 5.6 PCR amplification of FOXC1 orf in HekSPT1/2 and Hela cells. Genomic DNA from HekSPT1/2 and Hela cells was isolated using a genomic DNA isolation kit. Equal amounts of DNA template were amplified using PCR reaction and the product was resolved by an agarose gel. FOXC1 amplification band was observed at 1662 bp.

HekSPT1/2 cells. The cells were grown in culture and the western blot analysis was performed on the whole cell lysates. Comparison of protein from the cell lines revealed

To verify the effect of the low expression of FVT1 peptide in Hela cells the activity of 3KSR in the Hela and Hek SPT1/2 cells was determined by an *invitro* enzyme activity assay. The HPLC analysis of the activity assay indicated that Hela cells had activity of 0.27 pmol/µg/min for 3KSR as compared to 0.61 pmol/µg/min activity in Hek SPT1/2 cells. These finding suggest that the lack of FOXC1 results in lower expression and activity of 3KSR in Hela cells.

5.4.8 Analysis of FVT1 gene expression in the NCI60 cell panel

To compare the expression of 3KSR (FVT1) between a panel of cell lines including, Hela the mRNA abundance for FVT1 in the NCI60 cell panel was compared using the cell lines using the BioGPS browser [227]. The comparative analysis revealed that Hela cells (Fig 5.8) have among the lowest expression compared to other cell lines.

5.4.9 Evaluation of 3KSR enzyme activity in Hela cells after FOXC1 transfection

In order to rescue 3KSR activity and reverse the accumulation of 3-keto dihydroceramide in Hela cells, the human FOXC1 ORF was cloned as described in the methods section. Hela cells were grown in100 mm dishes and transfected with control (pcDNA) or FOXC1 vector for 48 hr, and subsequently incubated with 30 µM 3-ketosphinganine for 15 min. At the end of the time point the cells were scraped and the

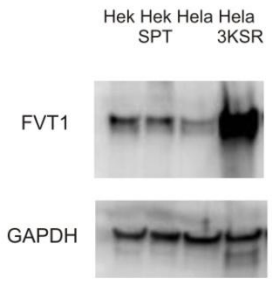

Fig 5.7 Comparison of 3KSR peptide in cell line. Whole cell lysates of Hek, HekSPT1/2, Hela and Hela-3KSR cells were prepared and equal amounts (15 μg) of protein were separated by an SDS-PAGE gel. The anti-FVT1 antibody was used to detect 3KSR peptide, while the detection of GAPDH with an anti-GAPDH antibody was used as a protein loading control.

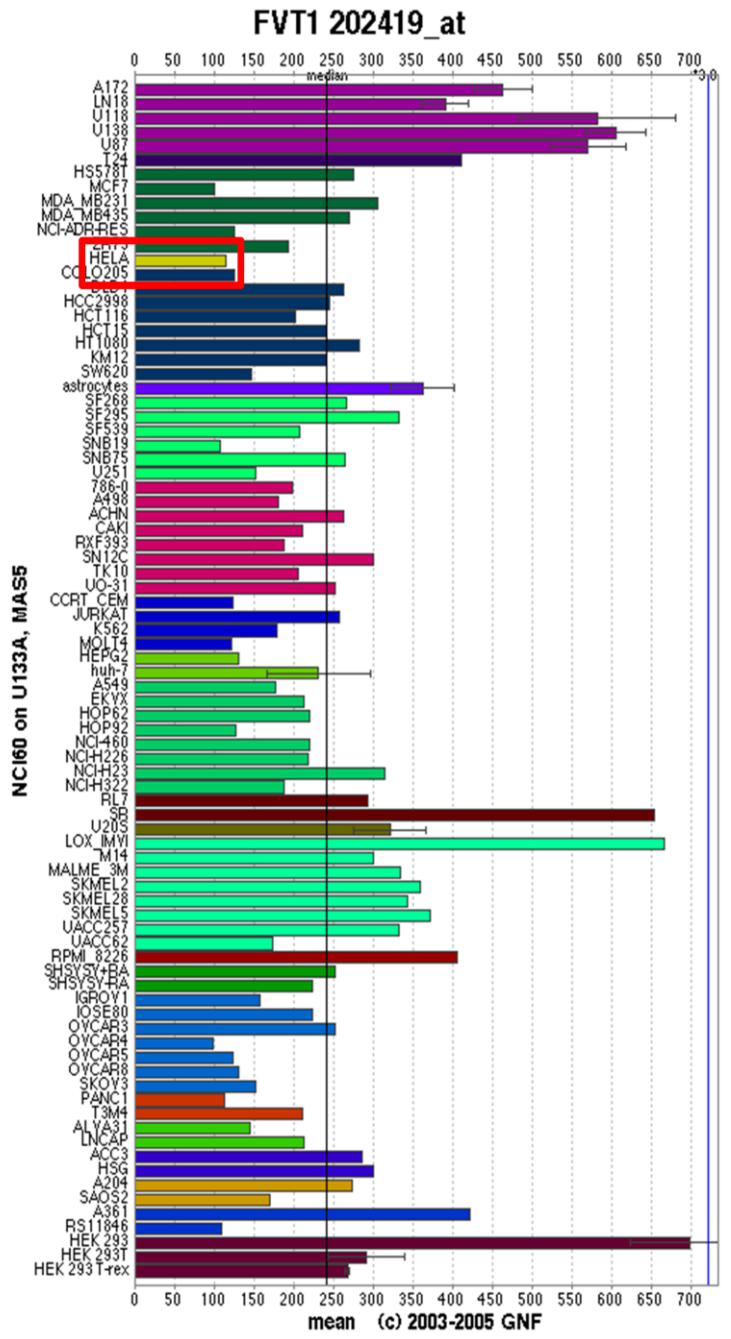

Fig 5.8 Global analysis of FVT1 expression in NCI60 cell panel. To compare the expression of FVT1 between a panel of cancer cell lines including Hela cell, a search was conducted using the BioGPS browser [227].

sphingolipids were extracted and analyzed by LC-ESI-MS/MS as previously described [211]. Hela cells transfected with FOXC1 had 2.64 $\pm$ 1.6 pmol total 3 keto-dihydroceramide /mg protein as compared to control transfected Hela cells, 2.3 $\pm$ 1.2 pmol total 3 keto- dihydroceramide /mg protein. These results suggest that transfection of FOXC1 was unable to cause a significant increase in 3KSR activity in Hela cells.

5.5 Conclusion

This study reports application of bioinformatics analysis in the successful identification of 3KSR. In vitro enzyme activity assay in Hela and Ecoli cells verified the 3KSR enzyme activity of human FVT1 ORF activity of human FVT1. Furthermore, using the knowledge of transcription factor binding studies and the Hela cell model the accumulation of N-acyl product of 3-ketosphinganine intermediate was detected. However the restoration of FOXC1 expression in Hela cells was unable to rescue 3KSR activity. This study demonstrates the advantage of combining sequence analysis with biochemistry in the discovery of unknown enzyme transcripts and their regulation.

CHAPTER 6

CHARACTERIZATION OF MUTANT SERINE PALMITOYLTRANSFERASE 1 IN LY-B CELLS AND ITS PARTIAL STABILIZATION, WITHOUT DETECTABLE ENZYMATIC ACTIVITY, BY CHEMICAL CHAPERONES

6.1 Introduction

Sphingoid base biosynthesis is initiated by serine palmitoyltransferase (SPT; EC2.3.1.50) [228], an activity that is essential for cells in culture unless the medium is supplemented with sphingolipids [229]. SPT is comprised of two [228], and possibly more subunits [147, 230], and homozygous deletion of two subunits (Sptlc1 and Sptlc2, also known as LCB1/LCB2 or SPT1/SPT2) in mice is embryonic lethal [231]. Because the mammalian SPT is a membrane protein, its crystallization has been a challenge. Bioinformatics based homology modelling is a possible approach to model SPT structure, since it is related to previously crystallized class of pyridoxal 5-phosphate dependent enzymes. This technique has been previously applied to study the impact of amino acid substitutions in SPT during hereditary sensory neuropathy type 1 (HSN1) [232, 233].

Sptlc1 subunit of LY-B cells lack SPT activity due to a mutation [229], and therefore they have been used as models for studies of *de novo* sphingolipid biosynthesis and the functions of sphingolipids [229]. However the cause of the dysfunctional SPT

activity in these cells is unclear. During this study sequencing of the *SPTLC1* mRNA from LY-B cells identified the mutation as a guanine to adenine change at nucleotide 738, causing a G246R transformation. Western blots revealed low expression of the mutant SPT1 peptide, but activity was not detectable by mass spectrometric analysis of [^{13}C]-palmitate incorporation into sphinganine, sphingosine, 1-deoxysphinganine, or 1-desoxymethylsphinganine. Treatment of LY-B cells with chemical chaperones (DMSO or glycerol) increased the amounts of mutant SPT1 as well as SPT2, but SPT activity was not restored. This study has established that G246R mutation in hamster SPT1 results in the loss of SPT activity.

6.2 Methods

6.2.1 Materials

Chinese hamster ovary (CHO) derived lines LY-B and LY-B/cLCB1 (which are stably transfected with the Chinese hamster LCB1 cDNA to restore SPT activity) were available from previous studies [229]. Ham's F12 medium was from Gibco (Carlsbad, CA) and fetal bovine serum was obtained from Hyclone (Logan, UT). The sources for the antibodies were BD Biosciences (San Jose, CA) for the anti-LCB1 monoclonal antibody, Cayman (Ann Arbor, MI) for the anti-SPT2 monoclonal antibody, Sigma (St. Louis, MO) for the anti-beta actin and anti-HA antibodies, Ambion (Austin, TX) for the anti-GAPDH antibody, and David Uhlinger (Johnson & Johnson Pharmaceutical Research & Development, Raritan, NJ) for another anti-SPT1 antibody [234]. The enhanced chemifluorescence (ECF) Western blotting kit was purchased from GE healthcare

(Piscataway, NJ). Mass spectrometry internal standards were obtained from Avanti Polar Lipids (Alabaster, AL) and [U-^{13}C]- palmitic acid was purchased from Cambridge Isotope (Andover, MA). Fumonisin B_1 (FB_1) was obtained from Biomol (Plymouth Meeting, PA). All other reagents and solvents were of high quality.

6.2.2 Cell culture and treatments

LY-B and LY-B/LCB1 cells were cultured in Ham's F12 medium containing 10% fetal bovine serum, penicillin G (100 U/ml) and streptomycin sulfate (100 μg/ml) in 5% CO_2 at 37 °C. During stable isotope labeling studies, the media was supplemented with 0.1 mM [U-^{13}C]-palmitic acid complexed with equimolar fatty acid free BSA (Calbiochem, Gibbstown, NJ). After 12 or 24 h, depending on the experiment, the incorporation of stable isotope into sphingolipids was measured by liquid chromatography, electrospray ionization tandem mass spectrometry (LC ESI-MS/MS) as previously described [235] except as noted below.

To analyze whether LY-B and LY-B/LCB1 cells produce both the "typical" sphingoid bases (i.e., sphinganine and sphingosine) and the recently discovered "atypical" sphingoid bases (1-deosysphinganine and 1-desoxymethylsphinganine) [11, 236], 25 μM FB1 was added to the cells one hour before addition of the 0.1 mM [U-^{13}C]-palmitic acid-BSA complex (and the FB_1 was included in the medium for the full 24 h incubation) to cause the sphingoid bases to accumulate [236].

For chemical chaperone treatment of LY-B cells, the cells were grown to approximately 50% confluence and changed to media supplemented with different

concentrations of DMSO (up to 3%) or glycerol (up to 1 M) for 24 h. To determine how this affected SPT amount, the SPT1 and SPT2 peptides were visualized by western blotting as described in 2.3. GAPDH was used as the protein loading control because DMSO and glycerol have been noted to influence the expression of actin [237-239]. To determine how SPT activity was affected, the cells were incubated for an 12 h in the same medium supplemented with 0.1 mM [U-^{13}C]-palmitic acid-BSA complex then the [^{13}C]-labeled sphingolipids were determined by LC ESI-MS/MS.

6.2.3 Cloning and sequencing of SPT1 from LY-B cells

Total RNA was extracted from LY-B cells by the Absolutely RNA Miniprep Kit (Qiagen, Valencia, CA) and reverse transcribed to cDNA using the cDNA Synthesis System Kit (TaKaRa, Mountain View, CA). PCR was performed to amplify the SPT1 transcript using primers (5'- atggcgatggcggcggagca and 3'- ctacagcagcacagcctgggca), which represents the start and stop codon for hamster SPT1 open reading frame. The amplified PCR transcript was ligated into pUC18 cloning vector and restriction digested with EcoRI to determine the clones with the correct inserts. 15 selected clones were sequenced (Nevada genomics center, Reno, NV) and compared to wildtype CHO SPT1 mRNA by multiple sequence alignment using T-coffee [224].

6.2.4 Western blotting

After the experiment the cells were scraped from the dishes into PBS solution containing Complete Mini protease inhibitor cocktail (Roche Diagnostics, Indianapolis,

IN) and lysed by sonication. The total cell lysate was incubated with Benzonase Nuclease (Novagen, Madison, WI) for DNA cleavage for 30 min at room temperature, following which equal amounts of protein (40 μg) were separated by 12% SDS-PAGE (Pierce, Rockford, IL) minigel (10 well) in Tris-HEPES-SDS (100mM Tris, 100mM HEPES, pH 8.0, 3mM SDS) running buffer and electrophoresed at 160 volts. The separated proteins were transferred onto a nitrocellulose membrane (Whatman, Florham park, NJ) and blocked with 5% milk-TBST (Tris buffered saline Tween-20) (20 mM Tris-HCl, pH 7.6, 137 mM NaCl, 0.1% Tween-20) solution. The membrane was incubated with primary antibodies (anti-LCB1, diluted 1:2000; Anti-SPT1, diluted 1:3000; anti-SPT2, diluted 1:1000) overnight at 4^{o} C and washed with TBST solution before being probed with a secondary anti–fluorescein antibody (ECF kit) for 1 h. The protein bands were visualized by incubating the membrane with the ECF substrate for 30 min and imaged using FLA-3000 imager (Fujifilm, Stamford, CT). Pixel density was measured using Multi Gauge (Fujifilm) image analysis software. Statistical significance was defined at a p-value of 0.05 using the Kruskal-Wallis rank sum test in R v2.61 (www.r-project.org).

6.2.5 LC ESI-MS/MS analysis of sphingolipids

The sphingolipids were analyzed in positive ionization mode by LC ESI-MS/MS [235] using ABI 3000 triple quadrupole and ABI 4000 quadrupole-linear ion trap mass spectrometers (Applied Biosystems, Foster City, CA). Since the major fragmentation products of ceramides and ceramide monohexosides (e.g., ions with *m/z* 264.4 for sphingosine and *m/z* 266.4 for sphinganine) retain the carbon atoms originally derived from palmitoyl-CoA, the sphingolipids made *de novo* via incorporation of [U-^{13}C]-

palmitate into the sphingoid base backbones were determined by adding 16 mass units to the precursor-product pairs for species labeled in only the sphingoid base backbone, and by adding 32 mass units to the precursor ion and 16 to the product for compounds labeled in both the fatty acid and the sphingoid base. Since these product ions are of very low abundance from sphingomyelins [235], the incorporation of [U-^{13}C]-palmitate into the sphingoid base backbones of SM was determined by treatment of an aliquot of the lipid extract with the phospholipase D from *Streptomyces chromofuscus* (Sigma) to produce ceramide 1-phosphates phosphates [240, 241], which do provide definitive information about [^{13}C] labeling of the sphingoid base backbone [211, 235]. This treatment was conducted by incubating dried lipid extracts with 50 units of the enzyme suspended in 0.1 ml of 100 mM Tris HCl, pH 8.0, and 3 mM decylglucopyranoside (Sigma), at 37^{o} C for 30 min. The reaction was dried by speedvac and analyzed by LC ESI-MS/MS.

Analysis of the biosynthesis of sphinganine (So), sphingosine (Sa) and the "atypical" sphingoid bases (1-deosysphinganine, 1-deoxy-Sa, and 1-desoxymethylsphinganine, 1-desoxymethyl-Sa) [11, 236] by cells incubated [U-^{13}C]-palmitate and 25 μM FB_1 was conducted by LC ESI-MS/MS using multiple reaction monitoring with Q1 and Q3 set to pass the following precursor and product ions in positive ionization mode: 316.5/298.3 ([^{13}C]-So), 318.5/300.3 ([^{13}C]-Sa), 302.4/284.4 ([^{13}C]-1-deoxy-Sa), and 288.3/270.3 ([^{13}C]-1-desoxymethyl-Sa). The LC conditions were the same as described previously [236], i.e. using a reverse phase LC column (Supelco 2.1 x 50 mm Discovery C18 column, Sigma, St. Louis, MO) and a binary solvent system at a flow rate of 0.6 mL/min delivered by a Shimadzu LC-10 AD VP binary pump; the binary system began with equilibration of the column with a solvent

mixture of 60% mobile phase A ($CH_3OH/H_2O/HCOOH$, 58/41/1, v/v/v, with 5 mM ammonium formate) and 40% mobile phase B ($CH_3OH/HCOOH$, 99/1, v/v, with 5 mM ammonium formate), sample injection (typically in 50 µL of the same mixture), elution with this mixture for 1.3 min followed by a linear gradient to 100% B over 2.8 min (then a column wash with 100% B for 0.5 min followed by a wash and re-equilibration with the original A/B mixture before the next run).

6.2.6 Homology modelling of mutant SPT1

Homology modelling was performed to predict the structure of the mutant SPT1 by comparing it with two crystallised POAS enzymes [233], including the newly crystallized serine palmitoyltransferase from the bacterium *Sphingomonas paucimobilis* (PDB ID: 2JG2) [232]. In the first step, two crystal structures were selected (PDB ID: 2JG2 and 1FC4) as templates by a blast search of the PDB database using the query SPT1 peptide, because they possess high sequence identity (30 %). The sequences of the template and mutant SPT1 protein were aligned using T-coffee [224] and refined manually into a PIR format alignment file. The homology model was generated by Modeller v6.1 [242] using the PDB template, alignment file and instruction files, and visualised by VMD v1.8.6 [243].

6.3 Results

6.3.1 Analysis of the gene sequence for mutant SPT1 in LY-B cells

Sequencing of the mutated SPT1 from LY-B cells revealed a guanine to adenine mutation at nucleotide residue 738, which would result in the substitution of Arg for Gly246, which is conserved across numerous species (hamster, mouse, human and *S. cerviceae*), as shown in Fig. 6.1A. Homology modeling (Fig. 6.1B) predicts that this transformation places Arg246 in the vicinity of the non-polar residues Phe, Gly, Val and Leu, which would be likely to interfere with the correct folding of SPT1.

6.3.2 Analysis of mutant SPT1 polypeptide in LY-B cells

Previous studies have not detected an SPT1 peptide in LY-B cells by Western blotting [229], however, a very faint band is discernable when larger amounts of protein (40 μg) are examined using two antibodies (anti-LCB1 and anti-SPT1) (Fig. 6.2A and C) but not using an antibody to another polypeptide epitope not found in the cells (HA) (Fig. 6.2B). Also shown is the staining of SPT1 in LY-B/cLCB1 cells, which have been stably transfected with the wild-type SPT1 gene (Fig. 6.2A and C).

A

LY-B	237	VTRRFIVVERLYMNTGT	253
C.griseus	237	VTRRFIVVEGLYMNTGT	253
H.sapiens	237	VTRRFIVVEGLYMNTGT	253
M.musculus	237	VTRRFIVVEGLYMNTGT	253
S.cerevisiae	283	IPRKFIVTEGIFHNSGD	299

*

B

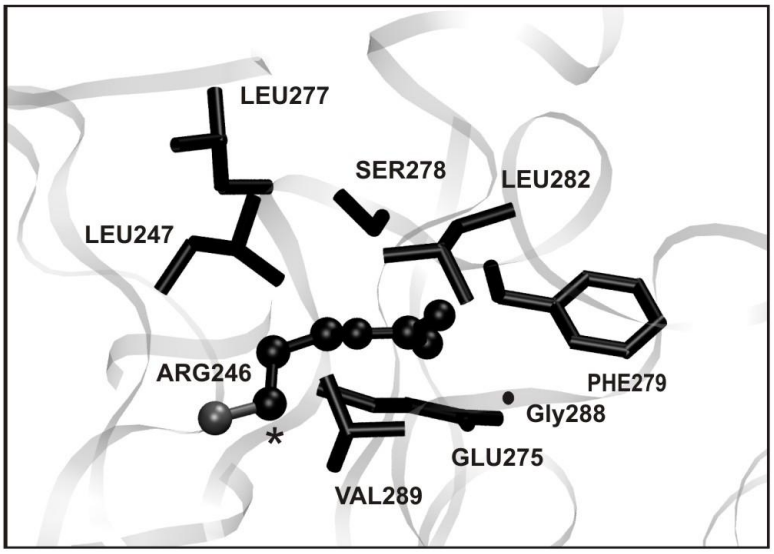

Fig. 6.1 Sequence comparison and homology model of the SPT1 mutant protein of LY-B cells. (A) Protein sequences of SPT1 were compared from LY-B cells, CHO, human, mouse and *S. cerviceae* using T-coffee. The point mutation G246R in LY-B cells is indicated by an asterisk. (B) This homology model for mutant SPT1 from LY-B cells was prepared using Modeller v6.1. The illustrated figure shows the G246R mutation (indicated in a ball and stick representation) to be located in a pocket of hydrophobic residues (Phe279, Leu282, Val289, Leu247, Ser 278) was visualized by VMD.

6.3.3 Analysis of mutant SPT activities in LY-B cells

To ascertain whether this small amount of mutant SPT1 afforded detectable *de novo* sphingolipid biosynthesis, cells were incubated with [^{13}C]-palmitic acid and analyzed for incorporation of [^{13}C] into the sphingoid base backbone (with free sphingoid bases in Fig. 6.3A and complex sphingolipids in Fig. 6B-D); LY-B/cLCB1 cells were used as a positive control because they have SPT activities comparable to wild-type CHO cells [229]. When all of the subspecies are summed, the amounts of backbone [^{13}C]-labeled sphingolipids in the LY-B/cLCB1 cells at 6 h were 62 $\pm$ 0.3 pmol Cer/mg protein, 54 $\pm$ 0.8 pmol HexCer/mg protein and 300 $\pm$ 14 pmol SM/mg protein, for a total of ~416 pmol/mg protein; for LY-B cells, the amounts were below the limits of detection for Cer and HexCer (~ 0.1 pmol/mg protein) and very low for SM (5.5 $\pm$ 16 pmol SM/mg protein) which, based on the high noise in the signal (reflected in the high SD), might be due to other compounds with similar ionization characteristics. Thus, even counting the possibility that this represents SM, the maximum amount of labeled backbone sphingolipids in the LY-B cells would only ~1% that in LY-B/cLCB1 cells**.**

As has been shown before [229], although LY-B cells are defective in sphingolipid biosynthesis *de novo*, they contain appreciable amounts of sphingolipids if grown in medium that contains sphingolipids (e.g., from serum). In these studies, the pmol of unlabelled sphingolipids/mg protein for LY-B vs LY-B/cLCB1 cells (measured by LC ESI-MS/MS) were, respectively: 140 $\pm$ 18 *vs* 1073 $\pm$ 17 for Cer; 122 $\pm$ 7 *vs* 447 $\pm$ 87 for HexCer; and 3474 $\pm$ 452 *vs* 5143 $\pm$ 167 for SM (data not shown).

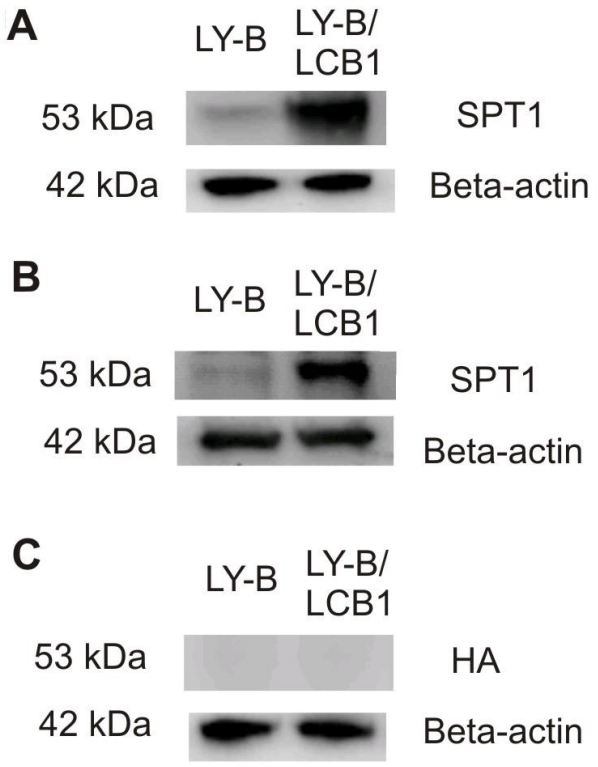

Fig. 6.2 Western blots of SPT1 in LY-B and LY-B/cLCB1 cells. Whole cell lysates of LY-B and LY-B/cLCB1 cells were prepared and equal amounts (40 μg) of protein were separated by an SDS-PAGE gel. Replicate membranes were probed with (A) a commercial LCB1 antibody; (B) an anti-HA antibody as a negative control, and (C) an independent anti-SPT1 polyclonal antibody. The detection of β-actin with an anti-β-actin antibody was used as a protein loading control.

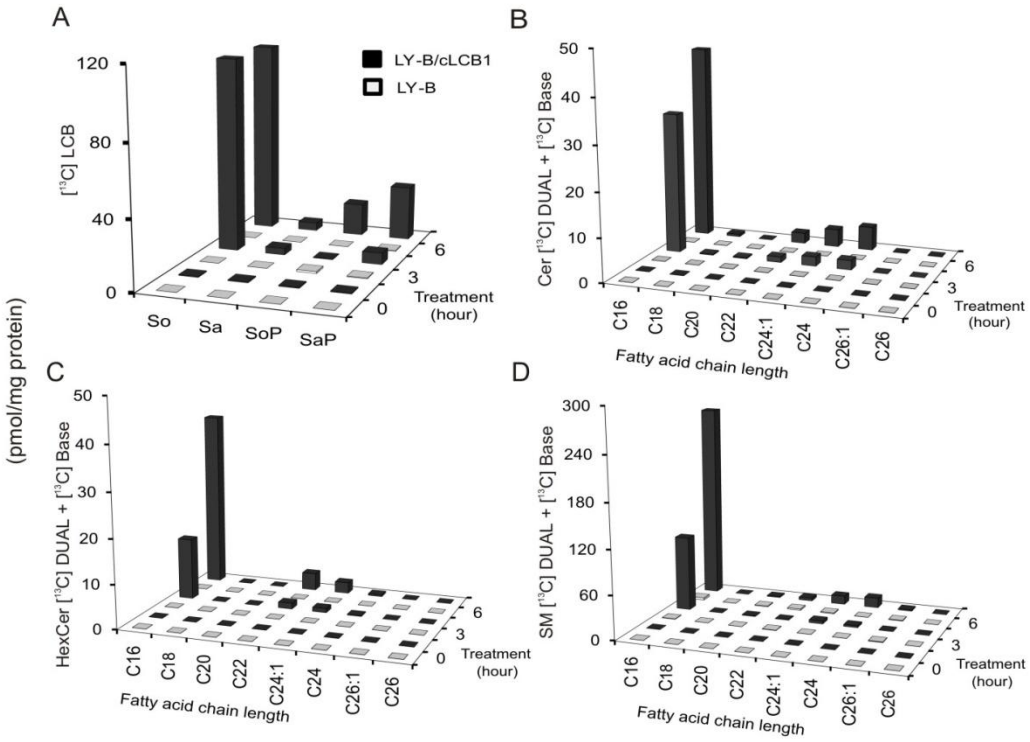

Fig. 6.3. Comparison of *de novo* sphingolipid biosynthesis in LY-B and LY-B/cLCB1 cells. LY-B and LY-B/cLCB1 cells were incubated with 0.1 mM [^{13}C]-palmitic acid for 0, 3 and 6 h and the sphingolipids labeled in the sphingoid base alone (BASE) plus the sphingoid base and fatty acid (DUAL) were measured by LC ESI-MS/MS. The black bars represent the sphingolipids in LY-B/cLCB1 cells while the white bars indicate the LY-B cells. (A) [^{13}C]-labeled long-chain bases (LCB) sphingosine, So; sphinganine, Sa; sphingosine 1-phosphate, SoP; and sphinganine 1-phosphate, SaP. (B-D) provide the sum of the label in the BASE and DUAL subspecies of ceramide, Cer, monohexosylceramides, HexCer, and sphingomyelins, SM, based on variation in the chain length of the amide-linked fatty acid (shown by chain length:number of double bonds).

As another way to assess sphingoid base biosynthesis, the cells were incubated with FB_1 to allow accumulation of the [^{13}C]-labeled sphingoid bases, which are otherwise rapidly N-acylated to complex sphingolipids, and thus less easily tracked. These results are shown in Fig. 5.4 as the relative ion yields for the precursor/product pairs as they elute from the reverse phase column. Production of [^{13}C]-So (Fig. 6.4A), [^{13}C]-Sa (Fig. 5.4C), [^{13}C]-1-deoxy-Sa (Fig. 6.4B) and [^{13}C]-1-desoxy-methyl-Sa (Fig 6.4D) were readily detected with the LY-B/cLCB1 cells, but the signal was but not above background for the LY-B cells, which further confirms the conclusion from Fig. 6.3 that the LY-B cells do not synthesize detectable amounts of sphingoid bases *de novo*. The appearance of [^{13}C]-sphingosine in LY-B/cLCB1 cells was somewhat surprising because desaturation of sphinganine is thought to occur only after N-acylation [244], but it is possible that this concentration of FB_1 did not completely block [^{13}C]-Cer biosynthesis and this [^{13}C]-sphingosine arose from turnover.

6.3.4 Partial stabilization of mutant SPT in LY-B cells

Some misfolded proteins can be stabilized by so-called chemical chaperones such as DMSO and glycerol [245-247]. When LY-B cells were treated for 24 h with DMSO or glycerol at concentrations where they have previously been effective, there were noticeable increases in both SPT1 and SPT2 by Western blotting (Fig. 6.5, upper), with the average increases in five experiments being between 2- and 3-fold (Fig. 6.5, lower). Lower concentrations had no effect, and higher were toxic (data not shown). In case these treatments also resulted in restoration of SPT activity, the incorporaton of [^{13}C]-palmitate into sphingolipids was measured after LY-B cells had been treated with either

3% DMSO or 1 M glycerol for 24 h (the [^{13}C]-palmitate was added to the same medium and the cells were incubated for 12 h before extraction for sphingolipid analysis by LC ESI-MS/MS). As noted earlier, the ion yields for the ^{13}C-labelled, we would estimate that the amounts were 2.0 $\pm$ 0.47 pmol/mg protein for the LY-B cells alone , 1.6 $\pm$ 0.2 pmol/mg protein for the LY- cells incubated with 3% DMSO and 2.33 $\pm$ 1.15 pmol/mg protein for LY-B cells in 1M glycerol.Therefore, there was no evidence that the small amounts of SPT1 detected upon treatment of the cells with these chemical chaperones restored SPT activity.

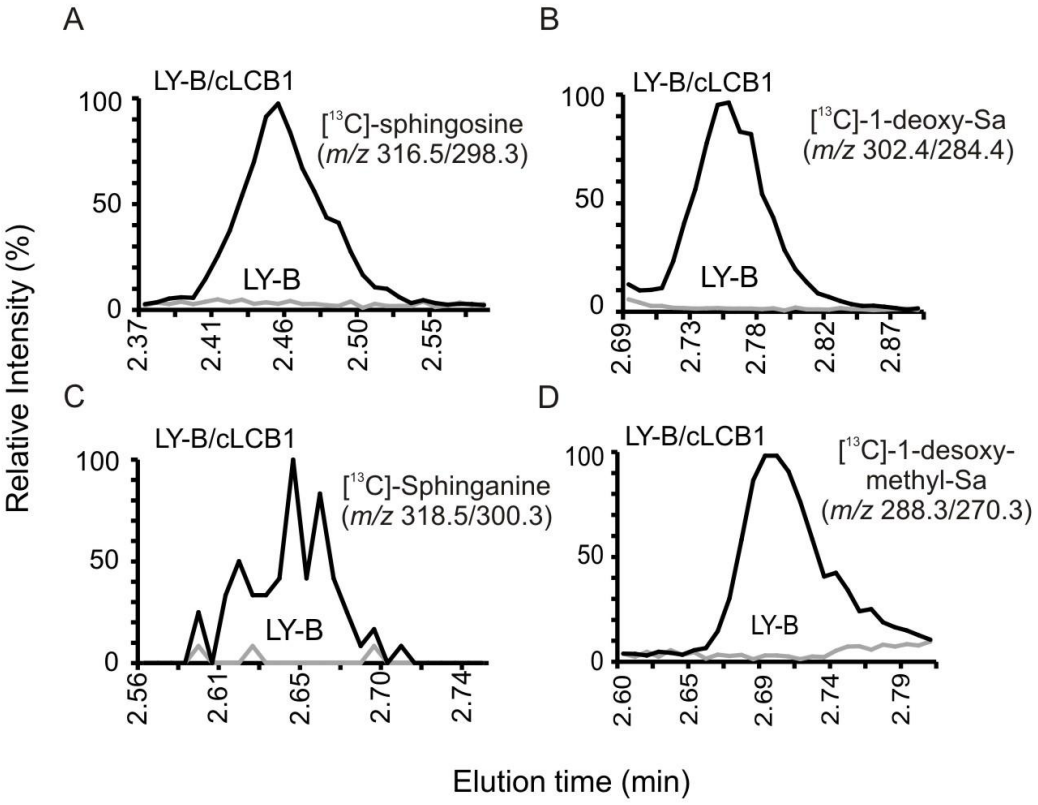

Fig. 6.4. Relative amounts of typical and atypical [^{13}C]-labelled sphingoid bases produced by LY-B and LY-B/cLCB1 cells upon co-treatment with FB_1. Shown are the relative ion intensities of the shown precursor/product pairs in the LC ESI-MS/MS eluates. The LC retention times for these species matched that of standards for these compounds (not shown). The samples for these analyses were obtained by incubating LY-B and LY-B/cLCB1 cells with 0.1 mM [^{13}C]-palmitic acid and 25 μM FB_1 for 24 h; the grey line indicates LY-B cells and the black line represents LY-B/cLCB1 cells.

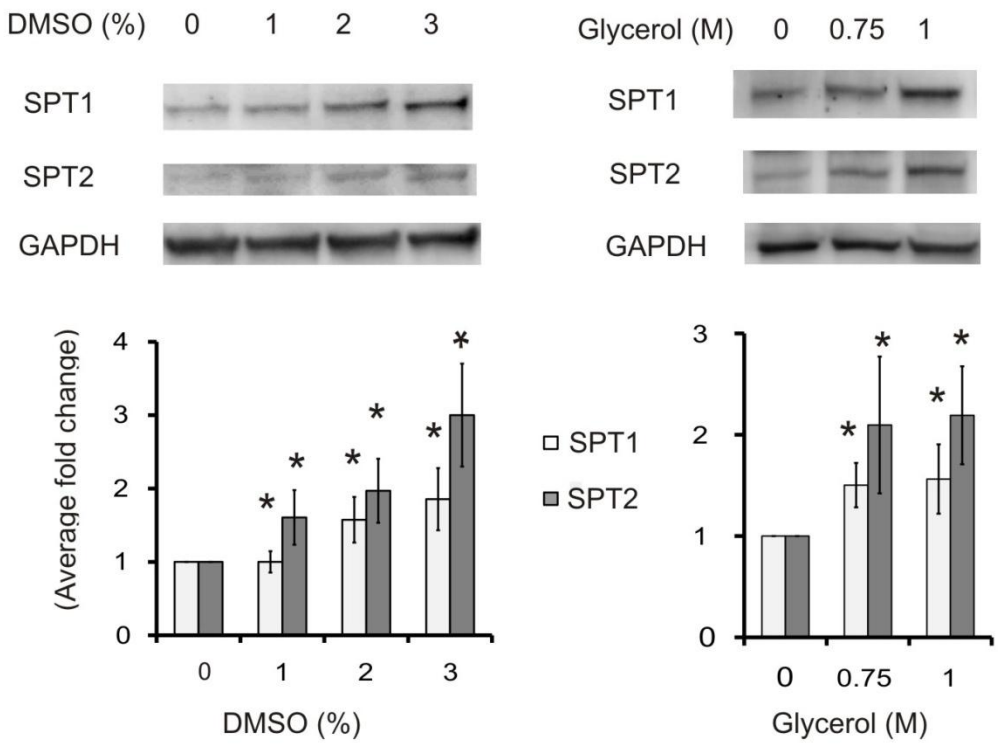

Fig. 6.5. Elevation of the amounts of SPT1 and SPT2 in LY-B cells treated with chemical chaperones. LY-B cell were treated with DMSO (left panels) or glycerol (right panels) at the shown concentrations for 24 h then analyzed by Western blotting (upper panels), with GAPDH as the loading control. The lower panels are the relative differences in protein amounts as estimated from the pixel densities of the bands from five independent Western blots (bottom panels), with the standard error indicated by the bars. Ratios that were significantly different from the control (no treatment, 0) at $P \leq 0.05$, as determined by the Kruskal Wallis rank sum test, are indicated by an asterisk.

6.4 Conclusion

Structure bioinformatics and sequence alignment provided valuable hypothesis that resulted in the sequencing and identification of nucleotide substitution in SPT1 transcript (G246R) from LY-B cells. These results are consistent with the fact that LY-B cells were produced using ethyl methanesulfonate [229], a mutagen that causes the random replacement of guanine(s) with adenine. Furthermore, the very low amounts of detectable mutant SPT1 polypeptide is consistent with the translated protein being unstable, which would be predicted upon localization of a positively charged Arg in a hydrophobic region of the enzyme, as suggested by the homology model [248]. It was worthwhile, nonetheless, to test for possible SPT activity given the recent discovery that SPT is able to produce not only sphinganine (and downstream sphingosine) but also the atypical sphingoid bases, 1-deoxysphinganine (from alanine) and 1-desoxymethylsphinganine (from glycine) [236]; furthermore, it has been suggested that these are elevated in the mutated SPTLC1 found in human sensory neuropathy type 1 (HSN1) [11]. However, the LY-B cells produced no detectable sphingoid bases of any of these types.

Therefore, for most studies, the presence of small amounts of mutant SPT1 polypeptide is not likely to interfere with the investigation. Its presence should be kept in mind, nonetheless, during investigations where the residual protein might become stabilized and complicate interpretation of studies of protein-protein interactions or other phenomena.

CHAPTER 7

Summary and future directions

Sphingolipids have important biological roles, and changes in their amounts have been linked to pathogenesis in wide range of diseases including cancers, where they promote cell adhesion, migration, proliferation and metastasis. However, it is challenge to characterize variations in all sphingolipid species due to their high structural diversity. The integration of different omics approaches such as transcriptomic and metabolic measurements provides new avenues to identify novel sphingolipid alterations. This dissertation aims to develop new and use existing bioinformatics techniques to investigate factors influencing sphingolipid biosynthesis.

To facilitate the integrative analysis of gene expression and sphingolipid amounts, updated pathway maps were prepared using an open access visualization tool, Pathvisio v1.1. The datasets were formatted using Perl scripts and visualized with the aid of color coded pathway diagrams. Comparative analysis of transcriptomics and sphingolipid alterations from experimental studies and published literature revealed 72.8 % correlation between mRNA and sphingolipid differences (p-value < 0.0001 by the Fisher's exact test). Conversely, pathway analysis of gene expression has also directed attention towards novel sphingolipid alteration, such as the elevation of phyto-sphingolipids and d16:1 Cer in MCF7 and MDA-MB-231 cells respectively. Thus comparison of gene expression and metabolite amounts using pathway diagrams has the potential to provide mechanistic

insight related to differential sphingolipid composition and also predict novel subspecies present in cancer cells and tissues. This approach has great potential to help the discovery of glycosphingolipids biomarkers in cancers and other disorders with specific knowledge of glycan head group and sphingoid base backbone.

As more dataset become available, visual analysis of gene expression pathway diagrams can be cumbersome. A solution to this challenge might be the development of mathematical algorithms for the prediction of putative branches of altered sphingolipids. Some of the potential approaches likely to provide such analysis my involve bayesian network and graph theory. Conversely, with wider availability of lipidomic datasets it could be possible to develop machine learning test to predict metabolite composition based on the gene expression signatures. These computational tools may be highly complementary to recent undertakings by Lipidmaps consortium to develop mass spectrometric methods for the quantitation of higher order glycosphingolipids.

During the preparation of the maps it was noted that a number of transcripts encoding sphingolipid biosynthetic enzymes were undiscovered. The human transcript for one such enzyme, 3-keto sphinganine reductase was identified and validated during this dissertation using molecular cloning and in vitro enzyme activity assay. Furthermore, mass spectrometry analysis of Hela cells which have defective FOXC1, a putative transcription regulator of FVT1 showed greater accumulation of N-acyl 3-ketosphinganine. However the transfection of FOXC1 into Hela cells was unable to alter 3KSR expression and reduce N-acyl 3-ketosphinganine amounts. Though this didn’t show the intended reversal with the gene transfection it is likely that additional subunits

of the transcription factor complex and post translational modification through protein kinases may play a role in regulation of FOXC1 activity.

The last study in this dissertation employs structure bioinformatics (homology modeling) and multiple sequence alignment to characterize SPT protein in LY-B cells that lack de novo sphingolipid biosynthesis. This in silico study identified a point mutation potentially resulting in the misfolding of SPT and loss of its enzyme activity. Treatment of LY-B cells with chemical chaperone partially stabilized SPT, without rescuing its activity. A potential application of structural modeling could be for the analysis of genomics alteration detected within genes in genome wide association studies and SNP's.

Thus studies in this dissertation demonstrate that the gene expression pathway maps are useful tools to notice alteration in different branches of sphingolipid biosynthesis pathway based on microarray and other transcriptomic analysis. The high correlation between gene expression differences and sphingolipid alterations highlights the application of this tool to evaluate molecular changes associate with sphingolipid alterations as well as predict differences in specific metabolites that can be experimentally verified using sensitive approaches such as mass spectrometry. Hence, the combination of different bioinformatics approaches, including protein and DNA sequence analysis, structure modeling and pathway diagrams can provide valuable inputs for biochemical and molecular studies of sphingolipid metabolism.

Appendix A – Tools for gene expression pathway analysis

1) Perl program to extract normalized glycosphingolipid gene expression values

```
!/usr/bin/Perl
# microarray filtering file
use strict;
use warnings;

my $Micro = $ARGV[0];  # Microarray file neme
my $GeneList = $ARGV[1];  # Gene or probelist file


open(MICRO, $Micro)||die"cannot open microarray file\n";
open(LIST, $GeneList)||die"cannot open genelist file\n";


my %hash= ();
while(my $line = <LIST>){


    chomp($line);
    my @words = split(/\t/,$line);
    my $id = $words[0];
    $hash{$id} = 0;

}

my @keys = keys(%hash);

my $num = @keys;

while(my $gene = <MICRO>)
{
   chomp($gene);
    for(my $i=0; $i < $num; $i++)
    {

      my $key = $keys[$i];
      chomp($key);
        if ($gene =~ m/$key/i)
        {
          print "$gene \n";

        }

     }
}

close(MICRO);
close(LIST);
```

Instructions for using Perl program for filtering sphingolipid genes: on windows PC install the Activeperl package from www.activestate.com (Perl is already installed on Mac OS in the X-terminal). Copy and paste the above script in text editor (notepad) and save it as 'genefilter.pl' in a separate folder. Next copy and paste the list of gene IDs and probe IDs into separate text file and save them as 'shingogene.txt' or 'sphingoprobe.txt' in the same folder as the Perl script. Save the normalized microarray dataset with gene expression values and gene ID or affymetrix probe IDs in a tab delineated text file in the folder along with the gene/probe list and the Perl script. To filter the sphingolipid related gene expression values from all the microarray gene probes run the Perl script on the command line (as shown in the figure below for windows PC).

'c:\perl> perl genefilter.pl microarrayfile.txt sphingogene.txt > microarraysphingo.txt'

The script generates an output text file 'microarraysphingo.txt' with the selected sphingolipid gene expression values, which is used to prepare pathvisio input dataset file.

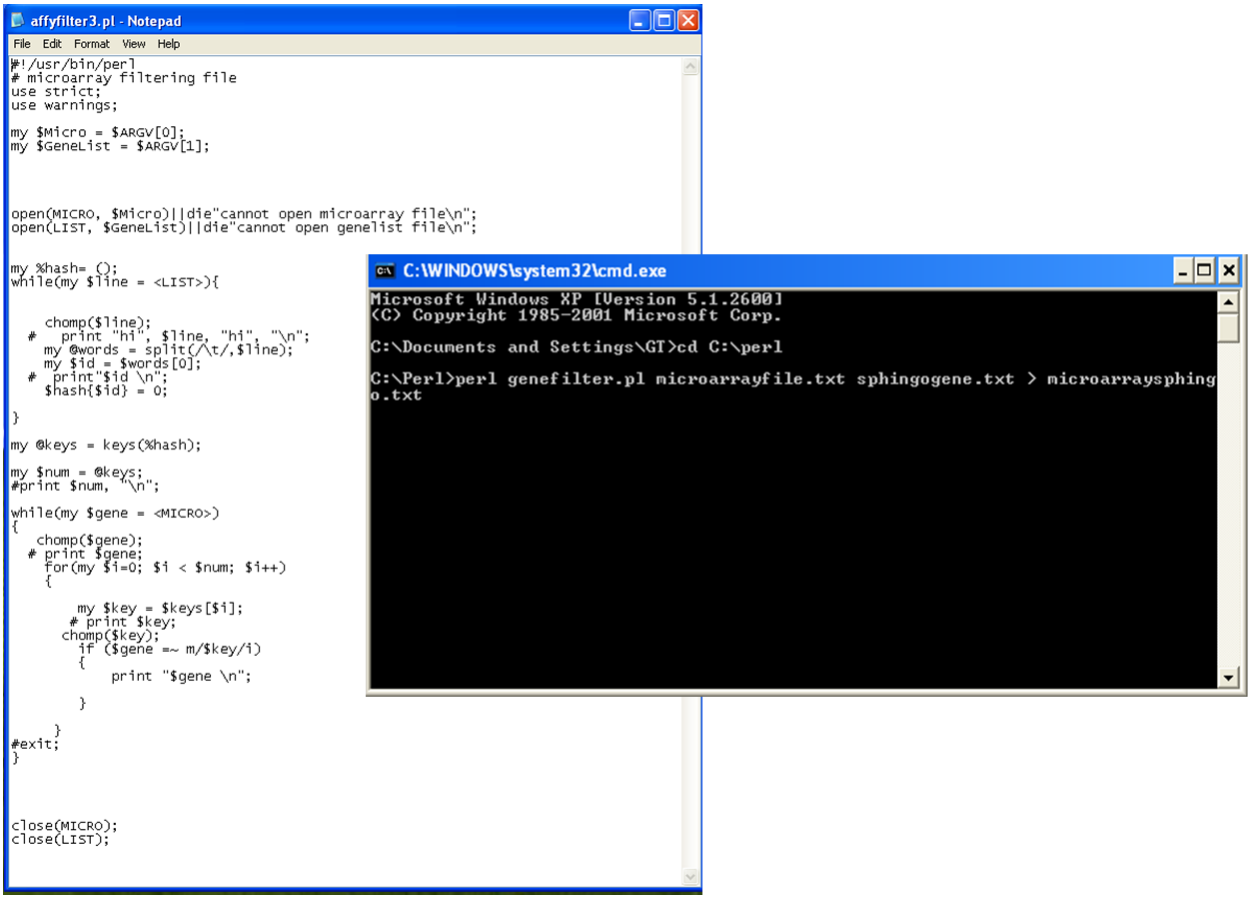

2) Gene list and preselected probe IDs for Affymetrix HG-U133 plus2

A user may use either gene list or preselected probe ids to extract gene expression information

Gene Symbol	Probe Set ID
A4GALT	219488_at
ABO	214504_at
AGA	204332_s_at
AOAH	205639_at
ASAH1	1555419_a_at
B3GALNT2	1562391_at
B3GALT1	222969_at
B3GALT2	210121_at
B3GALT4	210205_at
B3GALT5	206947_at
B3GALT6	1553959_a_at
B3GNT1	203188_at
B3GNT2	219326_s_at
B3GNT3	204856_at
B3GNT4	221240_s_at
B3GNT5	1554835_a_at
B3GNT6	1552833_at
B3GNT7	1552965_a_at
B3GNT8	237338_at
B4GALNT1	206435_at
B4GALNT2	1552903_at
B4GALNT3	1553727_at
B4GALNT4	238080_at
B4GALT1	216627_s_at
B4GALT2	209413_at
B4GALT3	210243_s_at
B4GALT4	210540_s_at
B4GALT6	206232_s_at
BGLAP	206956_at
CERK	218421_at

CERKL	243366_s_at
ELOVL1	218028_at
ELOVL2	220029_at
ELOVL3	234513_at
ELOVL4	219532_at
ELOVL5	208788_at
ELOVL6	210868_s_at
FUT1	206109_at
FUT10	235472_at
FUT11	238551_at
FUT2	208505_s_at
FUT9	207696_at
FVT1	202419_at
GAL3ST1	205670_at
GAL3ST2	1553046_s_at
GAL3ST3	1553257_at
GAL3ST4	219815_at
GALNT2	217787_s_at
GBGT1	231780_at
GCNT1	205505_at
GLA	214430_at
GM2A	209727_at
GM2A_1	215890_at
HEXA	1559932_at
HEXB	201944_at
LASS1	229448_at
LASS2	222212_s_at
LASS3	1554253_a_at
LASS4	218922_s_at
LASS5	224951_at
LASS6	242019_at
NAGA	202943_s_at
PHCA	222688_at

PPAP2A 209147_s_at

PPAP2B 232324_x_at

PPAP2C 209529_at

SGPL1 212322_at

SGPP2 244780_at

SMPD1 209420_s_at

SMPD1_2 217171_at

SMPD3 231732_at

SMS 202043_s_at

SPHK1 219257_s_at

SPHK2 209857_s_at

SPTLC1_2 1554053_at

SPTLC1 202278_s_at

SPTLC2 203127_s_at

SPTLC2_1 203128_at

SPTLC2_2 216203_at

SPTLC3_2 220456_at

SPTLC3 227752_at

ST3GAL1 208322_s_at

ST3GAL2 205346_at

ST3GAL3 1555171_at

ST3GAL4 203759_at

ST3GAL5 203217_s_at

ST3GAL6 213355_at

ST6GAL1 214971_s_at

ST6GAL2 1555123_at

ST6GALNAC1 227725_at

ST6GALNAC2 204542_at

ST6GALNAC3 235334_at

ST6GALNAC4 228163_at

ST6GALNAC5 220979_s_at

ST6GALNAC6 222571_at

ST8SIA1 210073_at

ST8SIA5 206258_at

TRAM2 1554383_a_at

UGCG 204881_s_at

UGT8 208358_s_at

COL4A3BP 223466_x_at

ASAH3 1553929_at

FUT3 216010_x_at

SLC33A1 203164_at

B3GALNT1 223374_s_at

A3GALT2

ASAH2 231791_at

DEGS1 209250_at

DEGS2 236496_at

SGMS1 212989_at

SGMS2 242963_at

3) Application of data to Pathvisio

Formatting the input file

Gene expression data for sphingolipid specific genes extracted with the perl Script (Supplement 1A) should be formatted into a pathvisio input file with three essential columns and saved as a comma separated file (.csv). An example is given below

GeneID	SystemCode	Fold
1552833_at	X	-1.143967291
1552903_at	X	1.010328449
1552965_a_at	X	1.422851697
1553046_s_at	X	1.220136212
1553257_at	X	1.113669687
1553727_at	X	4.407868628
1553959_a_at	X	1.83540546
1554053_at	X	-2.338778491
1554253_a_at	X	1.068452133
1554383_a_at	X	1.139011527
1554835_a_at	X	2.045004684
1555123_at	X	2.645276048
1555171_at	X	-1.123596112
1555419_a_at	X	-2.284137975

GeneID is the gene identifier or probe ID

SystemCode -- type of gene identifier

Fold – the calculated fold change for the specific gene probe.

Further information about the tile format can be obtained from www.pathvisio.org

Instruction of download of maps from wikipathways

Visit www.wikipathways.org

Browse for pathway and click for Sphingolipid metabolism

In the download link select PathVisio (.gmpl)

Save the pathway maps in a folder in the pathvisio directory

Creating Pathway diagrams with expression data in Pathvisio.

Open the pathway map in Pathvisio browser

Create a expression data using formatted expression file

In the menu select Data → Import expression data

Select the 'input file' (previously prepared .csv file) and 'output file'

Follow the steps by clicking next

Choose data delimiter → 'comma' , Next

Select 'systemcode' then Next

Visualization of expression values

Select the dataset Data → 'select expression data'

Select Data → 'visualization options'

Define the color criteria

After the completion the map should be colored according to the selected criteria.

For further details about the steps one can refer the Pathvisio user tutorial at www.pathvisio.org

Appendix B Sphingolipid Pathway maps for NCI60 cell panel

The fold change was for individual genes in cell lines were determined by taking a ratio of the gene expression values and the average expression of the gene among all 60 cell lines.

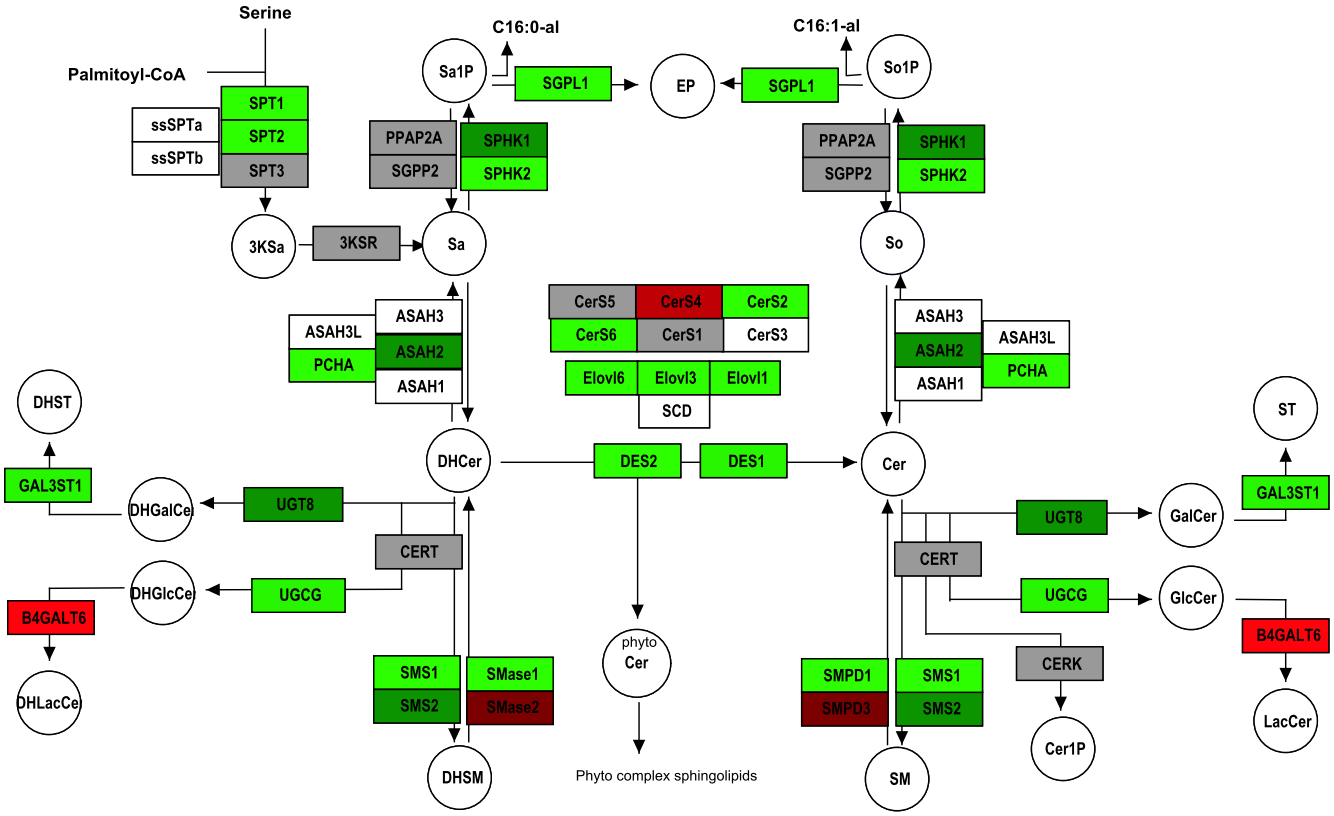

1: CCRF_CEM

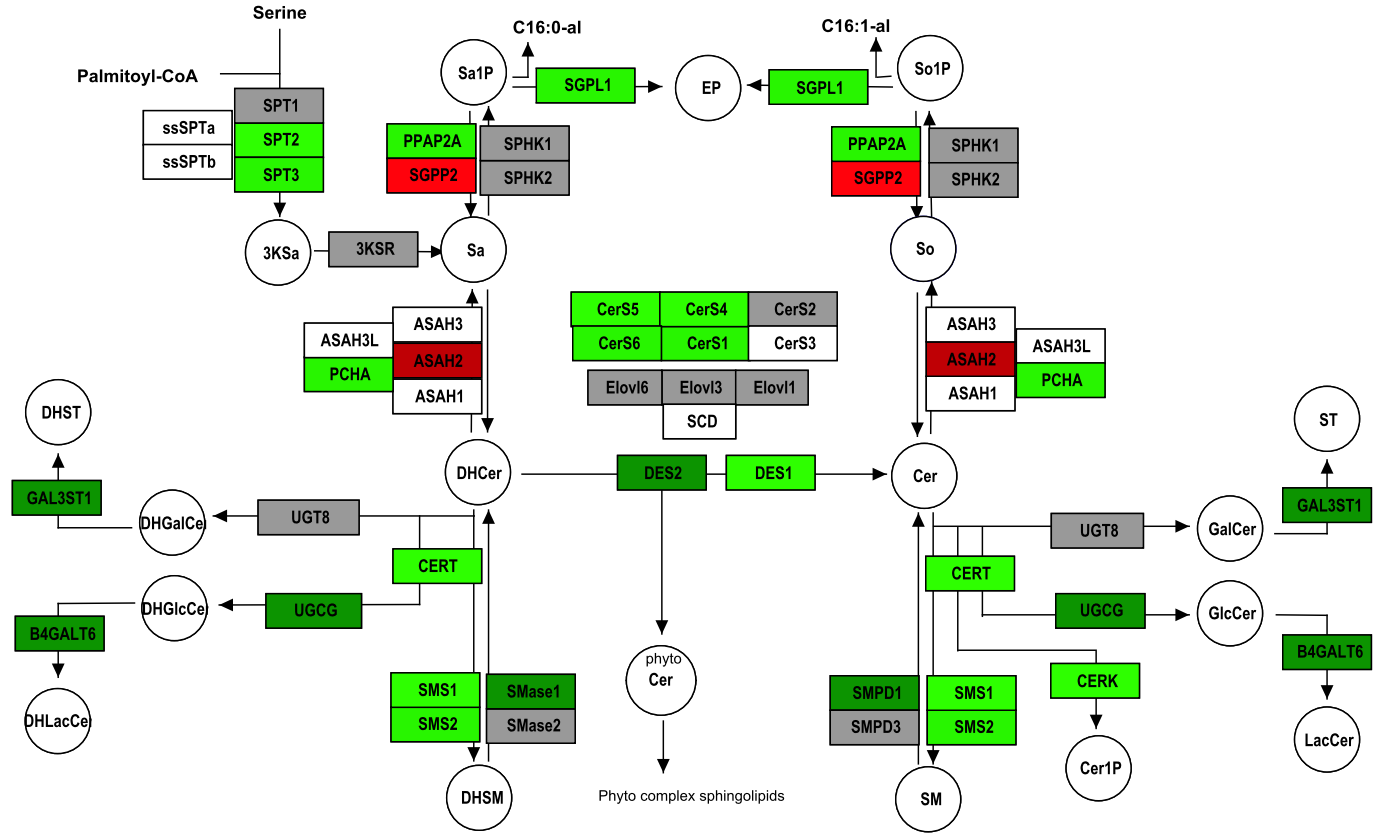

2: HL_60

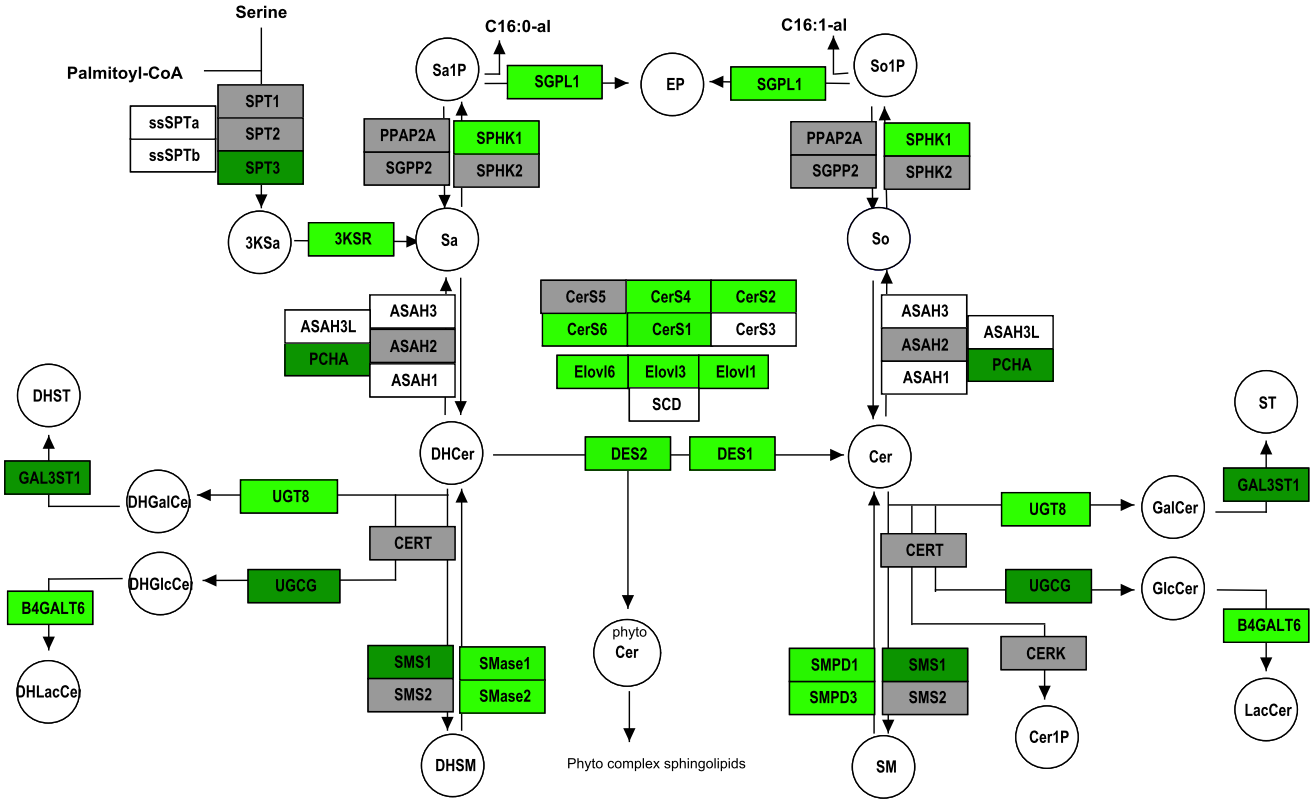

Sf 3: MOLT_4

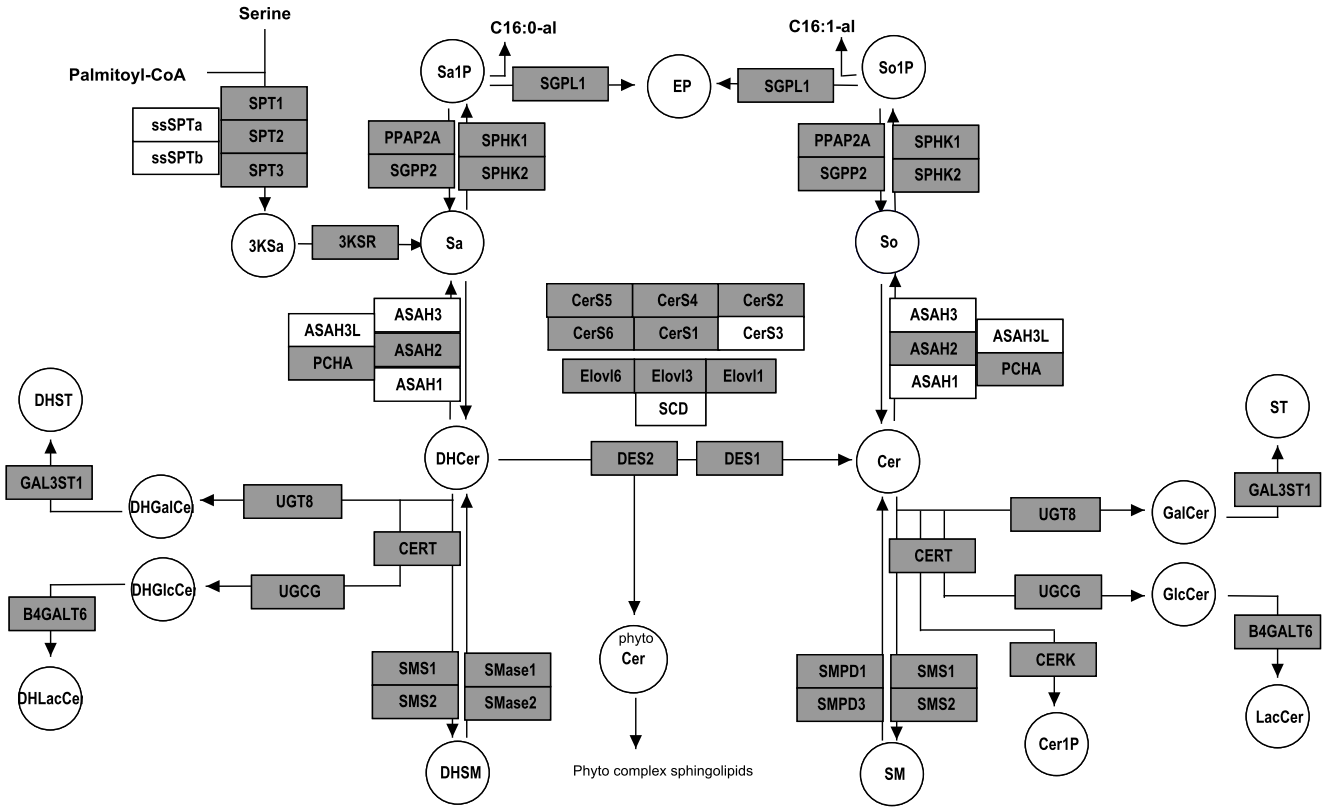

Sf 4: RPMI_8226

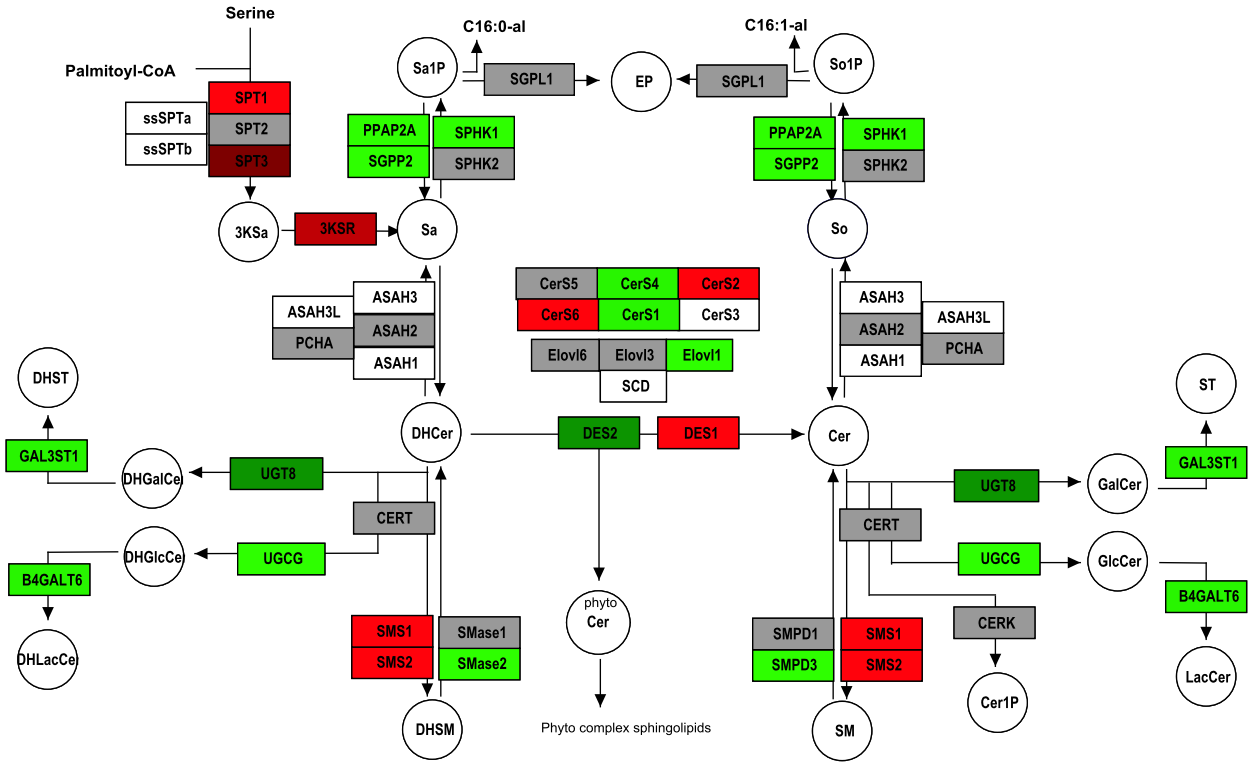

Sf 5: SR

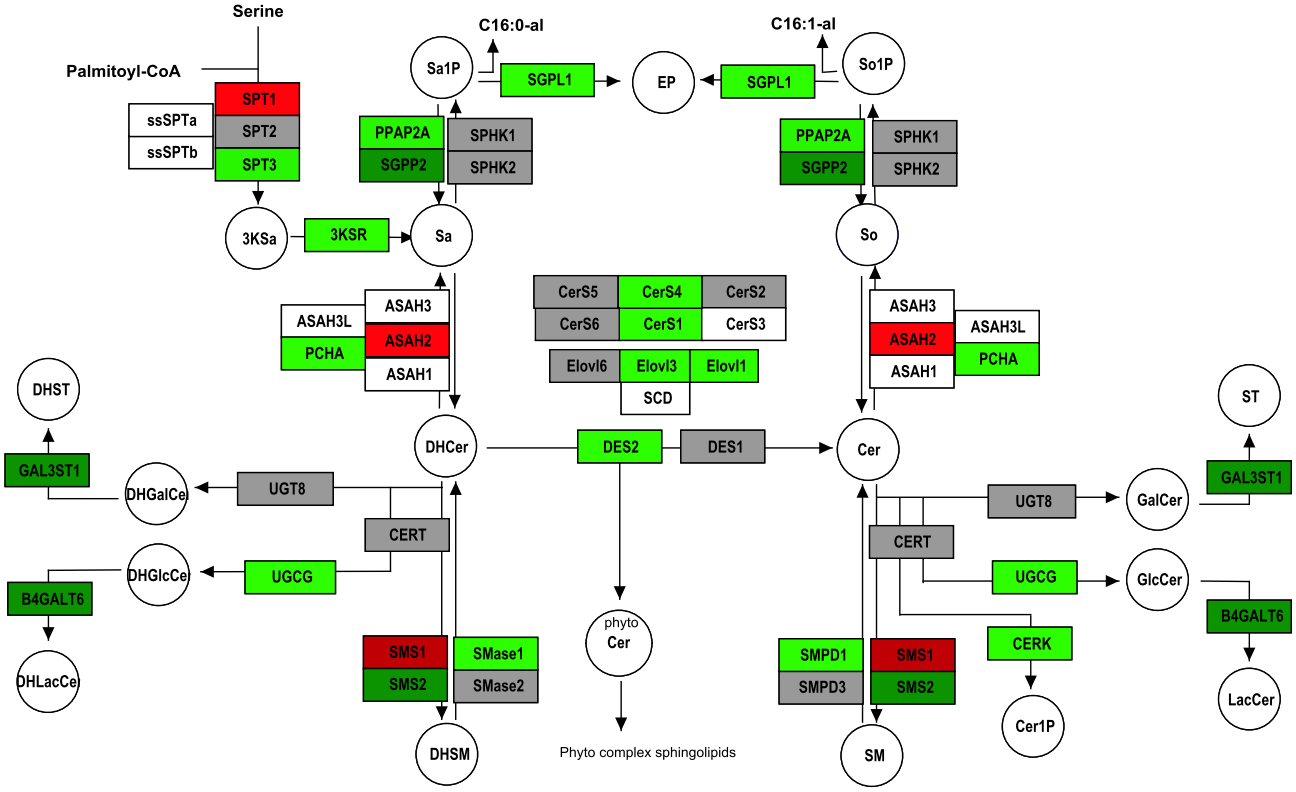

Sf 6: K_562

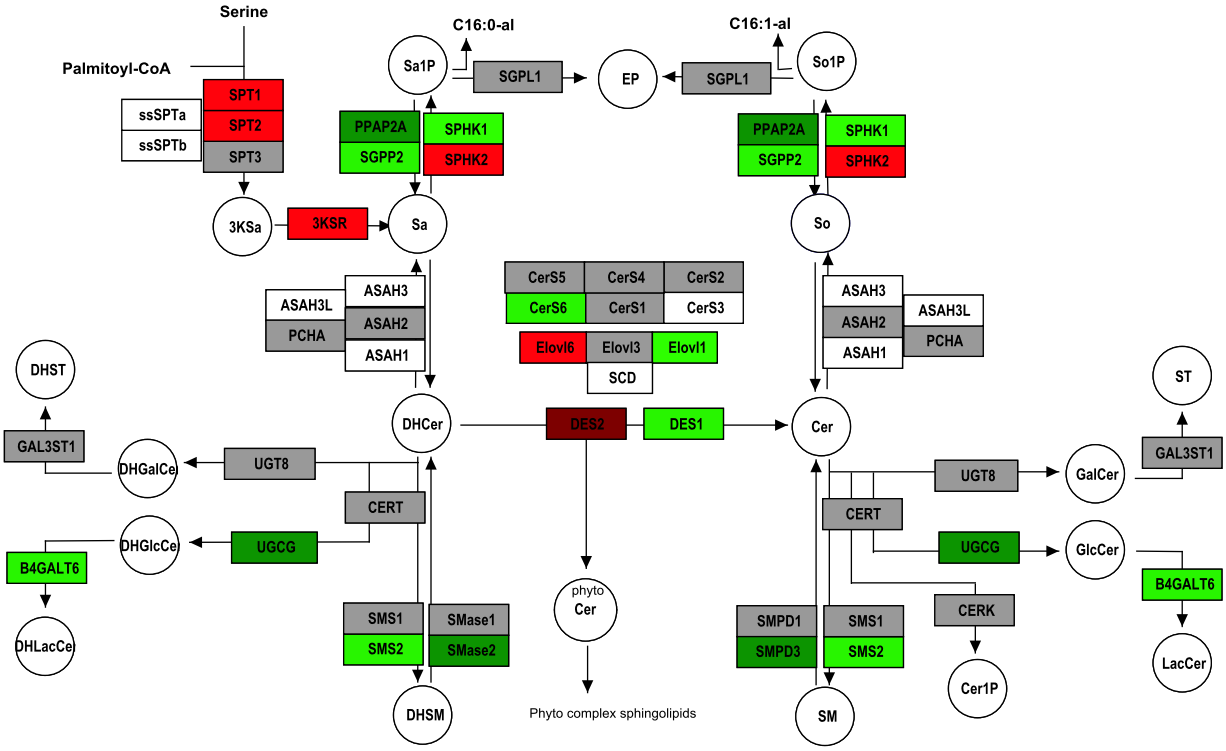

Sf 7: MCF_7

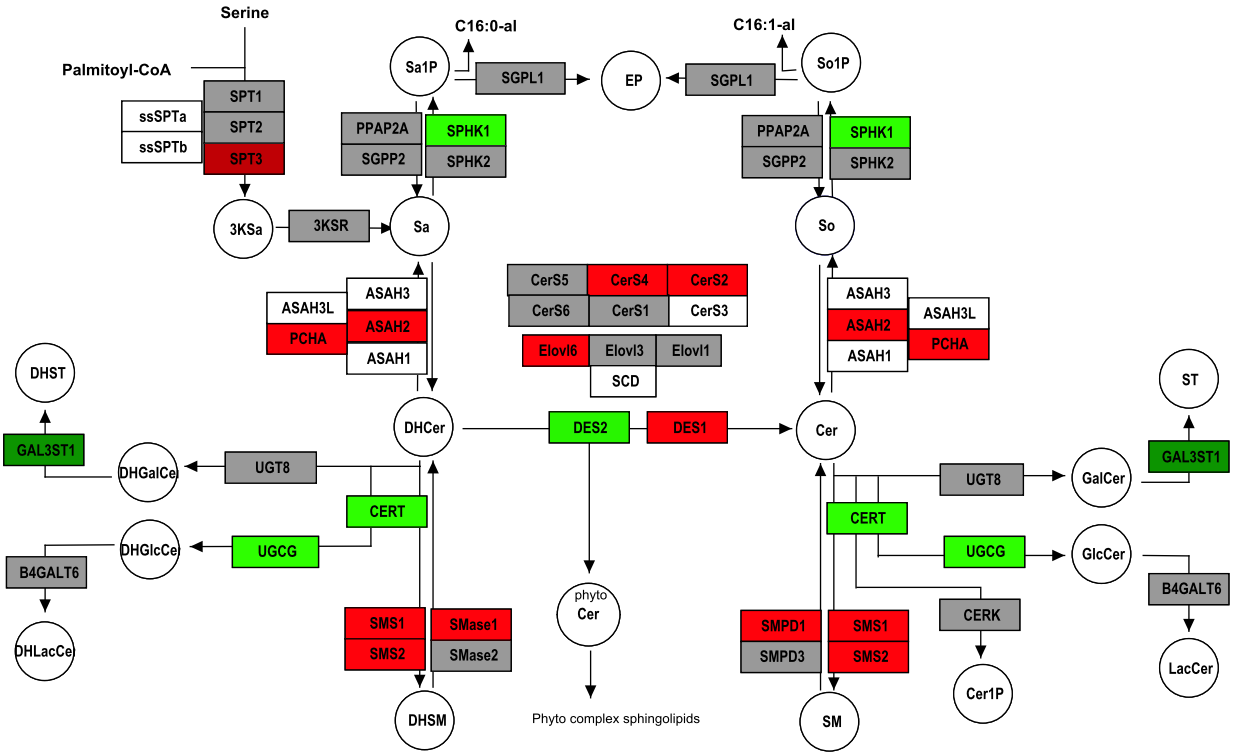

Sf 8: MDA_MB_231

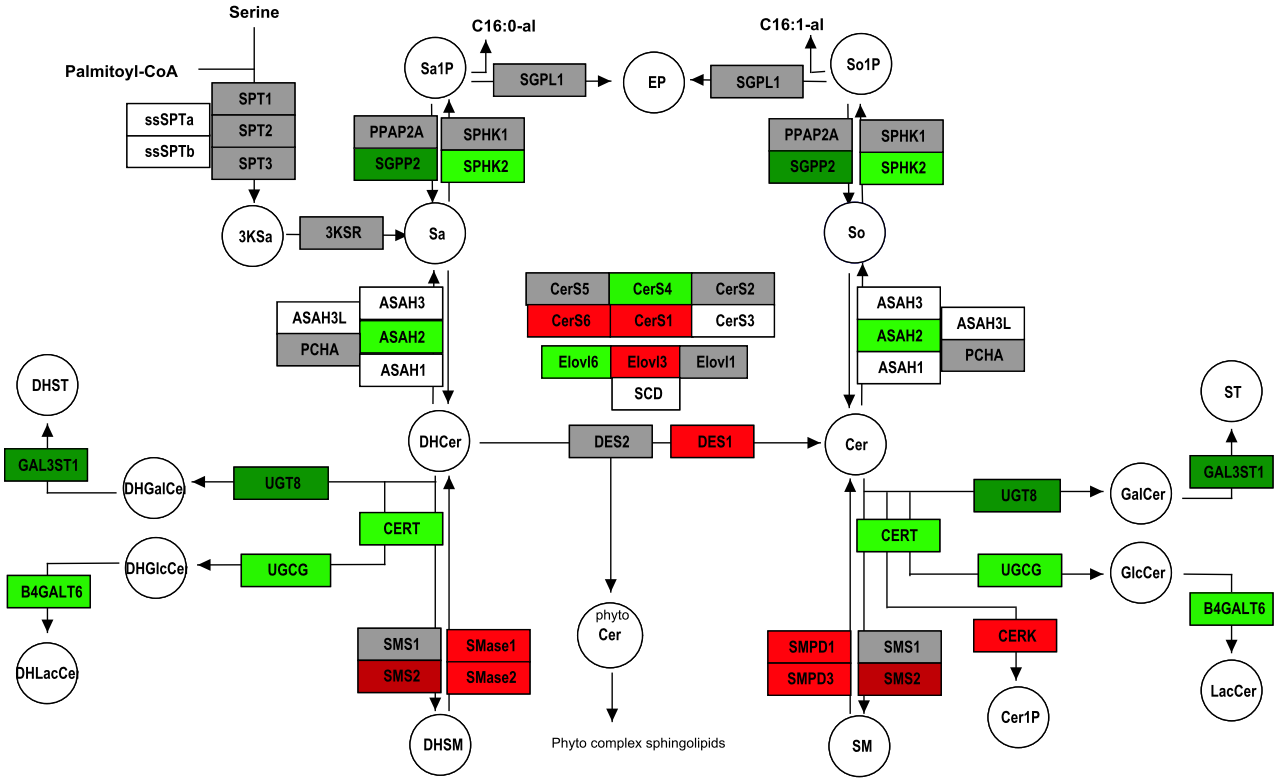

Sf 9: HS578T

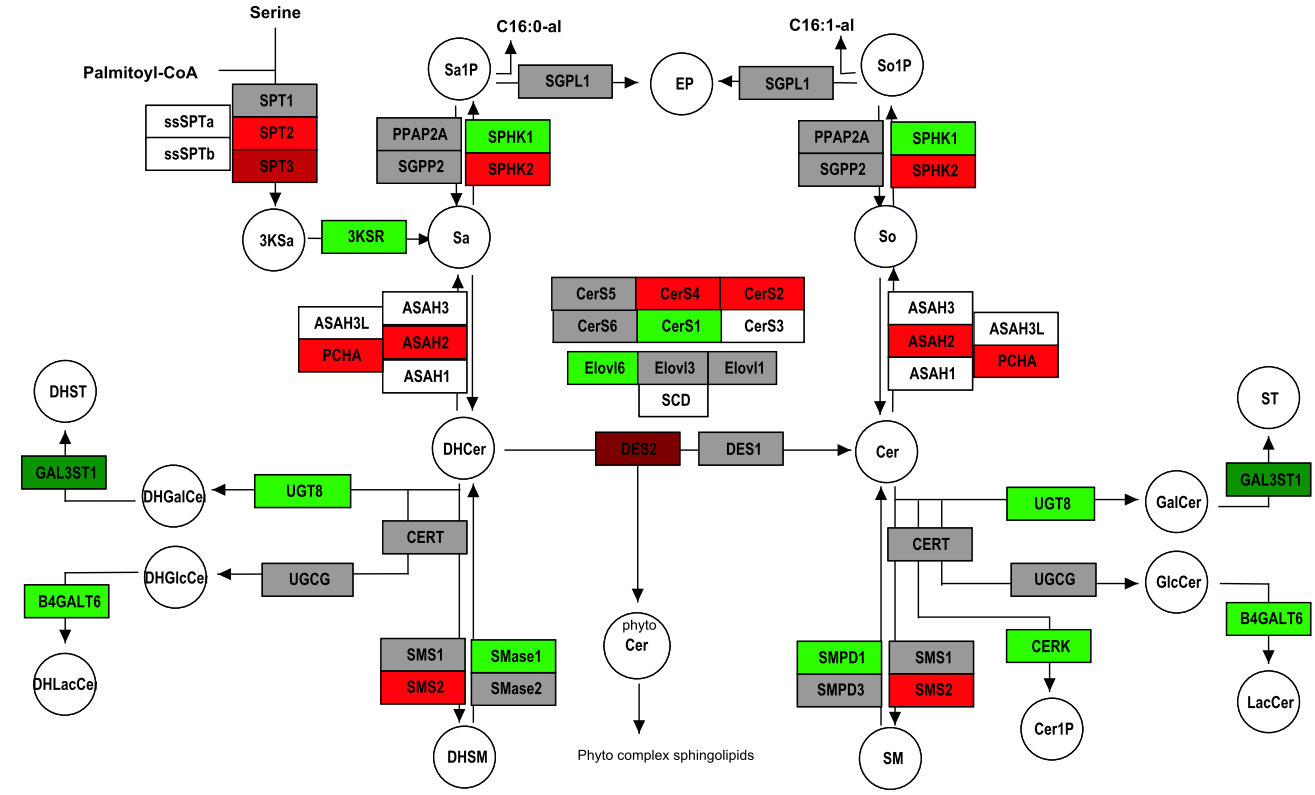

Sf 10: T47D

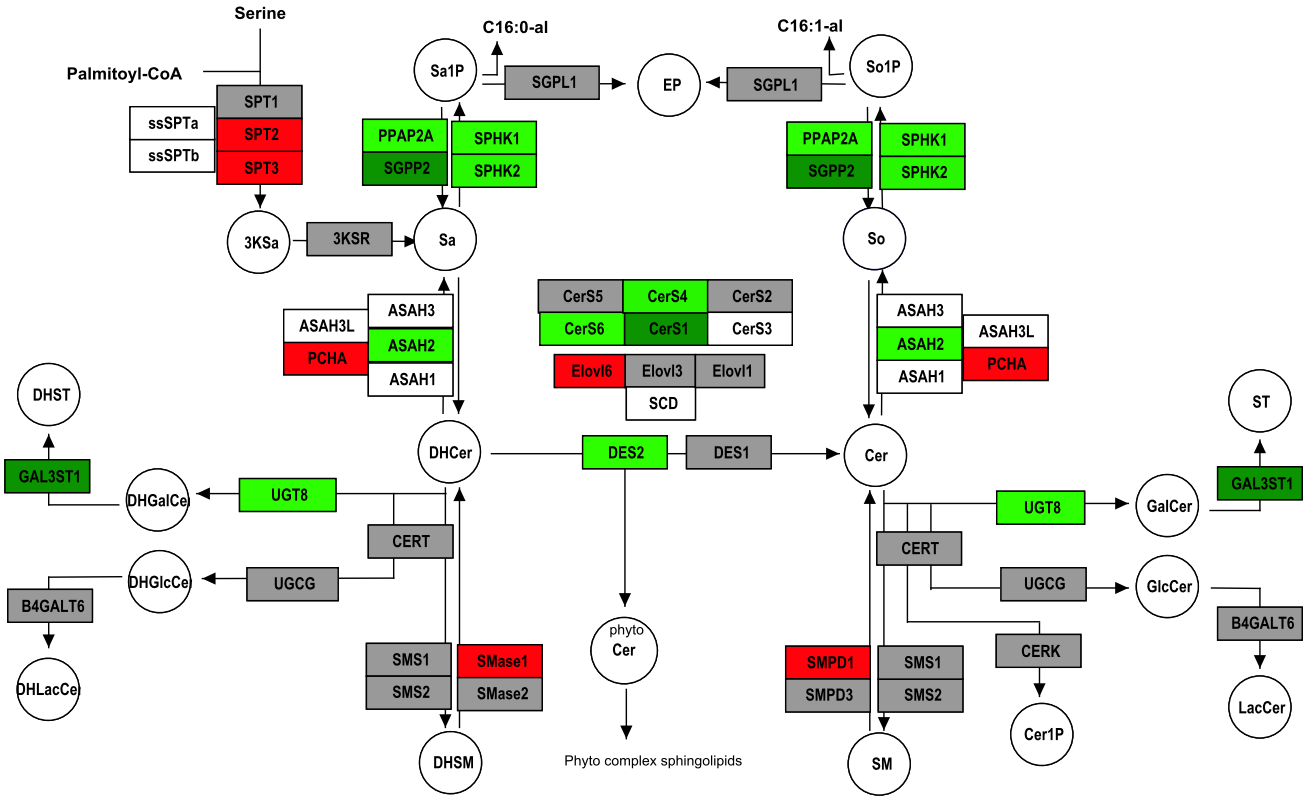

Sf 11: SF_268

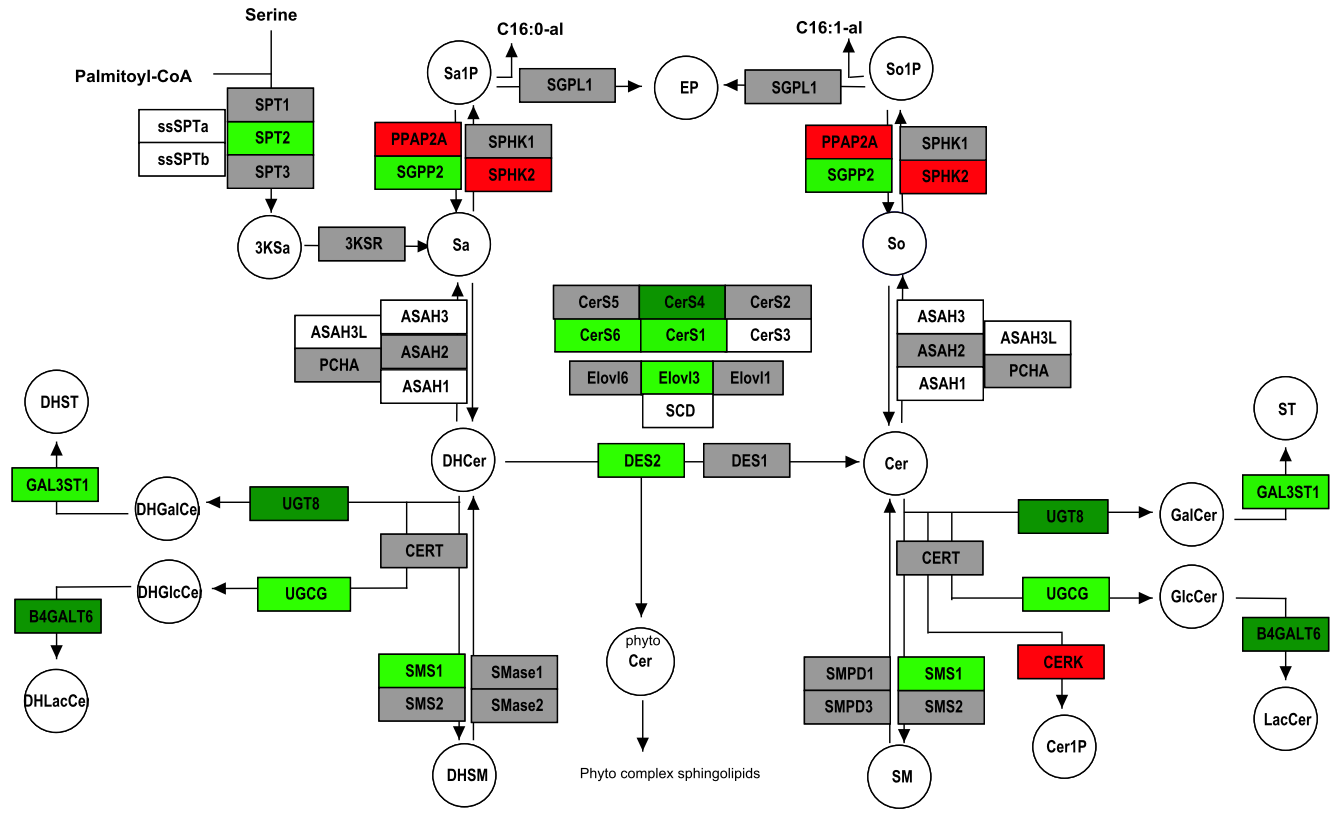

Sf 12: SF_295

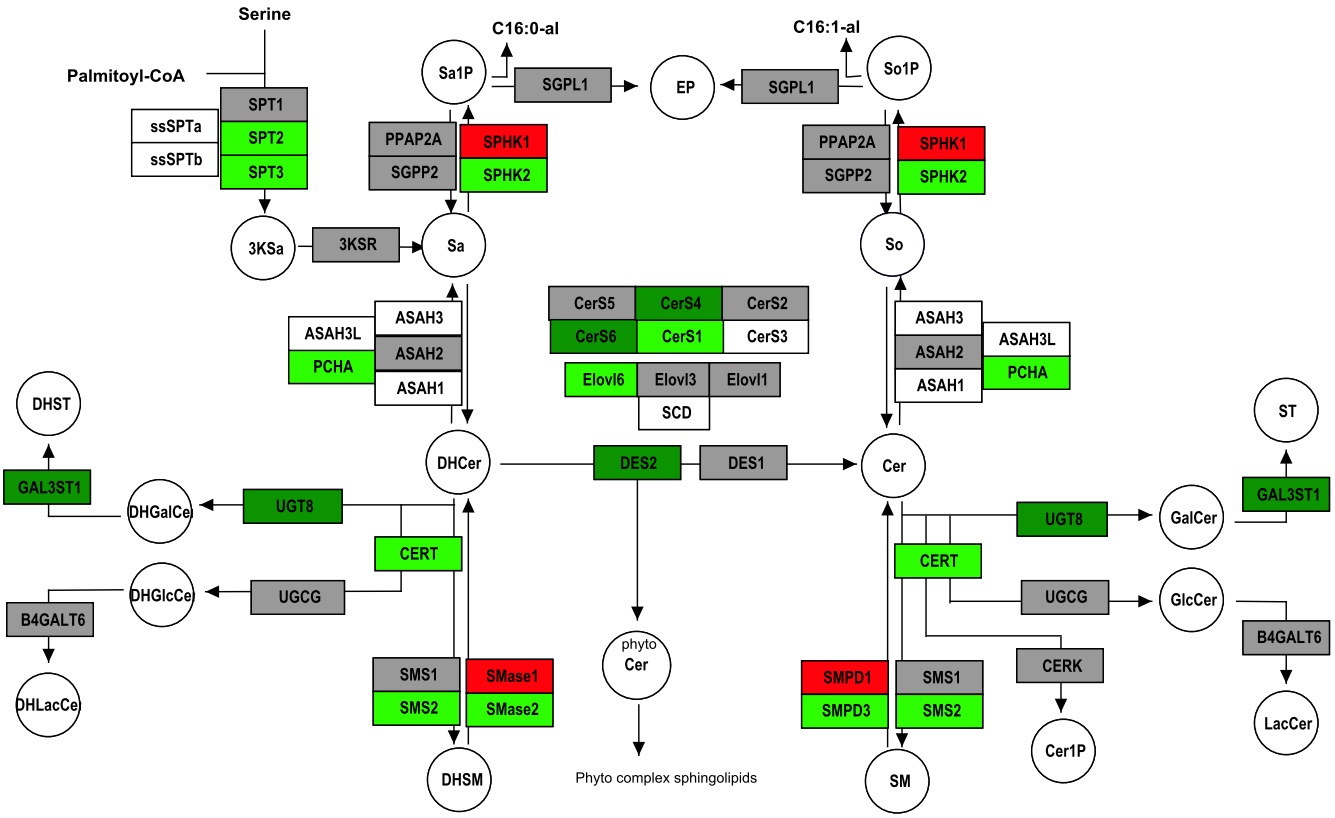

Sf 13: SF_539

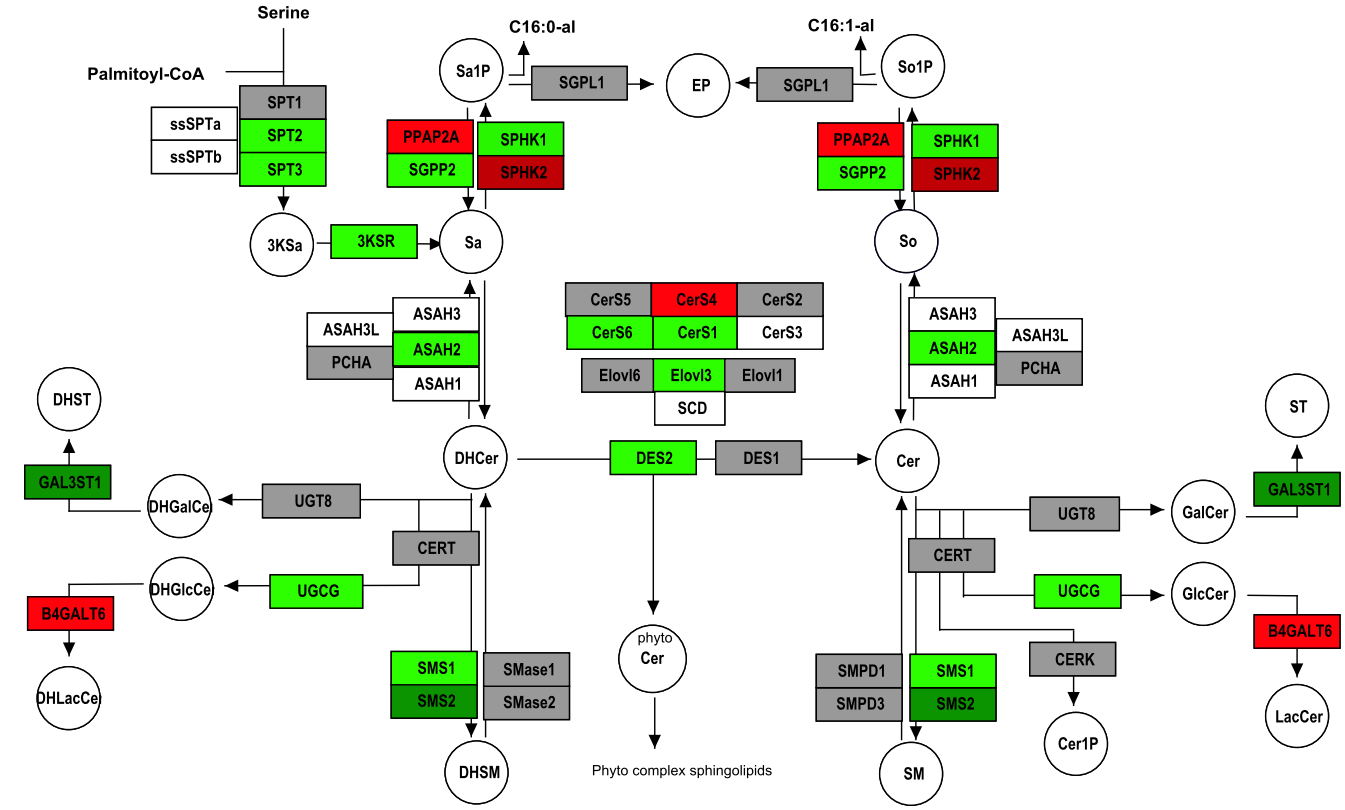

Sf 14: SNB_19

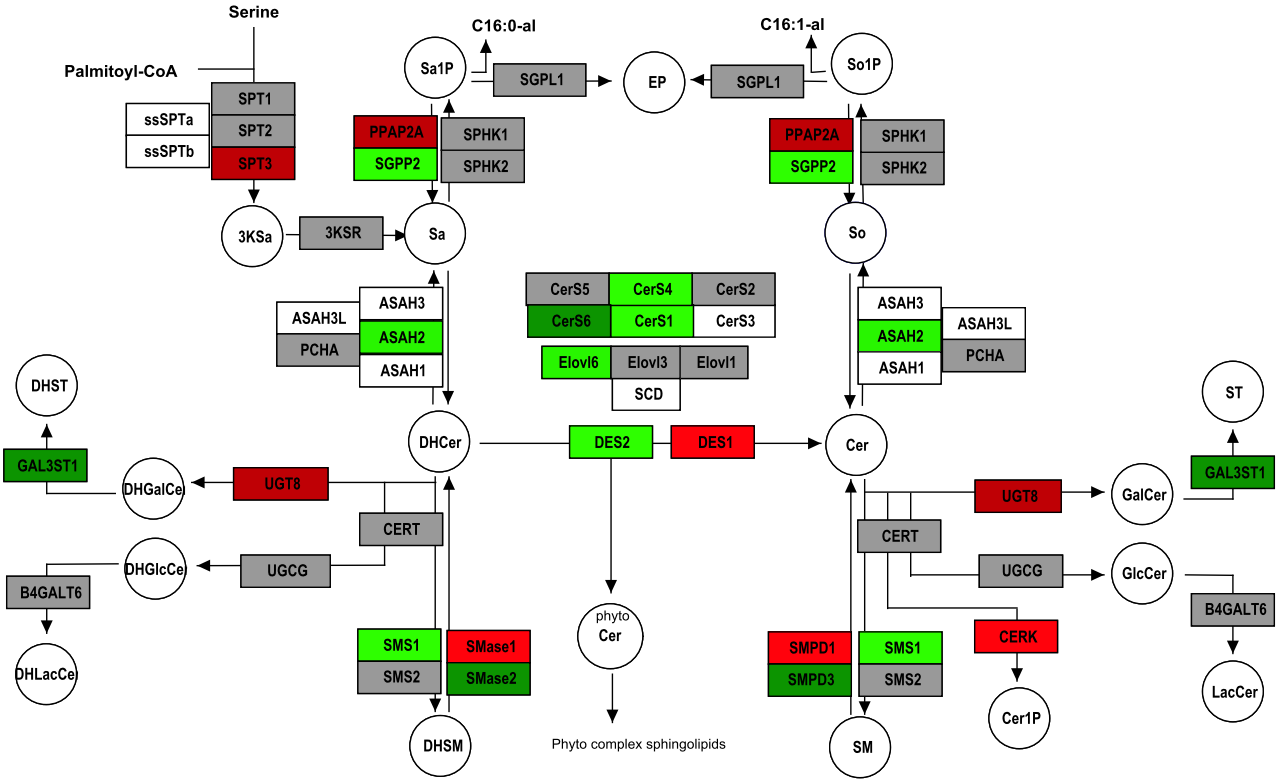

Sf 15: SNB_75

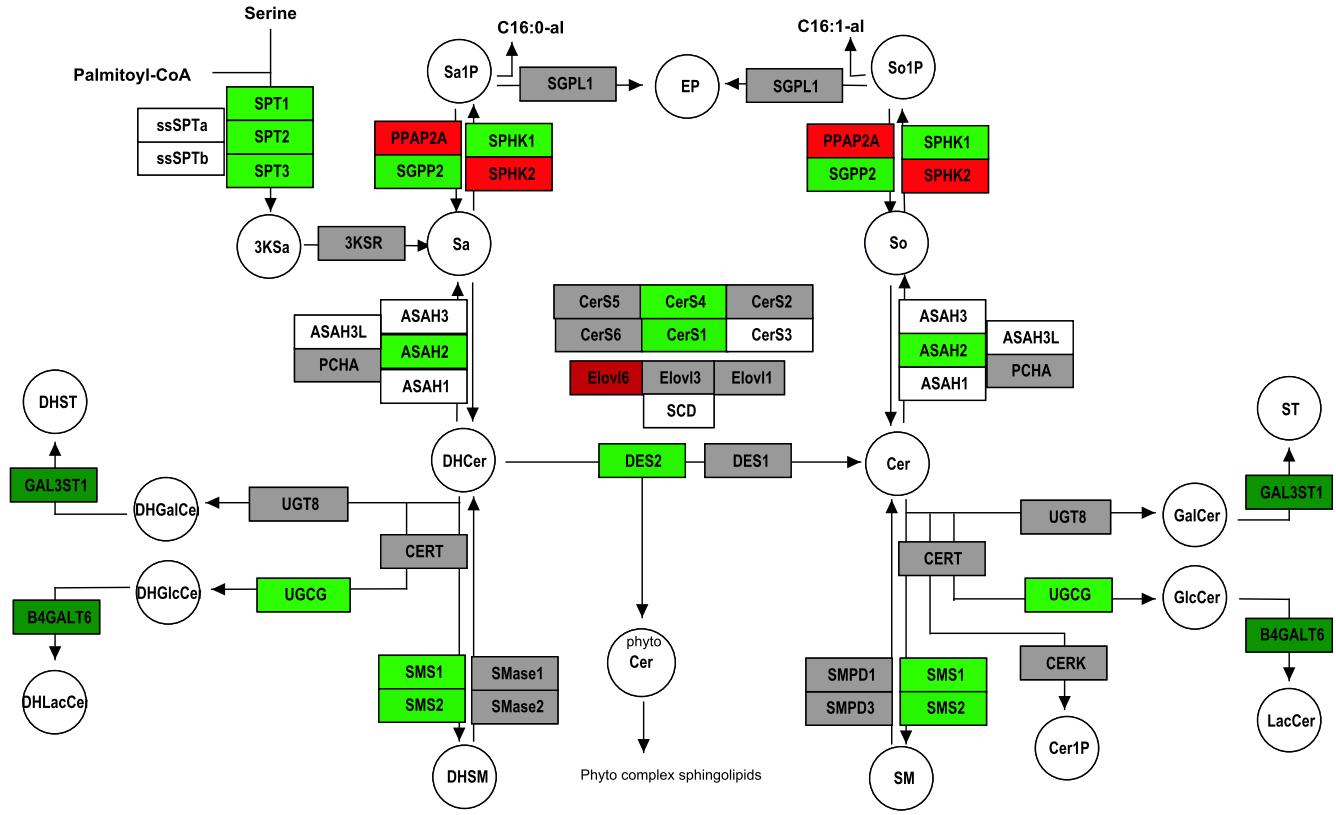

Sf 16: U251

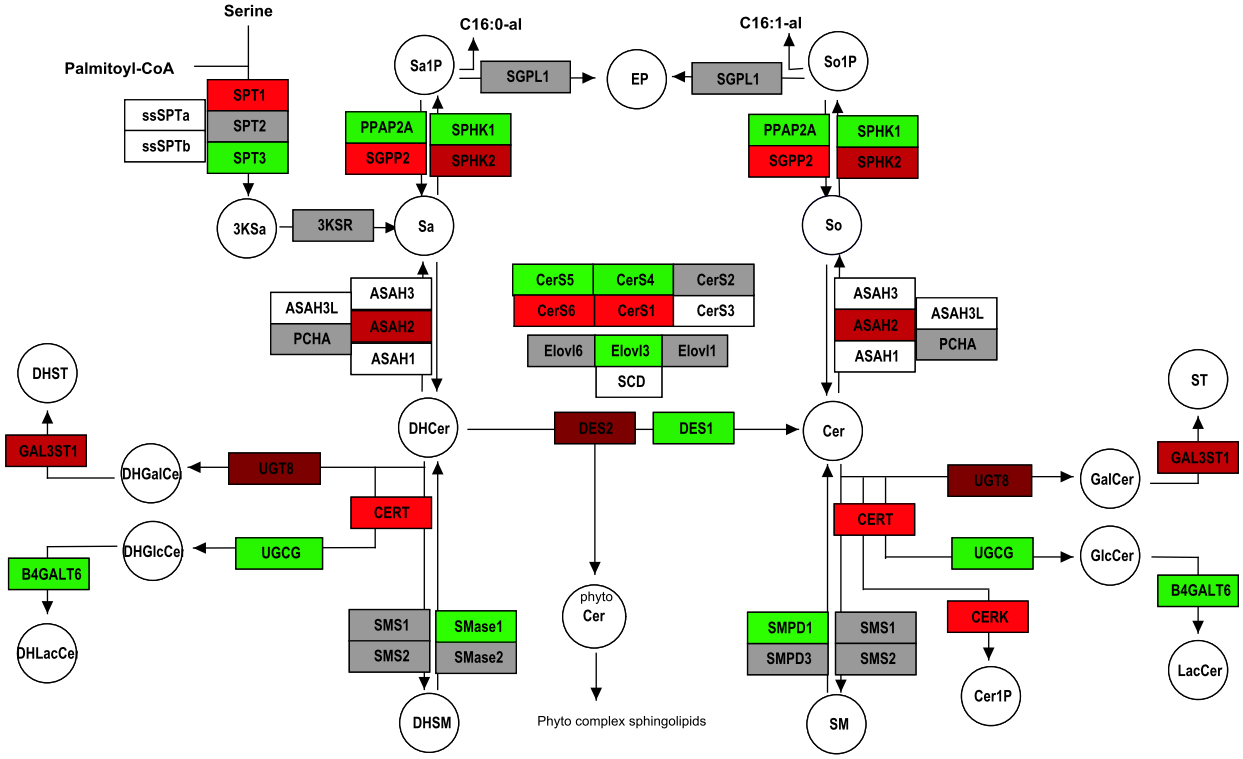

Sf 17: COLO205

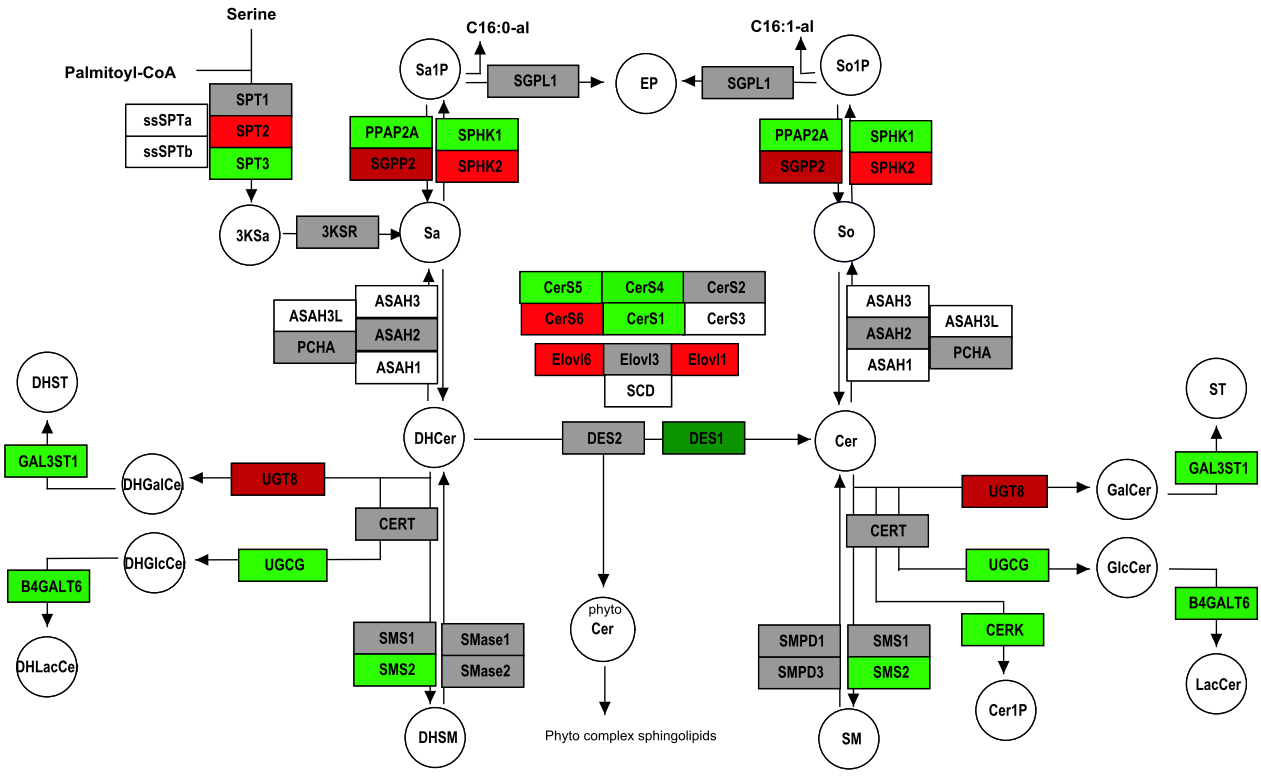

Sf 18: HCC_2998

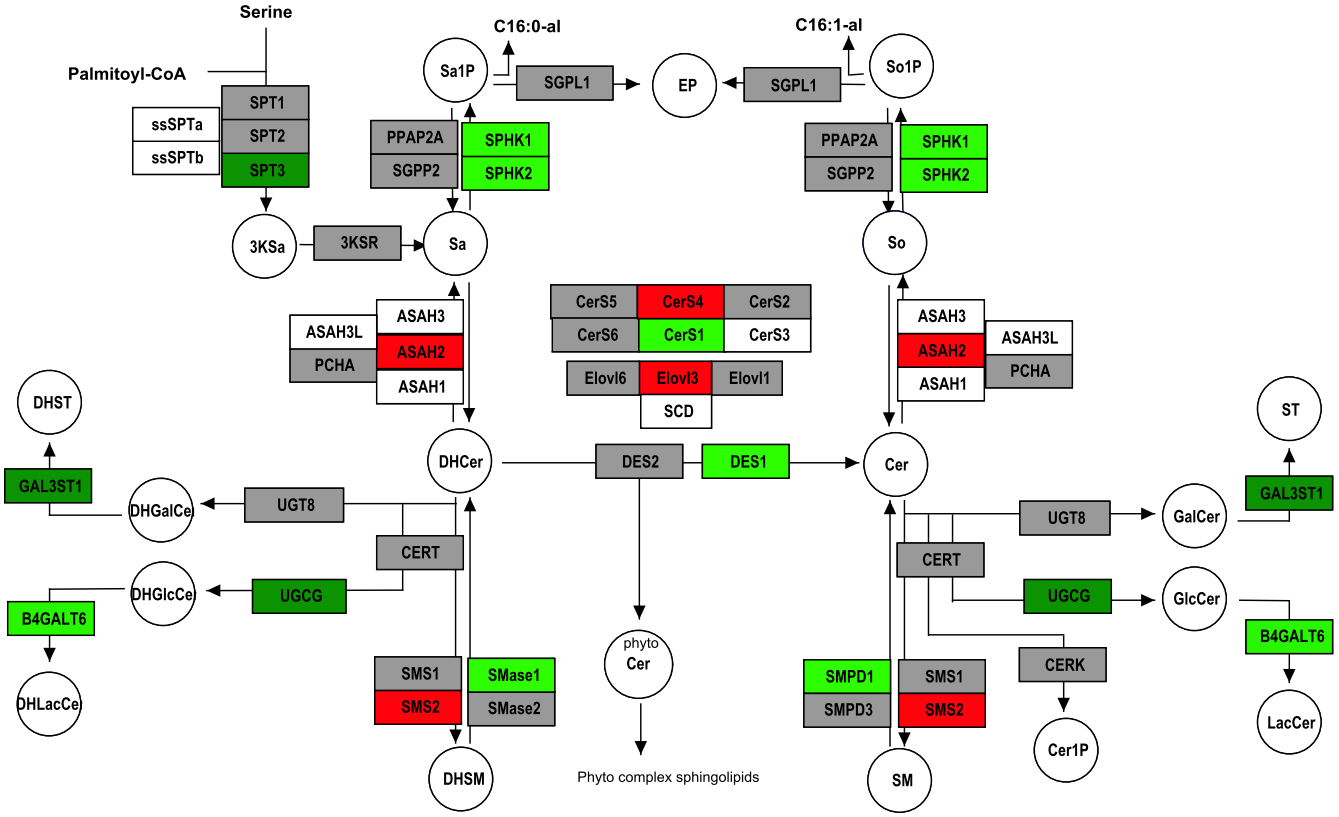

Sf 19: HCT_116

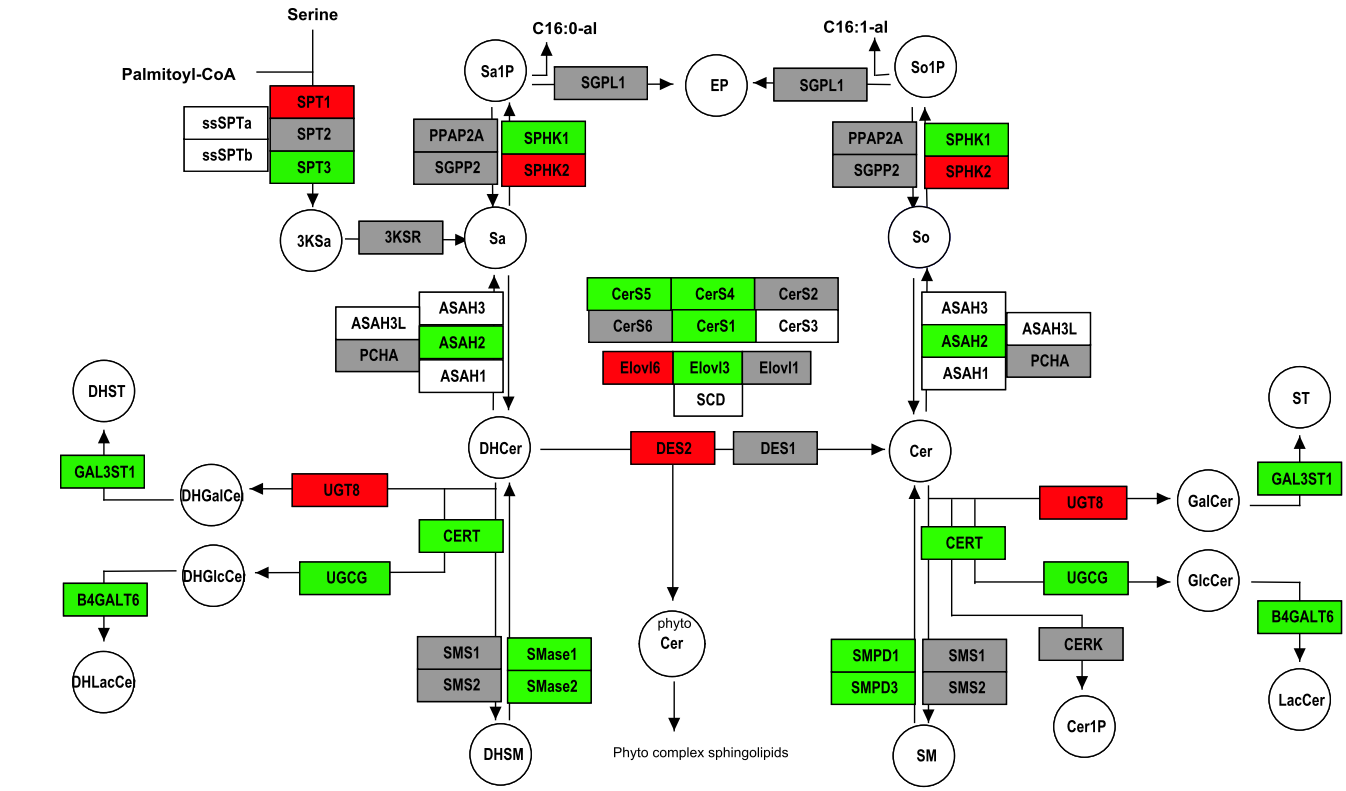

Sf 20: HCT_15

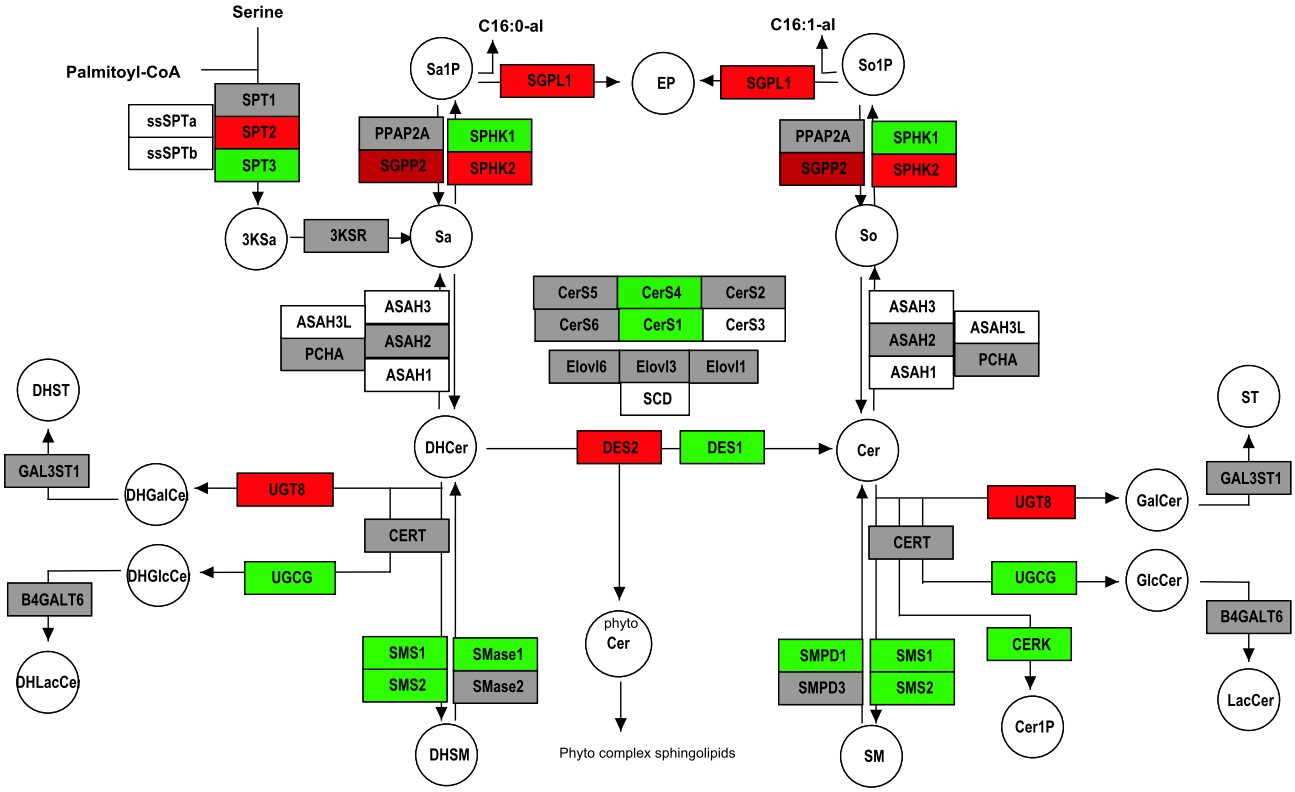

Sf 21: HT29

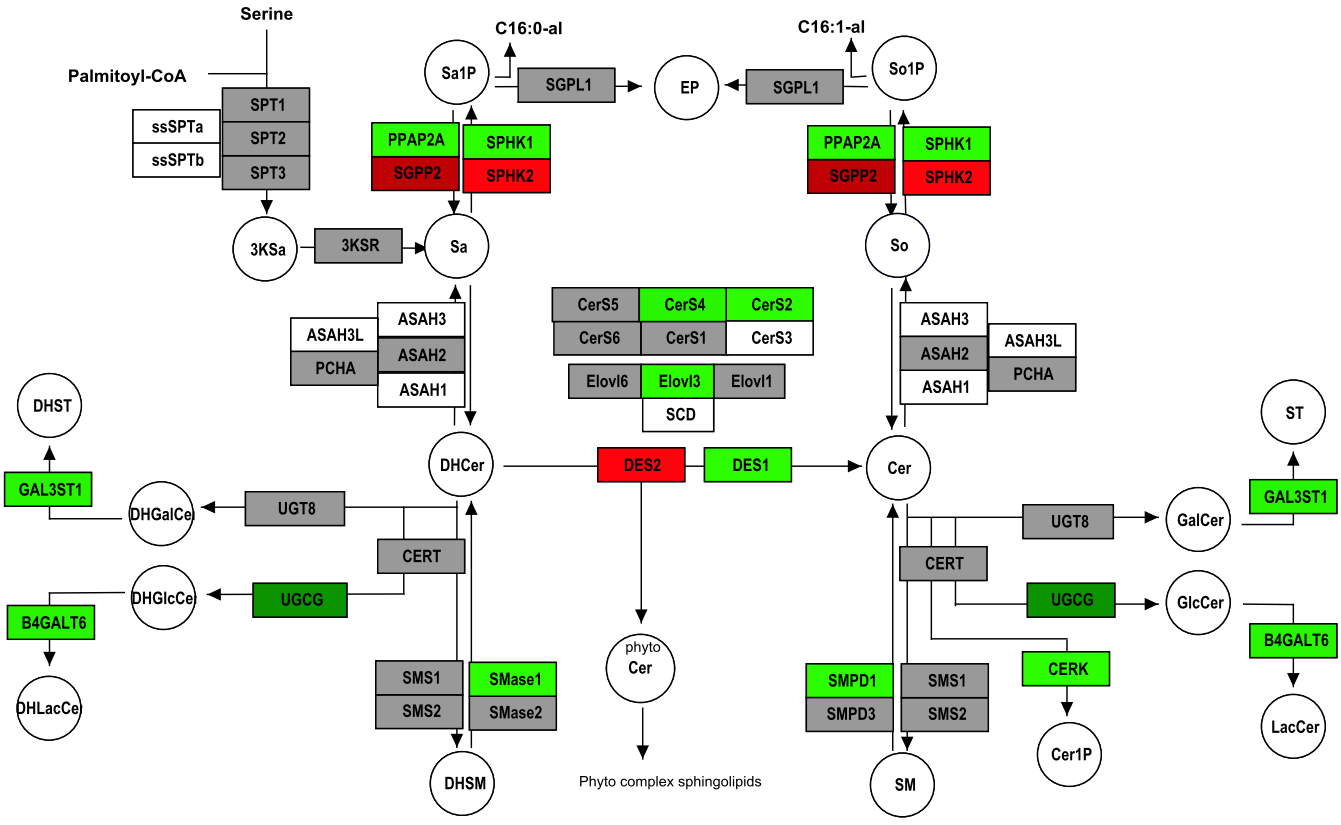

Sf 22: KM12

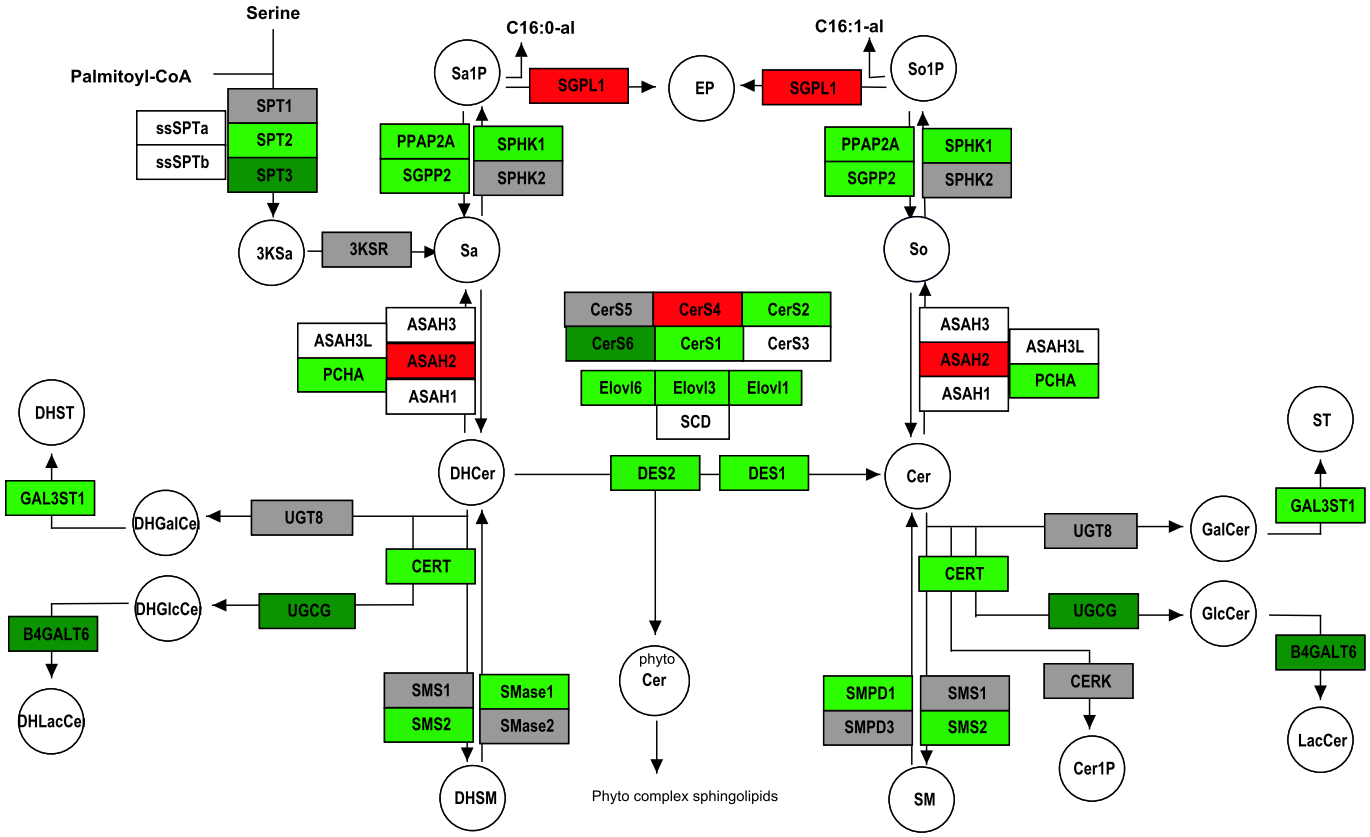

Sf 23: SW_620

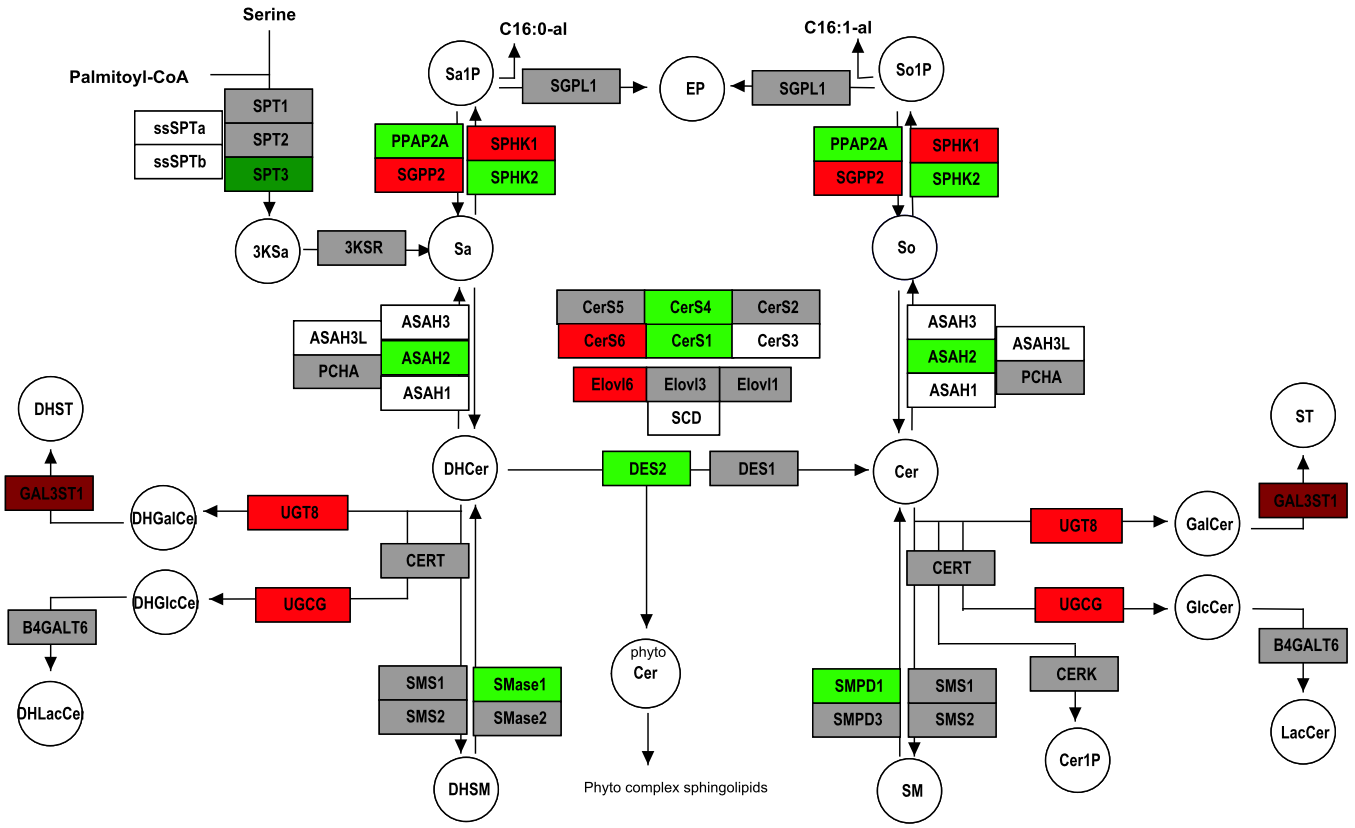

Sf 24: 786_0

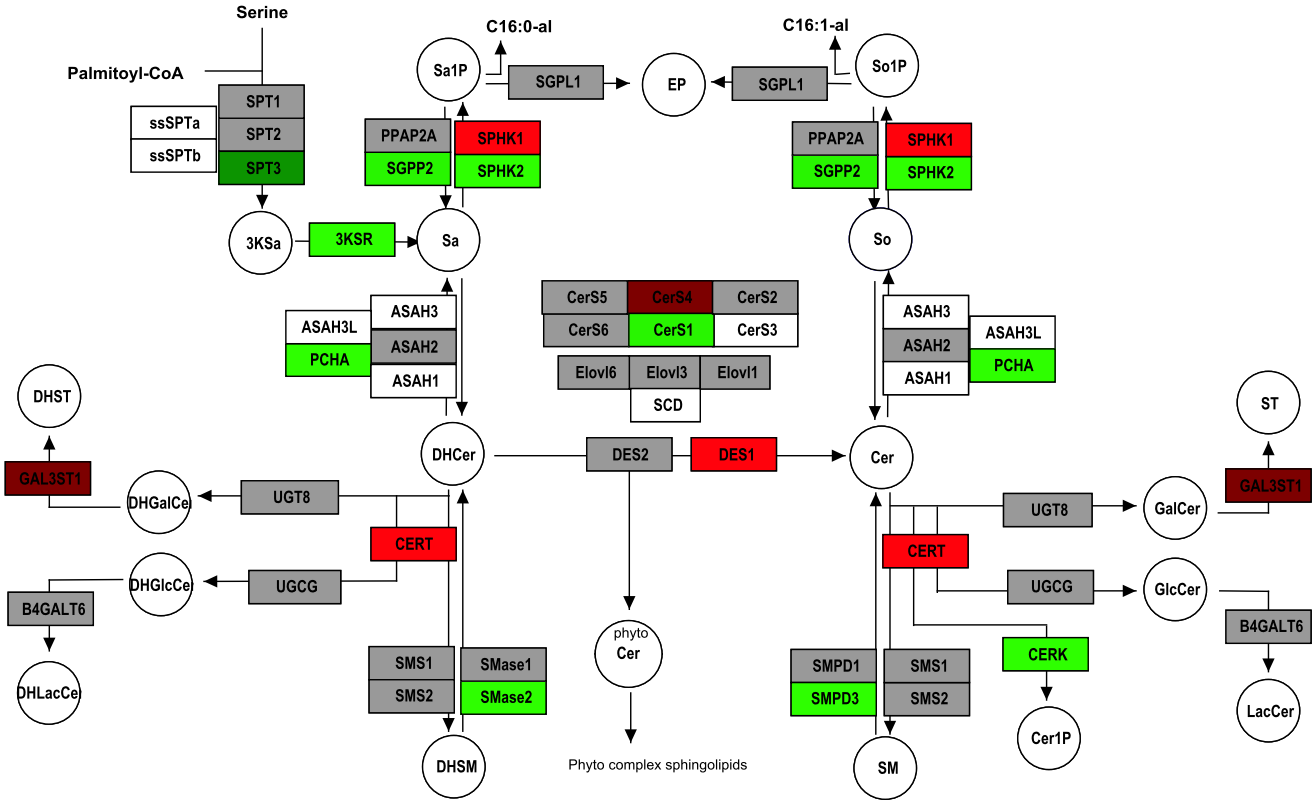

Sf 25: A498

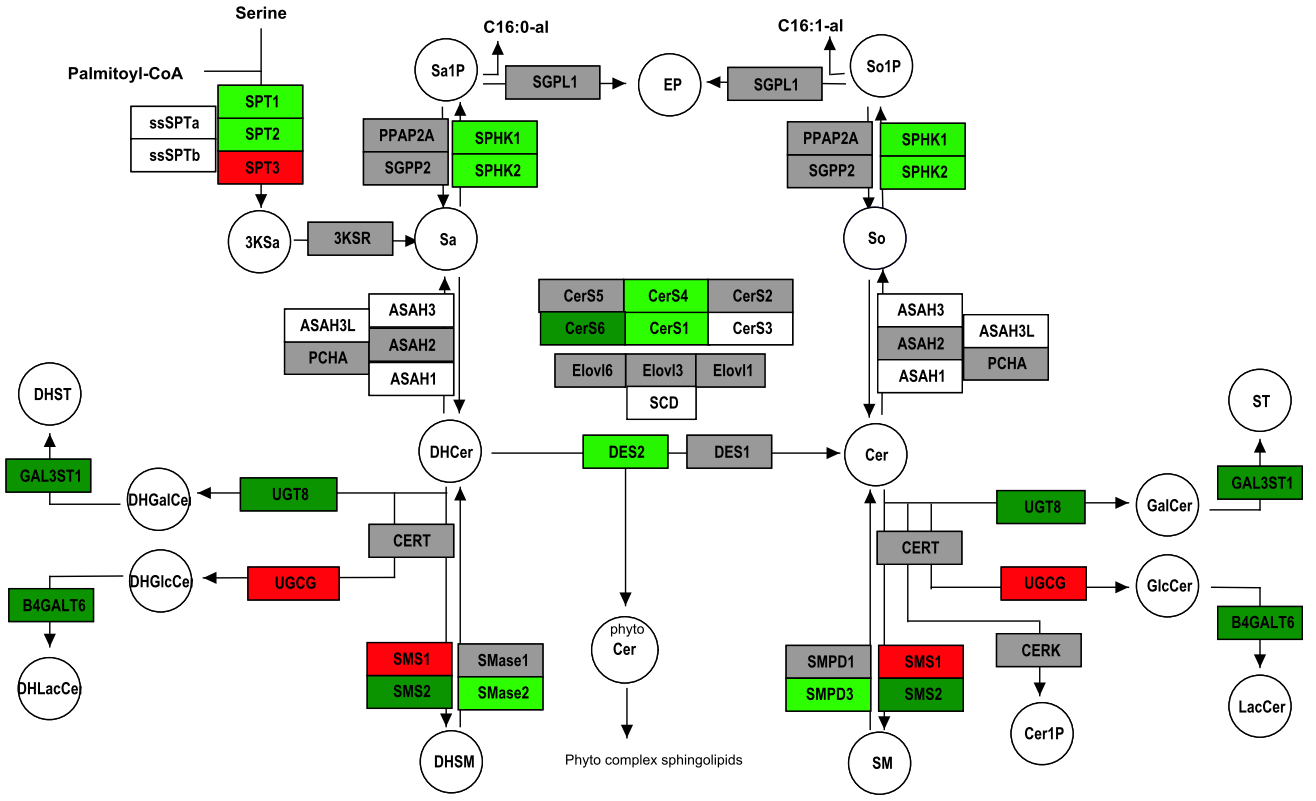

Sf 26: BT_549

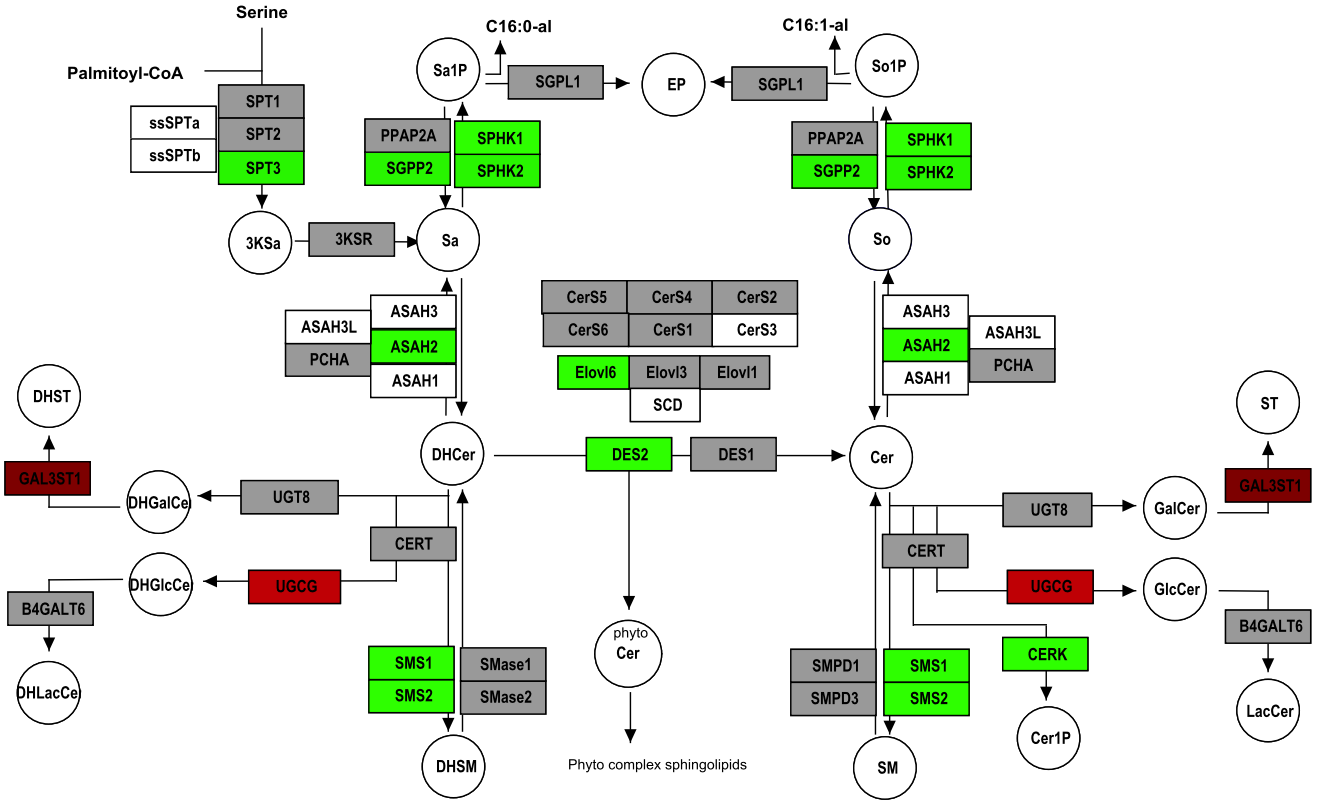

Sf 27: ACHN

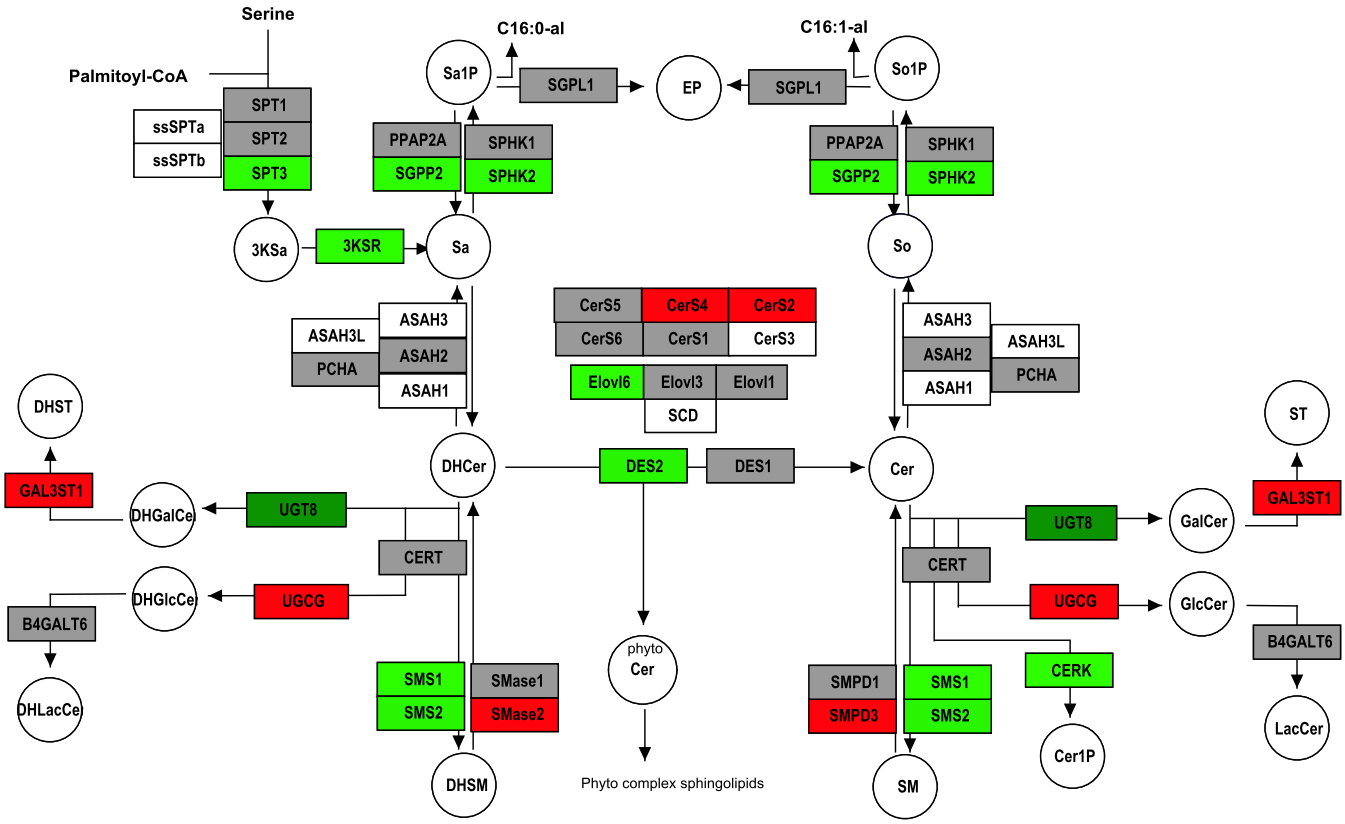

Sf 28: CAKI_1

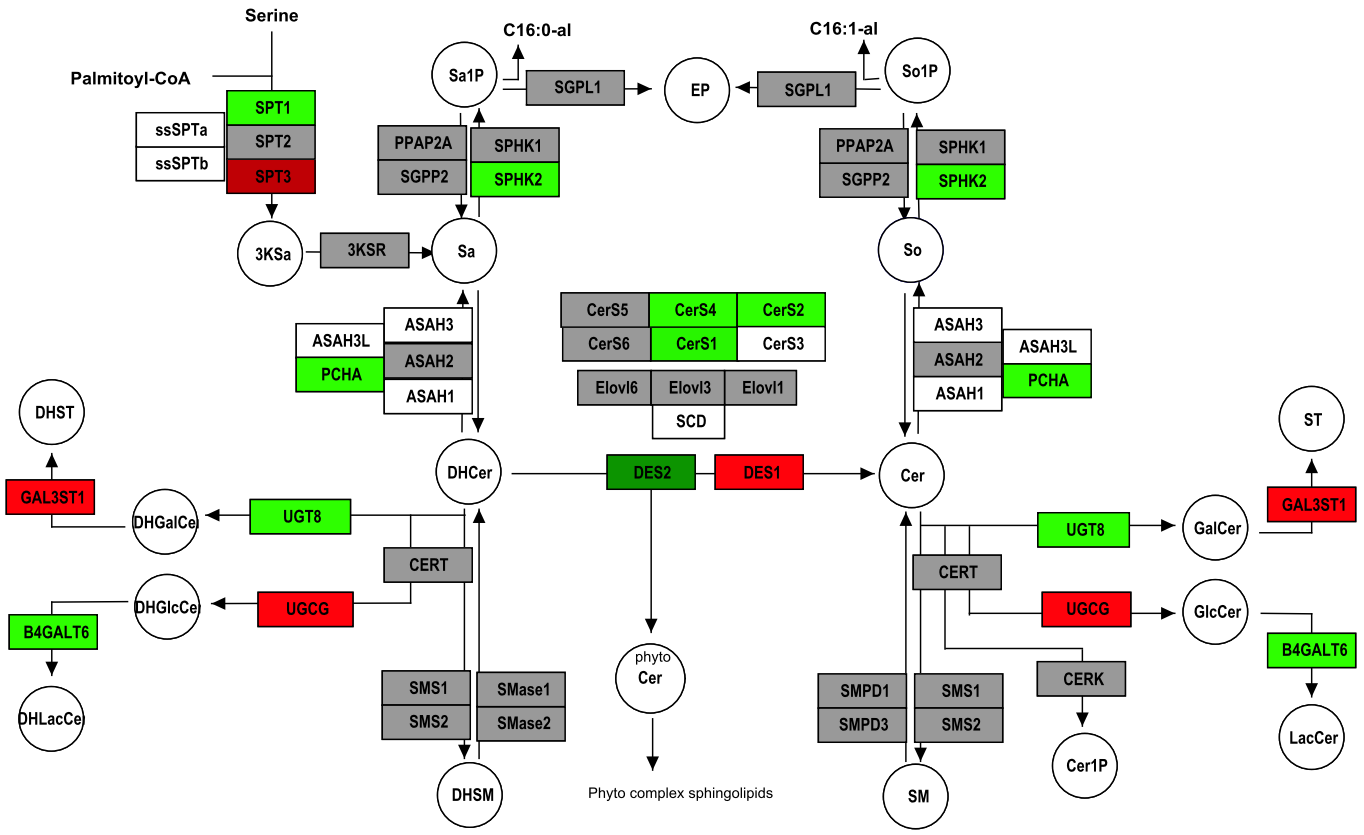

Sf 29: RXF_393

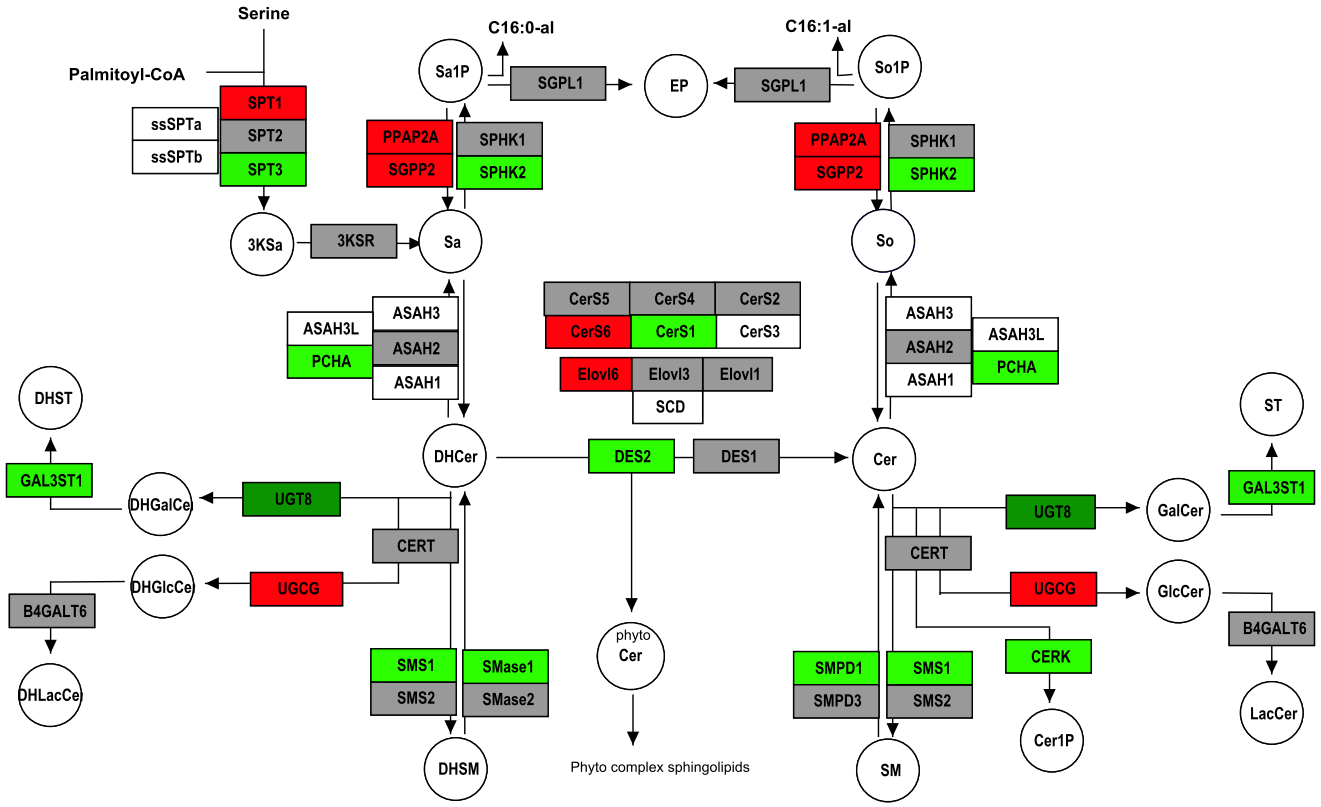

Sf 30: SN12C

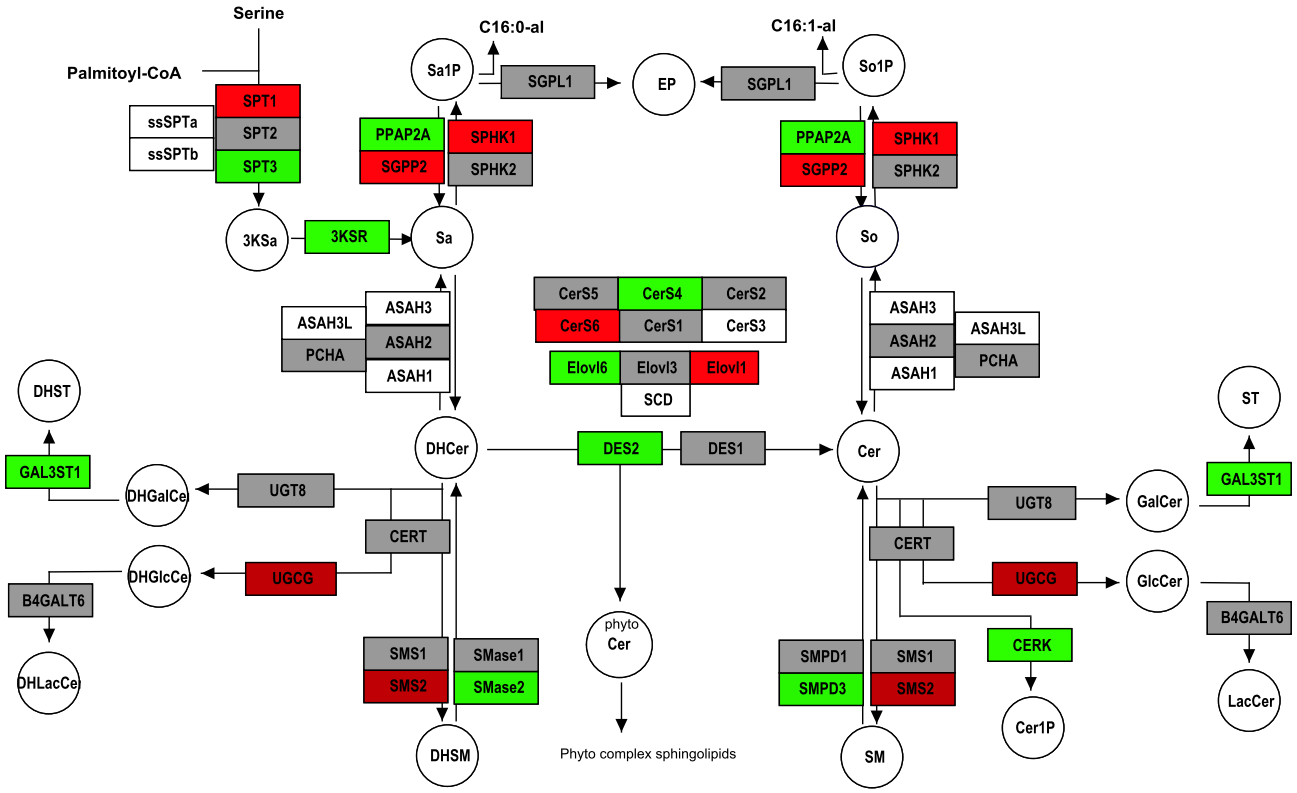

Sf 31: TK_10

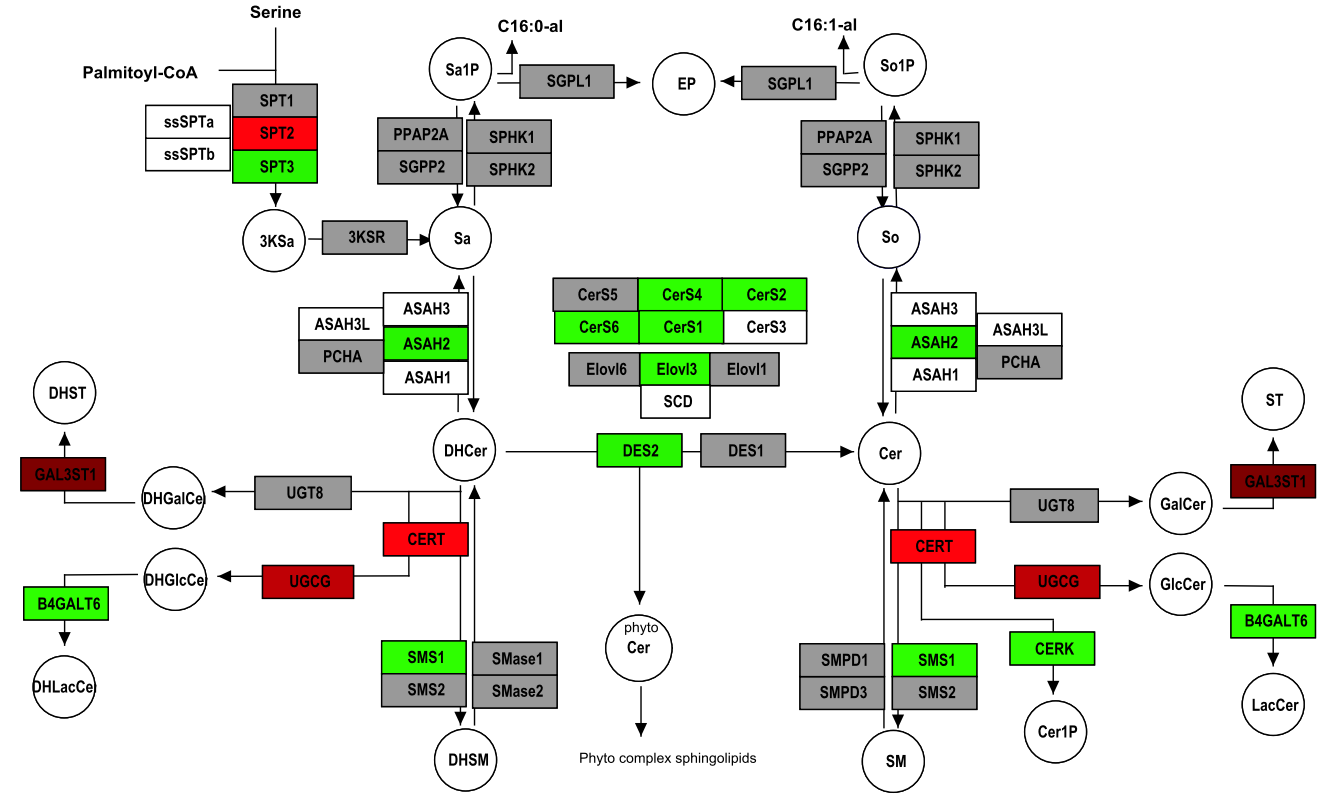

Sf 32: UO_31

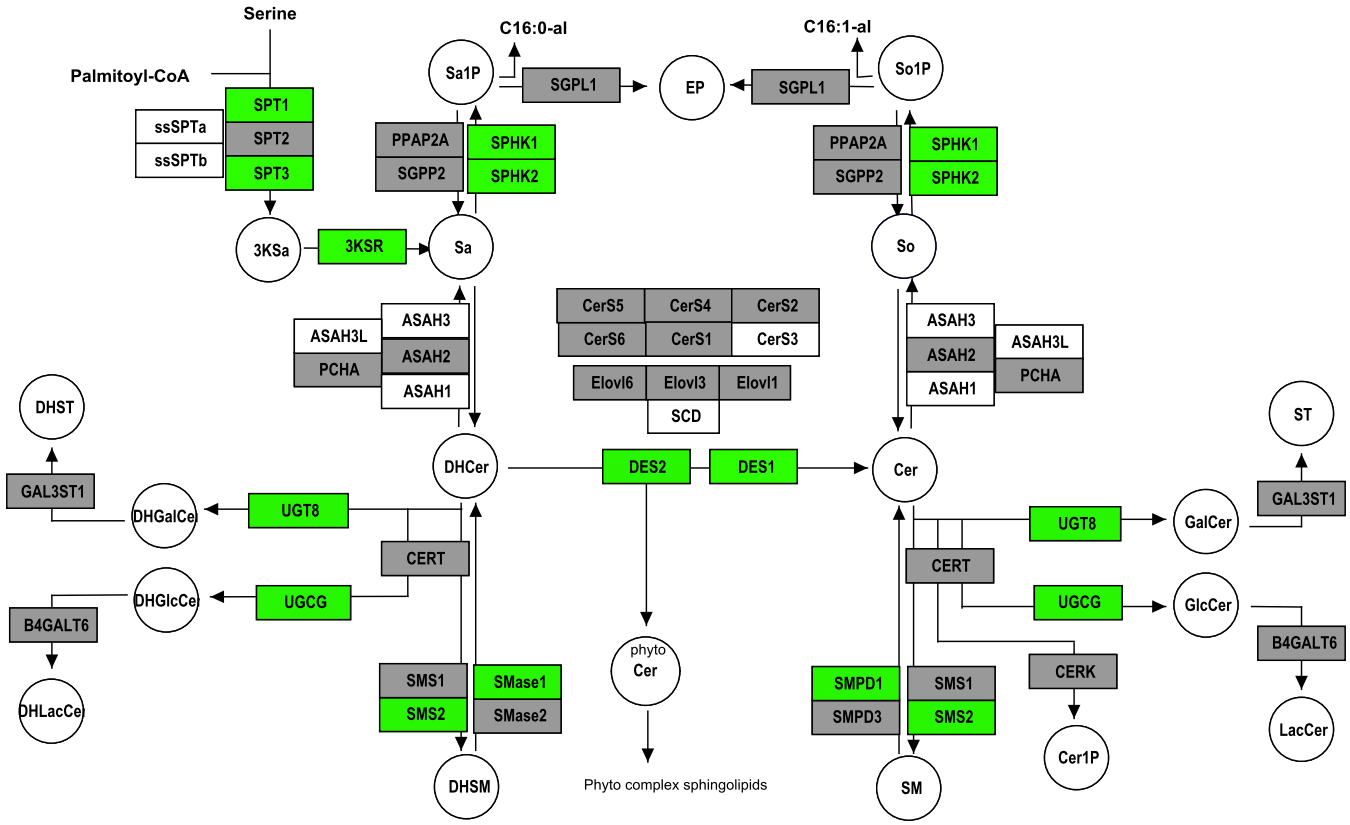

Sf 33: A549

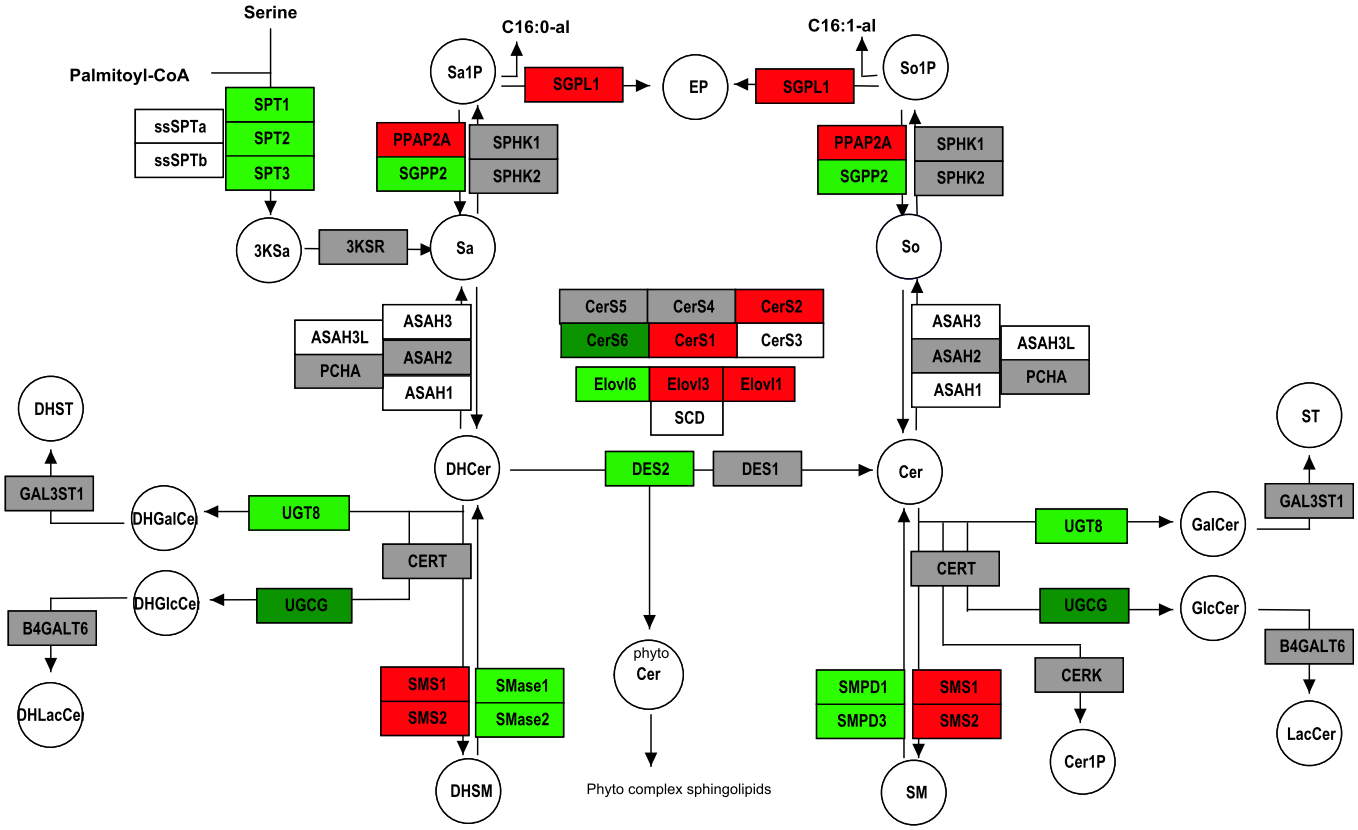

Sf 34: EKVX

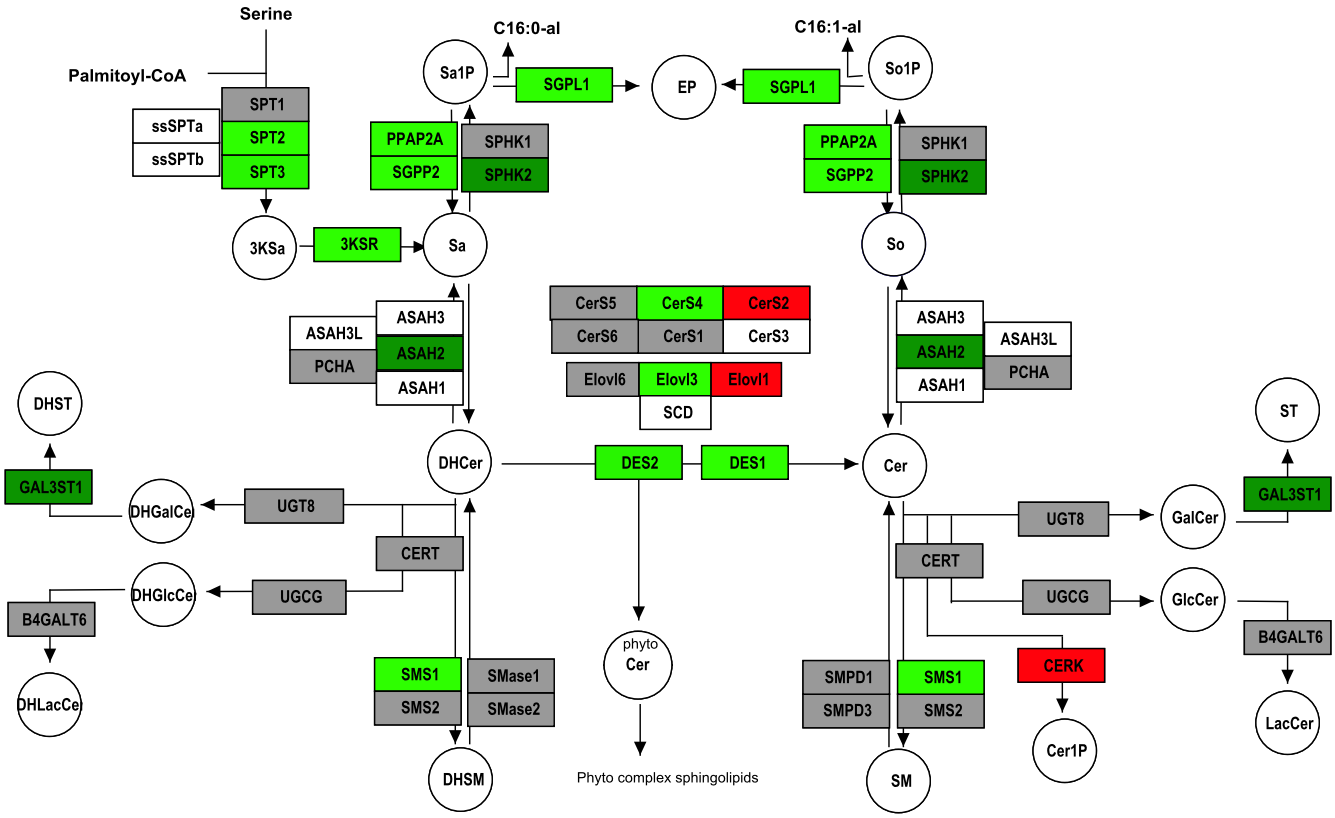

Sf 35: HOP_62

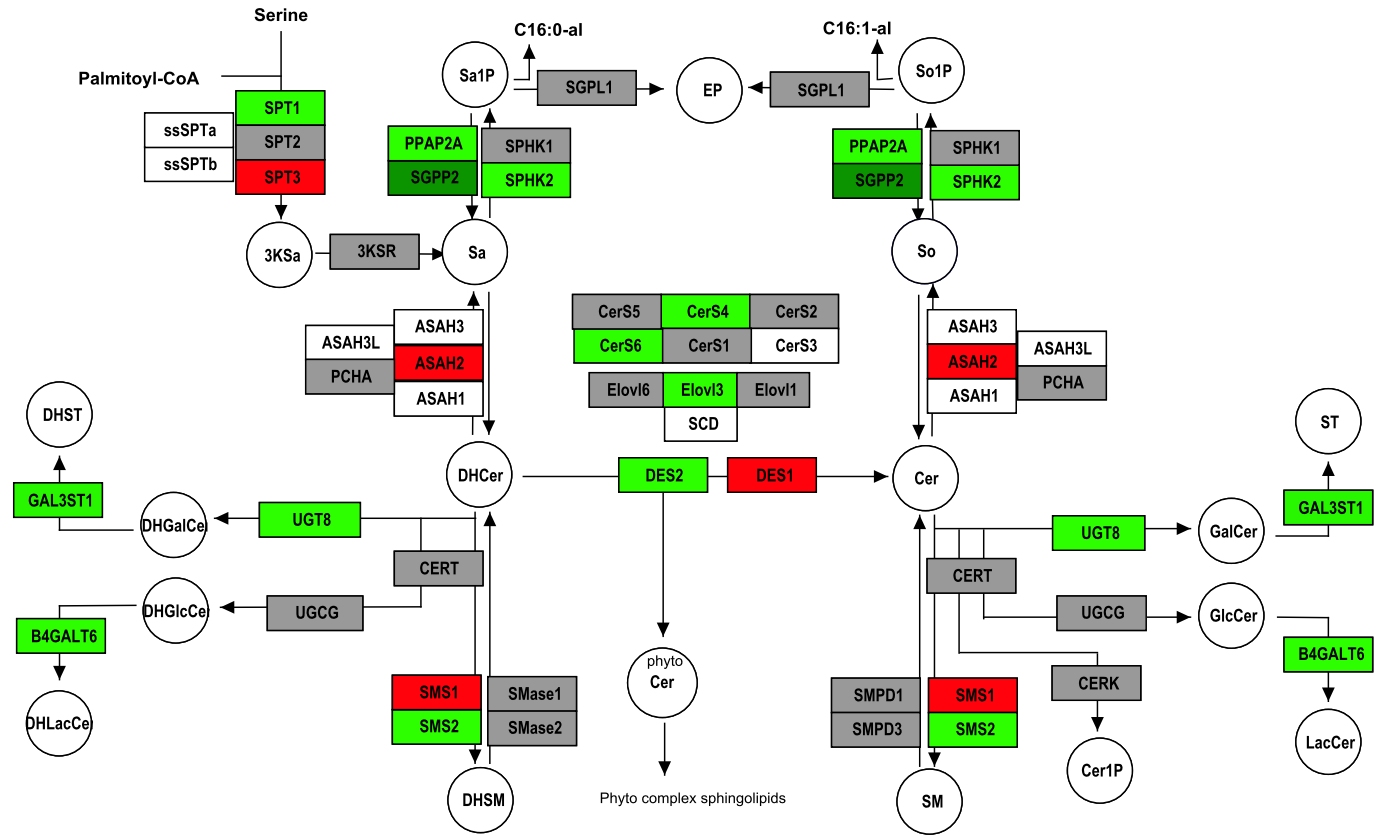

Sf 36: HOP_92

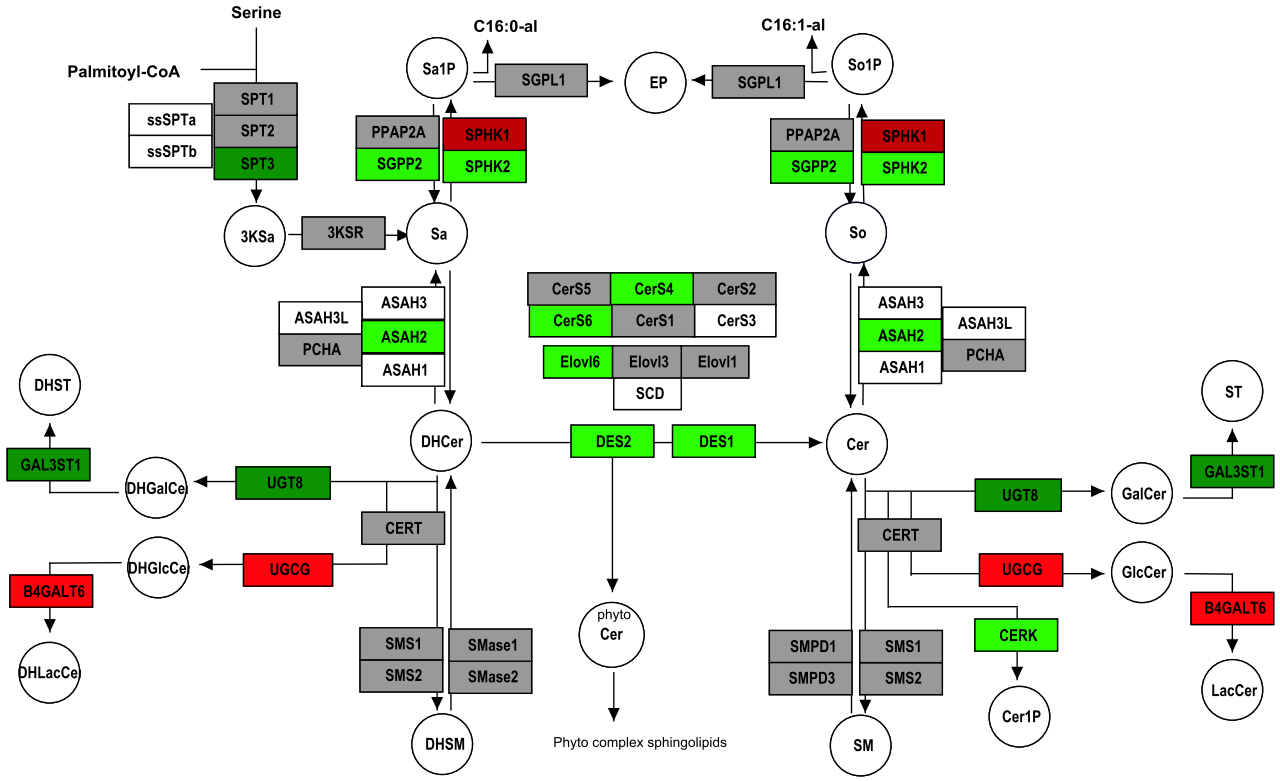

Sf 37: NCI_H226

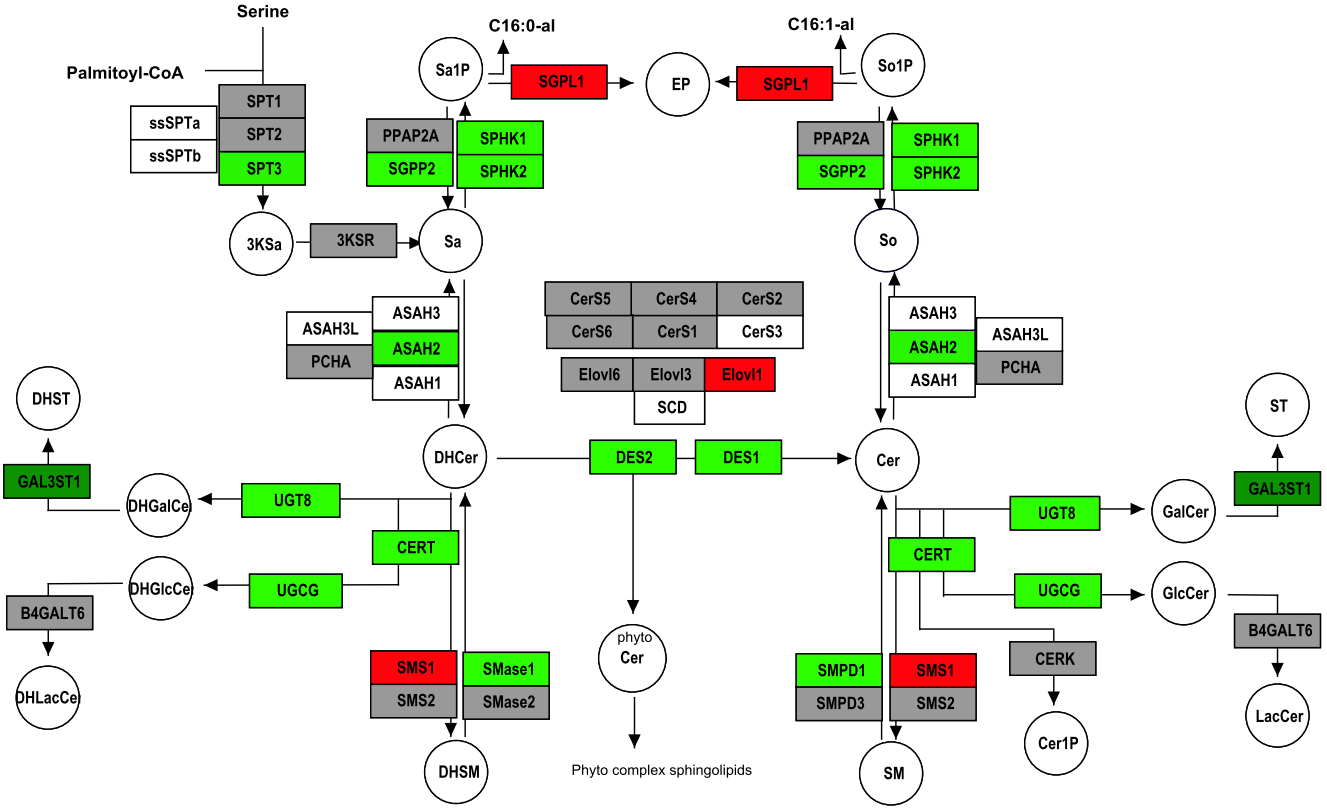

Sf 38: NCI_H322M

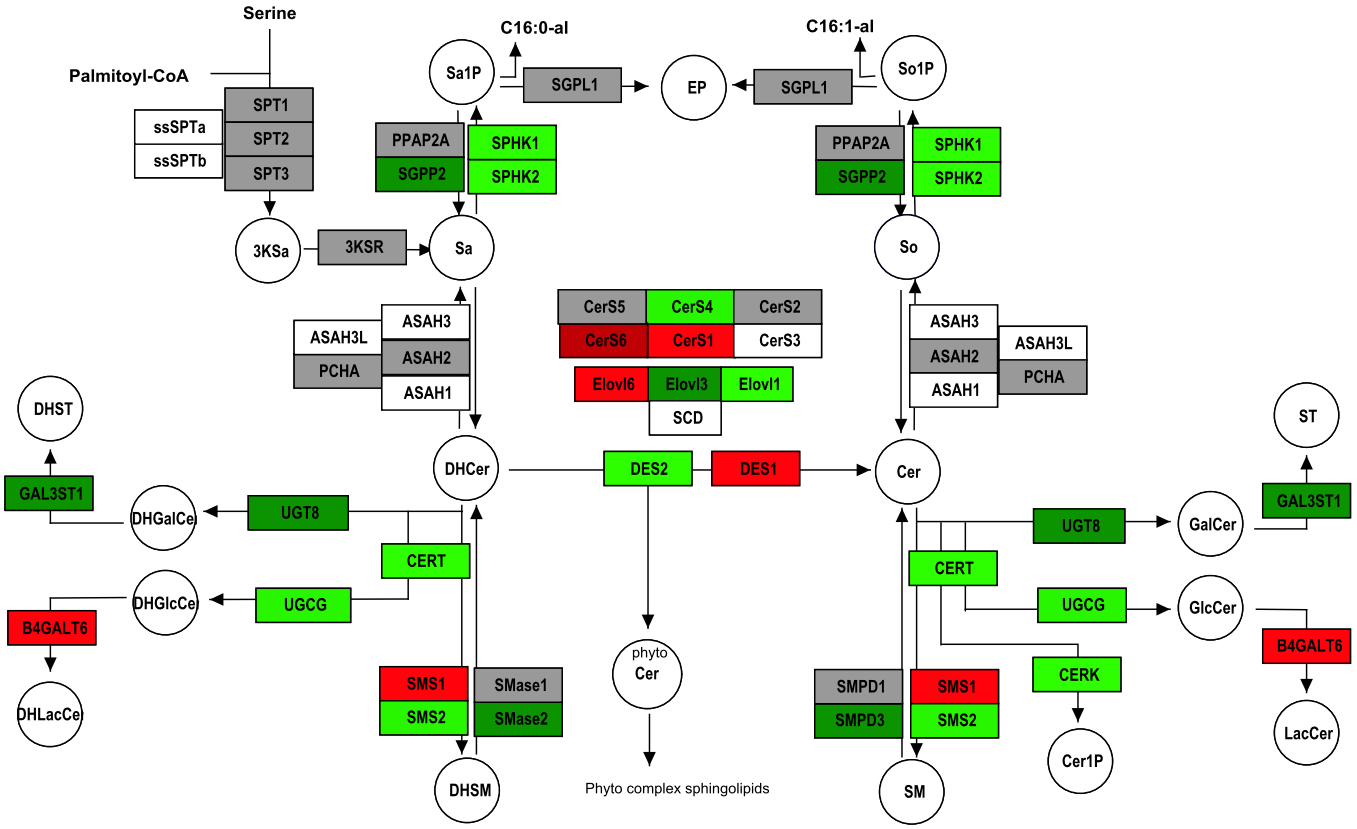

Sf 39: NCI_H460

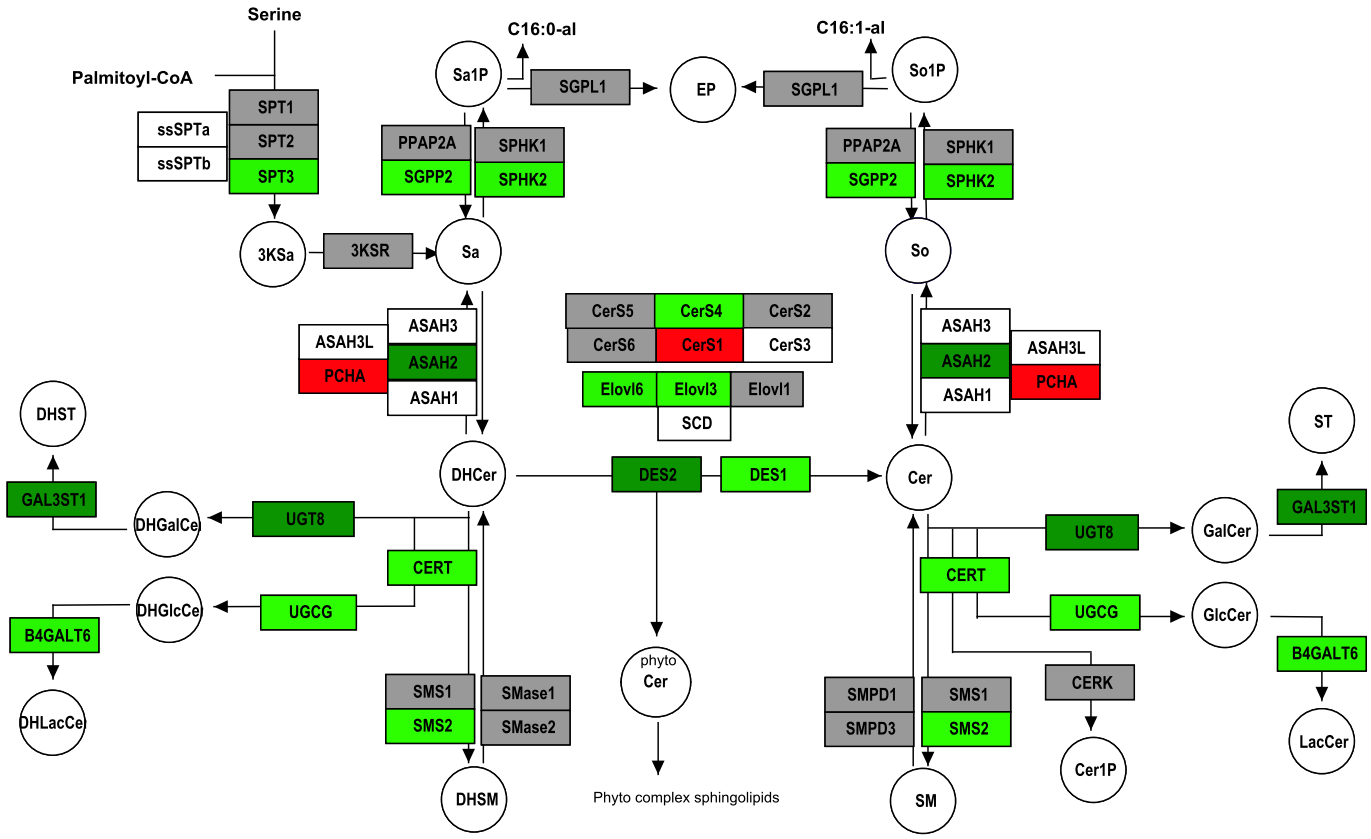

Sf 40: NCI_H522

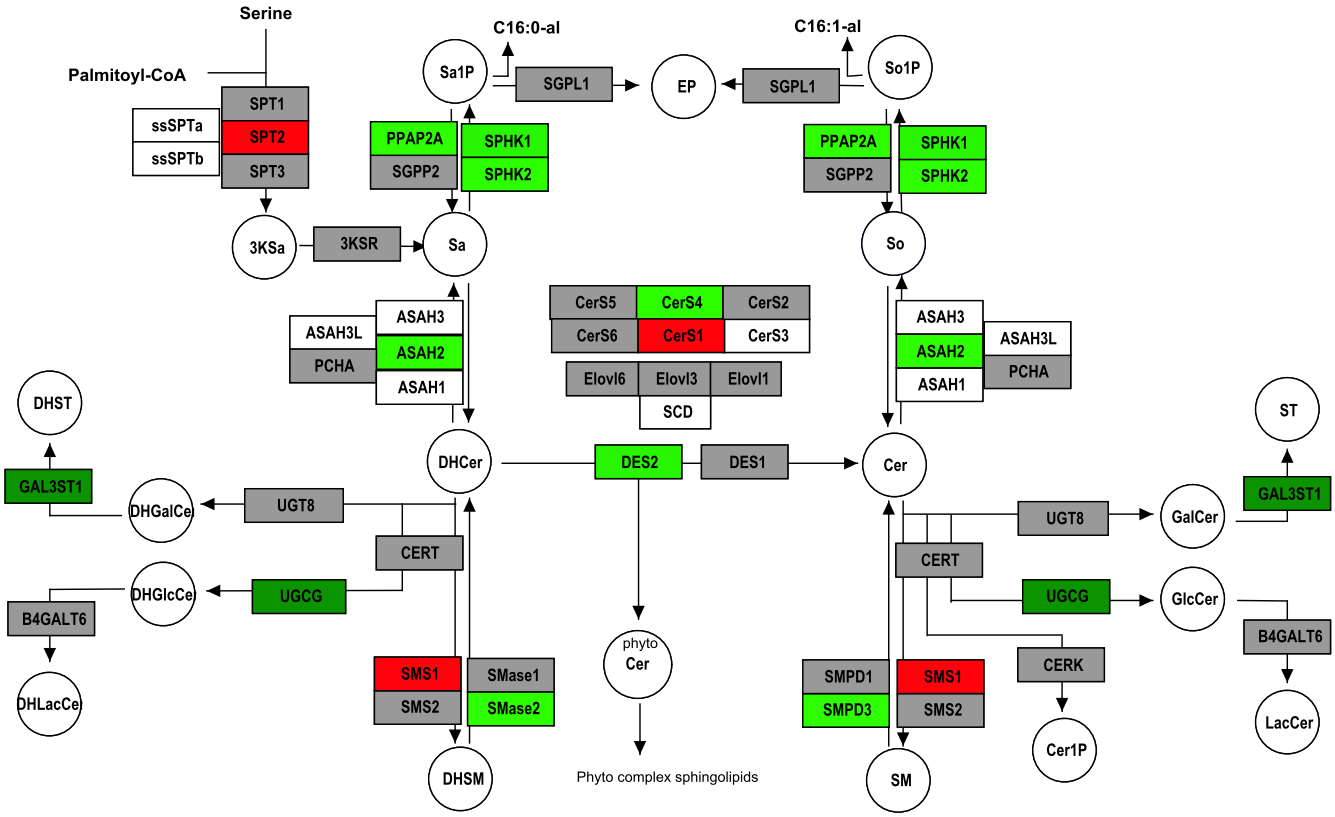

Sf 41: IGROV1

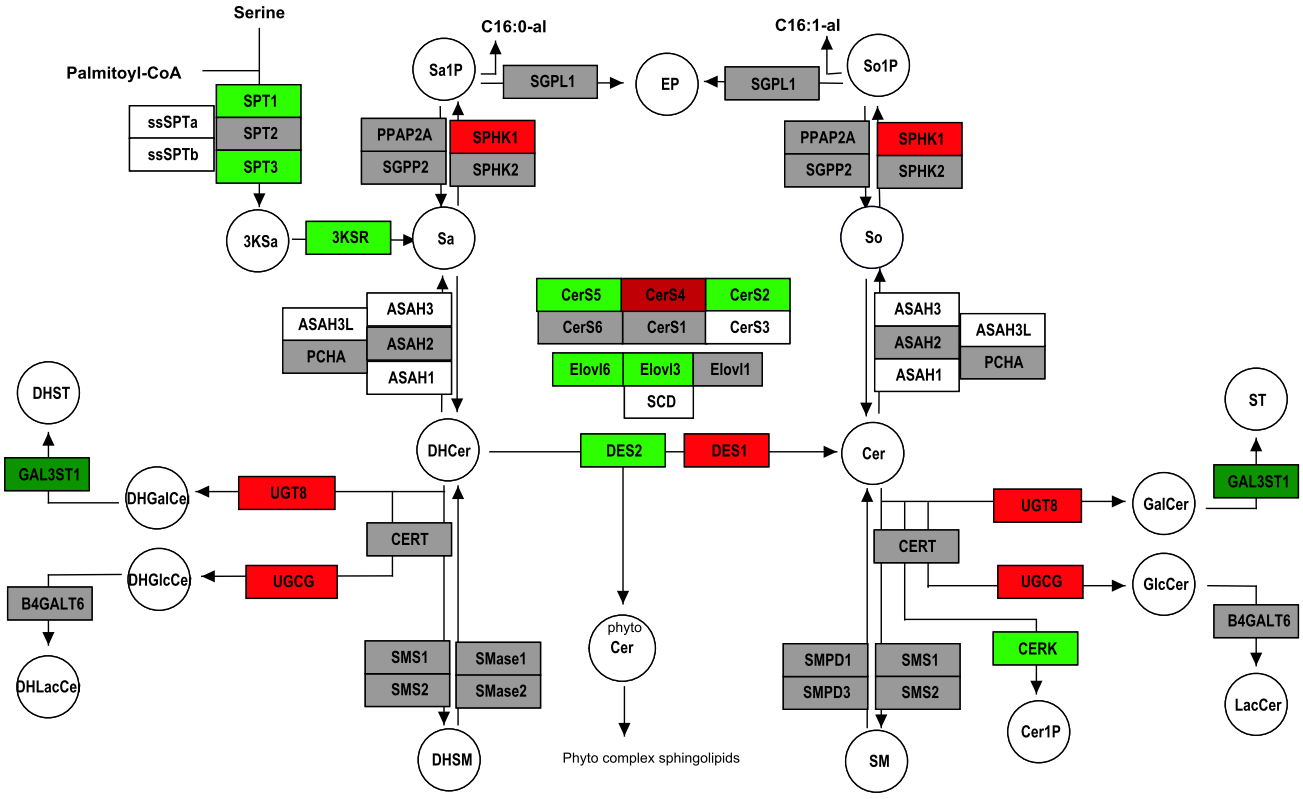

Sf 42: NCI_ADR_RES

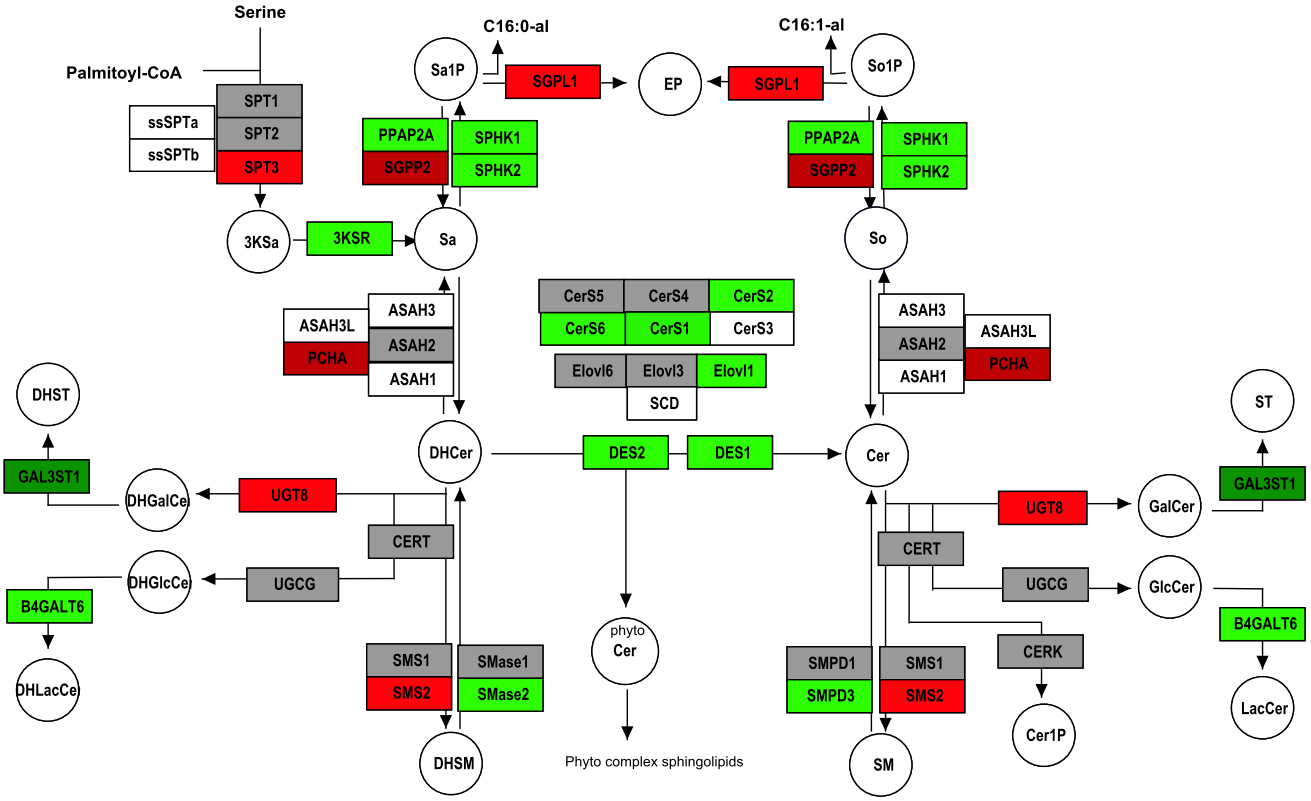

Sf 43: OVCAR_3

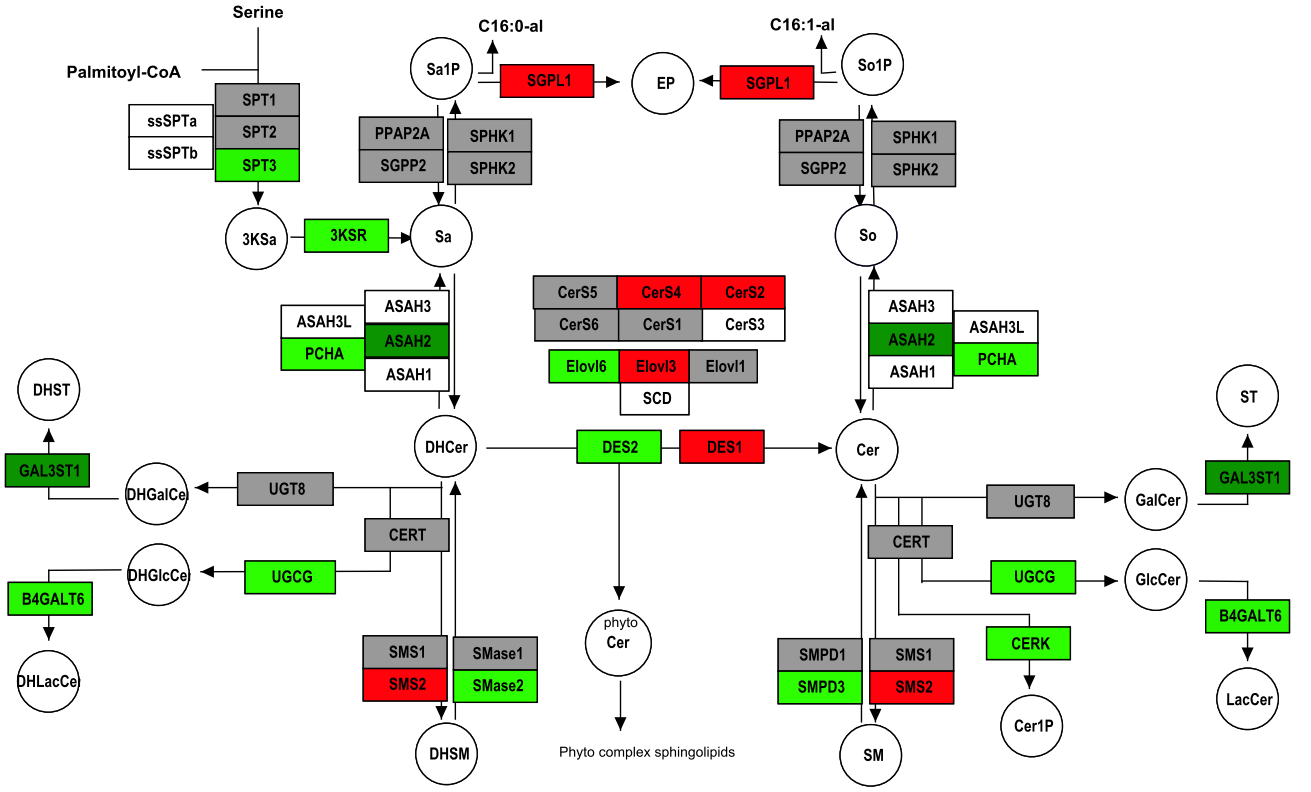

Sf 44: OVCAR_4

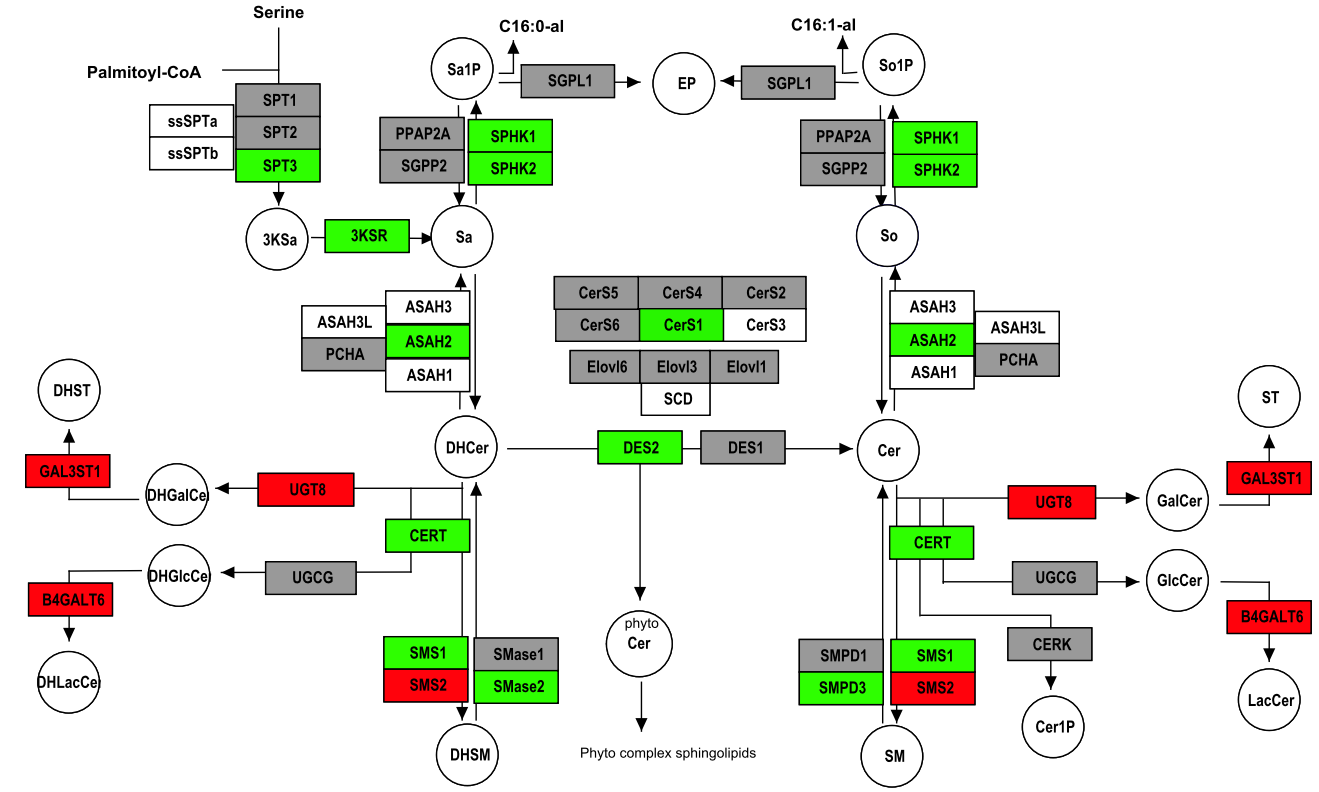

Sf 45: OVCAR_5

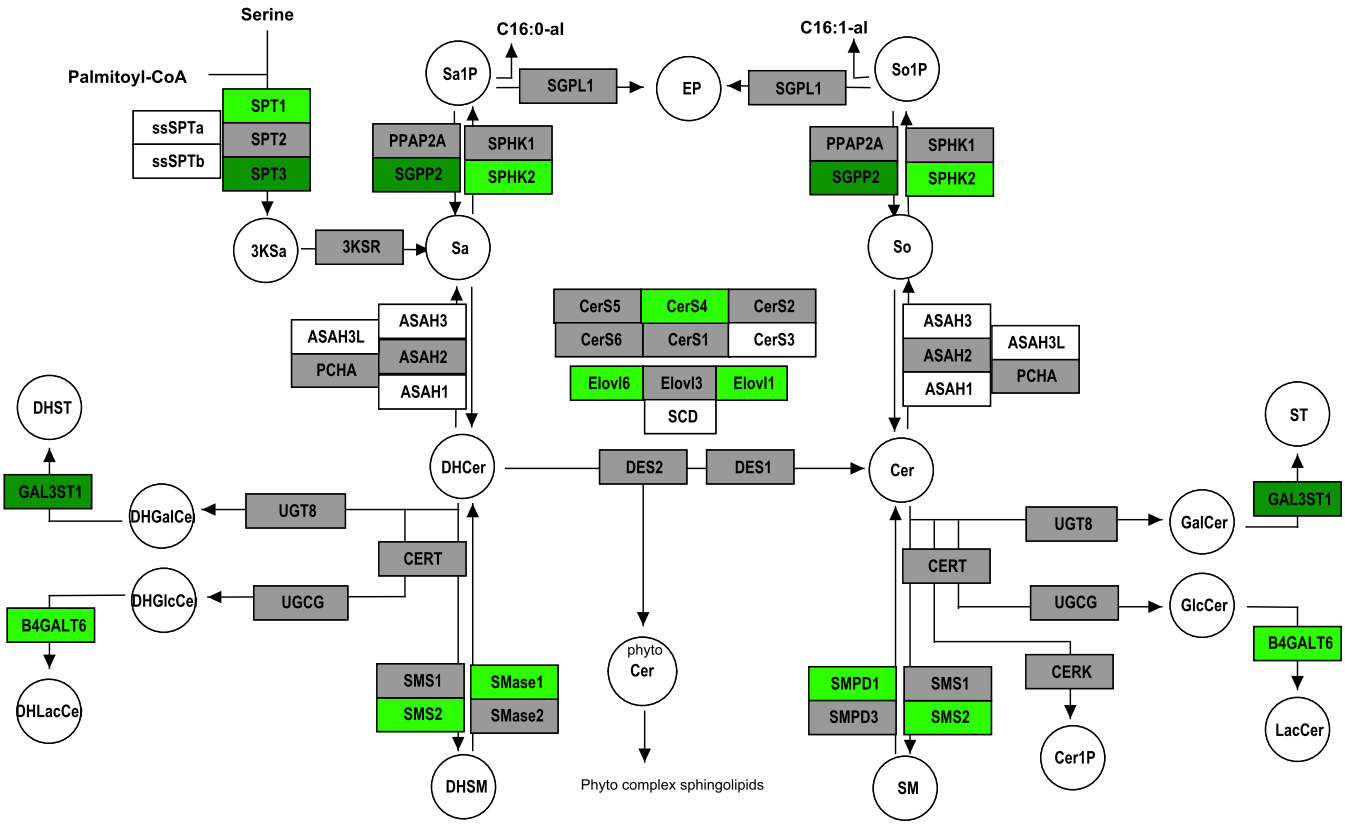

Sf 46: OVCAR_8

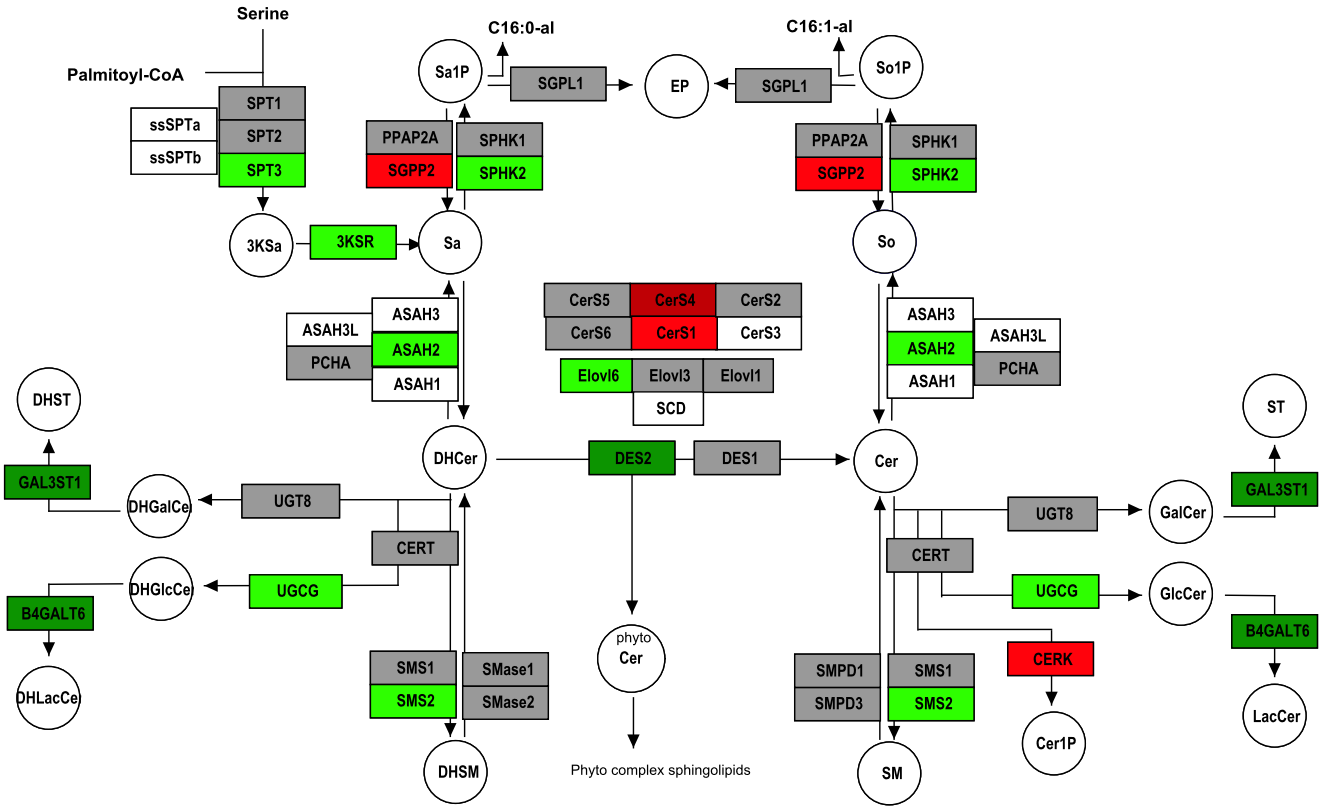

Sf 47: SK_OV_3

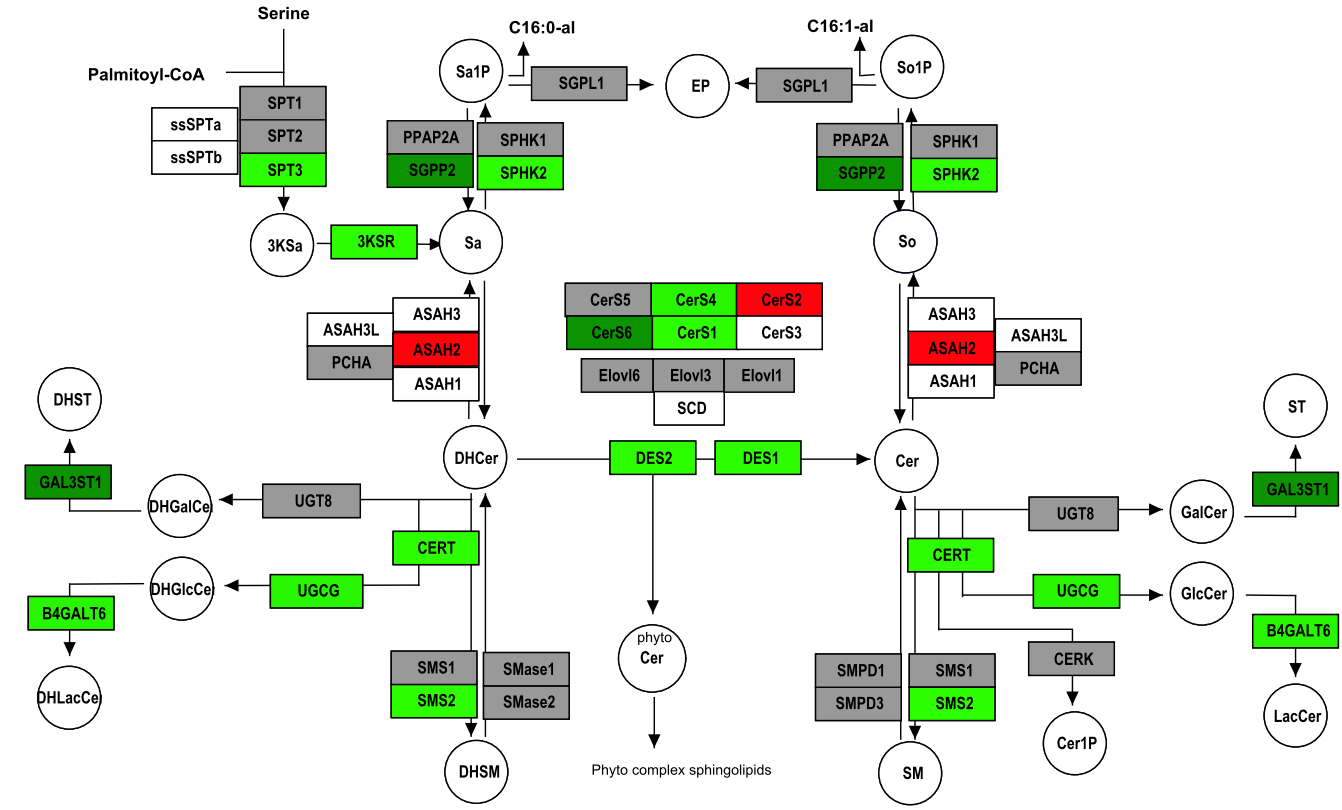

Sf 48: PC_3

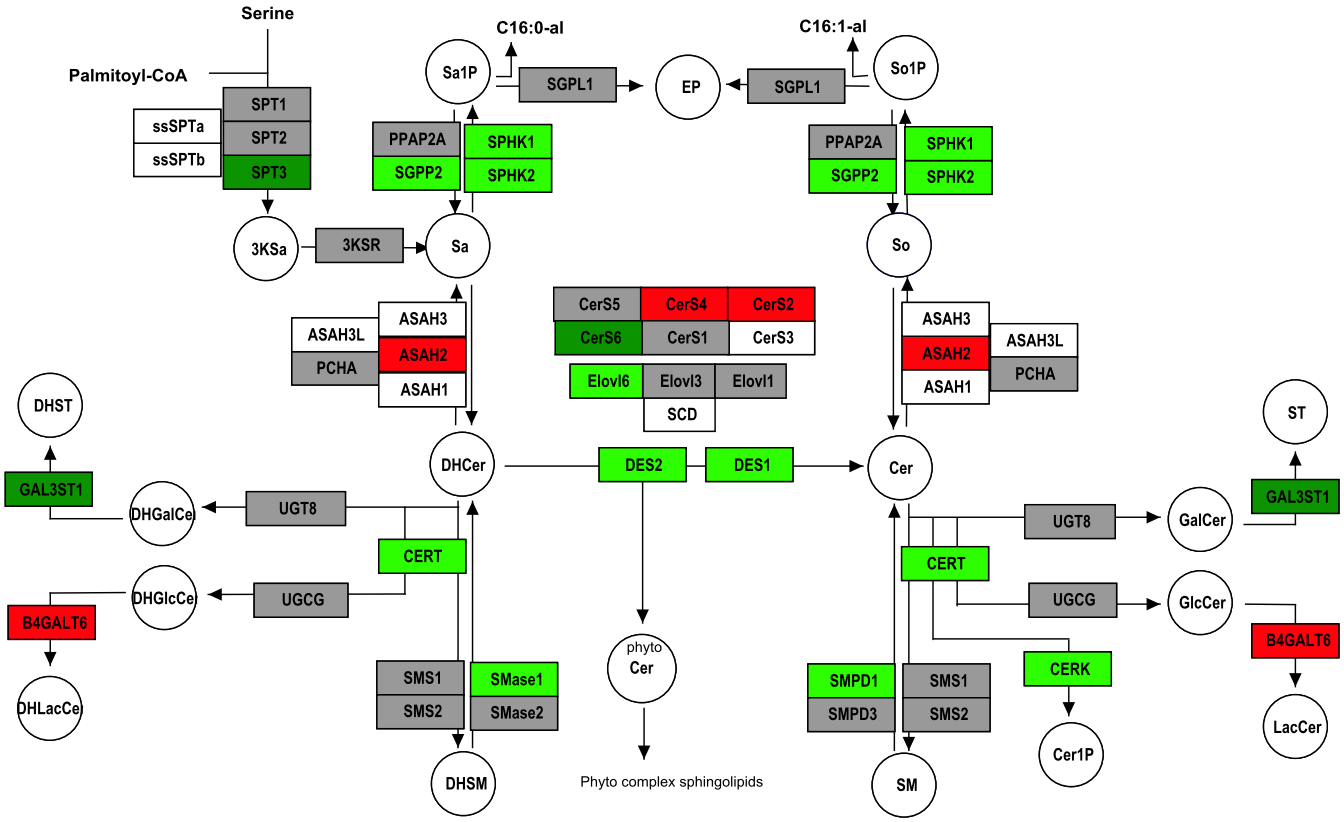

Sf 49: DU_145

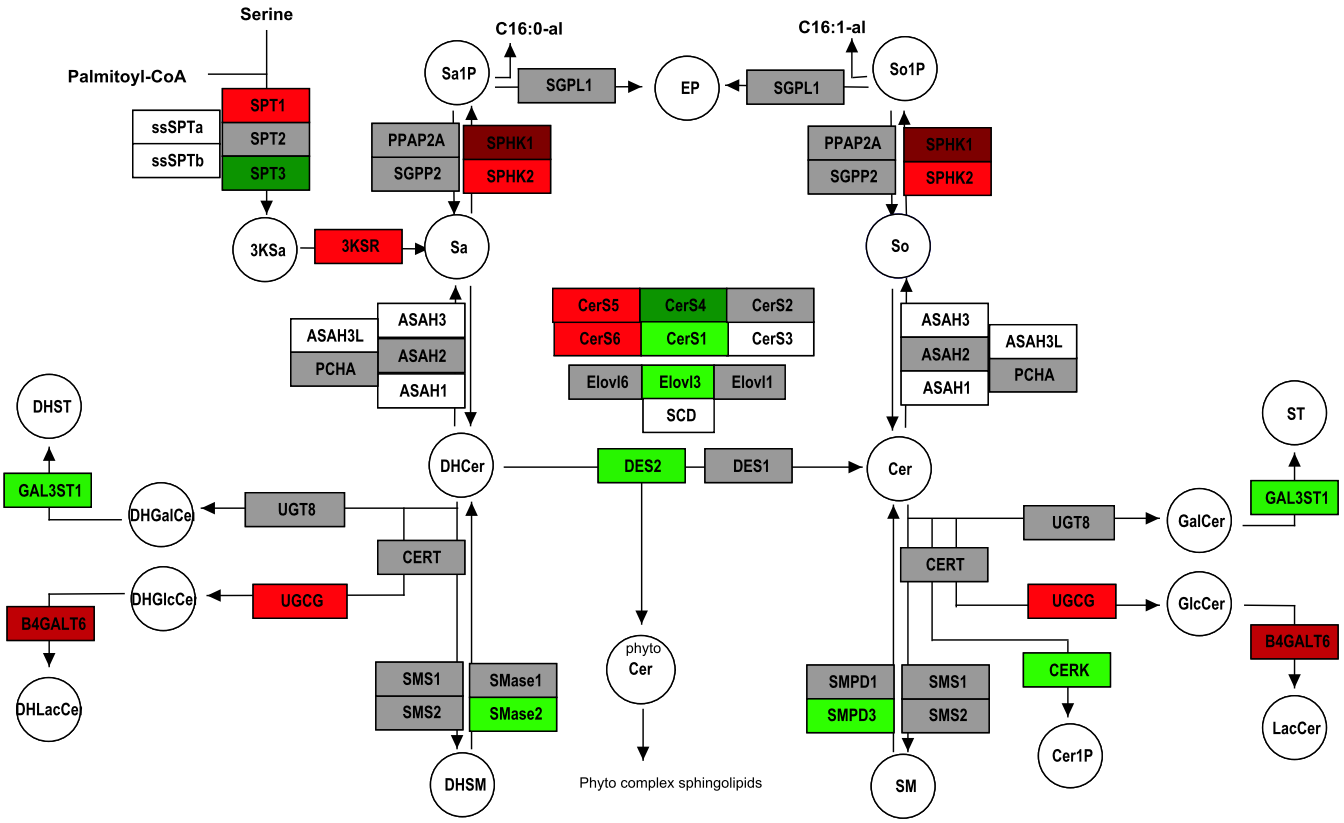

Sf 50: LOXIMVI

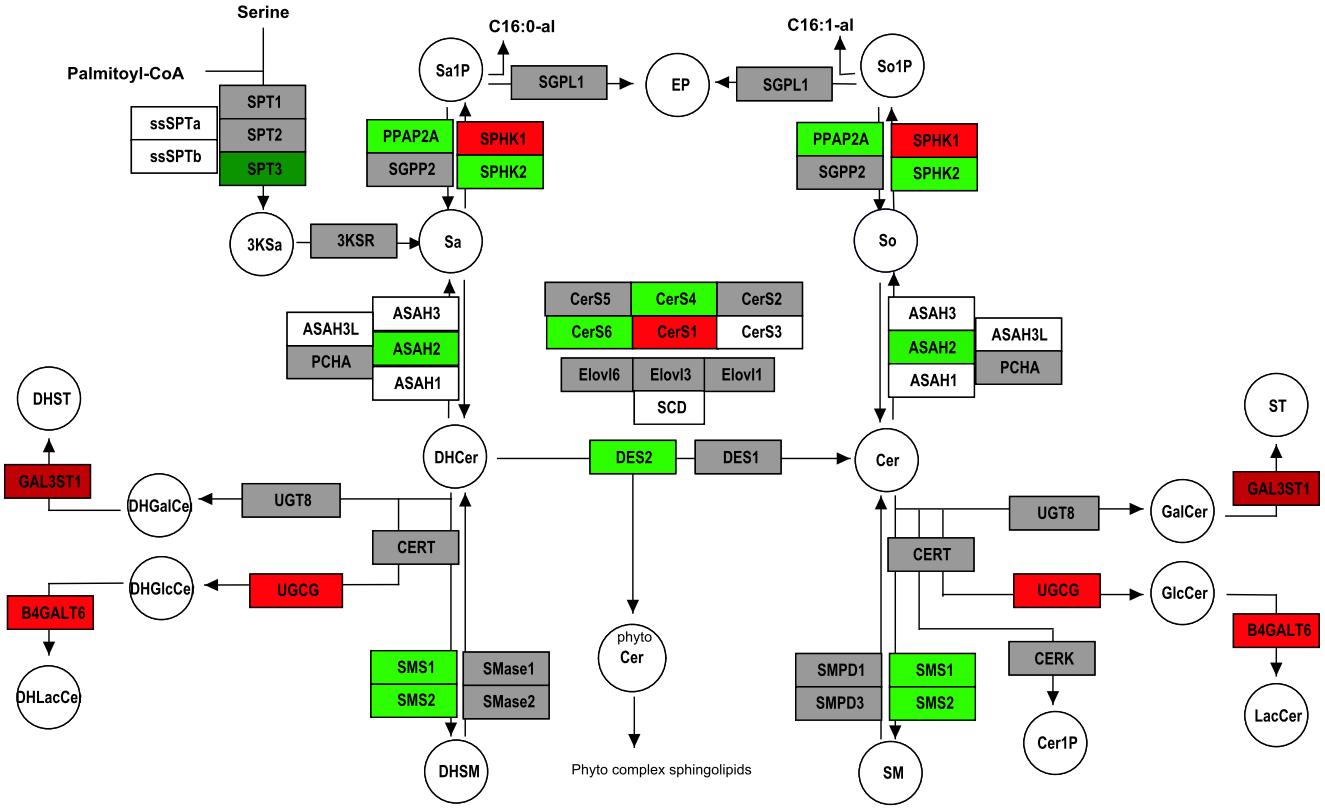

Sf 51: MALME_3M

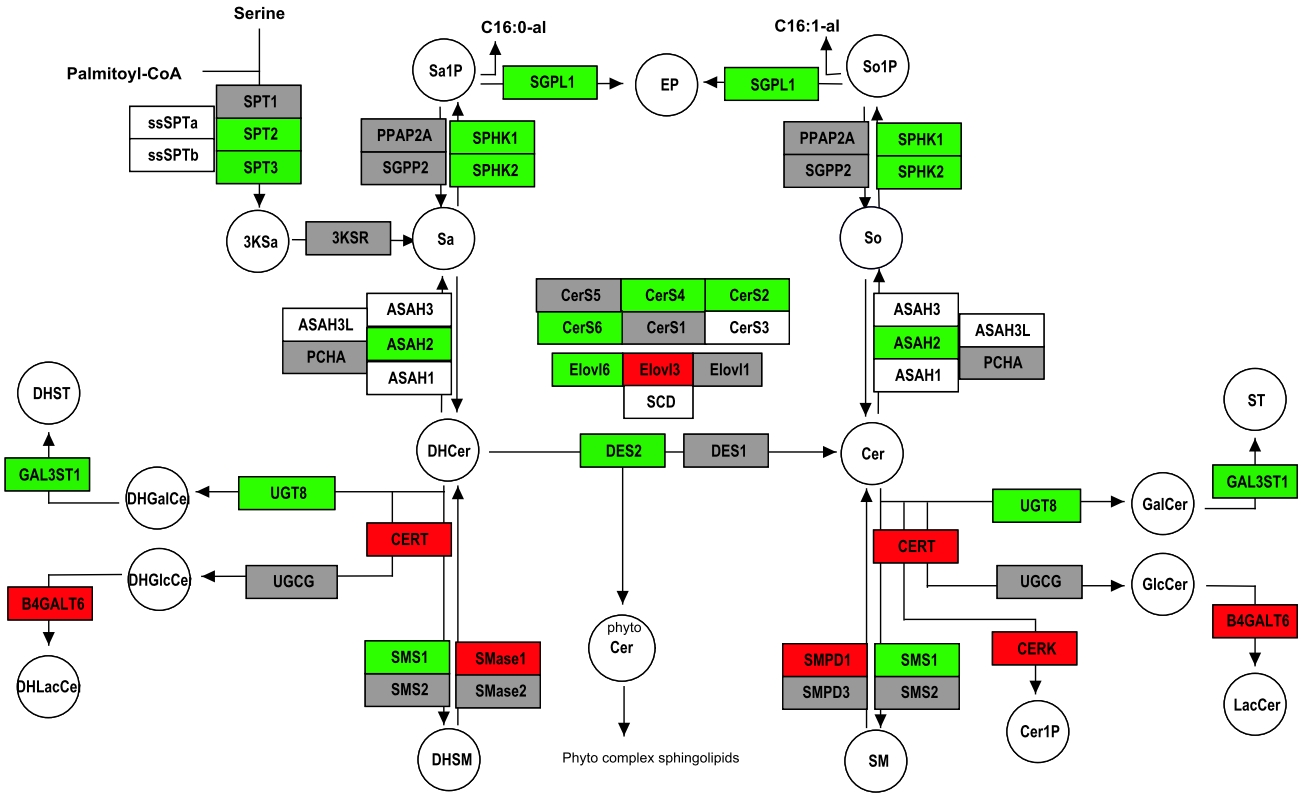

Sf 52: M14

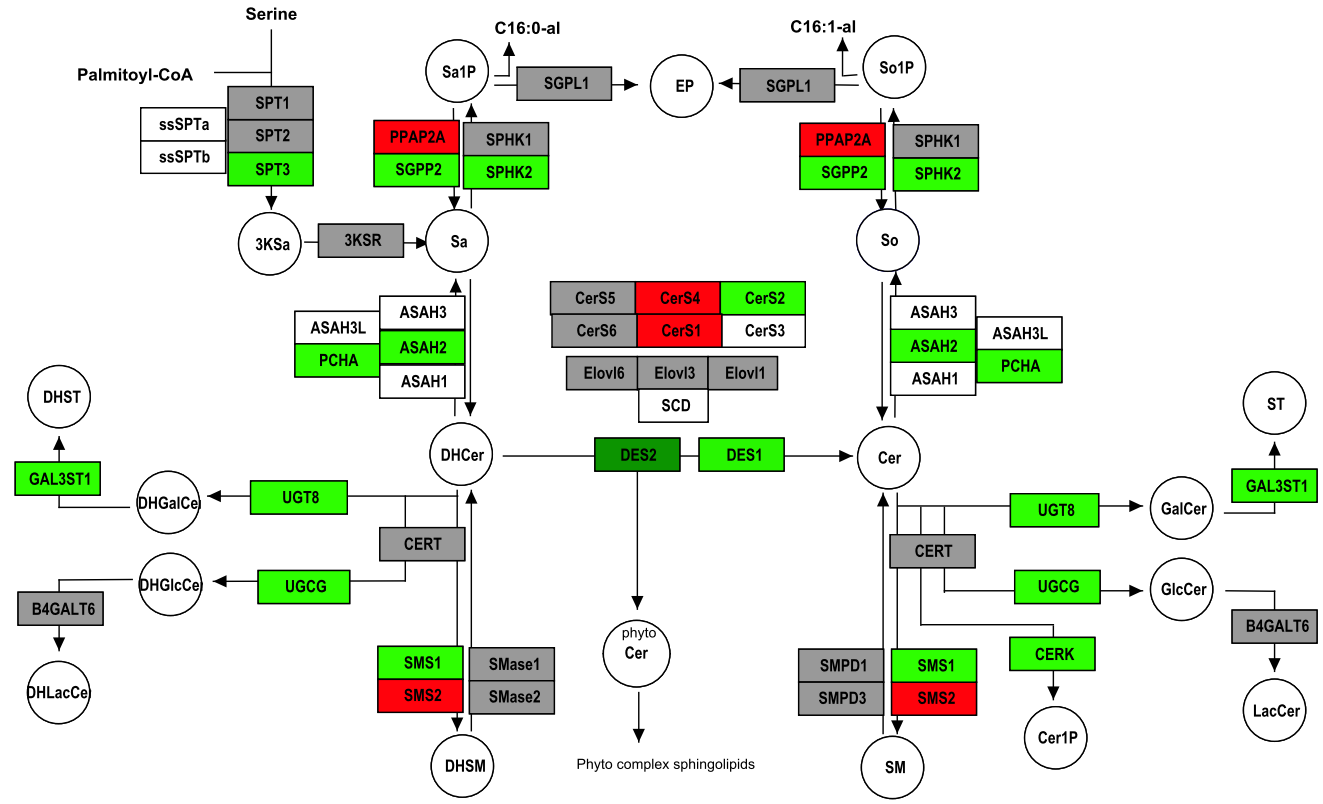

Sf 53: SK_MEL_2

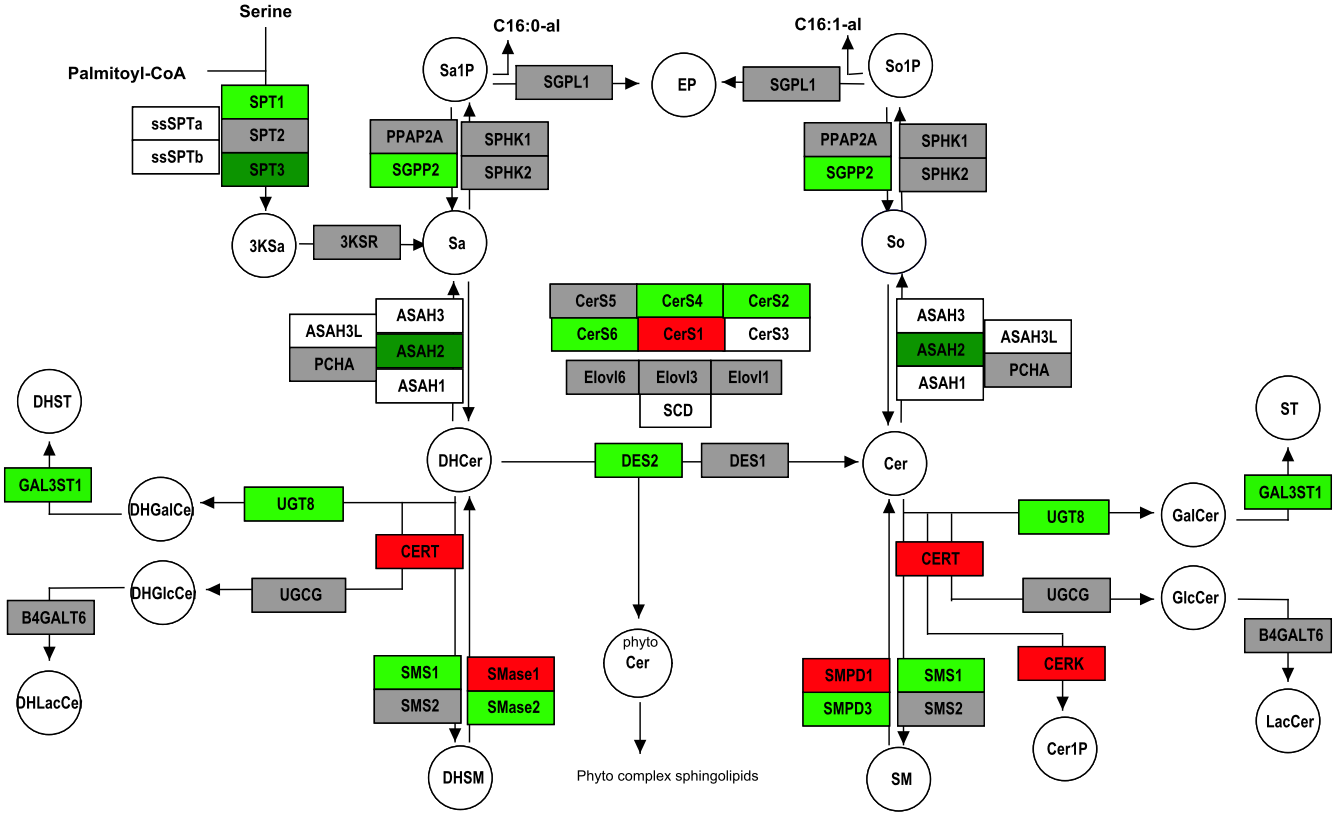

Sf 54: SK_MEL_28

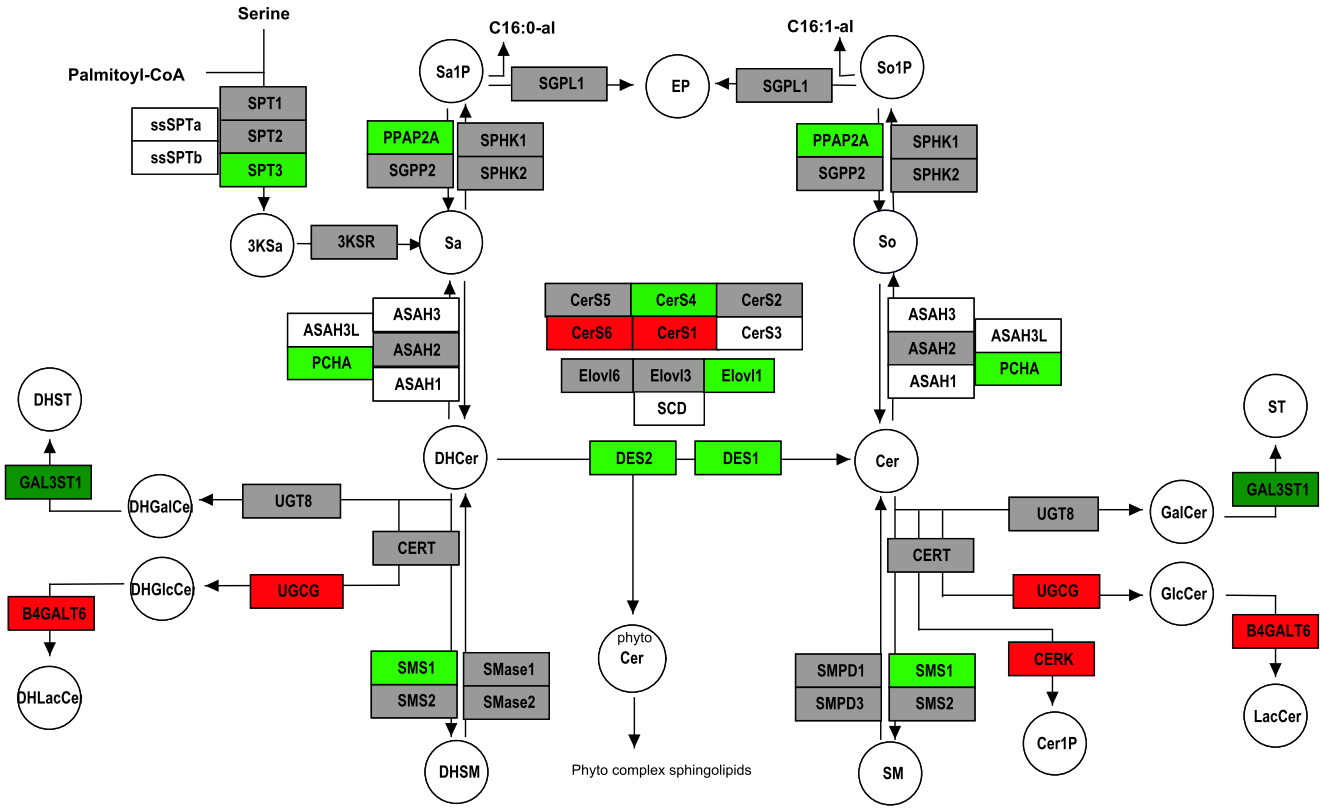

Sf 55: SK_MEL_5

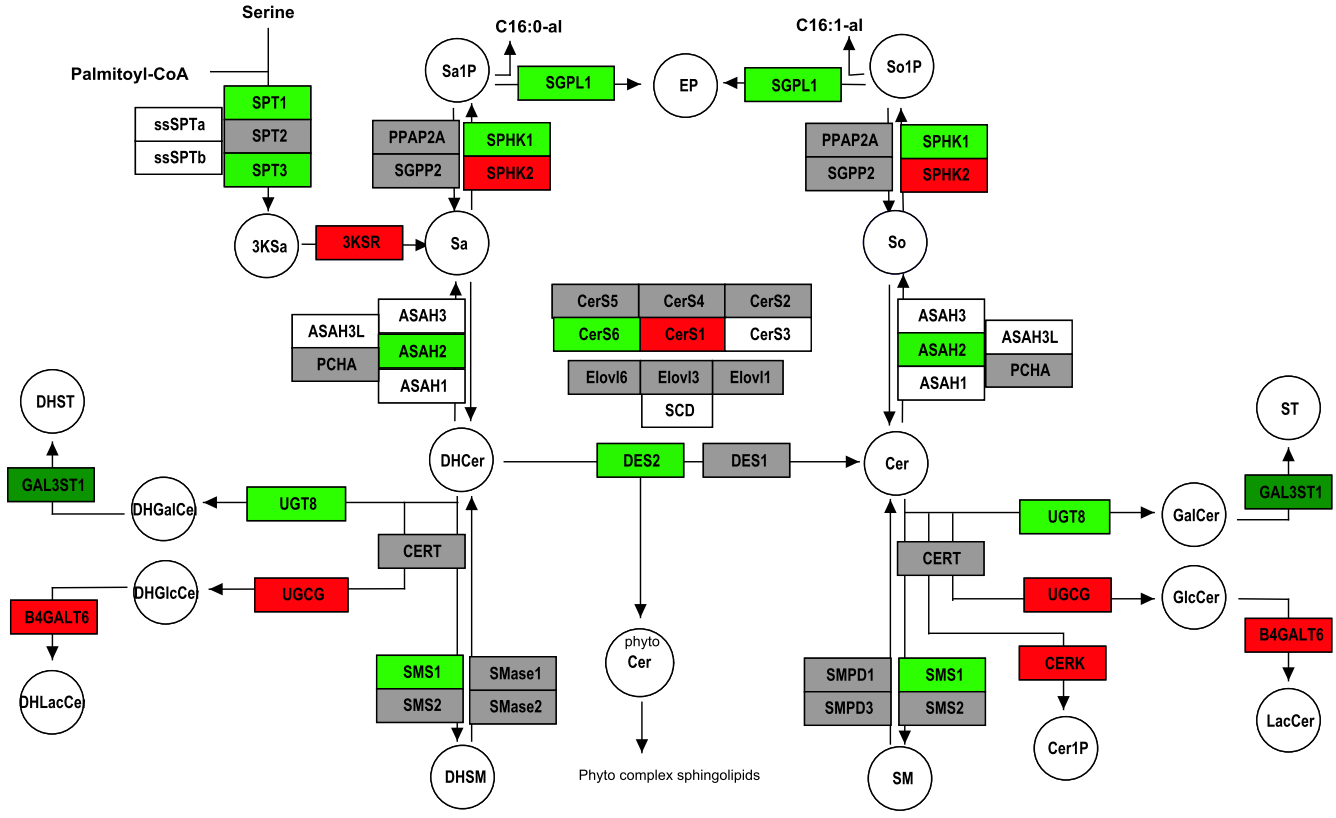

Sf 56: UACC_257

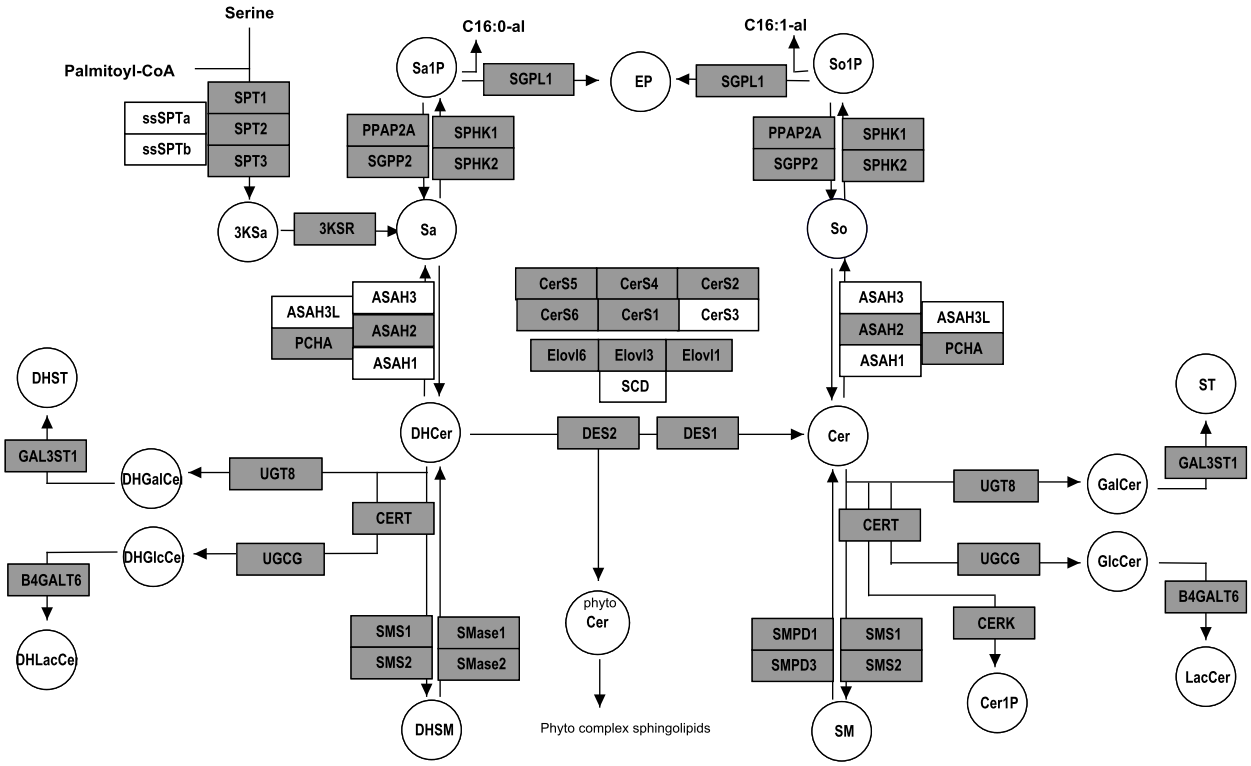

Sf 57: UACC_62

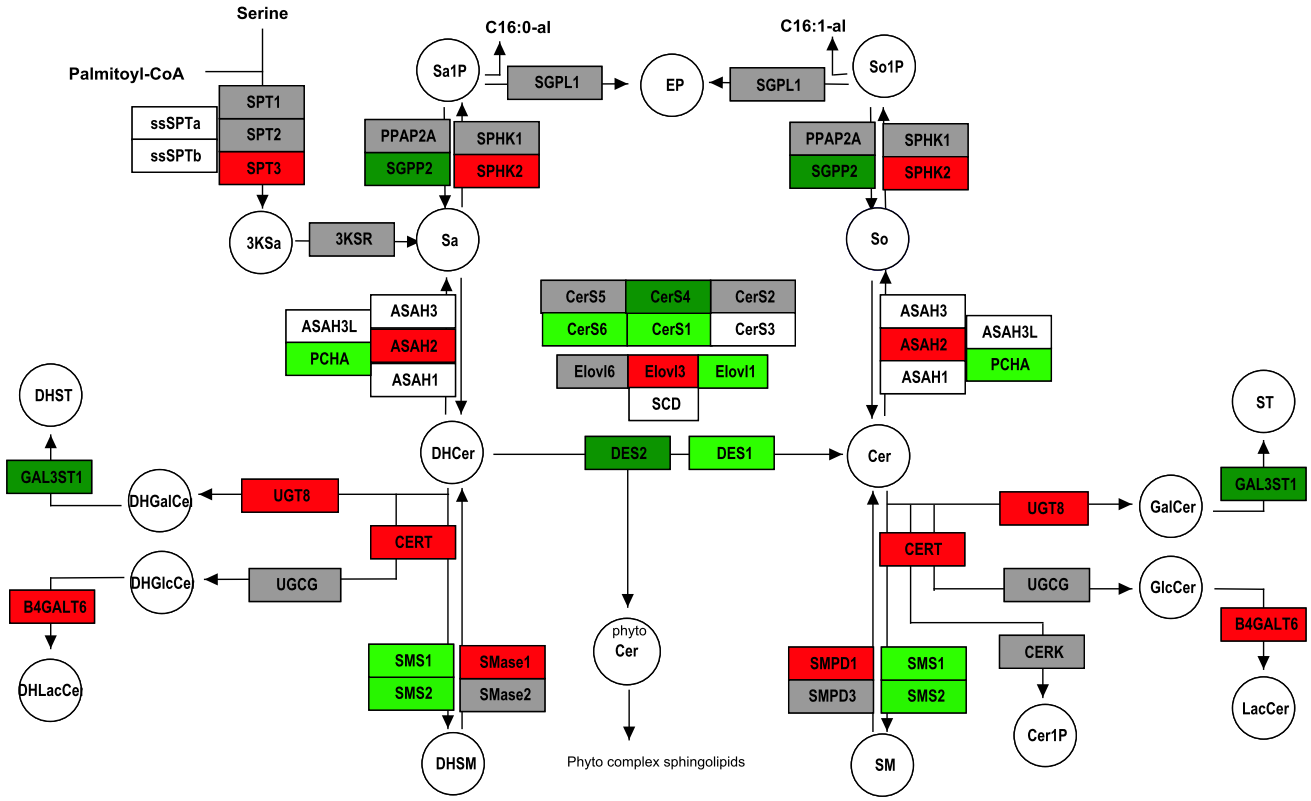

Sf 58: MDA_MB_435

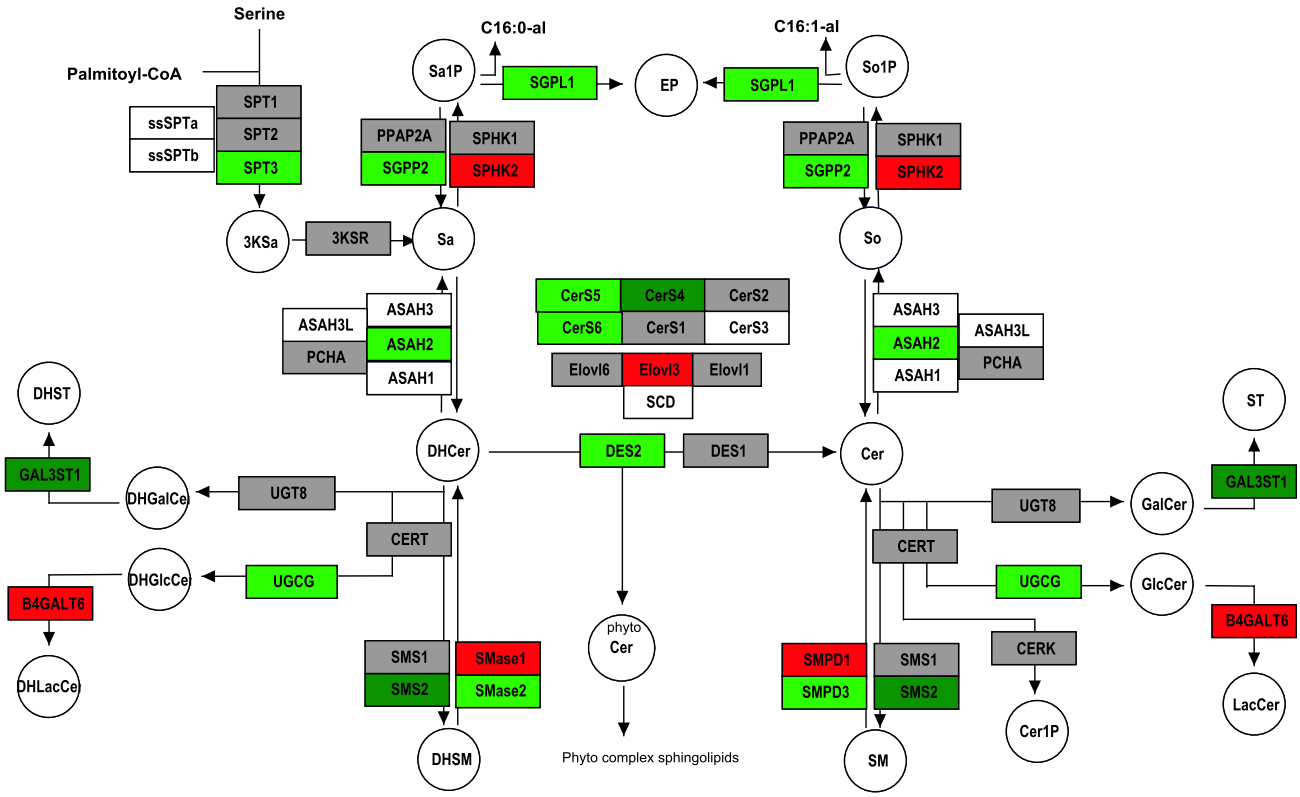
Serine
Palmitoyl-CoA
SPT1
ssSPTa
SPT2
ssSPTb
SPT3
3KSa
3KSR
Sa
Sa1P
C16:0-al
SGPL1
EP
SGPL1
C16:1-al
So1P
PPAP2A
SGPP2
SPHK1
SPHK2
PPAP2A
SGPP2
SPHK1
SPHK2
So
ASAH3L
PCHA
ASAH3
ASAH2
ASAH1
CerS5
CerS6
CerS4
CerS1
CerS2
CerS3
Elovl6
Elovl3
Elovl1
SCD
ASAH3
ASAH2
ASAH1
ASAH3L
PCHA
DHST
GAL3ST1
DHGalCe
UGT8
CERT
DHGlcCe
UGCG
B4GALT6
DHLacCe
DHCer
DES2
DES1
Cer
phyto
Cer
Phyto complex sphingolipids
SMS1
SMS2
SMase1
SMase2
DHSM
SMPD1
SMPD3
SMS1
SMS2
SM
UGT8
CERT
UGCG
CERK
Cer1P
GalCer
GlcCer
ST
GAL3ST1
B4GALT6
LacCer

Sf 59: MDA_N

REFERENCES

1. Merrill AH, Jr., Wang MD, Park M, Sullards MC: **(Glyco)sphingolipidology: an amazing challenge and opportunity for systems biology**. *Trends Biochem Sci* 2007, **32**(10):457-468.

2. Spiegel S: **Sphingosine 1-phosphate: a ligand for the EDG-1 family of G-protein-coupled receptors**. *Ann N Y Acad Sci* 2000, **905**:54-60.

3. Obeid LM, Linardic CM, Karolak LA, Hannun YA: **Programmed cell death induced by ceramide**. *Science* 1993, **259**(5102):1769-1771.

4. Stevens VL, Nimkar S, Jamison WC, Liotta DC, Merrill AH, Jr.: **Characteristics of the growth inhibition and cytotoxicity of long-chain (sphingoid) bases for Chinese hamster ovary cells: evidence for an involvement of protein kinase C**. *Biochim Biophys Acta* 1990, **1051**(1):37-45.

5. Bejaoui K, Wu C, Scheffler MD, Haan G, Ashby P, Wu L, de Jong P, Brown RH, Jr.: **SPTLC1 is mutated in hereditary sensory neuropathy, type 1**. *Nat Genet* 2001, **27**(3):261-262.

6. Dawkins JL, Hulme DJ, Brahmbhatt SB, Auer-Grumbach M, Nicholson GA: **Mutations in SPTLC1, encoding serine palmitoyltransferase, long chain base subunit-1, cause hereditary sensory neuropathy type I**. *Nat Genet* 2001, **27**(3):309-312.

7. Kolter T, Sandhoff K: **Sphingolipid metabolism diseases**. *Biochim Biophys Acta* 2006, **1758**(12):2057-2079.

8. Hakomori S: **Tumor-associated carbohydrate antigens defining tumor malignancy: basis for development of anti-cancer vaccines**. *Adv Exp Med Biol* 2001, **491**:369-402.

9. Hakomori S: **Glycosylation defining cancer malignancy: new wine in an old bottle**. *Proc Natl Acad Sci U S A* 2002, **99**(16):10231-10233.

10. Pruett ST, Bushnev A, Hagedorn K, Adiga M, Haynes CA, Sullards MC, Liotta DC, Merrill AH, Jr.: **Biodiversity of sphingoid bases ("sphingosines") and related amino alcohols**. *J Lipid Res* 2008, **49**(8):1621-1639.

11. Hornemann T, Penno A, von Eckardstein A: **The accumulation of two atypical sphingolipids cause hereditary sensory neuropathy type 1 (HSAN1)**. *Chemistry and Physics of Lipids* 2008, **154**:62-62.

12. Hornemann T, Penno A, Rutti MF, Ernst D, Kivrak-Pfiffner F, Rohrer L, von Eckardstein A: **The SPTLC3 subunit of serine palmitoyltransferase generates short chain sphingoid bases**. *J Biol Chem* 2009, **284**(39):26322-26330.

13. Gongshe Han SDG, Kenneth Gable, Somashekarappa Niranjanakumari, Prasun Moitra, Florian Eichler, Robert H. Brown,, Jr. JMHaTMD: **Identification of stimulatory subunits of serine palmitoyltransferase:**
multiple SPT isozymes with distinct substrate specificities. *Proc Natl Acad Sci U S A* 2010.

14. Laviad EL, Albee L, Pankova-Kholmyansky I, Epstein S, Park H, Merrill AH, Jr., Futerman AH: **Characterization of ceramide synthase 2: tissue distribution, substrate specificity, and inhibition by sphingosine 1-phosphate**. *J Biol Chem* 2008, **283**(9):5677-5684.

15. Mizutani Y, Kihara A, Igarashi Y: **Mammalian Lass6 and its related family members regulate synthesis of specific ceramides**. *Biochem J* 2005, **390**(Pt 1):263-271.

16. Mizutani Y, Kihara A, Igarashi Y: **LASS3 (longevity assurance homologue 3) is a mainly testis-specific (dihydro)ceramide synthase with relatively broad substrate specificity**. *Biochem J* 2006, **398**(3):531-538.

17. Riebeling C, Allegood JC, Wang E, Merrill AH, Jr., Futerman AH: **Two mammalian longevity assurance gene (LAG1) family members, trh1 and trh4, regulate dihydroceramide synthesis using different fatty acyl-CoA donors**. *J Biol Chem* 2003, **278**(44):43452-43459.

18. Venkataraman K, Riebeling C, Bodennec J, Riezman H, Allegood JC, Sullards MC, Merrill AH, Jr., Futerman AH: **Upstream of growth and differentiation factor 1 (uog1), a mammalian homolog of the yeast longevity assurance gene 1 (LAG1), regulates N-stearoyl-sphinganine (C18-(dihydro)ceramide) synthesis in a fumonisin B1-independent manner in mammalian cells**. *J Biol Chem* 2002, **277**(38):35642-35649.

19. Omae F, Miyazaki M, Enomoto A, Suzuki M, Suzuki Y, Suzuki A: **DES2 protein is responsible for phytoceramide biosynthesis in the mouse small intestine**. *Biochem J* 2004, **379**(Pt 3):687-695.

20. Tettamanti G: **Ganglioside/glycosphingolipid turnover: new concepts**. *Glycoconj J* 2004, **20**(5):301-317.

21. Bollinger CR, Teichgraber V, Gulbins E: **Ceramide-enriched membrane domains**. *Biochim Biophys Acta* 2005, **1746**(3):284-294.

22. Simons K, Ikonen E: **Functional rafts in cell membranes**. *Nature* 1997, **387**(6633):569-572.

23. Grassme H, Jekle A, Riehle A, Schwarz H, Berger J, Sandhoff K, Kolesnick R, Gulbins E: **CD95 signaling via ceramide-rich membrane rafts**. *J Biol Chem* 2001, **276**(23):20589-20596.

24. Cahuzac N, Baum W, Kirkin V, Conchonaud F, Wawrezinieck L, Marguet D, Janssen O, Zornig M, Hueber AO: **Fas Ligand is localized to membrane rafts where it displays increased cell death-inducing activity**. *Blood* 2005.

25. Huang Y, Yang J, Shen J, Chen FF, Yu Y: **Sphingolipids are involved in N-methyl-N'-nitro-N-nitrosoguanidine-induced epidermal growth factor receptor clustering**. *Biochem Biophys Res Commun* 2005, **330**(2):430-438.

26. Cremesti AE, Goni FM, Kolesnick R: **Role of sphingomyelinase and ceramide in modulating rafts: do biophysical properties determine biologic outcome?** *FEBS Lett* 2002, **531**(1):47-53.

27. Gulbins E, Kolesnick R: **Raft ceramide in molecular medicine**. *Oncogene* 2003, **22**(45):7070-7077.

28. Sjogren B, Svenningsson P: **Depletion of the lipid raft constituents, sphingomyelin and ganglioside, decreases serotonin binding at human 5-HT7(a) receptors in HeLa cells**. *Acta Physiol (Oxf)* 2007, **190**(1):47-53.

29. Gupta VR, Patel HK, Kostolansky SS, Ballivian RA, Eichberg J, Blanke SR: **Sphingomyelin functions as a novel receptor for Helicobacter pylori VacA**. *PLoS Pathog* 2008, **4**(5):e1000073.

30. Zheng M, Fang H, Tsuruoka T, Tsuji T, Sasaki T, Hakomori S: **Regulatory role of GM3 ganglioside in alpha 5 beta 1 integrin receptor for fibronectin-mediated adhesion of FUA169 cells**. *J Biol Chem* 1993, **268**(3):2217-2222.

31. Bremer EG, Hakomori S: **GM3 ganglioside induces hamster fibroblast growth inhibition in chemically-defined medium: ganglioside may regulate growth factor receptor function**. *Biochem Biophys Res Commun* 1982, **106**(3):711-718.

32. Iwabuchi K, Handa K, Hakomori S: **Separation of "glycosphingolipid signaling domain" from caveolin-containing membrane fraction in mouse melanoma B16 cells and its role in cell adhesion coupled with signaling**. *J Biol Chem* 1998, **273**(50):33766-33773.

33. Hakomori Si SI: **Inaugural Article: The glycosynapse**. *Proc Natl Acad Sci U S A* 2002, **99**(1):225-232.

34. Hakomori SI: **Structure and function of glycosphingolipids and sphingolipids: recollections and future trends**. *Biochim Biophys Acta* 2008, **1780**(3):325-346.

35. Ogawa D, Shikata K, Honke K, Sato S, Matsuda M, Nagase R, Tone A, Okada S, Usui H, Wada J *et al*: **Cerebroside sulfotransferase deficiency ameliorates L-selectin-dependent monocyte infiltration in the kidney after ureteral obstruction**. *J Biol Chem* 2004, **279**(3):2085-2090.

36. Crocker PR, Clark EA, Filbin M, Gordon S, Jones Y, Kehrl JH, Kelm S, Le Douarin N, Powell L, Roder J *et al*: **Siglecs: a family of sialic-acid binding lectins**. *Glycobiology* 1998, **8**(2):v.

37. Perillo NL, Marcus ME, Baum LG: **Galectins: versatile modulators of cell adhesion, cell proliferation, and cell death**. *J Mol Med* 1998, **76**(6):402-412.

38. Ono M, Handa K, Sonnino S, Withers DA, Nagai H, Hakomori S: **GM3 ganglioside inhibits CD9-facilitated haptotactic cell motility: coexpression of GM3 and CD9 is essential in the downregulation of tumor cell motility and malignancy**. *Biochemistry* 2001, **40**(21):6414-6421.

39. Meuillet EJ, Mania-Farnell B, George D, Inokuchi JI, Bremer EG: **Modulation of EGF receptor activity by changes in the GM3 content in a human epidermoid carcinoma cell line, A431**. *Exp Cell Res* 2000, **256**(1):74-82.

40. Zurita AR, Maccioni HJ, Daniotti JL: **Modulation of epidermal growth factor receptor phosphorylation by endogenously expressed gangliosides**. *Biochem J* 2001, **355**(Pt 2):465-472.

41. Karlsson KA: **On the character and functions of sphingolipids**. *Acta Biochim Pol* 1998, **45**(2):429-438.

42. Lingwood CA: **Verotoxin/globotriaosyl ceramide recognition: angiopathy, angiogenesis and antineoplasia**. *Biosci Rep* 1999, **19**(5):345-354.

43. Hannun YA, Obeid LM: **Principles of bioactive lipid signalling: lessons from sphingolipids**. *Nat Rev Mol Cell Biol* 2008, **9**(2):139-150.

44. Igarashi Y, Hakomori S, Toyokuni T, Dean B, Fujita S, Sugimoto M, Ogawa T, el-Ghendy K, Racker E: **Effect of chemically well-defined sphingosine and its N-methyl derivatives on protein kinase C and src kinase activities**. *Biochemistry* 1989, **28**(17):6796-6800.

45. Hannun YA, Loomis CR, Merrill AH, Jr., Bell RM: **Sphingosine inhibition of protein kinase C activity and of phorbol dibutyrate binding in vitro and in human platelets**. *J Biol Chem* 1986, **261**(27):12604-12609.

46. Chiang CW, Kanies C, Kim KW, Fang WB, Parkhurst C, Xie M, Henry T, Yang E: **Protein phosphatase 2A dephosphorylation of phosphoserine 112 plays the gatekeeper role for BAD-mediated apoptosis**. *Mol Cell Biol* 2003, **23**(18):6350-6362.

47. Xin M, Deng X: **Protein phosphatase 2A enhances Bax's proapoptotic function through dephosphorylation**. *J Biol Chem* 2006.

48. Wang G, Silva J, Krishnamurthy K, Tran E, Condie BG, Bieberich E: **Direct binding to ceramide activates protein kinase Czeta before the formation of a pro-apoptotic complex with PAR-4 in differentiating stem cells**. *J Biol Chem* 2005, **280**(28):26415-26424.

49. Kashiwagi K, Shirai Y, Kuriyama M, Sakai N, Saito N: **Importance of C1B domain for lipid messenger-induced targeting of protein kinase C**. *J Biol Chem* 2002, **277**(20):18037-18045.

50. Kajimoto T, Shirai Y, Sakai N, Yamamoto T, Matsuzaki H, Kikkawa U, Saito N: **Ceramide-induced apoptosis by translocation, phosphorylation, and activation of protein kinase Cdelta in the Golgi complex**. *J Biol Chem* 2004, **279**(13):12668-12676.

51. Aschrafi A, Franzen R, Shabahang S, Fabbro D, Pfeilschifter J, Huwiler A: **Ceramide induces translocation of protein kinase C-alpha to the Golgi compartment of human embryonic kidney cells by interacting with the C2 domain**. *Biochim Biophys Acta* 2003, **1634**(1-2):30-39.

52. Becker KP, Kitatani K, Idkowiak-Baldys J, Bielawski J, Hannun YA: **Selective inhibition of juxtanuclear translocation of protein kinase C betaII by a negative feedback mechanism involving ceramide formed from the salvage pathway**. *J Biol Chem* 2005, **280**(4):2606-2612.

53. Yellaturu CR, Bhanoori M, Neeli I, Rao GN: **N-Ethylmaleimide inhibits platelet-derived growth factor BB-stimulated Akt phosphorylation via activation of protein phosphatase 2A**. *J Biol Chem* 2002, **277**(42):40148-40155.

54. Ruvolo PP, Deng X, Ito T, Carr BK, May WS: **Ceramide induces Bcl2 dephosphorylation via a mechanism involving mitochondrial PP2A**. *J Biol Chem* 1999, **274**(29):20296-20300.

55. Heinrich M, Neumeyer J, Jakob M, Hallas C, Tchikov V, Winoto-Morbach S, Wickel M, Schneider-Brachert W, Trauzold A, Hethke A *et al*: **Cathepsin D links TNF-induced acid sphingomyelinase to Bid-mediated caspase-9 and -3 activation**. *Cell Death Differ* 2004, **11**(5):550-563.

56. Hobson JP, Rosenfeldt HM, Barak LS, Olivera A, Poulton S, Caron MG, Milstien S, Spiegel S: **Role of the sphingosine-1-phosphate receptor EDG-1 in PDGF-induced cell motility**. *Science* 2001, **291**(5509):1800-1803.

57. Lee MJ, Van Brocklyn JR, Thangada S, Liu CH, Hand AR, Menzeleev R, Spiegel S, Hla T: **Sphingosine-1-phosphate as a ligand for the G protein-coupled receptor EDG-1**. *Science* 1998, **279**(5356):1552-1555.

58. Cuvillier O, Pirianov G, Kleuser B, Vanek PG, Coso OA, Gutkind S, Spiegel S: **Suppression of ceramide-mediated programmed cell death by sphingosine-1-phosphate**. *Nature* 1996, **381**(6585):800-803.

59. Mandala SM, Thornton R, Tu Z, Kurtz MB, Nickels J, Broach J, Menzeleev R, Spiegel S: **Sphingoid base 1-phosphate phosphatase: a key regulator of sphingolipid metabolism and stress response**. *Proc Natl Acad Sci U S A* 1998, **95**(1):150-155.

60. Bremer EG, Schlessinger J, Hakomori S: **Ganglioside-mediated modulation of cell growth. Specific effects of GM3 on tyrosine phosphorylation of the epidermal growth factor receptor**. *J Biol Chem* 1986, **261**(5):2434-2440.

61. Yates AJ, VanBrocklyn J, Saqr HE, Guan Z, Stokes BT, O'Dorisio MS: **Mechanisms through which gangliosides inhibit PDGF-stimulated mitogenesis in intact Swiss 3T3 cells: receptor tyrosine phosphorylation, intracellular calcium, and receptor binding**. *Exp Cell Res* 1993, **204**(1):38-45.

62. Bremer EG, Hakomori S, Bowen-Pope DF, Raines E, Ross R: **Ganglioside-mediated modulation of cell growth, growth factor binding, and receptor phosphorylation**. *J Biol Chem* 1984, **259**(11):6818-6825.

63. Iwabuchi K, Yamamura S, Prinetti A, Handa K, Hakomori S: **GM3-enriched microdomain involved in cell adhesion and signal transduction through carbohydrate-carbohydrate interaction in mouse melanoma B16 cells**. *J Biol Chem* 1998, **273**(15):9130-9138.

64. Sorice M, Garofalo T, Misasi R, Longo A, Mikulak J, Dolo V, Pontieri GM, Pavan A: **Association between GM3 and CD4-Ick complex in human peripheral blood lymphocytes**. *Glycoconj J* 2000, **17**(3 -4):247-252.

65. Breslow DK, Collins SR, Bodenmiller B, Aebersold R, Simons K, Shevchenko A, Ejsing CS, Weissman JS: **Orm family proteins mediate sphingolipid homeostasis**. *Nature*, **463**(7284):1048-1053.

66. Han G, Gupta SD, Gable K, Niranjanakumari S, Moitra P, Eichler F, Brown RH, Jr., Harmon JM, Dunn TM: **Identification of small subunits of mammalian**

serine palmitoyltransferase that confer distinct acyl-CoA substrate specificities. *Proc Natl Acad Sci U S A* 2009, **106**(20):8186-8191.

67. Wagener R, Rohn G, Schillinger G, Schroder R, Kobbe B, Ernestus RI: **Ganglioside profiles in human gliomas: quantification by microbore high performance liquid chromatography and correlation to histomorphology and grading**. *Acta Neurochir (Wien)* 1999, **141**(12):1339-1345.

68. Sung CC, Pearl DK, Coons SW, Scheithauer BW, Johnson PC, Yates AJ: **Gangliosides as diagnostic markers of human astrocytomas and primitive neuroectodermal tumors**. *Cancer* 1994, **74**(11):3010-3022.

69. Vukelic Z, Kalanj-Bognar S, Froesch M, Bindila L, Radic B, Allen M, Peter-Katalinic J, Zamfir AD: **Human gliosarcoma-associated ganglioside composition is complex and distinctive as evidenced by high-performance mass spectrometric determination and structural characterization**. *Glycobiology* 2007, **17**(5):504-515.

70. Nudelman E, Hakomori S, Kannagi R, Levery S, Yeh MY, Hellstrom KE, Hellstrom I: **Characterization of a human melanoma-associated ganglioside antigen defined by a monoclonal antibody, 4.2**. *J Biol Chem* 1982, **257**(21):12752-12756.

71. Pukel CS, Lloyd KO, Travassos LR, Dippold WG, Oettgen HF, Old LJ: **GD3, a prominent ganglioside of human melanoma. Detection and characterisation by mouse monoclonal antibody**. *J Exp Med* 1982, **155**(4):1133-1147.

72. Ravindranath MH, Muthugounder S, Presser N: **Ganglioside signatures of primary and nodal metastatic melanoma cell lines from the same patient**. *Melanoma Res* 2008, **18**(1):47-55.

73. Popa I, Pons A, Mariller C, Tai T, Zanetta JP, Thomas L, Portoukalian J: **Purification and structural characterization of de-N-acetylated form of GD3 ganglioside present in human melanoma tumors**. *Glycobiology* 2007, **17**(4):367-373.

74. Ravindranath MH, Amiri AA, Bauer PM, Kelley MC, Essner R, Morton DL: **Endothelial-selectin ligands sialyl Lewis(x) and sialyl Lewis(a) are differentiation antigens immunogenic in human melanoma**. *Cancer* 1997, **79**(9):1686-1697.

75. Kiguchi K, Takamatsu K, Tanaka J, Nozawa S, Iwamori M, Nagai Y: **Glycosphingolipids of various human ovarian tumors: a significantly high expression of I3SO3GalCer and Lewis antigen in mucinous cystadenocarcinoma**. *Cancer Res* 1992, **52**(2):416-421.

76. Makhlouf AM, Fathalla MM, Zakhary MA, Makarem MH: **Sulfatides in ovarian tumors: clinicopathological correlates**. *Int J Gynecol Cancer* 2004, **14**(1):89-93.

77. Satoh M, Fukushi Y, Kawamura S, Ohyama C, Saito S, Orikasa S, Nudleman E, Hakamori S: **Glycolipid expression in prostatic tissue and analysis of the antigen recognized by antiprostatic monoclonal antibody APG1**. *Urol Int* 1992, **48**(1):20-24.

78. Marquina G, Waki H, Fernandez LE, Kon K, Carr A, Valiente O, Perez R, Ando S: **Gangliosides expressed in human breast cancer**. *Cancer Res* 1996, **56**(22):5165-5171.

79. Chang WW, Lee CH, Lee P, Lin J, Hsu CW, Hung JT, Lin JJ, Yu JC, Shao LE, Yu J *et al*: **Expression of Globo H and SSEA3 in breast cancer stem cells and the involvement of fucosyl transferases 1 and 2 in Globo H synthesis**. *Proc Natl Acad Sci U S A* 2008, **105**(33):11667-11672.

80. Menard S, Tagliabue E, Canevari S, Fossati G, Colnaghi MI: **Generation of monoclonal antibodies reacting with normal and cancer cells of human breast**. *Cancer Res* 1983, **43**(3):1295-1300.

81. Wiesner DA, Sweeley CC: **Circulating gangliosides of breast-cancer patients**. *Int J Cancer* 1995, **60**(3):294-299.

82. Nohara K, Wang F, Spiegel S: **Glycosphingolipid composition of MDA-MB-231 and MCF-7 human breast cancer cell lines**. *Breast Cancer Res Treat* 1998, **48**(2):149-157.

83. Vartanian T, Dawson G, Soliven B, Nelson DJ, Szuchet S: **Phosphorylation of myelin basic protein in intact oligodendrocytes: inhibition by galactosylsphingosine and cyclic AMP**. *Glia* 1989, **2**(5):370-379.

84. Suzuki E, Handa K, Toledo MS, Hakomori S: **Sphingosine-dependent apoptosis: a unified concept based on multiple mechanisms operating in concert**. *Proc Natl Acad Sci U S A* 2004, **101**(41):14788-14793.

85. Gewirtz DA: **Growth arrest and cell death in the breast tumor cell in response to ionizing radiation and chemotherapeutic agents which induce DNA damage**. *Breast Cancer Res Treat* 2000, **62**(3):223-235.

86. Kok JW, Sietsma H: **Sphingolipid metabolism enzymes as targets for anticancer therapy**. *Curr Drug Targets* 2004, **5**(4):375-382.

87. Senchenkov A, Litvak DA, Cabot MC: **Targeting ceramide metabolism--a strategy for overcoming drug resistance**. *J Natl Cancer Inst* 2001, **93**(5):347-357.

88. Scarlatti F, Bauvy C, Ventruti A, Sala G, Cluzeaud F, Vandewalle A, Ghidoni R, Codogno P: **Ceramide-mediated macroautophagy involves inhibition of protein kinase B and up-regulation of beclin 1**. *J Biol Chem* 2004, **279**(18):18384-18391.

89. Klionsky DJ, Emr SD: **Autophagy as a regulated pathway of cellular degradation**. *Science* 2000, **290**(5497):1717-1721.

90. Zheng W, Kollmeyer J, Symolon H, Momin A, Munter E, Wang E, Kelly S, Allegood JC, Liu Y, Peng Q *et al*: **Ceramides and other bioactive sphingolipid backbones in health and disease: lipidomic analysis, metabolism and roles in membrane structure, dynamics, signaling and autophagy**. *Biochim Biophys Acta* 2006, **1758**(12):1864-1884.

91. Yan G, Chen S, You B, Sun J: **Activation of sphingosine kinase-1 mediates induction of endothelial cell proliferation and angiogenesis by epoxyeicosatrienoic acids**. *Cardiovasc Res* 2008, **78**(2):308-314.

92. Liu Y, Wada R, Yamashita T, Mi Y, Deng CX, Hobson JP, Rosenfeldt HM, Nava VE, Chae SS, Lee MJ *et al*: **Edg-1, the G protein-coupled receptor for sphingosine-1-phosphate, is essential for vascular maturation**. *J Clin Invest* 2000, **106**(8):951-961.

93. Pinedo HM, Verheul HM, D'Amato RJ, Folkman J: **Involvement of platelets in tumour angiogenesis?** *Lancet* 1998, **352**(9142):1775-1777.

94. Chae SS, Paik JH, Furneaux H, Hla T: **Requirement for sphingosine 1-phosphate receptor-1 in tumor angiogenesis demonstrated by in vivo RNA interference**. *J Clin Invest* 2004, **114**(8):1082-1089.

95. Visentin B, Vekich JA, Sibbald BJ, Cavalli AL, Moreno KM, Matteo RG, Garland WA, Lu Y, Yu S, Hall HS *et al*: **Validation of an anti-sphingosine-1-phosphate antibody as a potential therapeutic in reducing growth, invasion, and angiogenesis in multiple tumor lineages**. *Cancer Cell* 2006, **9**(3):225-238.

96. Satoh M, Ito A, Nojiri H, Handa K, Numahata K, Ohyama C, Saito S, Hoshi S, Hakomori SI: **Enhanced GM3 expression, associated with decreased invasiveness, is induced by brefeldin A in bladder cancer cells**. *Int J Oncol* 2001, **19**(4):723-731.

97. Prinetti A, Iwabuchi K, Hakomori S: **Glycosphingolipid-enriched signaling domain in mouse neuroblastoma Neuro2a cells. Mechanism of ganglioside-dependent neuritogenesis**. *J Biol Chem* 1999, **274**(30):20916-20924.

98. Carr A, Mazorra Z, Alonso DF, Mesa C, Valiente O, Gomez DE, Perez R, Fernandez LE: **A purified GM3 ganglioside conjugated vaccine induces specific, adjuvant-dependent and non-transient antitumour activity against B16 mouse melanoma in vitro and in vivo**. *Melanoma Res* 2001, **11**(3):219-227.

99. Mazorra Z, Mesa C, Fernandez A, Fernandez LE: **Immunization with a GM3 ganglioside nanoparticulated vaccine confers an effector CD8(+) T cells-mediated protection against melanoma B16 challenge**. *Cancer Immunol Immunother* 2008, **57**(12):1771-1780.

100. Hamamura K, Furukawa K, Hayashi T, Hattori T, Nakano J, Nakashima H, Okuda T, Mizutani H, Hattori H, Ueda M *et al*: **Ganglioside GD3 promotes cell growth and invasion through p130Cas and paxillin in malignant melanoma cells**. *Proc Natl Acad Sci U S A* 2005, **102**(31):11041-11046.

101. Nakashima H, Hamamura K, Houjou T, Taguchi R, Yamamoto N, Mitsudo K, Tohnai I, Ueda M, Urano T, Furukawa K *et al*: **Overexpression of caveolin-1 in a human melanoma cell line results in dispersion of ganglioside GD3 from lipid rafts and alteration of leading edges, leading to attenuation of malignant properties**. *Cancer Sci* 2007, **98**(4):512-520.

102. Kang NY, Kim CH, Kim KS, Ko JH, Lee JH, Jeong YK, Lee YC: **Expression of the human CMP-NeuAc:GM3 alpha2,8-sialyltransferase (GD3 synthase) gene through the NF-kappaB activation in human melanoma SK-MEL-2 cells**. *Biochim Biophys Acta* 2007, **1769**(11-12):622-630.

103. Iglesias-Bartolome R, Crespo PM, Gomez GA, Daniotti JL: **The antibody to GD3 ganglioside, R24, is rapidly endocytosed and recycled to the plasma membrane via the endocytic recycling compartment. Inhibitory effect of brefeldin A and monensin**. *FEBS J* 2006, **273**(8):1744-1758.

104. Cheresh DA, Pierschbacher MD, Herzig MA, Mujoo K: **Disialogangliosides GD2 and GD3 are involved in the attachment of human melanoma and neuroblastoma cells to extracellular matrix proteins**. *J Cell Biol* 1986, **102**(3):688-696.

105. Sadeghlar F, Sandhoff K, van Echten-Deckert G: **Cell type specific localization of sphingomyelin biosynthesis**. *FEBS Lett* 2000, **478**(1-2):9-12.

106. Zeng G, Gao L, Birkle S, Yu RK: **Suppression of ganglioside GD3 expression in a rat F-11 tumor cell line reduces tumor growth, angiogenesis, and vascular endothelial growth factor production**. *Cancer Res* 2000, **60**(23):6670-6676.

107. Zhang S, Cordon-Cardo C, Zhang HS, Reuter VE, Adluri S, Hamilton WB, Lloyd KO, Livingston PO: **Selection of tumor antigens as targets for immune attack**

using immunohistochemistry: I. Focus on gangliosides. *Int J Cancer* 1997, **73**(1):42-49.

108. Ha KT, Lee YC, Kim CH: **Overexpression of GD3 synthase induces apoptosis of vascular endothelial ECV304 cells through downregulation of Bcl-2**. *FEBS Lett* 2004, **568**(1-3):183-187.

109. Okada M, Furukawa K, Yamashiro S, Yamada Y, Haraguchi M, Horibe K, Kato K, Tsuji Y, Furukawa K: **High expression of ganglioside alpha-2,8-sialyltransferase (GD3 synthase) gene in adult T-cell leukemia cells unrelated to the gene expression of human T-lymphotropic virus type I**. *Cancer Res* 1996, **56**(12):2844-2848.

110. Hamamura K, Furukawa K, Hayashi T, Hattori T, Nakano J, Nakashima H, Okuda T, Mizutani H, Hattori H, Ueda M *et al*: **Ganglioside GD3 promotes cell growth and invasion through p130Cas and paxillin in malignant melanoma cells**. *Proc Natl Acad Sci U S A* 2005, **102**(31):11041-11046.

111. Scorrano L, Petronilli V, Di Lisa F, Bernardi P: **Commitment to apoptosis by GD3 ganglioside depends on opening of the mitochondrial permeability transition pore**. *J Biol Chem* 1999, **274**(32):22581-22585.

112. Pilkington GJ, Parker K, Murray SA: **Approaches to mitochondrially mediated cancer therapy**. *Semin Cancer Biol* 2007.

113. Colell A, Garcia-Ruiz C, Mari M, Fernandez-Checa JC: **Mitochondrial permeability transition induced by reactive oxygen species is independent of cholesterol-regulated membrane fluidity**. *FEBS Lett* 2004, **560**(1-3):63-68.

114. Pastorino JG, Tafani M, Rothman RJ, Marcinkeviciute A, Hoek JB, Farber JL: **Functional consequences of the sustained or transient activation by Bax of the mitochondrial permeability transition pore**. *J Biol Chem* 1999, **274**(44):31734-31739.

115. Hasegawa T, Sugeno N, Takeda A, Matsuzaki-Kobayashi M, Kikuchi A, Furukawa K, Miyagi T, Itoyama Y: **Role of Neu4L sialidase and its substrate ganglioside GD3 in neuronal apoptosis induced by catechol metabolites**. *FEBS Lett* 2007, **581**(3):406-412.

116. Paris R, Morales A, Coll O, Sanchez-Reyes A, Garcia-Ruiz C, Fernandez-Checa JC: **Ganglioside GD3 sensitizes human hepatoma cells to cancer therapy**. *J Biol Chem* 2002, **277**(51):49870-49876.

117. Boyle PJ, Ma R, Tuteja N, Banerjee S, Basu S: **Apoptosis of human breast carcinoma cells in the presence of cis-platin and L-/D-PPMP: IV. Modulation**

of replication complexes and glycolipid: Glycosyltransferases. *Glycoconj J* 2006, **23**(3-4):175-187.

118. Corazzari M, Lovat PE, Oliverio S, Di Sano F, Donnorso RP, Redfern CP, Piacentini M: **Fenretinide: a p53-independent way to kill cancer cells**. *Biochem Biophys Res Commun* 2005, **331**(3):810-815.

119. Lovat PE, Corazzari M, Di Sano F, Piacentini M, Redfern CP: **The role of gangliosides in fenretinide-induced apoptosis of neuroblastoma**. *Cancer Lett* 2005, **228**(1-2):105-110.

120. Montaldo PG, Pagnan G, Pastorino F, Chiesa V, Raffaghello L, Kirchmeier M, Allen TM, Ponzoni M: **N-(4-hydroxyphenyl) retinamide is cytotoxic to melanoma cells in vitro through induction of programmed cell death**. *Int J Cancer* 1999, **81**(2):262-267.

121. Taraboletti G, Rao CN, Krutzsch HC, Liotta LA, Roberts DD: **Sulfatide-binding domain of the laminin A chain**. *J Biol Chem* 1990, **265**(21):12253-12258.

122. Roberts DD, Wewer UM, Liotta LA, Ginsburg V: **Laminin-dependent and laminin-independent adhesion of human melanoma cells to sulfatides**. *Cancer Res* 1988, **48**(12):3367-3373.

123. Aruffo A, Kolanus W, Walz G, Fredman P, Seed B: **CD62/P-selectin recognition of myeloid and tumor cell sulfatides**. *Cell* 1991, **67**(1):35-44.

124. Garcia J, Callewaert N, Borsig L: **P-selectin mediates metastatic progression through binding to sulfatides on tumor cells**. *Glycobiology* 2007, **17**(2):185-196.

125. Guo NH, Krutzsch HC, Negre E, Vogel T, Blake DA, Roberts DD: **Heparin- and sulfatide-binding peptides from the type I repeats of human thrombospondin promote melanoma cell adhesion**. *Proc Natl Acad Sci U S A* 1992, **89**(7):3040-3044.

126. Guo NH, Krutzsch HC, Negre E, Zabrenetzky VS, Roberts DD: **Heparin-binding peptides from the type I repeats of thrombospondin. Structural requirements for heparin binding and promotion of melanoma cell adhesion and chemotaxis**. *J Biol Chem* 1992, **267**(27):19349-19355.

127. Zhong Wu X, Honke K, Long Zhang Y, Liang Zha X, Taniguchi N: **Lactosylsulfatide expression in hepatocellular carcinoma cells enhances cell adhesion to vitronectin and intrahepatic metastasis in nude mice**. *Int J Cancer* 2004, **110**(4):504-510.

128. Kobayashi T, Honke K, Miyazaki T, Matsumoto K, Nakamura T, Ishizuka I, Makita A: **Hepatocyte growth factor specifically binds to sulfoglycolipids**. *J Biol Chem* 1994, **269**(13):9817-9821.

129. Sandhoff R, Grieshaber H, Djafarzadeh R, Sijmonsma TP, Proudfoot AE, Handel TM, Wiegandt H, Nelson PJ, Grone HJ: **Chemokines bind to sulfatides as revealed by surface plasmon resonance**. *Biochim Biophys Acta* 2005, **1687**(1-3):52-63.

130. Duchesneau P, Gallagher E, Walcheck B, Waddell TK: **Up-regulation of leukocyte CXCR4 expression by sulfatide: an L-selectin-dependent pathway on CD4+ T cells**. *Eur J Immunol* 2007, **37**(10):2949-2960.

131. Turutin DV, Kubareva EA, Pushkareva MA, Ullrich V, Sud'ina GF: **Activation of NF-kappa B transcription factor in human neutrophils by sulphatides and L-selectin cross-linking**. *FEBS Lett* 2003, **536**(1-3):241-245.

132. Kawakita M, Tsuji Y, Nakata Y, Ogasawara T, Takemura T, Isojima S, Koyama K: **Progesterone treatment decreases sulfate carbohydrate antigen on endometrial carcinoma cells and inhibits the cell binding to laminin**. *Gynecol Oncol* 1995, **57**(3):313-320.

133. Yamashiro S, Okada M, Haraguchi M, Furukawa K, Lloyd KO, Shiku H: **Expression of alpha 2,8-sialyltransferase (GD3 synthase) gene in human cancer cell lines: high level expression in melanomas and up-regulation in activated T lymphocytes**. *Glycoconj J* 1995, **12**(6):894-900.

134. Senkal CE, Ponnusamy S, Rossi MJ, Bialewski J, Sinha D, Jiang JC, Jazwinski SM, Hannun YA, Ogretmen B: **Role of human longevity assurance gene 1 and C18-ceramide in chemotherapy-induced cell death in human head and neck squamous cell carcinomas**. *Mol Cancer Ther* 2007, **6**(2):712-722.

135. Barrett T, Troup DB, Wilhite SE, Ledoux P, Rudnev D, Evangelista C, Kim IF, Soboleva A, Tomashevsky M, Edgar R: **NCBI GEO: mining tens of millions of expression profiles--database and tools update**. *Nucleic Acids Res* 2007, **35**(Database issue):D760-765.

136. Parkinson H, Sarkans U, Shojatalab M, Abeygunawardena N, Contrino S, Coulson R, Farne A, Lara GG, Holloway E, Kapushesky M *et al*: **ArrayExpress--a public repository for microarray gene expression data at the EBI**. *Nucleic Acids Res* 2005, **33**(Database issue):D553-555.

137. Rhodes DR, Yu J, Shanker K, Deshpande N, Varambally R, Ghosh D, Barrette T, Pandey A, Chinnaiyan AM: **ONCOMINE: a cancer microarray database and integrated data-mining platform**. *Neoplasia* 2004, **6**(1):1-6.

138. Kiguchi K, Iwamori Y, Suzuki N, Kobayashi Y, Ishizuka B, Ishiwata I, Kita T, Kikuchi Y, Iwamori M: **Characteristic expression of globotriaosyl ceramide in human ovarian carcinoma-derived cells with anticancer drug resistance**. *Cancer Sci* 2006, **97**(12):1321-1326.

139. van Iersel MP, Kelder T, Pico AR, Hanspers K, Coort S, Conklin BR, Evelo C: **Presenting and exploring biological pathways with PathVisio**. *BMC Bioinformatics* 2008, **9**(1):399.

140. Pico AR, Kelder T, van Iersel MP, Hanspers K, Conklin BR, Evelo C: **WikiPathways: pathway editing for the people**. *PLoS Biol* 2008, **6**(7):e184.

141. Liu G, Loraine AE, Shigeta R, Cline M, Cheng J, Valmeekam V, Sun S, Kulp D, Siani-Rose MA: **NetAffx: Affymetrix probesets and annotations**. *Nucleic Acids Res* 2003, **31**(1):82-86.

142. Kent WJ: **BLAT--the BLAST-like alignment tool**. *Genome Res* 2002, **12**(4):656-664.

143. Kent WJ, Sugnet CW, Furey TS, Roskin KM, Pringle TH, Zahler AM, Haussler D: **The human genome browser at UCSC**. *Genome Res* 2002, **12**(6):996-1006.

144. Yamaoka S, Miyaji M, Kitano T, Umehara H, Okazaki T: **Expression cloning of a human cDNA restoring sphingomyelin synthesis and cell growth in sphingomyelin synthase-defective lymphoid cells**. *J Biol Chem* 2004, **279**(18):18688-18693.

145. Jakobsson A, Westerberg R, Jacobsson A: **Fatty acid elongases in mammals: their regulation and roles in metabolism**. *Prog Lipid Res* 2006, **45**(3):237-249.

146. Miyazaki M, Ntambi JM: **Role of stearoyl-coenzyme A desaturase in lipid metabolism**. *Prostaglandins Leukot Essent Fatty Acids* 2003, **68**(2):113-121.

147. Hornemann T, Richard S, Rutti MF, Wei Y, von Eckardstein A: **Cloning and initial characterization of a new subunit for mammalian serine-palmitoyltransferase**. *J Biol Chem* 2006, **281**(49):37275-37281.

148. Kihara A, Igarashi Y: **FVT-1 is a mammalian 3-ketodihydrosphingosine reductase with an active site that faces the cytosolic side of the endoplasmic reticulum membrane**. *J Biol Chem* 2004, **279**(47):49243-49250.

149. Liu H, Sugiura M, Nava VE, Edsall LC, Kono K, Poulton S, Milstien S, Kohama T, Spiegel S: **Molecular cloning and functional characterization of a novel mammalian sphingosine kinase type 2 isoform**. *J Biol Chem* 2000, **275**(26):19513-19520.

150. Van Veldhoven PP, Gijsbers S, Mannaerts GP, Vermeesch JR, Brys V: **Human sphingosine-1-phosphate lyase: cDNA cloning, functional expression studies and mapping to chromosome 10q22(1)**. *Biochim Biophys Acta* 2000, **1487**(2-3):128-134.

151. Mao C, Xu R, Szulc ZM, Bielawski J, Becker KP, Bielawska A, Galadari SH, Hu W, Obeid LM: **Cloning and characterization of a mouse endoplasmic reticulum alkaline ceramidase: an enzyme that preferentially regulates metabolism of very long chain ceramides**. *J Biol Chem* 2003, **278**(33):31184-31191.

152. Koch J, Gartner S, Li CM, Quintern LE, Bernardo K, Levran O, Schnabel D, Desnick RJ, Schuchman EH, Sandhoff K: **Molecular cloning and characterization of a full-length complementary DNA encoding human acid ceramidase. Identification Of the first molecular lesion causing Farber disease**. *J Biol Chem* 1996, **271**(51):33110-33115.

153. El Bawab S, Roddy P, Qian T, Bielawska A, Lemasters JJ, Hannun YA: **Molecular cloning and characterization of a human mitochondrial ceramidase**. *J Biol Chem* 2000, **275**(28):21508-21513.

154. Xu R, Jin J, Hu W, Sun W, Bielawski J, Szulc Z, Taha T, Obeid LM, Mao C: **Golgi alkaline ceramidase regulates cell proliferation and survival by controlling levels of sphingosine and S1P**. *FASEB J* 2006, **20**(11):1813-1825.

155. Mao C, Xu R, Szulc ZM, Bielawska A, Galadari SH, Obeid LM: **Cloning and characterization of a novel human alkaline ceramidase. A mammalian enzyme that hydrolyzes phytoceramide**. *J Biol Chem* 2001, **276**(28):26577-26588.

156. Huitema K, van den Dikkenberg J, Brouwers JF, Holthuis JC: **Identification of a family of animal sphingomyelin synthases**. *EMBO J* 2004, **23**(1):33-44.

157. Ichikawa S, Sakiyama H, Suzuki G, Hidari KI, Hirabayashi Y: **Expression cloning of a cDNA for human ceramide glucosyltransferase that catalyzes the first glycosylation step of glycosphingolipid synthesis**. *Proc Natl Acad Sci U S A* 1996, **93**(10):4638-4643.

158. Bosio A, Binczek E, Le Beau MM, Fernald AA, Stoffel W: **The human gene CGT encoding the UDP-galactose ceramide galactosyl transferase (cerebroside synthase): cloning, characterization, and assignment to human chromosome 4, band q26**. *Genomics* 1996, **34**(1):69-75.

159. Lamour NF, Stahelin RV, Wijesinghe DS, Maceyka M, Wang E, Allegood JC, Merrill AH, Jr., Cho W, Chalfant CE: **Ceramide kinase uses ceramide provided**

by ceramide transport protein: localization to organelles of eicosanoid synthesis. *J Lipid Res* 2007, **48**(6):1293-1304.

160. Sugiura M, Kono K, Liu H, Shimizugawa T, Minekura H, Spiegel S, Kohama T: **Ceramide kinase, a novel lipid kinase. Molecular cloning and functional characterization**. *J Biol Chem* 2002, **277**(26):23294-23300.

161. Hanada K, Kumagai K, Tomishige N, Yamaji T: **CERT-mediated trafficking of ceramide**. *Biochim Biophys Acta* 2009, **1791**(7):684-691.

162. Hanada K, Kumagai K, Yasuda S, Miura Y, Kawano M, Fukasawa M, Nishijima M: **Molecular machinery for non-vesicular trafficking of ceramide**. *Nature* 2003, **426**(6968):803-809.

163. Schuchman EH, Suchi M, Takahashi T, Sandhoff K, Desnick RJ: **Human acid sphingomyelinase. Isolation, nucleotide sequence and expression of the full-length and alternatively spliced cDNAs**. *J Biol Chem* 1991, **266**(13):8531-8539.

164. Hofmann K, Tomiuk S, Wolff G, Stoffel W: **Cloning and characterization of the mammalian brain-specific, Mg2+-dependent neutral sphingomyelinase**. *Proc Natl Acad Sci U S A* 2000, **97**(11):5895-5900.

165. Takizawa M, Nomura T, Wakisaka E, Yoshizuka N, Aoki J, Arai H, Inoue K, Hattori M, Matsuo N: **cDNA cloning and expression of human lactosylceramide synthase**. *Biochim Biophys Acta* 1999, **1438**(2):301-304.

166. Han G, Gupta SD, Gable K, Niranjanakumari S, Moitra P, Eichler F, Brown RH, Jr., Harmon JM, Dunn TM: **Identification of small subunits of mammalian serine palmitoyltransferase that confer distinct acyl-CoA substrate specificities**. *Proc Natl Acad Sci U S A* 2009.

167. Shankavaram UT, Reinhold WC, Nishizuka S, Major S, Morita D, Chary KK, Reimers MA, Scherf U, Kahn A, Dolginow D *et al*: **Transcript and protein expression profiles of the NCI-60 cancer cell panel: an integromic microarray study**. *Mol Cancer Ther* 2007, **6**(3):820-832.

168. Turashvili G, Bouchal J, Baumforth K, Wei W, Dziechciarkova M, Ehrmann J, Klein J, Fridman E, Skarda J, Srovnal J *et al*: **Novel markers for differentiation of lobular and ductal invasive breast carcinomas by laser microdissection and microarray analysis**. *BMC Cancer* 2007, **7**:55.

169. Hoeflich KP, O'Brien C, Boyd Z, Cavet G, Guerrero S, Jung K, Januario T, Savage H, Punnoose E, Truong T *et al*: **In vivo antitumor activity of MEK and phosphatidylinositol 3-kinase inhibitors in basal-like breast cancer models**. *Clin Cancer Res* 2009, **15**(14):4649-4664.

170. Lee PL, Kohler JJ, Pfeffer SR: **Association of beta-1,3-N-acetylglucosaminyltransferase 1 and beta-1,4-galactosyltransferase 1, trans-Golgi enzymes involved in coupled poly-N-acetyllactosamine synthesis**. *Glycobiology* 2009, **19**(6):655-664.

171. Almeida R, Amado M, David L, Levery SB, Holmes EH, Merkx G, van Kessel AG, Rygaard E, Hassan H, Bennett E *et al*: **A family of human beta4-galactosyltransferases. Cloning and expression of two novel UDP-galactose:beta-n-acetylglucosamine beta1, 4-galactosyltransferases, beta4Gal-T2 and beta4Gal-T3**. *J Biol Chem* 1997, **272**(51):31979-31991.

172. Kumagai T, Tanaka M, Yokoyama M, Sato T, Shinkai T, Furukawa K: **Early lethality of beta-1,4-galactosyltransferase V-mutant mice by growth retardation**. *Biochem Biophys Res Commun* 2009, **379**(2):456-459.

173. Wandall HH, Pizette S, Pedersen JW, Eichert H, Levery SB, Mandel U, Cohen SM, Clausen H: **Egghead and brainiac are essential for glycosphingolipid biosynthesis in vivo**. *J Biol Chem* 2005, **280**(6):4858-4863.

174. Amado M, Almeida R, Carneiro F, Levery SB, Holmes EH, Nomoto M, Hollingsworth MA, Hassan H, Schwientek T, Nielsen PA *et al*: **A family of human beta3-galactosyltransferases. Characterization of four members of a UDP-galactose:beta-N-acetyl-glucosamine/beta-nacetyl-galactosamine beta-1,3-galactosyltransferase family**. *J Biol Chem* 1998, **273**(21):12770-12778.

175. Isshiki S, Togayachi A, Kudo T, Nishihara S, Watanabe M, Kubota T, Kitajima M, Shiraishi N, Sasaki K, Andoh T *et al*: **Cloning, expression, and characterization of a novel UDP-galactose:beta-N-acetylglucosamine beta1,3-galactosyltransferase (beta3Gal-T5) responsible for synthesis of type 1 chain in colorectal and pancreatic epithelia and tumor cells derived therefrom**. *J Biol Chem* 1999, **274**(18):12499-12507.

176. Keusch JJ, Manzella SM, Nyame KA, Cummings RD, Baenziger JU: **Expression cloning of a new member of the ABO blood group glycosyltransferases, iGb3 synthase, that directs the synthesis of isoglobo-glycosphingolipids**. *J Biol Chem* 2000, **275**(33):25308-25314.

177. Sasaki K, Kurata-Miura K, Ujita M, Angata K, Nakagawa S, Sekine S, Nishi T, Fukuda M: **Expression cloning of cDNA encoding a human beta-1,3-N-acetylglucosaminyltransferase that is essential for poly-N-acetyllactosamine synthesis**. *Proc Natl Acad Sci U S A* 1997, **94**(26):14294-14299.

178. Sekine M, Nara K, Suzuki A: **Tissue-specific regulation of mouse core 2 beta-1,6-N-acetylglucosaminyltransferase**. *J Biol Chem* 1997, **272**(43):27246-27252.

179. Nagata Y, Yamashiro S, Yodoi J, Lloyd KO, Shiku H, Furukawa K: **Expression cloning of beta 1,4 N-acetylgalactosaminyltransferase cDNAs that determine the expression of GM2 and GD2 gangliosides**. *J Biol Chem* 1992, **267**(17):12082-12089.

180. Yamamoto F, Marken J, Tsuji T, White T, Clausen H, Hakomori S: **Cloning and characterization of DNA complementary to human UDP-GalNAc: Fuc alpha 1----2Gal alpha 1----3GalNAc transferase (histo-blood group A transferase) mRNA**. *J Biol Chem* 1990, **265**(2):1146-1151.

181. Kijimoto S, Ishibashi T, Makita A: **Biosynthesis of Forssman hapten from globoside by alpha-N-acetylgalactosaminyltransferase of guinea pig tissues**. *Biochem Biophys Res Commun* 1974, **56**(1):177-184.

182. Yoda Y, Ishibashi T, Makita A: **Isolation, characterization, and biosynthesis of Forssman antigen in human lung and lung carcinoma**. *J Biochem* 1980, **88**(6):1887-1890.

183. Sarnesto A, Kohlin T, Hindsgaul O, Thurin J, Blaszczyk-Thurin M: **Purification of the secretor-type beta-galactoside alpha 1----2-fucosyltransferase from human serum**. *J Biol Chem* 1992, **267**(4):2737-2744.

184. Kelly RJ, Rouquier S, Giorgi D, Lennon GG, Lowe JB: **Sequence and expression of a candidate for the human Secretor blood group alpha(1,2)fucosyltransferase gene (FUT2). Homozygosity for an enzyme-inactivating nonsense mutation commonly correlates with the non-secretor phenotype**. *J Biol Chem* 1995, **270**(9):4640-4649.

185. Kukowska-Latallo JF, Larsen RD, Nair RP, Lowe JB: **A cloned human cDNA determines expression of a mouse stage-specific embryonic antigen and the Lewis blood group alpha(1,3/1,4)fucosyltransferase**. *Genes Dev* 1990, **4**(8):1288-1303.

186. Kumar R, Potvin B, Muller WA, Stanley P: **Cloning of a human alpha(1,3)-fucosyltransferase gene that encodes ELFT but does not confer ELAM-1 recognition on Chinese hamster ovary cell transfectants**. *J Biol Chem* 1991, **266**(32):21777-21783.

187. Weston BW, Nair RP, Larsen RD, Lowe JB: **Isolation of a novel human alpha (1,3)fucosyltransferase gene and molecular comparison to the human Lewis blood group alpha (1,3/1,4)fucosyltransferase gene. Syntenic, homologous, nonallelic genes encoding enzymes with distinct acceptor substrate specificities**. *J Biol Chem* 1992, **267**(6):4152-4160.

188. Koszdin KL, Bowen BR: **The cloning and expression of a human alpha-1,3 fucosyltransferase capable of forming the E-selectin ligand**. *Biochem Biophys Res Commun* 1992, **187**(1):152-157.

189. Natsuka S, Gersten KM, Zenita K, Kannagi R, Lowe JB: **Molecular cloning of a cDNA encoding a novel human leukocyte alpha-1,3-fucosyltransferase capable of synthesizing the sialyl Lewis x determinant**. *J Biol Chem* 1994, **269**(24):16789-16794.

190. Johnson PH, Yates AD, Watkins WM: **Human salivary fucosyltransferases : evidence for two distinct alpha-3-L-fucosyltransferase activities one or which is associated with the Lewis blood group Le gene**. *Biochem Biophys Res Commun* 1981, **100**(4):1611-1618.

191. Nishihara S, Iwasaki H, Kaneko M, Tawada A, Ito M, Narimatsu H: **Alpha1,3-fucosyltransferase 9 (FUT9; Fuc-TIX) preferentially fucosylates the distal GlcNAc residue of polylactosamine chain while the other four alpha1,3FUT members preferentially fucosylate the inner GlcNAc residue**. *FEBS Lett* 1999, **462**(3):289-294.

192. Rearick JI, Sadler JE, Paulson JC, Hill RL: **Enzymatic characterization of beta D-galactoside alpha2 leads to 3 sialyltransferase from porcine submaxillary gland**. *J Biol Chem* 1979, **254**(11):4444-4451.

193. Sadler JE, Rearick JI, Paulson JC, Hill RL: **Purification to homogeneity of a beta-galactoside alpha2 leads to 3 sialyltransferase and partial purification of an alpha-N-acetylgalactosaminide alpha2 leads to 6 sialyltransferase from porcine submaxillary glands**. *J Biol Chem* 1979, **254**(11):4434-4442.

194. Kono M, Takashima S, Liu H, Inoue M, Kojima N, Lee YC, Hamamoto T, Tsuji S: **Molecular cloning and functional expression of a fifth-type alpha 2,3-sialyltransferase (mST3Gal V: GM3 synthase)**. *Biochem Biophys Res Commun* 1998, **253**(1):170-175.

195. Sjoberg ER, Kitagawa H, Glushka J, van Halbeek H, Paulson JC: **Molecular cloning of a developmentally regulated N-acetylgalactosamine alpha2,6-sialyltransferase specific for sialylated glycoconjugates**. *J Biol Chem* 1996, **271**(13):7450-7459.

196. Okajima T, Fukumoto S, Ito H, Kiso M, Hirabayashi Y, Urano T, Furukawa K: **Molecular cloning of brain-specific GD1alpha synthase (ST6GalNAc V) containing CAG/Glutamine repeats**. *J Biol Chem* 1999, **274**(43):30557-30562.

197. Okajima T, Chen HH, Ito H, Kiso M, Tai T, Furukawa K, Urano T: **Molecular cloning and expression of mouse GD1alpha/GT1aalpha/GQ1balpha synthase (ST6GalNAc VI) gene**. *J Biol Chem* 2000, **275**(10):6717-6723.

198. Eppler CM, Morre DJ, Keenan TW: **Ganglioside biosynthesis in rat liver: characterization of cytidine-5'-monophospho-n-acetylneuraminic acid:hematoside (GM3) sialyltransferase**. *Biochim Biophys Acta* 1980, **619**(2):318-331.

199. Yoshida Y, Kojima N, Kurosawa N, Hamamoto T, Tsuji S: **Molecular cloning of Sia alpha 2,3Gal beta 1,4GlcNAc alpha 2,8-sialyltransferase from mouse brain**. *J Biol Chem* 1995, **270**(24):14628-14633.

200. Kono M, Yoshida Y, Kojima N, Tsuji S: **Molecular cloning and expression of a fifth type of alpha2,8-sialyltransferase (ST8Sia V). Its substrate specificity is similar to that of SAT-V/III, which synthesize GD1c, GT1a, GQ1b and GT3**. *J Biol Chem* 1996, **271**(46):29366-29371.

201. Mitsumoto Y, Oka S, Sakuma H, Inazawa J, Kawasaki T: **Cloning and chromosomal mapping of human glucuronyltransferase involved in biosynthesis of the HNK-1 carbohydrate epitope**. *Genomics* 2000, **65**(2):166-173.

202. Chou DK, Tobet SA, Jungalwala FB: **Restoration of synthesis of sulfoglucuronylglycolipids in cerebellar granule neurons promotes dedifferentiation and neurite outgrowth**. *J Biol Chem* 1998, **273**(14):8508-8515.

203. Kojima Y, Fukumoto S, Furukawa K, Okajima T, Wiels J, Yokoyama K, Suzuki Y, Urano T, Ohta M: **Molecular cloning of globotriaosylceramide/CD77 synthase, a glycosyltransferase that initiates the synthesis of globo series glycosphingolipids**. *J Biol Chem* 2000, **275**(20):15152-15156.

204. Okajima T, Nakamura Y, Uchikawa M, Haslam DB, Numata SI, Furukawa K, Urano T: **Expression cloning of human globoside synthase cDNAs. Identification of beta 3Gal-T3 as UDP-N-acetylgalactosamine:globotriaosylceramide beta 1,3-N-acetylgalactosaminyltransferase**. *J Biol Chem* 2000, **275**(51):40498-40503.

205. Kanamori A, Nakayama J, Fukuda MN, Stallcup WB, Sasaki K, Fukuda M, Hirabayashi Y: **Expression cloning and characterization of a cDNA encoding a novel membrane protein required for the formation of O-acetylated ganglioside: a putative acetyl-CoA transporter**. *Proc Natl Acad Sci U S A* 1997, **94**(7):2897-2902.

206. Sean D, Meltzer PS: **GEOquery: a bridge between the Gene Expression Omnibus (GEO) and BioConductor**. *Bioinformatics* 2007, **23**(14):1846-1847.

207. Gentleman RC, Carey VJ, Bates DM, Bolstad B, Dettling M, Dudoit S, Ellis B, Gautier L, Ge Y, Gentry J *et al*: **Bioconductor: open software development for computational biology and bioinformatics**. *Genome Biol* 2004, **5**(10):R80.

208. Sullards MC, Allegood JC, Kelly S, Wang E, Haynes CA, Park H, Chen Y, Merrill AH, Jr.: **Structure-specific, quantitative methods for analysis of sphingolipids by liquid chromatography-tandem mass spectrometry: "inside-out" sphingolipidomics**. *Methods Enzymol* 2007, **432**:83-115.

209. Sturn A, Quackenbush J, Trajanoski Z: **Genesis: cluster analysis of microarray data**. *Bioinformatics* 2002, **18**(1):207-208.

210. Kishimoto Y, Radin NS: **Biosynthesis of Nervonic Acid and Its Homologues from Carboxyl-Labeled Oleic Acid**. *J Lipid Res* 1963, **4**:444-447.

211. Shaner RL, Allegood JC, Park H, Wang E, Kelly S, Haynes CA, Sullards MC, Merrill AH, Jr.: **Quantitative analysis of sphingolipids for lipidomics using triple quadrupole and quadrupole linear ion trap mass spectrometers**. *J Lipid Res* 2008.

212. Haynes CA, Allegood JC, Sims K, Wang EW, Sullards MC, Merrill AH, Jr.: **Quantitation of fatty acyl-coenzyme As in mammalian cells by liquid chromatography-electrospray ionization tandem mass spectrometry**. *J Lipid Res* 2008, **49**(5):1113-1125.

213. Ruckhaberle E, Karn T, Rody A, Hanker L, Gatje R, Metzler D, Holtrich U, Kaufmann M: **Gene expression of ceramide kinase, galactosyl ceramide synthase and ganglioside GD3 synthase is associated with prognosis in breast cancer**. *J Cancer Res Clin Oncol* 2009, **135**(8):1005-1013.

214. Ruckhaberle E, Holtrich U, Engels K, Hanker L, Gatje R, Metzler D, Karn T, Kaufmann M, Rody A: **Acid ceramidase 1 expression correlates with a better prognosis in ER-positive breast cancer**. *Climacteric* 2009:1-12.

215. Bredel M, Bredel C, Juric D, Duran GE, Yu RX, Harsh GR, Vogel H, Recht LD, Scheck AC, Sikic BI: **Tumor necrosis factor-alpha-induced protein 3 as a putative regulator of nuclear factor-kappaB-mediated resistance to O6-alkylating agents in human glioblastomas**. *J Clin Oncol* 2006, **24**(2):274-287.

216. Hendrix ND, Wu R, Kuick R, Schwartz DR, Fearon ER, Cho KR: **Fibroblast growth factor 9 has oncogenic activity and is a downstream target of Wnt signaling in ovarian endometrioid adenocarcinomas**. *Cancer Res* 2006, **66**(3):1354-1362.

217. Schrump DS, Furukawa K, Yamaguchi H, Lloyd KO, Old LJ: **Recognition of galactosylgloboside by monoclonal antibodies derived from patients with primary lung cancer**. *Proc Natl Acad Sci U S A* 1988, **85**(12):4441-4445.

218. Riker AI, Enkemann SA, Fodstad O, Liu S, Ren S, Morris C, Xi Y, Howell P, Metge B, Samant RS *et al*: **The gene expression profiles of primary and metastatic melanoma yields a transition point of tumor progression and metastasis**. *BMC Med Genomics* 2008, **1**:13.

219. Stoffel W, LeKim D, Sticht G: **Metabolism of sphingosine bases. 8. Distribution, isolation and properties of D-3-oxosphinganine reductase. Stereospecificity of the NADPH-dependent reaction of 3-oxodihydrospingosine (2-amino-1-hydroxyoctadecane-3-one)**. *Hoppe Seylers Z Physiol Chem* 1968, **349**(12):1637-1644.

220. Ardail D, Popa I, Alcantara K, Pons A, Zanetta JP, Louisot P, Thomas L, Portoukalian J: **Occurrence of ceramides and neutral glycolipids with unusual long-chain base composition in purified rat liver mitochondria**. *FEBS Lett* 2001, **488**(3):160-164.

221. Beeler T, Bacikova D, Gable K, Hopkins L, Johnson C, Slife H, Dunn T: **The Saccharomyces cerevisiae TSC10/YBR265w gene encoding 3-ketosphinganine reductase is identified in a screen for temperature-sensitive suppressors of the Ca2+-sensitive csg2Delta mutant**. *J Biol Chem* 1998, **273**(46):30688-30694.

222. Zhou Y, Kato H, Asanoma K, Kondo H, Arima T, Kato K, Matsuda T, Wake N: **Identification of FOXC1 as a TGF-beta1 responsive gene and its involvement in negative regulation of cell growth**. *Genomics* 2002, **80**(5):465-472.

223. Merrill AH, Jr., Wang E, Mullins RE, Jamison WC, Nimkar S, Liotta DC: **Quantitation of free sphingosine in liver by high-performance liquid chromatography**. *Anal Biochem* 1988, **171**(2):373-381.

224. Notredame C, Higgins DG, Heringa J: **T-Coffee: A novel method for fast and accurate multiple sequence alignment**. *J Mol Biol* 2000, **302**(1):205-217.

225. Tanabe T, Tanaka N, Uchikawa K, Kabashima T, Ito K, Nonaka T, Mitsui Y, Tsuru M, Yoshimoto T: **Roles of the Ser146, Tyr159, and Lys163 residues in the catalytic action of 7alpha-hydroxysteroid dehydrogenase from Escherichia coli**. *J Biochem* 1998, **124**(3):634-641.

226. Tamimi Y, Lines M, Coca-Prados M, Walter MA: **Identification of target genes regulated by FOXC1 using nickel agarose-based chromatin enrichment**. *Invest Ophthalmol Vis Sci* 2004, **45**(11):3904-3913.

227. Wu C, Orozco C, Boyer J, Leglise M, Goodale J, Batalov S, Hodge CL, Haase J, Janes J, Huss JW, 3rd *et al*: **BioGPS: an extensible and customizable portal for querying and organizing gene annotation resources**. *Genome Biol* 2009, **10**(11):R130.

228. Hanada K: **Serine palmitoyltransferase, a key enzyme of sphingolipid metabolism**. *Biochim Biophys Acta* 2003, **1632**(1-3):16-30.

229. Hanada K, Hara T, Fukasawa M, Yamaji A, Umeda M, Nishijima M: **Mammalian cell mutants resistant to a sphingomyelin-directed cytolysin. Genetic and biochemical evidence for complex formation of the LCB1 protein with the LCB2 protein for serine palmitoyltransferase**. *J Biol Chem* 1998, **273**(50):33787-33794.

230. Gable K, Slife H, Bacikova D, Monaghan E, Dunn TM: **Tsc3p is an 80-amino acid protein associated with serine palmitoyltransferase and required for optimal enzyme activity**. *J Biol Chem* 2000, **275**(11):7597-7603.

231. Hojjati MR, Li Z, Jiang XC: **Serine palmitoyl-CoA transferase (SPT) deficiency and sphingolipid levels in mice**. *Biochim Biophys Acta* 2005, **1737**(1):44-51.

232. Yard BA, Carter LG, Johnson KA, Overton IM, Dorward M, Liu H, McMahon SA, Oke M, Puech D, Barton GJ *et al*: **The structure of serine palmitoyltransferase; gateway to sphingolipid biosynthesis**. *J Mol Biol* 2007, **370**(5):870-886.

233. Gable K, Han G, Monaghan E, Bacikova D, Natarajan M, Williams R, Dunn TM: **Mutations in the yeast LCB1 and LCB2 genes, including those corresponding to the hereditary sensory neuropathy type I mutations, dominantly inactivate serine palmitoyltransferase**. *J Biol Chem* 2002, **277**(12):10194-10200.

234. Batheja AD, Uhlinger DJ, Carton JM, Ho G, D'Andrea MR: **Characterization of serine palmitoyltransferase in normal human tissues**. *J Histochem Cytochem* 2003, **51**(5):687-696.

235. Merrill AH, Jr., Sullards MC, Allegood JC, Kelly S, Wang E: **Sphingolipidomics: high-throughput, structure-specific, and quantitative analysis of sphingolipids by liquid chromatography tandem mass spectrometry**. *Methods* 2005, **36**(2):207-224.

236. Zitomer NC, Mitchell T, Voss KA, Bondy GS, Pruett ST, Garnier-Amblard EC, Liebeskind LS, Park H, Wang E, Sullards MC *et al*: **Ceramide synthase inhibition by fumonisin B1 causes accumulation of 1-deoxy-sphinganine: A novel category of bioactive 1-deoxy-sphingoid bases and 1-deoxy-**

dihydroceramides biosynthesized by mammalian cell lines and animals. *J Biol Chem* 2008.

237. Iwatani M, Ikegami K, Kremenska Y, Hattori N, Tanaka S, Yagi S, Shiota K: **Dimethyl sulfoxide has an impact on epigenetic profile in mouse embryoid body**. *Stem Cells* 2006, **24**(11):2549-2556.

238. Hegner B, Weber M, Dragun D, Schulze-Lohoff E: **Differential regulation of smooth muscle markers in human bone marrow-derived mesenchymal stem cells**. *J Hypertens* 2005, **23**(6):1191-1202.

239. Wiebe JP, Kowalik A, Gallardi RL, Egeler O, Clubb BH: **Glycerol disrupts tight junction-associated actin microfilaments, occludin, and microtubules in Sertoli cells**. *J Androl* 2000, **21**(5):625-635.

240. Malmqvist T, Mollby R: **Enzymatic hydrolysis by bacterial phospolipases C and D of immobilized radioactive sphingomyelin and phosphatidylcholine**. *Acta Pathol Microbiol Scand [B]* 1981, **89**(5):363-367.

241. Brogden KA, Engen RL, Songer JG, Gallagher J: **Changes in ovine erythrocyte morphology due to sphingomyelin degradation by Corynebacterium pseudotuberculosis phospholipase D**. *Microb Pathog* 1990, **8**(2):157-162.

242. Marti-Renom MA, Stuart AC, Fiser A, Sanchez R, Melo F, Sali A: **Comparative protein structure modeling of genes and genomes**. *Annu Rev Biophys Biomol Struct* 2000, **29**:291-325.

243. Humphrey W, Dalke A, Schulten K: **VMD: visual molecular dynamics**. *J Mol Graph* 1996, **14**(1):33-38, 27-38.

244. Rother J, van Echten G, Schwarzmann G, Sandhoff K: **Biosynthesis of sphingolipids: dihydroceramide and not sphinganine is desaturated by cultured cells**. *Biochem Biophys Res Commun* 1992, **189**(1):14-20.

245. Burrows JA, Willis LK, Perlmutter DH: **Chemical chaperones mediate increased secretion of mutant alpha 1-antitrypsin (alpha 1-AT) Z: A potential pharmacological strategy for prevention of liver injury and emphysema in alpha 1-AT deficiency**. *Proc Natl Acad Sci U S A* 2000, **97**(4):1796-1801.

246. Kubota K, Niinuma Y, Kaneko M, Okuma Y, Sugai M, Omura T, Uesugi M, Uehara T, Hosoi T, Nomura Y: **Suppressive effects of 4-phenylbutyrate on the aggregation of Pael receptors and endoplasmic reticulum stress**. *J Neurochem* 2006, **97**(5):1259-1268.

247. Ohashi T, Uchida K, Uchida S, Sasaki S, Nihei H: **Intracellular mislocalization of mutant podocin and correction by chemical chaperones**. *Histochem Cell Biol* 2003, **119**(3):257-264.

248. Myers JK, Pace CN: **Hydrogen bonding stabilizes globular proteins**. *Biophys J* 1996, **71**(4):2033-2039.